Documentation for the 2008 Update of the United States National Seismic Hazard Maps

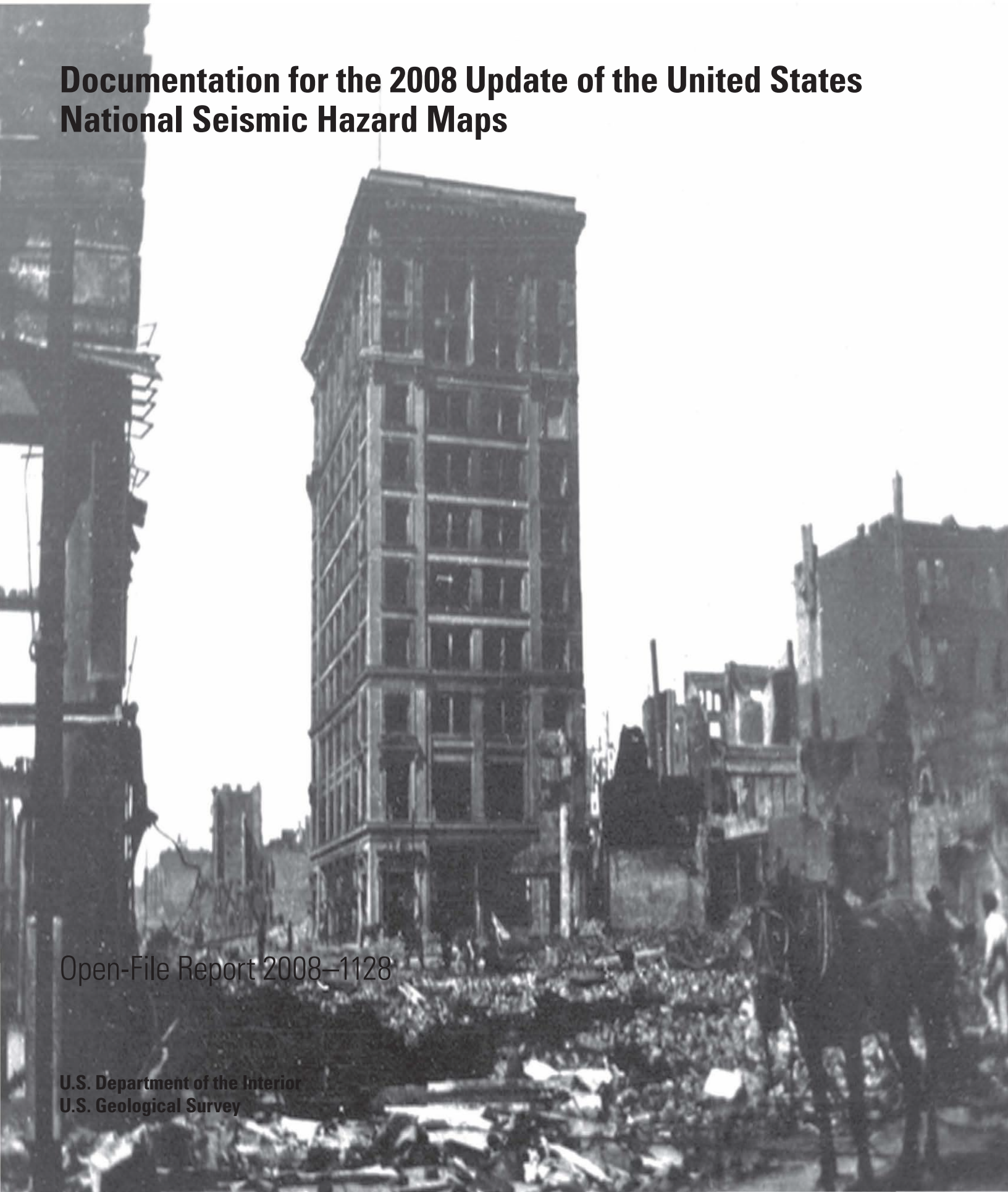

Open-File Report 2008–1128

U.S. Department of the Interior
U.S. Geological Survey

Documentation for the 2008 Update of the United States National Seismic Hazard Maps

By Mark D. Petersen, Arthur D. Frankel, Stephen C. Harmsen, Charles S. Mueller, Kathleen M. Haller, Russell L. Wheeler, Robert L. Wesson, Yuehua Zeng, Oliver S. Boyd, David M. Perkins, Nicolas Luco, Edward H. Field, Chris J. Wills, and Kenneth S. Rukstales

Open-File Report 2008–1128

U.S. Department of the Interior
U.S. Geological Survey

U.S. Department of the Interior
DIRK KEMPTHORNE, Secretary

U.S. Geological Survey
Mark D. Myers, Director

U.S. Geological Survey, Reston, Virginia: 2008

For product and ordering information:
World Wide Web: http://www.usgs.gov/pubprod
Telephone: 1-888-ASK-USGS

For more information on the USGS--the Federal source for science about the Earth, its natural and living resources, natural hazards, and the environment:
World Wide Web: http://www.usgs.gov
Telephone: 1-888-ASK-USGS

Suggested citation:
Petersen, Mark D., Frankel, Arthur D., Harmsen, Stephen C., Mueller, Charles S., Haller, Kathleen M., Wheeler, Russell L., Wesson, Robert L., Zeng, Yuehua, Boyd, Oliver S., Perkins, David M., Luco, Nicolas, Field, Edward H., Wills, Chris J., and Rukstales, Kenneth S., 2008, Documentation for the 2008 Update of the United States National Seismic Hazard Maps: U.S. Geological Survey Open-File Report 2008–1128, 61 p.

Contents

Figures

Tables

Appendix Figures:

Appendix Tables:

Documentation for the 2008 Update of the United States National Seismic Hazard Maps

By Mark D. Petersen,[1] Arthur D. Frankel,[1] Stephen C. Harmsen,[1] Charles S. Mueller,[1] Kathleen M. Haller,[1] Russell L. Wheeler,[1] Robert L. Wesson,[1] Yuehua Zeng,[1] Oliver S. Boyd,[2] David M. Perkins,[1] Nicolas Luco,[1] Edward H. Field,[3] Chris J. Wills,[4] and Kenneth S. Rukstales[1]

Introduction

The 2008 U.S. Geological Survey (USGS) National Seismic Hazard Maps display earthquake ground motions for various probability levels across the United States and are applied in seismic provisions of building codes, insurance rate structures, risk assessments, and other public policy. This update of the maps incorporates new findings on earthquake ground shaking, faults, seismicity, and geodesy. The resulting maps are derived from seismic hazard curves calculated on a grid of sites across the United States that describe the frequency of exceeding a set of ground motions. The USGS National Seismic Hazard Mapping Project developed these maps by incorporating information on potential earthquakes and associated ground shaking obtained from interaction in science and engineering workshops involving hundreds of participants, review by several science organizations and State surveys, and advice from two expert panels. The new probabilistic hazard maps represent an update of the 2002 seismic hazard maps developed by Frankel and others (2002), which used the methodology developed for the 1996 version of the maps (Frankel and others, 1996). Algermissen and Perkins (1976) published the first probabilistic seismic hazard map of the United States which was updated in Algermissen and others (1990). The National Seismic Hazard Maps represent our assessment of the "best available science" in earthquake hazards estimation for the United States (maps of Alaska and Hawaii as well as further information on hazard across the United States are available on our Web site at *http://earthquake.usgs.gov/research/hazmaps/*).

USGS probabilistic seismic hazard maps are revised every 6 years or so to reflect newly published or thoroughly reviewed earthquake science and to keep pace with regular updates of the building code. We discussed potential changes in the national seismic hazard model and maps at a series of topical and regional USGS National Seismic Hazard Mapping Project (NSHMP) workshops and committee meetings held in 2005 and 2006 (fig. 1). Two workshops were convened in Menlo Park, Calif., to discuss ground shaking issues for the Central and Eastern United States (CEUS), led by Jack Boatwright, and the Western United States (WUS). In addition, we conducted regional seismic hazard workshops for the Pacific Northwest in Seattle, Wash., the CEUS in Boston, Mass., the Intermountain West in Reno, Nev., and California in San Francisco, Calif. A National User Needs workshop was held in San Mateo, Calif., by the Applied Technology Council. Additional information regarding our workshops can be found at: *http://earthquake.usgs.gov/research/hazmaps/whats_new/workshops/index.php* and *http://www.atcouncil.org/* (The Third ATC-35/USGS National Earthquake Ground-Motion Mapping Workshop, December 7–8, 2006; CD–ROM available).

In addition to workshops, the USGS assembled two expert panels to provide advice on issues in updating the National Seismic Hazard Maps. The NSHMP Next Generation Attenuation Relation Advisory Panel included: Ralph Archeleta, John Anderson, Martin Chapman, C.B. Crouse, Robert Graves, Tom Heaton, William Holmes, Jonathan Stewart, and David Wald met in Berkeley, Calif. The panel focused on implementation of the new Pacific Earthquake Engineering Research Center (PEER) Next Generation Attenuation Relations (NGA) in the national maps. Information from this meeting can be found at *http://earthquake.usgs.gov/research/hazmaps/whats_new/workshops/index.php*. The NSHM Advisory Panel, was composed of seismic hazard experts and met in Golden, Colo., to review progress on the maps, hazard curves, input data, and procedures used in this update. In addition, they provided final technical review of the 2008 National Seismic Hazard Maps. This group included: John Anderson, Kenneth Campbell, Allin Cornell, C.B. Crouse, John Ebel, Jeff Kimball, William Lettis, Michael Reichle, Paul Somerville, and regional coordinators of the USGS earthquake program Mike Blanpied, Tom Brocher, Susan Hough, Buddy Schweig, and Craig Weaver.

Additional advice was provided by several science and engineering organizations and geological surveys. The Western States Seismic Policy Council convened a 3-day workshop

[1]Golden, Colorado

[2]Memphis, Tennessee

[3]Pasadena, California

[4]California Geological Survey, Sacramento, California

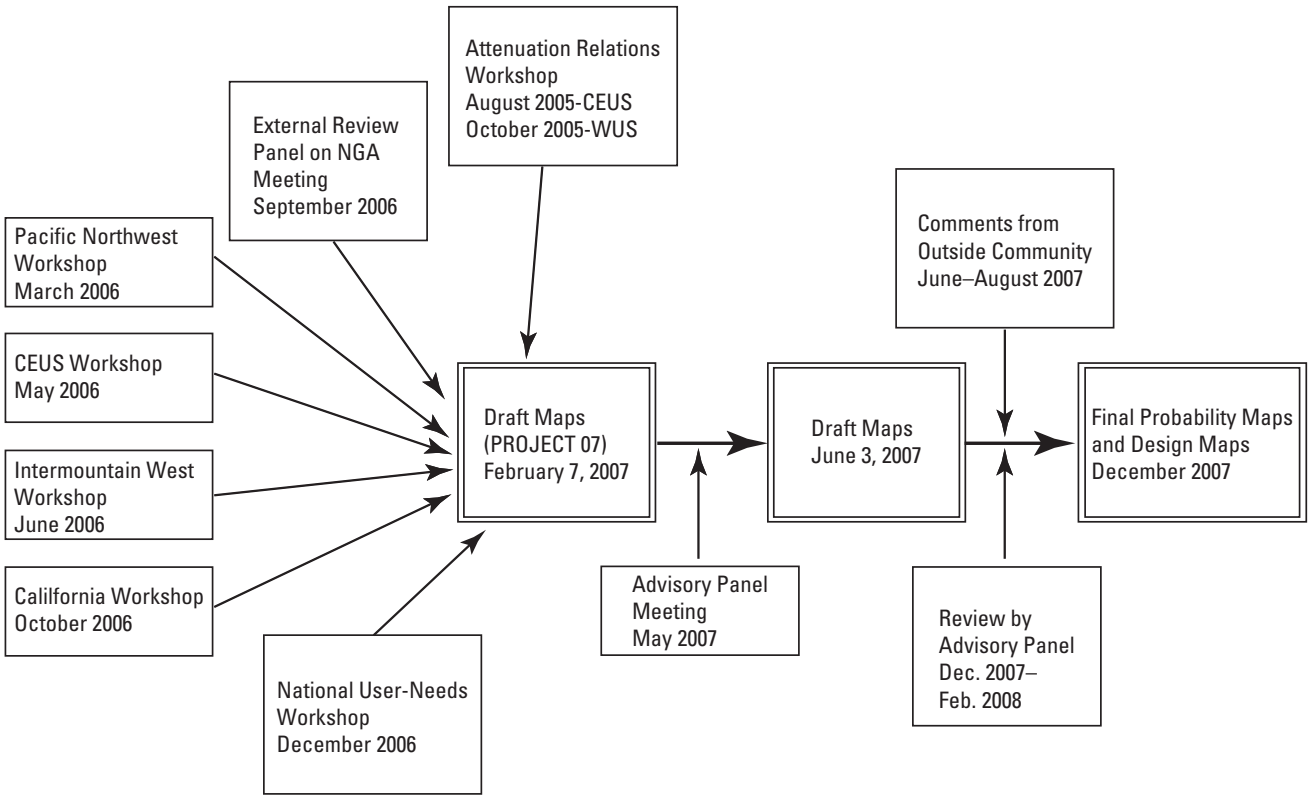

Figure 1. Process for developing the 2008 USGS National Seismic Hazard Maps. CEUS, Central United States; WUS, Western United States.

to develop recommendations to the NSHMP on Intermountain West hazard issues (March 2006 in Salt Lake City). Their recommendations can be found at *http://geology.utah.gov/online/ofr/ofr-477.pdf* (Lund, 2006). The Utah Geological Survey convened a working group and held several meetings to recommend recurrence information for Quaternary faults in Utah (Lund, 2005). The Working Group on California Earthquake Probabilities involving the USGS, California Geological Survey, and Southern California Earthquake Center held several meetings and workshops to determine parameters and methodologies in developing a uniform earthquake forecast model for California, at *http://gravity.usc.edu/WGCEP/*. The Pacific Earthquake Engineering Research Center (PEER) held several meetings to update the Western United States crustal attenuation relations (*http://peer.berkeley.edu/products/nga_project.html*). Scientists, engineers, and policy makers from government agencies, academic institutions, and private sector groups contributed to the meetings and workshops. As was the case for the 1996 and 2002 hazard maps, the California Geological Survey (CGS) cooperated in developing the 2008 maps for the State (see Field and others, 2008). Further information on California hazards can be found at *http://www.consrv.ca.gov/CGS/geologic_hazards/earthquakes/index.htm.*

Table 1 outlines the significant changes that were implemented in the 2008 hazard maps. One primary goal of this update was to include the best available science including information on fault slip rates, paleoseismologic data from fault trenching studies, earthquake catalogs, and strong-motion recordings from global earthquakes. As much as possible, we used consistent methodologies to develop a uniform hazard assessment across the country, although we also accounted for regional differences where needed. Draft documentation and maps were available for review by State geological surveys and the public from June to August 2007 (fig. 1). Draft versions of the new maps were delivered on February 15, 2007, September 30, 2007, and December 21, 2007, to the Building Seismic Safety Council (BSSC) for discussions of potential implementation in the 2012 building code as part of the Federal Emergency Management Agency (FEMA) and USGS-sponsored PROJECT 07, a Building Seismic Safety Council committee that evaluates potential changes to building code design criteria. Draft design maps based on these hazard maps (MCE maps) were provided to the BSSC on January 17, 2008, for their consideration in the 2009 National Earthquake Hazard Reduction Program (NEHRP) provisions.

This documentation focuses on the new input parameters and output hazard products. The principal methodologies of probabilistic seismic hazard analysis can be found in other literature (for example, McGuire, 2004). However, it is important to recognize that in this analysis we calculate probabilistic

Table 1. Significant changes to National Seismic Hazard Maps.

A. California
   a. Revised earthquake catalog and accounted for magnitude round off and uncertainty
   b. Constrained model to fit within 2 sigma historical or observed seismicity rates (suggested by WGCEP—Science review panel)
      i. Reduced moment rate on faults by 10 percent to account for aftershocks, foreshocks, afterslip, and smaller earthquakes
      ii. Reduced earthquakes M≥6.5 in smoothed gridded seismicity to 1/3 of the rate to account for earthquakes already modeled on faults (generally not applied outside California)
      iii. Implemented a branch of Gutenberg-Richter model with b=0, which is consistent with modeling of several of the large multisegment ruptures on the San Andreas system
      iv. Eliminated the epistemic magnitude uncertainty, which is accounted for by implementing the two magnitude-area relations
   c. Implemented four new recurrence models for southern California Type-A faults from WGCEP (based on moment-balanced models, paleoseismic recurrence models, Ellsworth Type-B (Ellsworth, 2003) magnitude-area relations and Hanks and Bakun (2002) magnitude-area relations)
   d. Developed new multisegment ruptures for several California Type-B faults
   e. Implemented new SCEC CFM model for geometry in southern California
   f. Revised slip rates for sections of the San Andreas fault, San Jacinto fault, and nine Type-B faults
   g. Developed new zones of distributed shear in southern California and revised geometry in northern California (rates considered are about 50 percent of the total strain rate
   h. Included new documentation for logic tree (see fig. 23)

B. Intermountain West
   a. Updated catalog through 2006 and accounted for magnitude round off and uncertainty
   b. Updated fault parameters on more than 10 percent of faults, added several new faults (see Appendix G)
   c. Changed preferred dip for most normal faults from 60° to 50°
   d. Allowed for distribution of dips on normal faults (40°, 50°, and 60° with 0.2, 0.6, 0.2 weights, see Appendix G) as recommended by Western States Seismic Policy Council
   e. Implemented Wasatch fault floating rupture (M7.4) model to account for random multisegment rupture
   f. Applied California weights for Gutenberg-Richter and characteristic magnitude-frequency distributions, 1/3 and 2/3 respectively, as recommended by Western States Seismic Policy Council
   g. Revised geometry of zones of distributed shear in Nevada (rates based on 50 percent of the total strain rate)
   h. Included new documentation for logic trees (see figs. 12, 17, and 18)

C. Pacific Northwest
   a. Updated catalog through 2006 and accounted for magnitude round off and uncertainty
   b. Added new recurrence distribution for Cascadia that includes M 8.0–8.7 and M8.8–9.2 models weighted 1/3 and 2/3, respectively
   c. Added new source zone around Portland and the coast to account for potential of large deep earthquakes, based on extrapolating the rate of small-magnitude earthquakes (M<4.0)
   d. Added new faults (Lake–Creek–Boundary Creek fault, Boulder Creek fault, and Stonewall Anticline structure)
   e. Included new documentation for logic trees (see figs. 19 and 20)
   f. Modified fault geometry for South Whidbey Island fault to include three hypothetical strands

D. Central and Eastern United States
   a. Updated catalog through 2006 and accounted for magnitude uncertainty (see fig. 2)
   b. Reduced magnitudes in northern New Madrid seismic zone by 0.2 unit and added logic-tree branch for recurrence rate of 1/750 years
   c. Added logic-tree branch for 1/1,000-year recurrence rate of earthquakes in New Madrid (recommended by advisory panel)
   d. Implemented temporal cluster model for New Madrid earthquakes (see Appendix F for example calculation)
   e. Modified fault geometry for New Madrid to include five hypothetical strands and increased weight on central strand to 0.7
   f. Revised dip of Reelfoot fault to 38°
   g. Developed maximum magnitude distribution for seismicity-derived hazard sources (see fig. 2)
   h. Revised geometry of large Charleston zone, extending it farther offshore to include the Helena Banks fault

Table 1. Significant changes to National Seismic Hazard Maps.—Continued

zone (agreed with members of advisory panel that we would hold workshop to discuss these issues for future versions of the maps)

i. Added documentation for logic trees (see figs. 2, 6, and 8)

E. Attenuation relations

a. Applied the three new PEER NGA equations for crustal faults in the Western United States. Accounted for additional epistemic uncertainties in ground motions (from ±23 percent to ±50 percent depending the number of samples in the particular magnitude-distance bin)

b. Implemented depth to the top of rupture parameter in two NGA equations in the Western United States

c. Implemented new depth to top of rupture for gridded seismicity in the Western United States

d. Implemented virtual dipping faults in the Western United States for seismicity-derived sources

e. Implemented new published equations (see fig. 2, 6, and 8) for Central and Eastern United States (Toro and others, 1997; Silva and others, 2002; Atkinson and Boore, 2006; and Tavakoli and Pezeshk, 2005) and revised weights

f. Replaced Sadigh and others (1997) ground-motion model with new Zhao and others (2006) model for Cascadia subduction interface earthquakes

g. Added the Atkinson and Boore (2003) attenuation relations for interface earthquakes on the Cascadia subduction zone

F. General methodology

a. Used two depths to top of rupture values for gridded seismicity hazard calculation for the WUS, 5 kilometers for M<6.5 and 1 kilometer for M≥6.5, and different depth to top of rupture for faults (see Appendix A)

b. Applied new magnitude binning scheme to more precisely quantify magnitude distribution and allow for better sampling of the distribution

hazard curves that depict the annual frequency of exceedance at given ground-motion levels (the inverse of the total annual frequency of exceedance is the return period of the ground-motion exceedance). To obtain a probability from an annual frequency of exceedance we apply the Poisson equation (time independent). For example, if the acceptable risk is defined as having a 2-percent chance of one or more exceedances in 50 years then the Poisson equation yields an annual frequency of exceedance of 0.000404. We interpolate the hazard curves at this annual frequency of exceedance to obtain the hazard maps. The maps were developed for 2-percent, 5-percent, and 10-percent probability of exceedance in 50 years for several spectral accelerations. In this documentation we concentrate on the 0.2-s and 1-s spectral acceleration and peak horizontal ground acceleration on uniform firm rock site condition (760 m/s shear-wave velocity in the upper 30 m of the crust) that is applied in current building codes.

The 2008 hazard maps are significantly different from the 2002 maps in many parts of the United States. The new maps generally show 10- to 15-percent reductions in acceleration across much of the Central and Eastern United States for 0.2-s and 1.0-s spectral acceleration and peak horizontal ground acceleration for 2-percent probability of exceedance in 50 years. The new maps for the Western United States indicate about 10-percent reductions for 0.2-s spectral acceleration and peak horizontal ground acceleration and up to 30-percent reductions in 1.0-s spectral acceleration at similar hazard levels. Most of the changes in the new maps can be attributed to the introduction of new attenuation relations for crustal and subduction earthquakes; however, changes to the fault and seismicity parameters also can be significant.

General Methodology

In this documentation, we explain the methodology and highlight important changes to the procedures and input parameters used. Further details of the methodology can be found in the earlier documentations (Frankel and others, 1996; Frankel and others, 2002; Petersen and others, 1996). Details of some of the models can be found in working group reports and recent literature (for example, Campbell and Bozorgnia, 2008; Field and others, 2008; Lund, 2005). Probabilistic hazard is calculated by developing models of seismicity-derived hazard sources, models of earthquakes on faults, and models of ground shaking resulting from these earthquakes.

As in the 2002 and 1996 maps, we include four different classes of earthquake source models in the 2008 maps: (1) smoothed-gridded seismicity, (2) uniform background source zones, (3) geodetically derived source zones, and (4) faults. The first two models are based on the earthquake catalog and characterize the hazard from earthquakes between about M5 and M6.5–7.0. The geodetically derived source zones are used to derive the hazard between M6.5 and the largest potential earthquake in a region. In most cases, the faults contribute most to the hazard for earthquakes larger than M6.5.

Seismicity-Derived Hazard Component

Random seismicity-derived sources account for two types of earthquakes: those that occur off known faults, and moderate-size earthquakes that are not modeled on faults. The gridded-seismicity models are based on historical earthquakes and account for the observation that larger earthquakes occur at or near clusters of previous smaller earthquakes (Frankel, 1995; Kafka, 2002; Kafka and Levin, 2000). Uniform background zones account for the possibility of future random seismicity in areas without historical seismicity and establish a floor to the seismic-hazard calculations. Special zones allow for local variability in seismicity characteristics within a zone (for example, changes in b-value, changes in maximum magnitude M_{max}, and uniform seismicity characteristics). These models are combined to account for the suite of potential earthquakes that can affect a site (see example logic tree in fig. 2).

Seismicity models require a declustered earthquake catalog of independent events for calculation of Poissonian (time-independent) earthquake rates. The earthquake catalogs are constructed by merging catalogs developed by different institutions. Duplicate events and manmade events are deleted. The catalog is then declustered to remove dependent events such as foreshocks or aftershocks using the routines of Gardner and Knopoff (1974). The CEUS catalog includes m_{bLg} magnitudes, whereas several of the ground-shaking equations require moment magnitudes. Therefore, when determining the hazard from a bin centered on a certain m_{bLg}, we convert this m_{bLg} to a moment magnitude when calculating the ground motions from most of the attenuation relations. Completeness levels are estimated from the earthquake catalog, and parameters of the magnitude-rate distribution (regional b-values and 10^a-values in cells or zones) are computed using a maximum-likelihood method (Weichert, 1980) that accounts for variable completeness. In the 2008 update of the maps, we have taken into account the uncertainty in magnitudes represented in the catalogs. This tends to reduce the rate of earthquakes in the model because magnitudes are more likely to be lower than the reported magnitude for a Gutenberg-Richter distribution with positive b-value that predicts more small earthquakes.

To calculate the hazard from a particular source, we apply a truncated-exponential or Gutenberg-Richter magnitude-frequency distribution (Gutenberg and Richter, 1944). The hazard is calculated using a minimum magnitude of 5.0 (moment magnitude in the WUS and m_{bLg} in the CEUS). M_{max} values are determined from paleoseismic information, historical seismicity, or global analogy. Seismicity rate parameters (a- and b-values) are obtained from analysis of the catalog. For the gridded-seismicity models, the earthquake rates determined for the cells (0.1 degree in latitude and longitude) are spatially smoothed using a two-dimensional Gaussian smoothing operator (Frankel, 1995).

The hazard is calculated for potential earthquakes at each grid cell. Earthquakes smaller than M6.0 are characterized as point sources at the center of each cell, whereas earthquakes larger than M6 assume hypothetical finite vertical or dipping faults centered on the source grid cell (Appendix B). Lengths of the finite faults are determined using the Wells and Coppersmith (1994) relations for all faulting styles taken together. In 1996 and 2002, the strike of each fault was chosen randomly (except for zones of distributed shear where the strike is fixed). In the 2008 update, we precalculate average distances from virtual faults with strike directions uniformly distributed from 0 to 180° (Appendixes B and C). (The fixed-strike zones have the same distance calculation as in previous seismic hazard models.) The average-distance calculation ensures that no receiver is assigned a biased distance based on an arbitrary draw from a random-number generator. This algorithm modification has little visible effect on probabilistic motion at 10^{-4} or greater probability of exceedance, but it does have an effect at smaller probabilities. In addition to the average distance calculation, we also apply virtual dipping faults for grids in the Western United States to account for hanging-wall terms included in the ground-motion prediction equations (Appendix D).

Fault Sources

Earthquake recurrence rates for faults are based on geologic measurements, geodesy, and seismicity measurements and interpretations. An important consideration in the hazard analysis is estimating the sizes of earthquakes that can rupture along a fault. We estimate the maximum magnitude along a fault by using the mapped surface geology and recorded earthquake location and depth distributions to obtain fault length or area. Using the fault dimensions and, in some cases, estimates of where earthquake ruptures may initiate and terminate (segmentation models), we can calculate the maximum or characteristic magnitudes from relationships that are dependent on fault length or area (for example, Wells and Coppersmith, 1994; Ellsworth, 2003; and Hanks and Bakun, 2002). These parameters, along with the fault slip rate, are needed to define the characteristic (Schwartz and Coppersmith, 1984) and Gutenberg-Richter (Gutenberg and Richter, 1944) magnitude-frequency distributions (Frankel and others, 1996; Petersen and others, 1996). We have sampled the Gutenberg-Richter distribution as described in Appendix E. The rates of these earthquakes can be inferred from paleoseismic investigations (both paleoliquefaction and fault trenching studies) or slip-rate estimates (from geodetic or geologic studies).

We develop weighted alternative source models based on tectonic, geodetic, and geologic considerations. Alternative models are included to account for epistemic uncertainty (the uncertainty between alternative models) in the sizes and rates of future earthquakes the sources may generate. We also account for aleatory variability (random variability in data used to constrain the model) in the locations and magnitudes of future earthquakes by including alternative magnitudes and fault traces or source areas along which future ruptures may occur. This uncertainty is described further in the sections below using logic-tree analyses. These analyses indicate the

epistemic uncertainty and the associated weights at each decision point in the analysis. Often a given parameter contains both epistemic uncertainty and aleatory variability.

Attenuation Relations

Ground-motion prediction equations or attenuation relations relate the source characteristics of the earthquake and propagation path of the seismic waves to the ground motion at a site. The predicted ground motion is typically quantified in terms of a median value (a function of magnitude, distance, style of faulting, and other factors) and a probability density function of peak horizontal ground acceleration or spectral accelerations. We apply ground-motion equations specific to the Central and Eastern United States earthquakes, to the Western United States crustal fault earthquakes, and to subduction-zone interface and in-slab earthquakes. In the Central and Eastern United States, we generally calculate ground motions from sources that are up to 1,000 kilometers from the site. In the Western United States, we calculate ground motion from crustal sources less than 200 kilometers and subduction sources less than 1,000 kilometers from the site.

Central and Eastern United States

As in 1996 and 2002, we include the northern and central Rocky Mountains and the Colorado Plateau in the CEUS region since earthquake stress drops and the attenuation parameter Q are poorly constrained in these areas. The CEUS fault model includes four finite fault sources (New Madrid, Mo., and adjacent States; Charleston, S.C.; Meers, Okla.; and Cheraw, Colo.). These four sources are the only ones in the CEUS that have paleoseismic data to constrain large-earthquake recurrence rates.

Source Model: Seismicity-Derived Hazard Component

Catalog

The earthquake catalog for central and eastern North America (CENA) has been updated through 2006. We include earthquakes outside the national border because they influence the hazard within the United States. As in the 1996 and 2002 updates, we combine earthquakes from several (reformatted) source catalogs, choose one preferred record for each event that is listed more than once and decluster to remove aftershocks and foreshocks (Mueller and others, 1997). As before, our goal is to make a CENA catalog that is dominated by the well-researched NCEER91 catalog (see below). The final declustered catalog used in the hazard analysis (hereinafter called emb.cc) lists approximately 3,350 earthquakes from 1700 through 2006 with magnitude equal to or greater than 3.0. Most small to moderate-size earthquakes in CENA are cataloged using a short-period surface-wave magnitude like m_{bLg} or its equivalent. A magnitude m_{bLg} of 5.0 is consistent with a M_w of 4.5–4.7 (emb.cc is based on magnitude m_{bLg}).

We use earthquakes from the following original source catalogs (listed in order of our preference for choosing between multiple listings). The National Center for Earthquake Engineering Research—NCEER91 catalog (Seeber and Armbruster, 1991; J. Armbruster, email communication, 2003) lists about 3,630 events (m_{bLg}2.5 or greater) in the Central and Eastern United States and southeastern Canada from 1627 to 1985 (~2370 in emb.cc). A major strength of NCEER91 is its thorough and consistent treatment of preinstrumental earthquakes. Sanford and others (1995) contribute a list of earthquakes in New Mexico from 1963 to 1993 from a special study (~20 in emb.cc). Stover and Coffman's (1993) catalog of significant United States earthquakes lists about 400 CENA events (magnitude ~4.5 or greater and (or) MMI VI or greater) from 1774 to 1989 (~30 in emb.cc). Stover and others (1984) compiled a series of State-by-State catalogs, listing about 4,280 CENA events (magnitude 2.5 or greater) from 1752 to 1986 (~240 in emb.cc); they include many smaller earthquakes than do Stover and Coffman (1993). The USGS Preliminary Determination of Epicenters (PDE) bulletin lists about 550 CENA earthquakes (magnitude 3.0 or greater) from 1960 to 1972 and about 4,000 (magnitude 2.5 or greater) from 1,973 through 2006 (total ~630 in emb.cc). Finally, the catalog compiled by the Decade of North American Geology project (Engdahl and Rinehart, 1991) lists about 2,300 CENA events (magnitude 3.0 or greater) from 1534 to 1985 (~60 in emb.cc). There are two primary changes from the 2002 version of emb.cc: (1) updates to the NCEER catalog (~220 additions and ~20 deletions) recommended by J. Armbruster (email communication, 2003) and (2) the addition of about 170 post-2001 earthquakes from the USGS PDE.

If more than one magnitude is listed in the original source-catalog record for an earthquake, a preferred magnitude is selected during the reformatting step. Only about 10 percent of the earthquakes in emb.cc do not have a listed m_{bLg} or m_b; in these cases, the preferred magnitude—of whatever type—is assumed to be m_{bLg} for the hazard analysis. The use of a preferred magnitude, rather than the previously used weighted average, also accounts for some minor differences with the 2002 catalog. It should be noted that the choice of m_{bLg} for the catalog necessitates conversions between m_{bLg} and moment magnitude at several stages in the hazard analysis. Foreshocks and aftershocks are deleted using the declustering methodology of Gardner and Knopoff (1974); this simple algorithm requires no tuning parameters (that is, prejudgments about what are or are not aftershocks), and results are easily reproducible. Manmade seismic events are deleted if they are associated with a transient process that is no longer active (for example, earthquakes caused by deep fluid injection at the Rocky Mountain Arsenal near Denver), or if the process is ongoing but we have no reason to expect that future large,

hazardous events will be associated with the activity (for example, earthquakes caused by fluid injection in the Paradox Valley of western Colorado, mining-related events in Colorado and Utah, and events related to oil production at the Dagger Draw field in New Mexico).

The final declustered catalog lists approximately 3,350 CENA earthquakes from 1700 through 2006 with magnitude equal to or greater than 3.0; about 70 percent and 16 percent are contributed by the NCEER and PDE source catalogs, respectively. Previously derived catalog completeness levels and b-values (0.76 for the high-seismicity zone near Charlevoix, Mich., and 0.95 elsewhere in CENA) are maintained in the current model.

Maximum Magnitude

The size of the largest expected earthquake is region dependent, and it should be estimated from tectonic or geologic principles rather than from examination of an earthquake catalog that spans a time period that is a fraction of the recurrence times of the largest modeled events. The maximum-magnitude (M_{max}) zonation carries over from 2002, but for the 2008 hazard analysis we model uncertainty in maximum magnitude using four distributed M_{max} values in a weighted logic tree (fig. 2).

The maximum magnitude is chosen based on the tectonic setting of the region and global analogs (Johnston and others, 1994). Wheeler (1995) and Wheeler and Frankel (2000) define the boundary between the craton and an outboard region of crustal extension (fig. 3) as the landward limit of rifting of Precambrian crust during the opening of the Iapetan (proto-Atlantic) ocean about 500 Ma. Wheeler (1995) argues that different maximum magnitudes are appropriate in the two regions, and we select values based on analogy with other stable continental regions worldwide (Johnston and others, 1996a; Wheeler and Frankel, 2000; Wheeler and Cramer, 2002). The histograms of figure 3B show strong peaks at moment magnitude 6.7. The stable-continental-region dataset includes earthquakes from various continents and tectonic histories. This geologic diversity suggests that M_{max} could exceed 6.7 throughout CENA. The high-magnitude tails of the histograms suggest that M_{max} could be larger. For the 2008 model, we use four values of moment magnitude distributed between M6.6 and 7.2 for characterizing hazard within the craton and four values between M7.1 and 7.7 for the extended margin (fig. 2).

For the extended margin, M7.1 is similar to the magnitudes inferred for the Charleston, S.C., earthquake (Johnston, 1996b; Bakun and Hopper, 2004), and M7.7 is the magnitude calculated for the 2001 Bhuj, India, earthquake (U.S. Geological Survey, *http://earthquake.usgs.gov*). As in the 1996 and 2002 models, we use a maximum magnitude of M7.2 for the Charleston areal zones, to avoid overlap with the mainshock, and M7.0 for the Colorado Plateau and Rocky Mountain zones, consistent with the value used for the seismicity models in the Western United States (fig. 4). Although the Wabash Valley region in southern Indiana and Illinois is part of the craton, M7.5 is used for M_{max} there, based on the distribution of paleoliquefaction features resulting from past large earthquakes (Wheeler and Cramer, 2002). Note that we convert M_{max} from moment magnitude to m_b for the hazard calculation, using the equations of Johnston (1996a) and Atkinson and Boore (1995) with equal weights.)

Smoothed-Gridded Seismicity

The gridded-seismicity source model accounts for the expectation that future large, damaging earthquakes will occur near previous small and moderate-size earthquakes. As in 1996 and 2002, we develop three models based on the completeness levels observed in the CENA catalog. East of about long 105°W., Model 1 counts magnitude 3.0 and larger earthquakes since 1924, Model 2 uses 4.0 and larger events since 1860, and Model 3 uses 5.0 and larger events since 1700. Completeness levels west of long 105°W. are 1976, 1924, and 1860 for Models 1–3, respectively. Seismicity rates for Models 1–3 are determined by counting earthquakes in each grid cell with dimensions 0.1° longitude by 0.1° latitude and adjusting for completeness, giving a maximum-likelihood estimate of the local rate (Frankel, 1995). Note that in the simplest application of the method, a magnitude-5 earthquake counts the same as a magnitude-3 earthquake in determining the rate. Hence, in contrast to the single model with variable completeness used for the Western United States, we apply three separate models to better represent the hazard in areas like the Nemaha Ridge of eastern Nebraska and Kansas, where moderate-size to large earthquakes have occurred but smaller events are underrepresented in the catalog.

There are two regions where the spatial patterns of small historical earthquakes might not represent the future hazard. These are Eastern Tennessee and New Madrid seismic zones (fig. 4). For these regions, we implement uniform source zones, with average seismicity rates determined from magnitude 3.0 or greater earthquakes since 1976 in each zone. These source zones replace the gridded seismicity and are added before smoothing (see below).

A two-dimensional spatial Gaussian function is used to smooth the gridded rates. We use correlation distances of 50 kilometers for Model 1 and 75 kilometers for Models 2 and 3; choices of smoothing parameters are based on judgments about earthquake location uncertainties and spatial trends observed in historical seismicity (Frankel and others, 1996). The resulting "agrid" gives the annual rate of earthquakes with magnitude between –0.05 and +0.05 in each grid cell (incremental 10^a in the Gutenberg-Richter notation, for a magnitude bin centered on m=0 with width=0.1 magnitude unit).

For the 2008 model, the seismicity rates are adjusted to account for magnitude uncertainty using results published by Tinti and Mulargia (1985) and Felzer (2007). As a rough first step to account for this effect, we assume standard errors of about 0.1 magnitude unit for earthquakes in 1972–2006, 0.2 for 1932–1971, and 0.3 for 1700–1931 (following guidelines

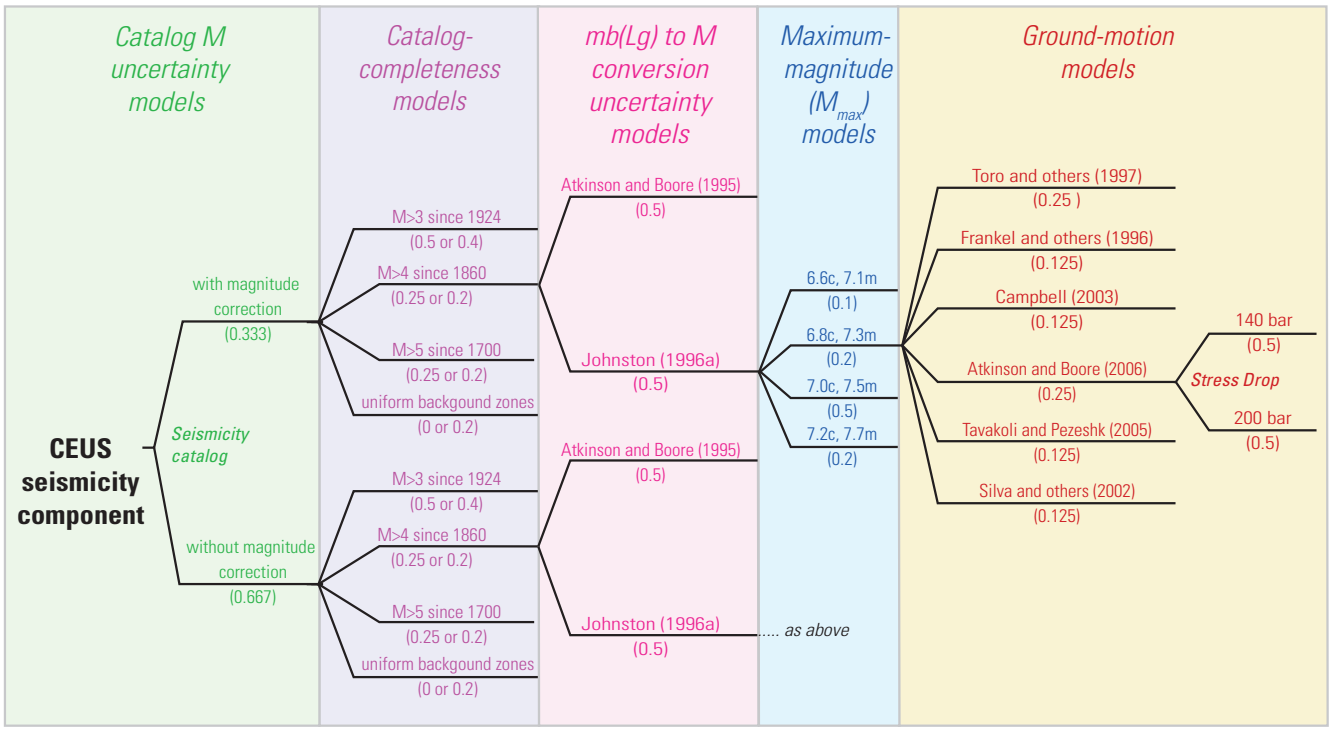

Figure 2. Logic tree for seismicity-derived hazard component in the Central and Eastern United States (CEUS). Each maximum-magnitude branch includes craton (c) and margin (m) estimates. Parameters in this figure include some aleatory variability as well as depicted epistemic uncertainty. We treat aleatory variability in ground motion in the hazard code.

suggested by Felzer for earthquakes in California), and apply the Tinti and Mulargia (1985) correction, which reduces modeled rates about 5 to 10 percent depending on the region and era. These uncertainty assumptions are untested for CENA. Furthermore, rate reductions can be severe near some of the old, large earthquakes that we have made a special effort to represent in the hazard model (see the above discussion about the Nemaha Ridge). For these reasons, gridded-seismicity models with and without magnitude-uncertainty corrections are combined with respective weights of 1/3 and 2/3. We feel it is important to model magnitude uncertainty in a preliminary way, but we do not implement it fully in CENA pending more analysis and research. We make no attempt to account for possible magnitude rounding effects (see WUS below), lacking CENA data.

We recognize that, in an effort to include as many earthquakes in the model as possible in the low-seismicity CEUS, we may have been somewhat optimistic in our choices of catalog completeness levels. To account for this, seismicity rates in each grid cell are multiplied by factors (ranging from about 1.0 to 2.1, depending on the model and subregion) that account for regional differences between modern completeness levels, determined from the catalog since 1976, and the assumed levels (see Mueller and others, 1997).

Uniform Background Zones

To supplement the gridded-seismicity sources, we also implement (as in the 1996 and 2002 models) four nonoverlapping regional uniform background source zones (Model 4); these zones are designed to provide a hazard floor to account for future random earthquakes in areas with little or no historical seismicity. The four zones cover regions that are geologically and seismologically distinct: the Colorado Plateau region, Rocky Mountains, craton, and extended margin (see fig. 4 and the previous discussion on maximum-magnitude zonation). For example, the largest historical earthquakes in CENA have occurred in the extended margin, and the average historical seismicity rate there is greater than twice the craton rate. An average seismicity rate for each regional zone is determined from the catalog since 1976.

As in 1996 and 2002, Model 4 is implemented in a way that does not penalize areas of high seismicity in order to provide a hazard floor in areas of low seismicity. In each grid cell, the historical seismicity rate is computed by combining Models 1–3 with respective weights of 0.5, 0.25, and 0.25. If this historical rate exceeds the floor value (Model 4), the final cell rate simply equals the historical rate. If, however, the floor value exceeds the historical rate, Models 1–4 are combined with respective weights 0.4, 0.2, 0.2, and 0.2 to give the final cell rate. Nowhere is the final cell rate less than the historical

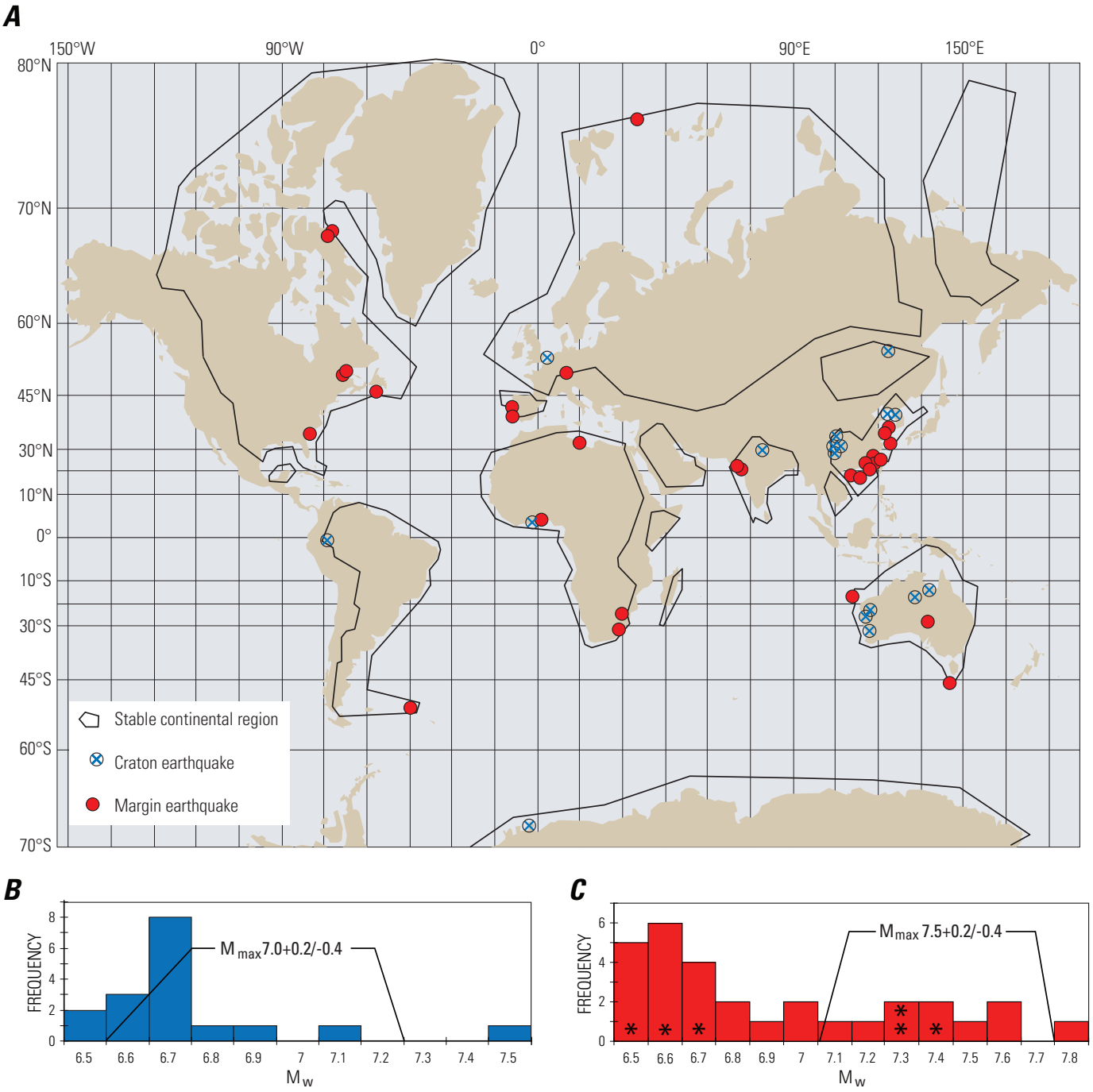

Figure 3. (*A*) Location of craton and margin worldwide earthquakes used to evaluate M_{max} for the area outlined in figure 3 (Wheeler and Johnston, 2007) and histograms showing magnitudes for (*B*) craton (n=17) and (*C*) margin (n=30) earthquakes. Asterisk indicates earthquake located in North America. The New Madrid earthquakes of 1811–1812 are not shown or used because the New Madrid seismic zone is treated as a special case (see section "New Madrid Seismic Zone").

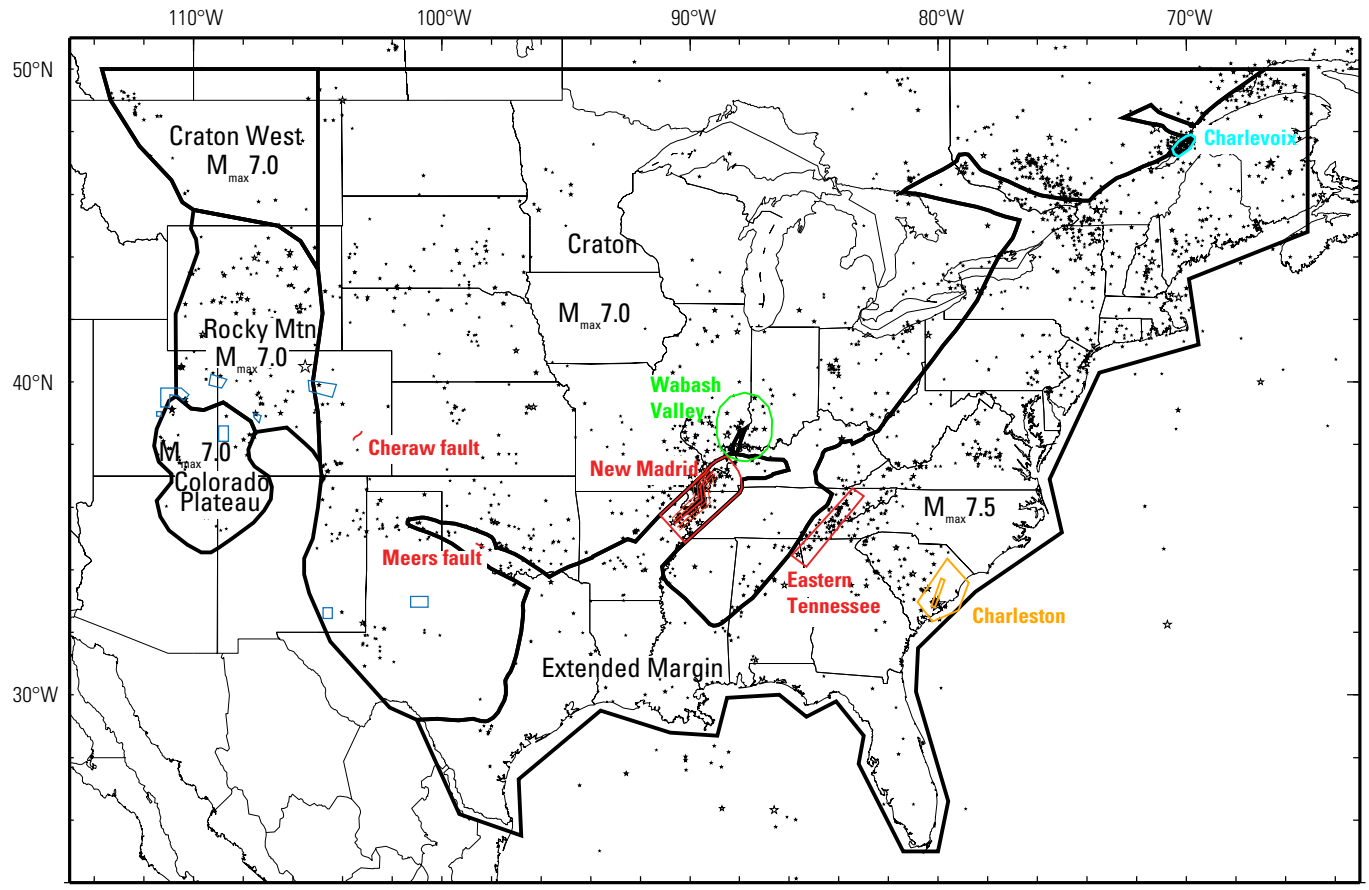

Figure 4. Map of special zones, faults, and regional M_{max} zones (shown by colors) in the Central and Eastern United States (see text for details). Blue polygons west of long 100°W. denote areas where nontectonic seismic events are removed from the catalog.

rate, and the total modeled seismicity rate exceeds the total historical rate by about 10 percent (Frankel and others, 1996). A special weighting scheme implemented in 2002 for the Colorado Front Range region (Frankel and others, 2002) also carries over to 2008: the floor rate is given full weight in grid cells in the Rocky Mountain zone where the floor rate exceeds the historical rate.

Special Zones

As previously described in the gridded seismicity and maximum magnitude sections, five special zones are used to account for variations in catalog completeness, uniform seismicity, maximum magnitude, and b-value. We implement uniform source zones for the Eastern Tennessee and New Madrid seismic zones, with average seismicity rates determined from earthquakes in each zone with magnitude 3.0 or greater since 1976. These zones are smoothed on the edges. The Wabash Valley zone incorporates an M_{max} of 7.5. The Charlevoix zone incorporates a b-value of 0.76. The region west of long 105°W. includes different completeness parameters than elsewhere in the CEUS. All of these special zones carry over from the 2002 model and are shown in figure 4.

Source Model—Faults

Figure 4 shows the locations of the four finite fault sources included in the CEUS source model (New Madrid, Mo., and adjacent States; Charleston, S.C.; Meers, Okla.; and Cheraw, Colo.).

New Madrid Seismic Zone

Rupture Sources

Three large earthquakes in 1811–1812 are thought to have ruptured the Reelfoot fault and locations to the north and south (fig. 5). The locations of these three large events are controversial because the only evidence of surface rupture for these events is along the Reelfoot fault. Thus, earthquake locations are generally constrained only by recorded

intensities, paleoseismic data, and historical seismicity patterns.

In 1996 and 2002, we included three "hypothetical" faults to account for uncertainty in future earthquake ruptures on the New Madrid fault zone. These rupture sources were developed by geological interpretation of the Reelfoot fault, mapped geologic structures, and seismicity characteristics. Fault traces in 2008 are similar to the 2002 model except we have revised the dip of the central segment and have used five rather than three subparallel traces to account for the spatial variability in future earthquakes (fig. 5). The five traces fill the same space as occupied by the previous three traces. Formerly, all three arms were modeled as vertical faults, but for 2008 we have changed the central (Reelfoot) arm from a vertical fault to a fault dipping 38° to the southwest. This modification was made to reflect the seismicity patterns as seen in cross sections perpendicular to the fault (Mueller and Pujol, 2001). The central trace, which most closely follows the seismicity, is weighted significantly higher than the other traces. The central trace is weighted 0.7, the traces just outside of the central trace are weighted 0.1 each, and the outer traces are weighted 0.05 each (fig. 6).

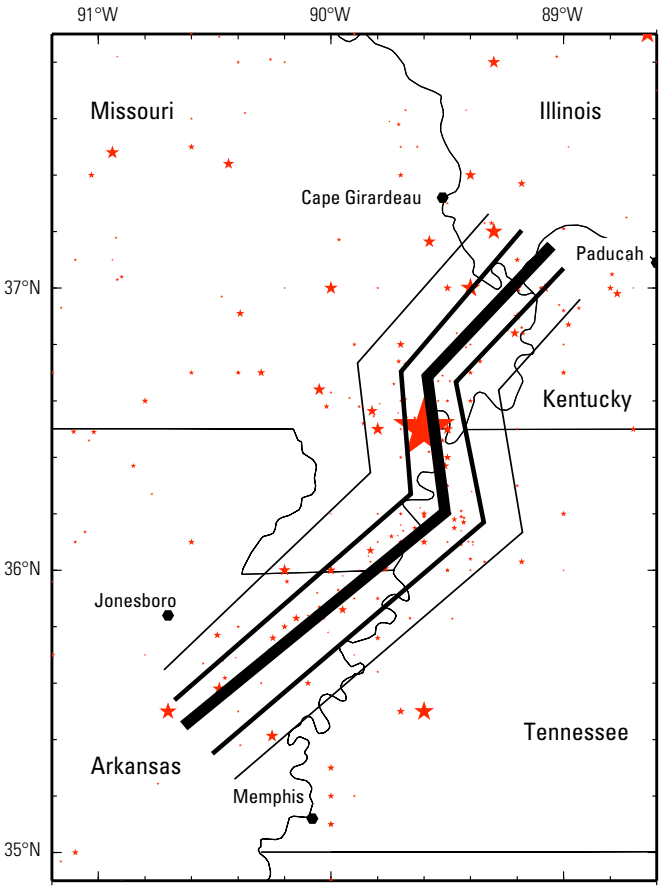

Figure 5. Historical seismicity (M≥3) and locations of the modeled New Madrid hypothetical faults. Relative weights assigned to the hypothetical faults shown by line width. Size of red stars indicates relative size of earthquake.

Magnitudes

Magnitudes of the 1811–1812 events have been controversial, with suggestions generally ranging from M7.0 up to M8.1 (table 2). Of the three largest New Madrid earthquakes, the one in January 1812 is the most likely to have ruptured the northern arm of the seismic zone. Three widely accepted magnitude estimates for the New Madrid sequence suggest that the January 1812 earthquake was about 0.2 magnitude units smaller than the December shock (table 2; Johnston, 1996b; Hough and others, 2000; Bakun and Hopper, 2004).

In the 2002 model, we applied a distribution of magnitudes for earthquakes on the New Madrid fault. The three arms that compose each hypothetical trace ruptured together with the following magnitudes and weights: M7.3 (0.15), M7.5 (0.2), M7.7 (0.5), and M8.0 (0.15). In the 2008 model, we assign magnitudes for the northern section that are 0.2 unit lower than those assigned to the central and southern sections. For the northern arm model, we applied the following weights: M7.1 (0.15), M7.3 (0.2), M7.5 (0.5), and M7.8 (0.15). The central and southern segments remain the same as in the 2002 model. The logic-tree branches for magnitude uncertainty are shown in figure 6.

Table 2. Magnitudes and rupture locations for New Madrid 1811–1812 earthquakes.

Event	Rupture segment	Hough and others (2000) Hough and Martin (2002)	Bakun and Hopper (2004)	Johnston (1996b)
December 16, 1811	southern	M7.2–7.3	M7.6	M8.1
December 16, 1811 (aftershock)	southern	M7.0		
January 23, 1812	northern	M7.0	M7.5	M7.8
February 7, 1812	central (Reelfoot)	M7.4–7.5	M7.8	M8.0

Earthquake Recurrence

Estimated recurrence intervals of large New Madrid earthquakes have been refined with additional paleoseismic data. In 1996, sparse data loosely constrained recurrence intervals; Frankel and others (1996) estimated an average value of 1,000 years. By 2002, paleoliquefaction and historical-earthquake data provided evidence for a 500-year recurrence (Cramer, 2001; Frankel and others, 2002; Tuttle and others, 2002). At least one large earthquake at about A.D. 300 and three sequences of large earthquakes at about A.D. 900, A.D. 1450, and A.D. 1811–1812 were recognized from crosscutting relationships and radiometric dating of liquefaction features (Tuttle and others, 2002; Tuttle and others, 2005). The occurrence of three sequences between A.D. 300 and A.D. 1811–1812 (about 1,500 years) implies an average recurrence of about

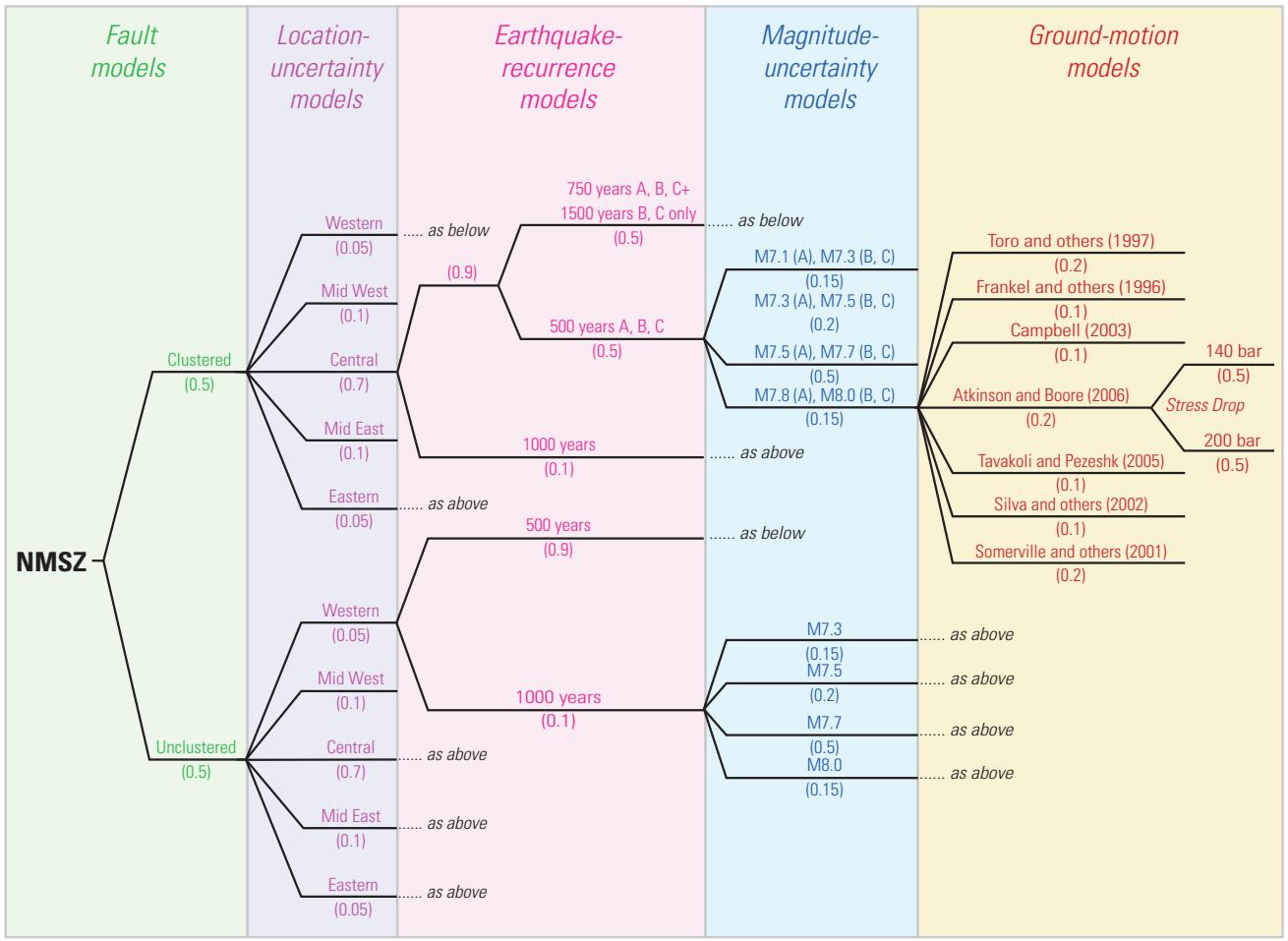

Figure 6. Logic tree for the New Madrid seismic zone (NMSZ). Parameters in this figure include some aleatory variability as well as depicted epistemic uncertainty. A, B, and C refer to the northern, central, and southern segments shown in figure 5. Location and magnitude branches may include aleatory variability and epistemic uncertainty; we have not treated these separately. We treat aleatory variability in ground motion in the hazard code.

500 years. However, it is unclear whether or not the northern arm ruptured in the A.D. 1450 sequence. If it did not, then this arm has experienced only two events in the past 1,500 years, suggesting an average recurrence of about 750 years. We have weighted the 500-year and 750-year earthquake recurrence alternatives for the northern arm equally (fig. 6).

In addition to these alternative recurrence models, some recent research suggests that the New Madrid seismic zone may rupture on average every 1,000 years as suggested by abrupt changes in meander patterns of the Mississippi River that were used to estimate earthquake activity on the Reelfoot fault (Holbrook and others, 2006). They infer that large, reverse-faulting ruptures are episodic. Within relatively active periods, average recurrence intervals are several centuries long, but during the less common quiescent periods, average recurrence intervals are interpreted to be about 1,000 years. Accordingly, we added a 1,000-year branch to the recurrence model. At present the meander-pattern methodology cannot detect small reverse-slip ruptures of the Reelfoot fault or large strike-slip ruptures of other faults in the seismic zone, so we assigned the 1,000-year branch a weight of 0.1.

For the 2008 update, we consider temporal clustering in modeling large New Madrid earthquakes (Appendix F; Appendix E in Toro and Silva, 2001). As mentioned previously, Tuttle and others (2002) provide evidence that large prehistoric earthquakes in the New Madrid seismic zone typically occur in sequences of three events, similar to those observed in 1811–1812. In the 2002 maps, we modeled large New Madrid earthquakes with a 500-year recurrence and as single events that ruptured across all three arms of the fault source. Modeling three independent events every 500 years would result in much higher hazard but would not be a reasonable approach

since the events are thought to be temporally dependent on each other and are on separate arms of the New Madrid source zone. Toro and Silva (2001) suggested that these sequences should instead be treated as a temporally dependent cluster of earthquakes. For hazard calculations, this means that the probability of exceeding a ground-motion level at a site will be higher when considering three dependent events rather than one independent event. Appendix F shows the details of the cluster model and some examples illustrating the impact of the model on hazard. Figure 6 presents the four clustering scenarios that we consider along with their weights. We assign equal weight to the clustered models and to a 2002-type unclustered source model.

Charleston, South Carolina, Seismic Zone

The Charleston region (fig. 7) was affected by an earthquake of about M7.3 in 1886. Two areal source zones were used in the 2002 hazard maps to account for uncertainty in the location of the source of future earthquakes. One was a geographically narrow zone that follows the Woodstock lineament and an area of river anomalies; a broader zone encompassed many of the known liquefaction features resulting from past earthquakes (Frankel and others, 2002; Wheeler and Perkins, 2000). At the urging of the NSHMP Advisory Panel, we extended the southeastern edge of the larger zone offshore to enclose the Helena Banks fault zone of Behrendt and others (1981) and Behrendt and Yuan (1987). Marine seismic-reflection profiles across strands of the Helena Banks fault zone show Miocene strata that are warped in a reverse-faulting sense. For the 2008 maps, the two zones were weighted equally (fig. 8). For each zone, we combined a characteristic model with magnitudes of 6.8 (wt 0.2), 7.1 (wt 0.2), 7.3 (wt 0.45), 7.5 (wt 0.15) and a recurrence time of 550 years. Additionally, a truncated Gutenberg-Richter model with m_{bLg} from 5.0 to 7.5 accounts for background events in the extended margin, including the Charleston zone. The background seismicity has random fault strike.

Meers Fault, Oklahoma, and Cheraw Fault, Colorado

The Meers fault in southwestern Oklahoma and the Cheraw fault in eastern Colorado (fig. 4) represent the only faults within the stable craton with adequately defined surface-faulting history constrained by radiometric dating. However, like the New Madrid seismic zone, these faults also may alternate between periods of relative quiescence and more active phases resulting in more frequent surface-rupturing earthquakes. This fault model allows for earthquake magnitude aleatory variability (2 sigma=0.24) and epistemic uncertainty (delta M=±0.2) with 0.2, 0.6, 0.2 weighting for the low, mean, and high values.

Two surface-faulting events have occurred on the Meers fault in the past 3,000 years (Kelson and Swan, 1990). Middle Pleistocene deposits have only been deformed by the late Holocene events; thus, surface deformation that preceded these two Holocene events occurred more than 100 k.y. earlier and possibly many hundreds of thousands of years earlier. As in the 2002 maps, the Meers fault is modeled using a characteristic moment magnitude of 7.0 and a recurrence time of 4,500 years.

The Cheraw fault in eastern Colorado (fig. 4) shows evidence of Holocene and earlier faulting based on a study by Crone and others (1997). They infer that surface-rupturing events on the fault occurred at about 8 ka, 12 ka, and 20–25 ka, which may represent an active earthquake phase. In contrast, events older than about 25 ka must have occurred prior to 100 ka, thus representing a quiescent period of some 75 k.y. or more. All parameters for the Cheraw fault are retained from 2002; the fault was modeled using a slip rate of 0.15 mm/yr based on data from the last two events and a maximum magnitude of 7.0±0.2 determined from the Wells and Coppersmith (1994) fault length for all slip types together relation. We use a fixed recurrence time of 17,400 years with a truncated Gutenberg-Richter model from M6.5 to 7.0. This yields a mean recurrence time of 5,000 years for earthquakes with minimum magnitude of 6.5.

Ground-Motion Relations

The 2008 hazard maps include several new attenuation relations based on simulated ground motions that were not available in 2002 (figs. 9 and 10). In 1996 and 2002, we used equations based on a single corner-frequency (source spectrum has a single corner similar to a Brune point source model), double corner-frequency (source spectrum has two corners to account for a finite fault), hybrid (source spectrum from empirical sources in WUS are modified to fit CEUS parameters), and finite-source models (full waveform simulations considering a finite source and propagation effects). The attenuation relations that we retain from the earlier model include the Frankel and others (1996) single-corner model, Somerville and others (2001) extended-source model, and the Campbell (2003) hybrid model. New models that have been implemented are Toro and others (1997), a single-corner extended source model; Atkinson and Boore (2006), a dynamic-corner frequency source model; Tavakoli and Pezeshk (2005), a hybrid model; and Silva and others (2002), a constant stress drop with magnitude saturation model. We use the weighting scheme for the attenuation models as shown in table 3 and figure 6. The weights are based on the following categories: single-corner finite fault model (accounts for magnitude saturation; 0.3), single-corner point-source model (accounts for Moho bounce and 1/r geometric spreading; 0.1), dynamic-corner-frequency models (account for magnitude saturation and variable stress drop; 0.2), full-waveform simulations (account for finite rupture of large earthquakes in CEUS crust; 0.2), and hybrid model (translates WUS empirical strong motion data for assumed CEUS parameters; 0.2).

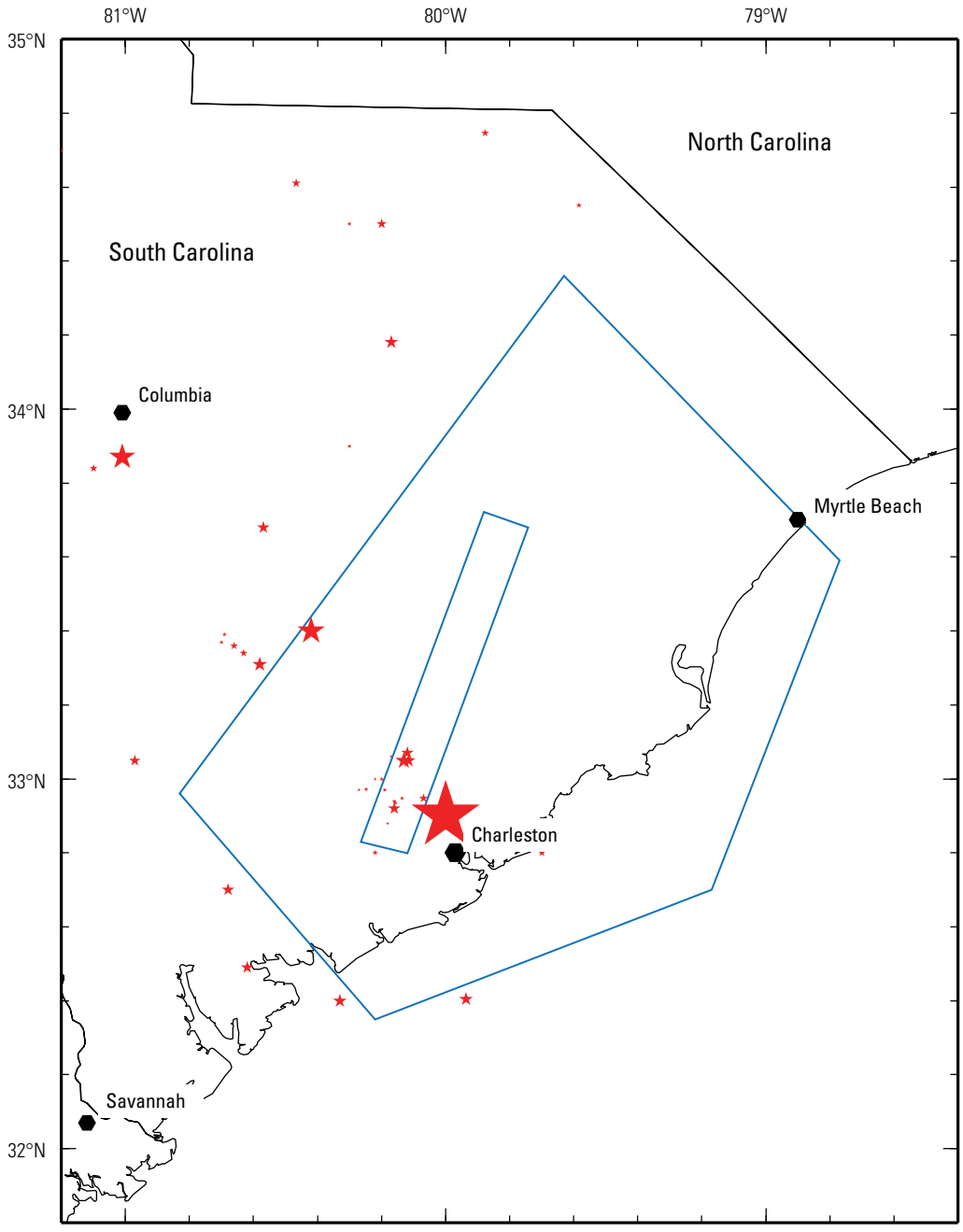

Figure 7. Historical seismicity (M≥3) and alternative source zones near Charleston, South Carolina. Size of red stars indicates relative size of earthquake.

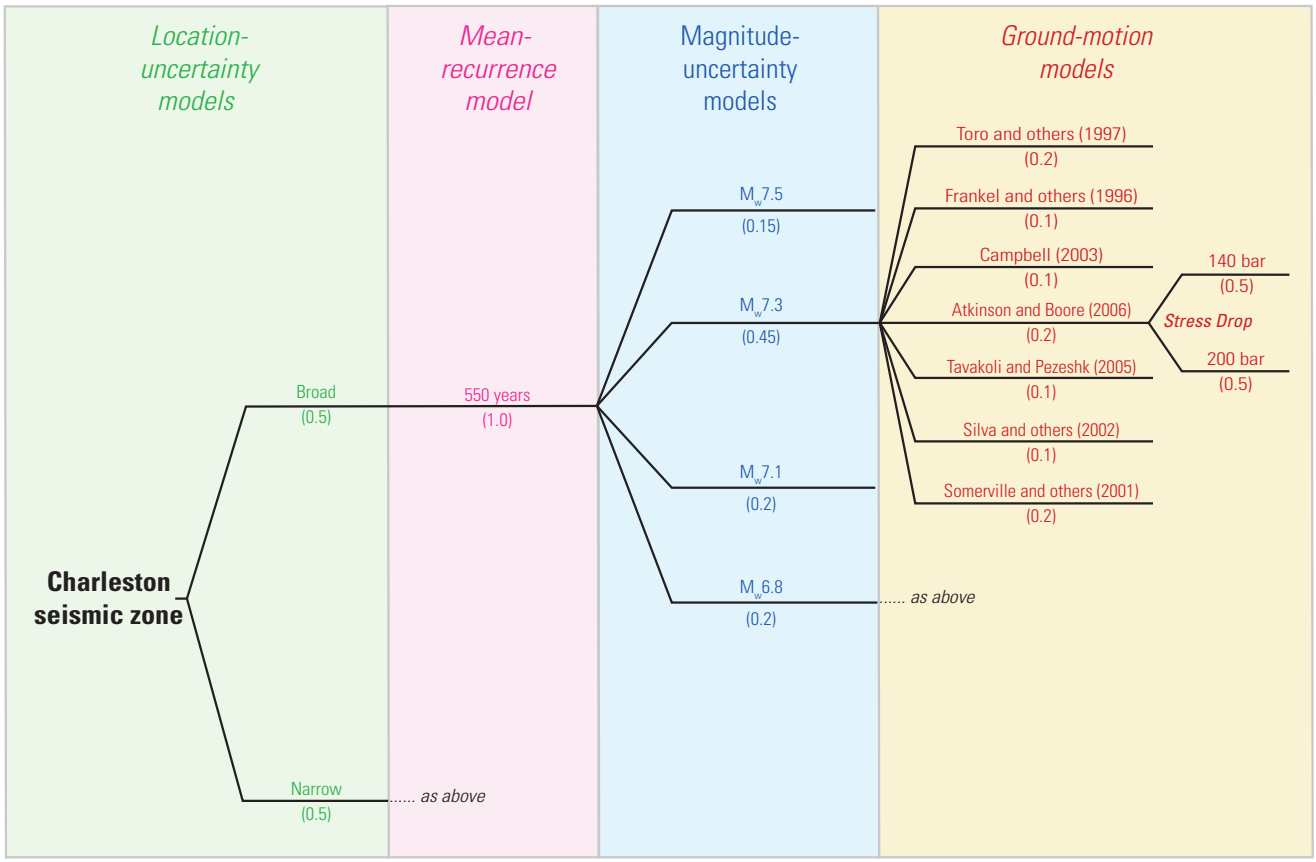

Figure 8. Logic tree for the Charleston seismic zone. Parameters in this figure include some aleatory variability as well as depicted epistemic uncertainty. Additional aleatory variability may be associated with location and magnitude models. We treat aleatory variability in ground motion in the hazard code.

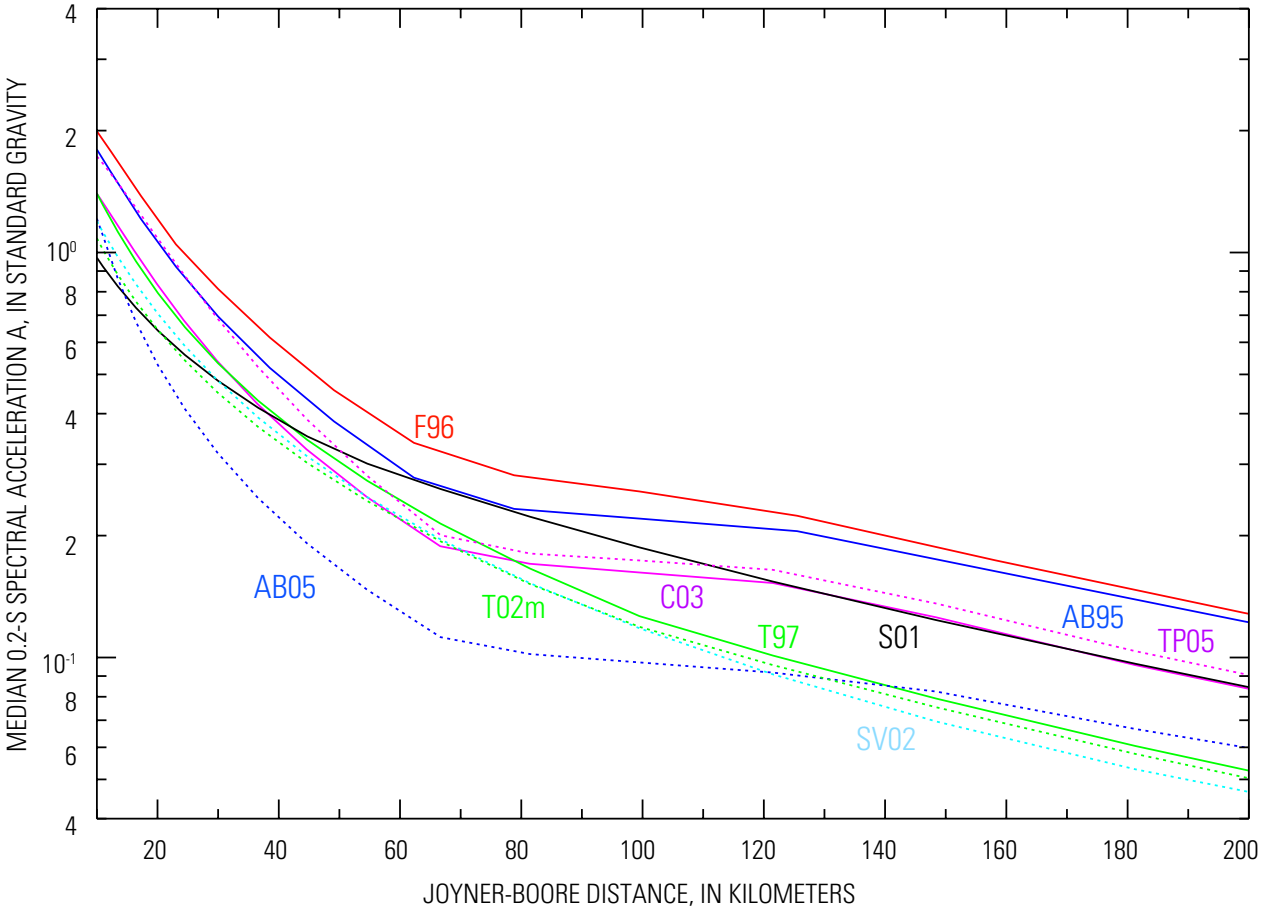

Figure 9. Central and Eastern United States 0.2-s spectral acceleration attenuation relations for M7 earthquake on a vertical strike-slip fault and Vs30 760-m/s site conditions: AB95 (Atkinson and Boore, 1995), AB05 (Atkinson and Boore, 2006), F96 (Frankel and others, 1996), T97 (Toro and others, 1997), T02m (Toro, 2002), C03 (Campbell, 2003), S01 (Somerville, 2001), SV02 (Silva and others, 2002), and TP05 (Tavakoli and Pezeshk, 2005). Figure provided by Chris H. Cramer.

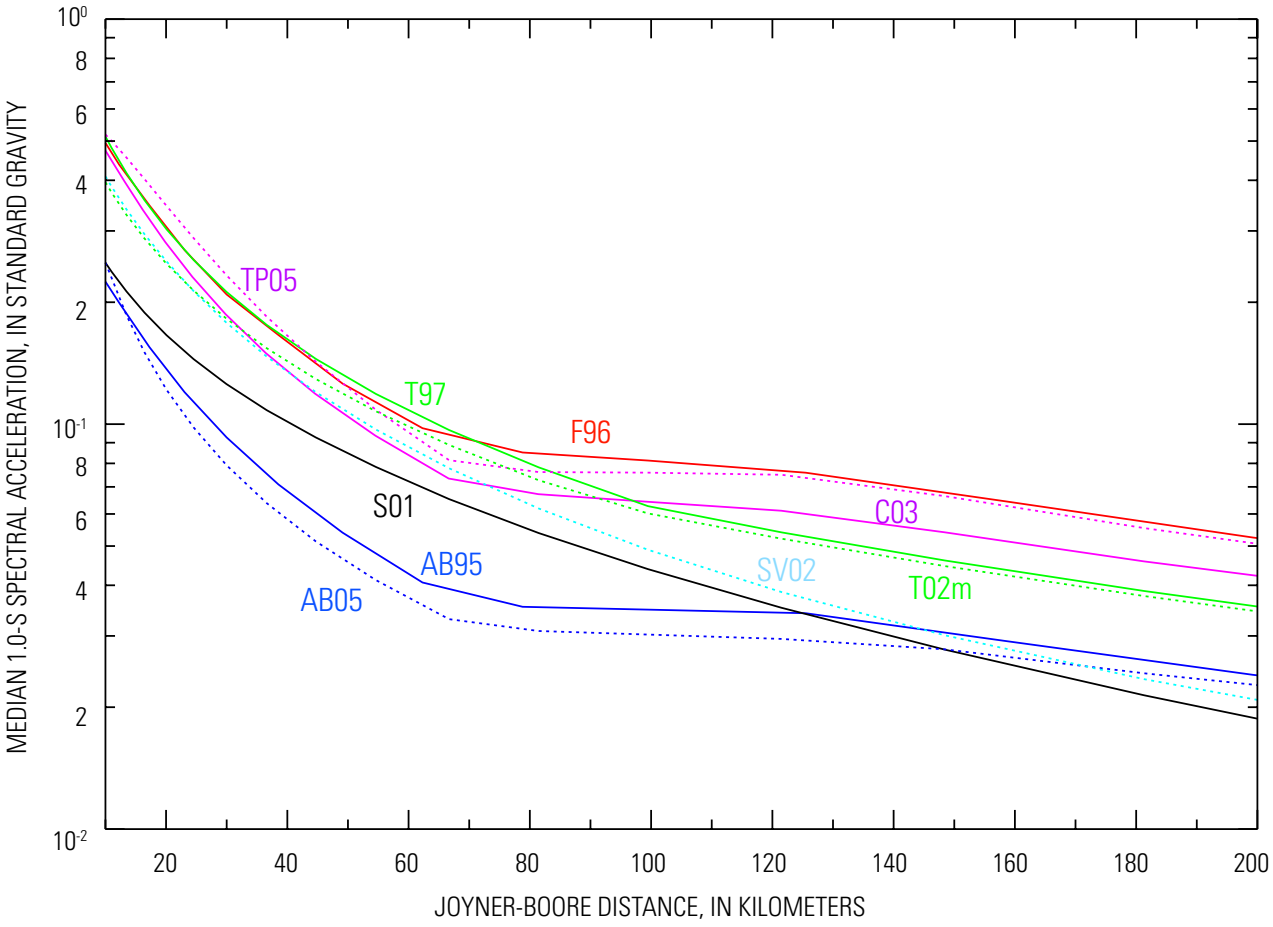

Figure 10. Central and Eastern United States 1-s spectral acceleration (SA) attenuation relations for M7 earthquake on a vertical strike-slip fault and Vs30 760-m/s site conditions: AB95 (Atkinson and Boore, 1995), AB05 (Atkinson and Boore, 2006), F96 (Frankel and others, 1996), T97 (Toro and others, 1997), T02m (Toro, 2002), C03 (Campbell, 2003), S01 (Somerville, 2001), SV02 (Silva and others, 2002), and TP05 (Tavakoli and Pezeshk, 2005). Figure provided by Chris H. Cramer.

Table 3. Weights for CEUS attenuation relations.

Single corner—finite fault	Weight
Toro and others (1997)	0.2
Silva and others (2002)—constant stress drop w/ saturation	0.1
Single corner—point source with Moho bounce	
Frankel and others (1996)	0.1
Dynamic corner frequency	
Atkinson and Boore (2006) 140 bar stress drop	0.1
Atkinson and Boore (2006) 200 bar stress drop	0.1
Full waveform simulation	
Somerville and others (2001) for large earthquakes	0.2
Hybrid empirical model	
Campbell (2003)	0.1
Tavakoli and Pezeshk (2005)	0.1

The National Seismic Hazard Maps use a reference site condition that is specified to be the boundary between NEHRP site classes B and C, with an average shear-wave velocity in the upper 30 m of the crust of 760 m/s. However, some attenuation relations are not developed for this shear-wave velocity. Therefore, we have typically converted hard-rock attenuation relations to approximate ground motions for a site with shear velocity on the NEHRP B-C boundary. Kappa is a key parameter in this conversion that defines the high-frequency near-surface site attenuation of the ground motion. For this and past versions of the maps, we applied a kappa of 0.01 for the CEUS to convert from hard rock to firm rock site conditions (see Frankel and others, 1996). The new Atkinson and Boore (2006) attenuation relations apply a kappa of 0.02 for a class BC site condition, which brings additional epistemic uncertainty into the 2008 maps. We use their attenuation relations for B/C sites directly in the hazard calculation. For several of these models, we used frequency-dependent factors to convert from hard rock (NEHRP site class A) to firm rock (NEHRP site class BC). These factors are: 1.52 for peak ground acceleration, 1.74 for 0.1-s, 1.76 for 0.2-s, 1.72 for 0.3-s, 1.58 for 0.5-s, 1.34 for 1.0-s, and 1.20 for 2.0-s spectral acceleration (see Frankel and others, 1996).

Another parameter that is important in ground-motion simulations for CEUS attenuation relations is stress drop. We have applied two alternative stress drops of 140 bars and 200 bars for the Atkinson and Boore (2006) model to account for epistemic uncertainty in that parameter. The effect of the stress drop alternatives is seen in figure 11.

To apply the background seismicity models, we assume a 5-kilometer source depth. For calculating ground motions, we convert m_b-values to moment magnitude using the Johnston (1994, 1996a) factors. We cap or truncate calculated ground-motion values to avoid unacceptably large ground motions. Capping and truncation do not significantly affect the results at probability levels of 2 percent in 50 years and greater. Median ground motions are capped at 1.5 g for peak ground acceleration and at 3.0 g for the 0.2-s spectral acceleration. In addition, we truncate the distribution of ground motions at three standard deviations above the median for peak ground acceleration and spectral accelerations. The ground-motion distribution for peak ground acceleration is truncated at 3 g and for 0.2-s spectral acceleration at 6 g, when these values are less than the 3-sigma cutoff.

Western United States

Source Model—Seismicity Derived Hazard Component

The background seismicity model, which accounts for random moderate-size earthquakes, is based on historical seismicity patterns (gridded), uniform broad regional zones (regional zones), and local seismicity variations (special zones). This background seismicity model requires a declustered earthquake catalog (consisting of independent events) for calculation of Poissonian earthquake rates.

Catalog

The earthquake catalog for western North America (WNA) has been updated through 2006. As in the 1996 and 2002 updates, we combine earthquakes from several (reformatted) source catalogs, choose one preferred record for each event that is listed more than once, and decluster to remove aftershocks and foreshocks (Mueller and others, 1997). Our goal is to make a WNA catalog that is dominated by well-researched source catalogs like the CGS/WGCEP catalog in California and the UNR/Pancha catalog in the Intermountain West. The final declustered catalog used in the hazard analysis (hereinafter called wmm.cc) lists approximately 3,260 earthquakes from 1850 through 2006 with magnitude equal to or greater than 4.0. Moment magnitude (M_w) has been determined for many moderate-size to large earthquakes in the WUS, and M_w is used in all the WUS ground-motion relations, so the WNA catalog is based on M_w.

We use earthquakes from the following original source catalogs (listed in order of our preference for choosing between multiple listings). Pancha and others (2006) at the University of Nevada, Reno developed a catalog (designed for studies of crustal deformation) that lists about 800 WNA events (M_w equal to or greater than about 4.8) from 1855 to 1999 (~200 in wmm.cc). The UNR/Pancha catalog provides new moment-magnitude estimates for many older earthquakes. The catalog originally developed and maintained by the California Geological Survey (CGS) has been updated and extended through 2006 (Felzer and Cao, 2007). The CGS/WGCEP catalog lists about 5,390 events (M_w or m_L 4.0 or greater) from 1769 through 2006 (~2070 in wmm.cc), and dominates the hazard from the seismicity models in California. Geological Survey of Canada provided a catalog of deep

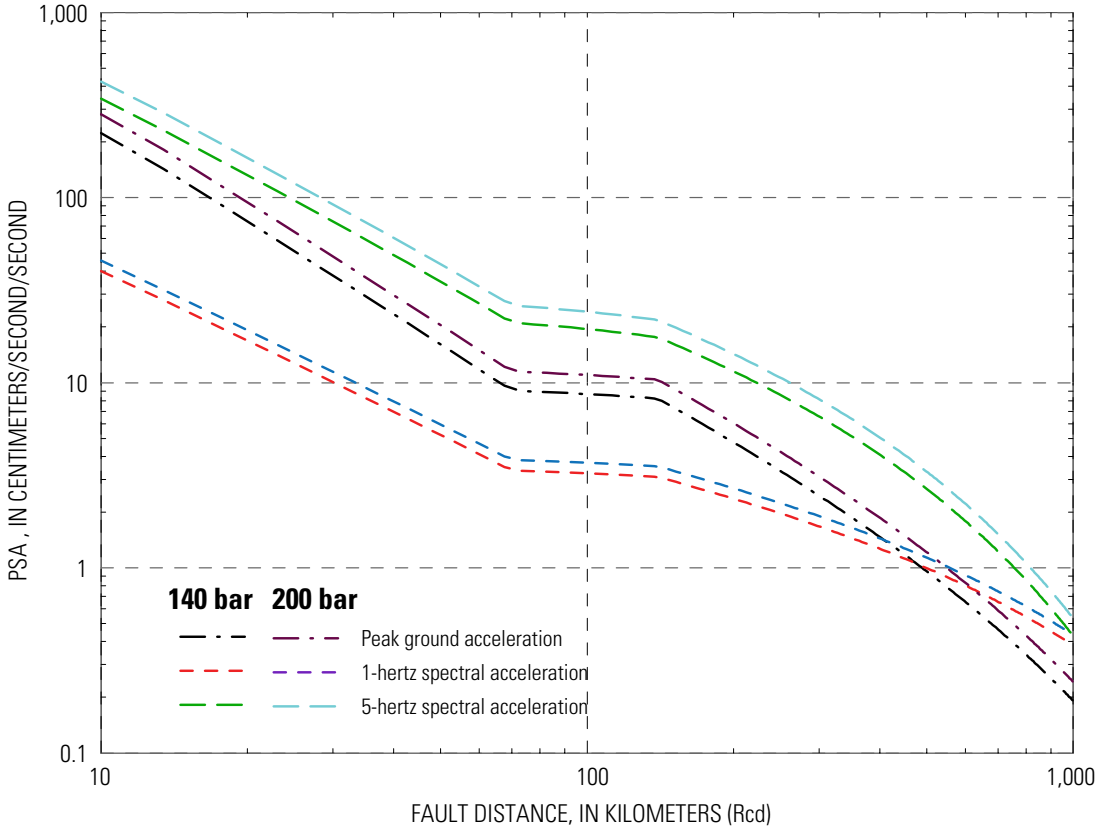

Figure 11. Comparison of Atkinson and Boore (2006) attenuation relations for peak ground acceleration and 1-hertz and 5-hertz spectral acceleration with 140-bar and 200-bar stress drop.

earthquakes beneath the Georgia Strait–Puget Sound region (magnitude 4.0 or greater) from 1909 to 1989 (15 in wmm.cc). Engdahl and Villaseñor (2002) compiled a global catalog that contributes 18 earthquakes (magnitude ~5.5 or greater, 1900–1999) to wmm.cc. Stover and Coffman's (1993) catalog of significant United States earthquakes lists about 2,050 WNA events (magnitude ~4.5 or greater and (or) MMI VI or greater) from 1769 to 1989 (~110 in wmm.cc). Stover and others (1984) compiled a series of State-by-State catalogs (excluding California, Oregon, and Washington), listing about 4,790 WNA events (magnitude 3.0 or greater) from 1857 to 1986 (~150 in wmm.cc); they include many smaller earthquakes than do Stover and Coffman (1993). The USGS Preliminary Determination of Epicenters (PDE) bulletin lists about 17,700 WNA events (magnitude ~3.2 or greater) from 1960 through 2006 (~550 in wmm.cc). Finally, the catalog compiled by the Decade of North American Geology project (Engdahl and Rinehart, 1991) lists ~6,220 WNA events (magnitude 4.0 or greater) from 1808 to 1985 (~150 in wmm.cc). Primary changes from the 2002 version of emb.cc are due to: (1) updates to the CGS/WGCEP catalog, (2) a decision to extend the predominance of the CGS/WGCEP catalog well beyond the California border (a region much larger than was used in 1996 and 2002), and (3) the addition of the UNR/Pancha catalog.

If more than one magnitude is listed in the original source catalog record for an earthquake, a preferred magnitude is selected during the reformatting step. M_w, m_b, M_s, or m_L is the preferred magnitude type for about 95 percent of the earthquakes in wmm.cc. These are all assumed to be M_w as listed for the hazard analysis, except in about 20 cases where magnitude is adjusted to M_w using published relations to account for saturation or other scaling effects. We use Sipkin (2003) for m_b and bilinear or trilinear approximations to the curves plotted by Utsu (2002) for M_s and m_L. All other magnitude types (the other 5 percent including ~80 cases of "unknown" type—most from the DNAG catalog) are also assumed to be M_w as listed for the hazard analysis. Foreshocks and aftershocks are deleted using the declustering methodology of Gardner and Knopoff (1974); this simple algorithm requires no tuning parameters (that is, prejudgments about what are or are not aftershocks), and results are easily reproducible. Manmade seismic events are deleted from the catalog if they are associated with a transient process that is no longer active (for example, nuclear explosions at the Nevada Test Site), or if the process is ongoing but we have no reason

to expect that future large, hazardous events will be associated with the activity (for example, mining-related events in Utah).

The final declustered catalog lists approximately 3,260 earthquakes from 1850 through 2006 with moment magnitude equal to or greater than 4.0; about 64 percent, 6 percent, and 17 percent are contributed by the CGS/WGCEP, UNR/Pancha, and PDE source catalogs, respectively. Previously derived catalog completeness levels and b-values are maintained in the current WUS seismicity model.

Deep earthquakes have caused considerable damage in the Puget Sound region (major events in 1949, 1965, and 2001), and these earthquakes have different ground-motion properties than shallow earthquakes. Earthquakes deeper than 35 kilometers occur beneath the Pacific Northwest and northern California. We maintain the two hazard models for deep seismicity from 2002 (Frankel and others, 2002). (1) For the Puget Sound region we apply completeness levels of M4.0 or greater since 1963 and M5.0 or greater since 1940, and a b-value of 0.40. (2) For northern California we use completeness levels of M4.0 or greater since 1963, and M5.0 or greater since 1930, and M6.0 or greater since 1950, and a b-value of 0.8. Based on recent seismicity near Portland, we add a new zone in northeastern Oregon for deep earthquakes using a b-value of 0.8 (described below in section "Special Zones").

Maximum Magnitude

We maintain the maximum-magnitude (M_{max}) models for the WUS seismicity hazard calculations from 2002 but have updated the input files where needed. For shallow seismicity we use M_{max} 7.0 in most regions. Exceptions include areas near modeled faults (see below), and the Central Nevada seismic zone and Puget Lowland regions where M_{max} is increased as a proxy to account for deficits between geodetic and seismic deformation rates (see section "Special Zones"). We use M_{max} 7.2 for deep seismicity (the commonly reported moment magnitude for the 1949 Puget Sound earthquake is 7.1).

In developing the 2002 hazard maps, we recognized that our methodology for combining hazard from gridded seismicity and faults potentially double-counts earthquakes in the magnitude range 6.5 to 7.0 where the models overlap (Petersen and others, 2000; Frankel and others, 2002). Although it has only a minor effect on the computed hazard, we resolved this issue in 2002 by decreasing M_{max} over dipping faults and within 10 kilometers of vertical faults so that there was no magnitude overlap. When the hazard from gridded seismicity is calculated, computer runs are performed using the M_{max} grids that correspond to the characteristic and Gutenberg-Richter fault cases. The hazard curves from these runs are then added with the appropriate weights used for the characteristic and Gutenberg-Richter models for faults in that area. For the Gutenberg-Richter epistemic branch, M_{max} for the gridded-seismicity model is set to **M**6.5, the M_{min} of the Gutenberg-Richter relation for each fault. For the characteristic branch, M_{max} is the same as M_{char} or 7.0, whichever is smaller. M_{max} is set to 7.0 for the gridded-seismicity calculation for areas away from faults. For 2008, we update this model using the new magnitude data for faults in the WUS.

Smoothed-Gridded Seismicity

Gridded-seismicity models include earthquakes that are not on faults or in zones of distributed shear and are calculated by smoothing the earthquake recurrence rates across a grid of points. The gridded-seismicity models are based on the assumption that future large, damaging earthquakes will occur near past small and moderate-size events.

Seismicity rates for the gridded-seismicity model (Model 1) are determined by counting earthquakes in each grid cell with dimensions 0.1° longitude by 0.1° latitude, accounting for variable catalog completeness using Weichert's (1980) maximum-likelihood method. For shallow seismicity (depth ≤35 kilometers) in a zone covering most of California (including the most seismically active regions near the coast), we use completeness levels of $4.0 \le M_w < 5.0$ since 1933, $5.0 \le M_w < 6.0$ since 1900, and $M_w \ge 6.0$ since 1850. For the rest of the WUS, we use $4.0 \le M_w < 5.0$ since 1963, $5.0 \le M_w < 6.0$ since 1930, and $M_w \ge 6.0$ since 1850. For deep seismicity (depth >35 kilometers), we use $4.0 \le M_w < 5.0$ since 1963 and $M_w \ge 5.0$ since 1940 for the Puget Sound region, and $4.0 \le M_w < 5.0$ since 1963, $5.0 \le M_w < 6.0$ since 1930, and $M_w \ge 6.0$ since 1850 for the northern California region. (These completeness levels are the same as 2002). Unlike the CEUS (above), we feel that a single model is sufficient to capture the hazard from the historical seismicity in the WUS, since virtually all earthquakes with magnitude 5 or greater have occurred near clusters of smaller events. It is important to note that the maximum-likelihood scheme counts one large earthquake the same as one magnitude 4 event in determining the rate. The resulting "agrid" gives the annual rate of earthquakes in each grid cell as an incremental 10^a in the Gutenberg-Richter notation, between M–0.05 and M+0.05, or a 0.1 bin width centered on M=0. For the WUS, we apply a b-value of 0.8, which was calculated from a magnitude-frequency analysis of the declustered catalog.

Based on seismic observatory data and historical practice, Felzer (2007) and Frankel and Mueller (2008) provided estimates of magnitude uncertainties and rounding errors for earthquakes in the CGS/WGCEP catalog, and we extend the guidelines given in her work to estimate magnitude uncertainty and rounding errors for earthquakes in the rest of the WNA catalog. As rough first steps to account for these effects, we assume standard errors of about 0.1 magnitude unit for earthquakes in 1972–2006, 0.2 for 1932–1971, and 0.3 for 1850–1931. We also assume that for earthquakes from 1900–1941 a magnitude listed as x.0 or x.5 has been rounded to the nearest 0.5, and that otherwise magnitudes have been rounded to the nearest 0.1 or 0.01 as reported. Magnitude uncertainty is accounted for following Tinti and Mulargia (1985). Each rounded magnitude is "unrounded" into a binned distribution of possible "true" magnitudes, and counted following the completeness rules. Both effects tend to reduce

modeled seismicity rates, generally in the neighborhood of 2 to 15 percent depending on the region and time period.

In the 1996 and 2002 maps, we computed separate agrids from shallow seismicity in extensional and nonextensional regions of the WUS and used corresponding combinations of ground motion relations to compute the hazard (fig. 12). This overall scheme is maintained for the current update, although it is implemented somewhat differently using the NGA relations (below). The nonextensional region covers most of California, the Pacific Northwest, and the northwest part of the Basin and Range source zone (the "Yakima" zone described in the 2002 documentation); the rest of the WUS is modeled as extensional.

A two-dimensional spatial Gaussian function with a correlation distance of 50 kilometers is used to smooth the gridded rates in most of the WUS (for both shallow and deep seismicity). Smoothing parameters are based on earthquake location uncertainties and spatial trends seen in historical seismicity (Frankel and others, 1996). One problem with the smoothing method is apparent in some parts of California where seismicity that occurs in narrow linear zones is oversmoothed into nearby aseismic regions. We follow the 2002 methodology by implementing an anisotropic smoothing scheme that provides some smoothing but generally keeps the modeled hazard closer to the original seismicity. Using respective correlation distances of 75 and 10 kilometers for directions parallel and normal to dominant seismicity trends, we apply this method (table 4) to earthquakes within 10 kilometers of the Brawley seismic zone in southern California, within 20 kilometers of the creeping section of the San Andreas fault in central California, and within 25 kilometers of the Mendocino fracture zone in offshore northern California (also removing the Mendocino fault source that was used in previous models).

The gridded-seismicity model is based on analysis of the historical earthquake catalog and should predict the total number of earthquakes observed in California from M_w5 to 7. But in addition to this model we also allow earthquakes between M_w6.5 and 7.0 to occur on modeled faults. In this case, we expect the total modeled rate of M_w6.5 to 7.0 earthquakes to exceed the total historical rate. To achieve a match, we need to reduce the rate of modeled earthquakes, either on faults or in the gridded seismicity. Our preliminary studies indicate that about two-thirds of the large earthquakes in California are associated with modeled faults (this percentage was confirmed in the research by the Working Group on California Earthquake Probabilities reported by Field and others, 2008). For the 2008 model, we have simply reduced the rate of earthquakes with $M_w \geq 6.5$ in the gridded model by a factor of two-thirds in an effort to match the historical rate in a region surrounding California (fig. 13). We recognize that additional research is needed to provide a more satisfactory long-term solution and to address this problem outside of California.

Table 4. Source parameters for anisotropically smoothed seismicity sources.

[SAF, San Andreas Fault]

Zone	M_{min}	M_{max}	Virtual fault strike (°)	b-value	Ratio of strike slip: Reverse: Normal
Brawley zone	5.0	6.5	157	0.8	0.5: 0: 0.5
Creeping section of SAF	5.0	6.0	–42.5	0.9	1.0: 0: 0
Mendocino fracture zone	5.0	7.0	90	0.8	0.5: 0.5: 0

Uniform Background Zones

In contrast to the gridded-(smoothed-) seismicity model, regional background zones account for earthquake potential spread uniformly across tectonic or geologic regions with constant geologic or strain characteristics. These zones are designed to provide a hazard floor and account for future random earthquakes in areas with little or no historical seismicity. The earthquake rate for each WUS background zone is determined by counting earthquakes with $M_w \geq 4$ since 1963, computing an annualized rate, and prorating this rate uniformly across the entire zone.

As in the 1996 and 2002 maps, we model background seismicity (WUS Model 2) in five nonoverlapping regional zones: the Basin and Range Province extended to include the Rio Grande rift, parts of Arizona and New Mexico, western Texas, eastern Washington, and northern Montana and Idaho; the Cascade volcanic province; the Snake River Plain province; the Yellowstone seismicity parabola province; and a region of southeastern California and southwestern Arizona (figs. 14 and 15). These regions are geologically and seismologically distinct, and the reasoning behind the zonation is discussed in detail in the 1996 documentation.

As in 1996 and 2002, the regional zone model (Model 2) is implemented in a way that does not penalize areas of high seismicity in order to provide a hazard floor in areas of low seismicity. In each grid cell, the historical gridded-seismicity rate (Model 1) is compared with the floor value from Model 2. If the historical rate exceeds the floor value, the final cell rate simply equals the historical rate. If, however, the floor value exceeds the historical rate, Models 1 and 2 are combined with respective weights 0.67 and 0.33 to calculate the final cell rate. Nowhere is the final cell rate less than the historical rate, and the total modeled seismicity rate in the WUS exceeds the total historical rate by about 16 percent.

Special Zones

Models 1 and 2 do not account for all of the local variations in earthquake potential that we would like to include in the hazard analysis. Special zones can be used to account for variations in catalog completeness, magnitude-rate distribution, maximum magnitude, depth, and b-value.

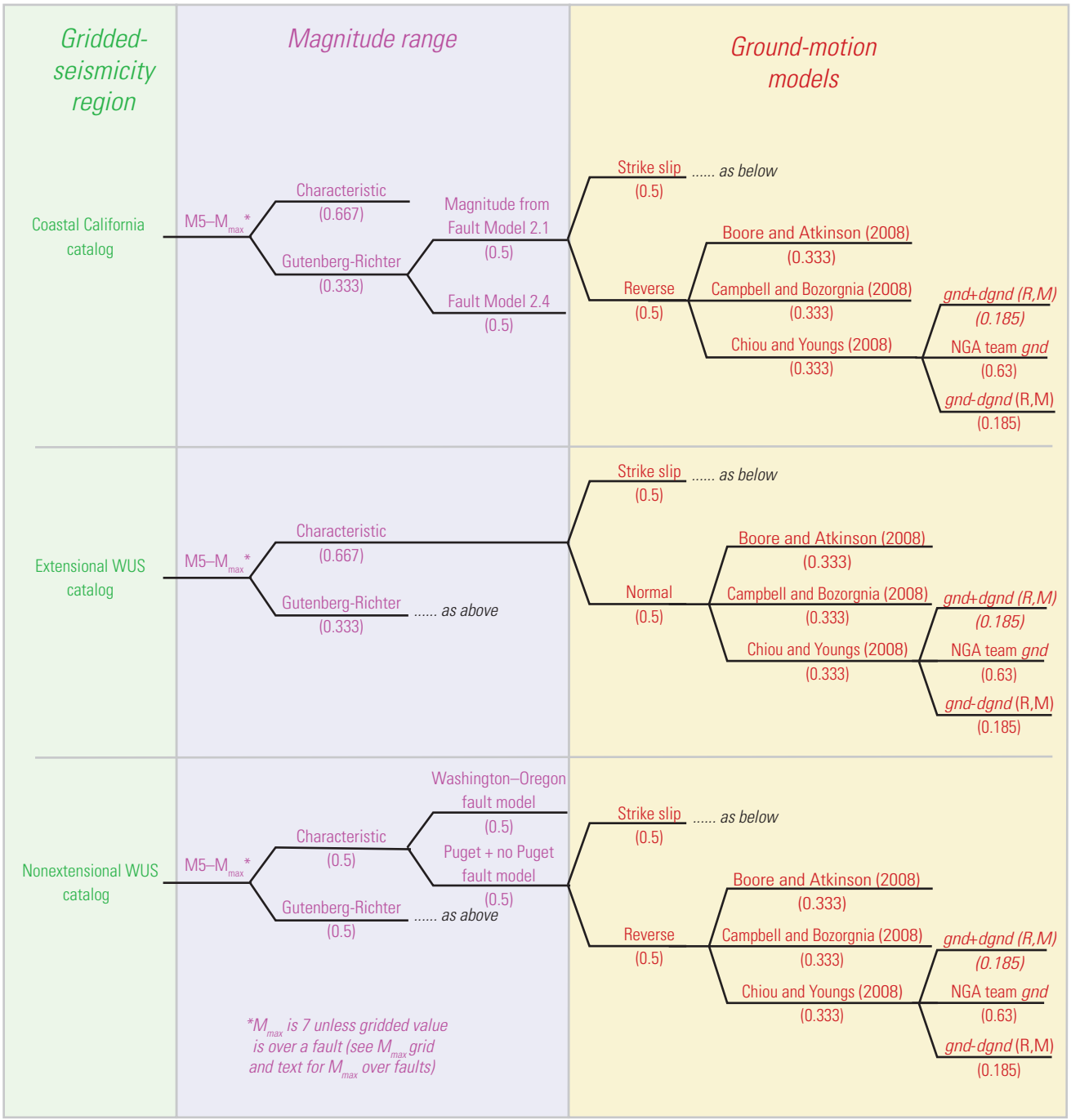

Figure 12. Logic tree for seismicity-derived hazard component in the Western United States (WUS). Parameters in this figure include some aleatory variability as well as depicted epistemic uncertainty. We treat aleatory variability in ground motion in the hazard code. NGA, Next Generation Attenuation; *gnd* is the logarithm of median spectral acceleration or peak ground acceleration; *dgnd* is uncertainty in median spectral acceleration or peak ground acceleration at a given distance (R) and magnitude (M). See table 6.

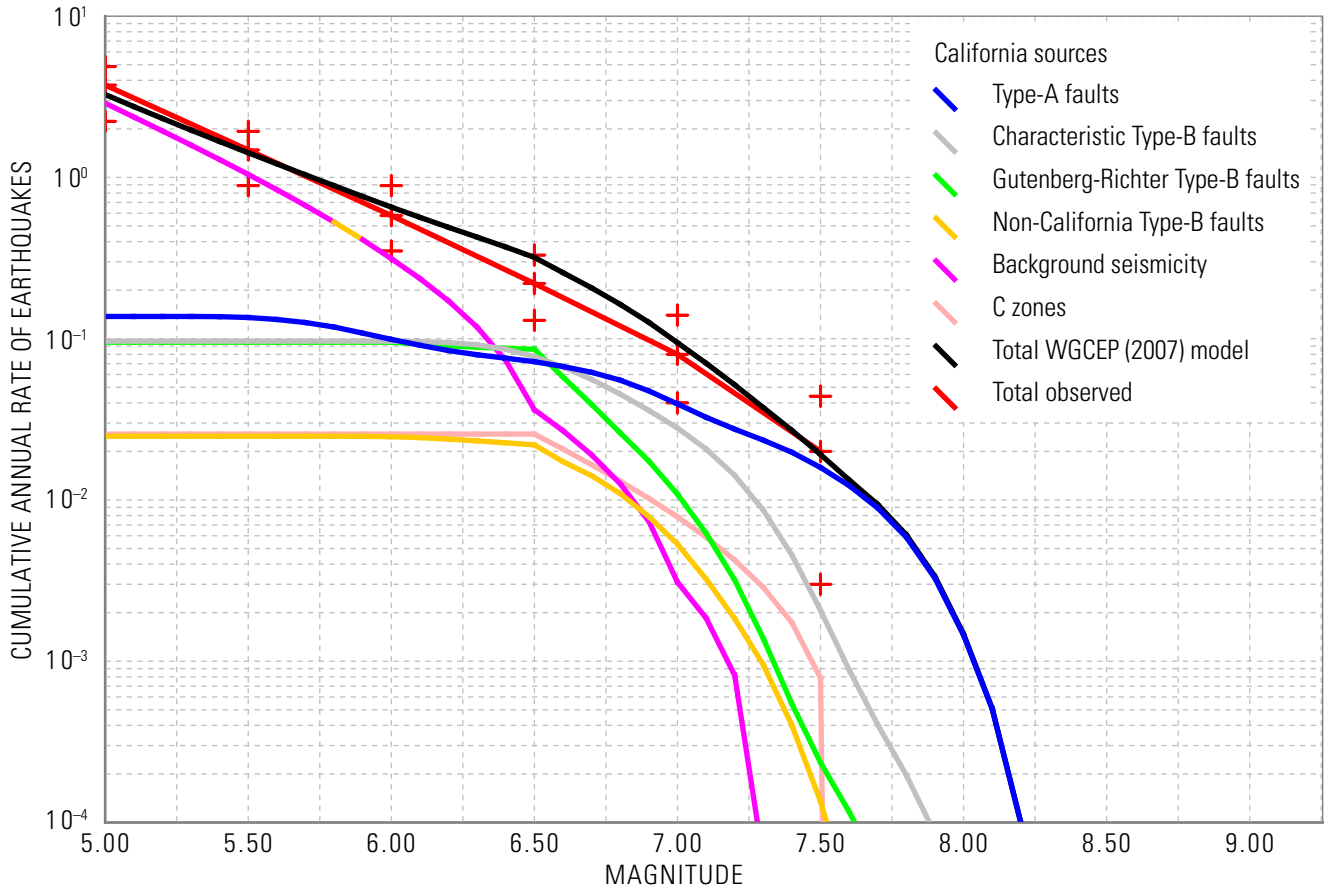

Figure 13. The total, cumulative magnitude-frequency distribution implied by the Working Group on California Earthquake Probability (Field and others, 2008) source model (black) as well as from the contributions from various types of sources in the model. The cumulative rates inferred from the historical earthquake catalog are shown in red; the outer red crosses represent the 95-percent confidence bounds described in Appendix I of Field and others (2008).

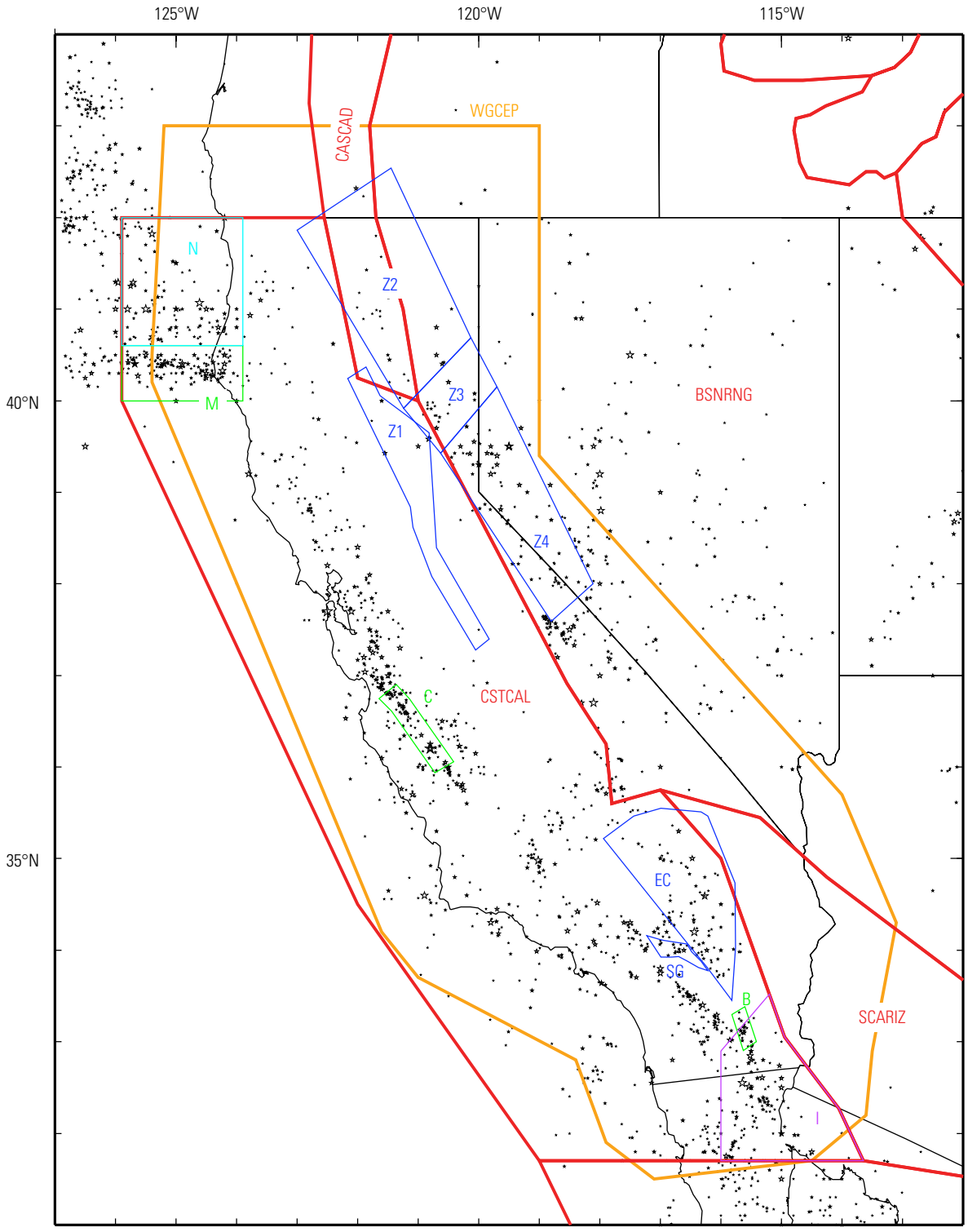

Figure 14. Historical seismicity patterns (gridded seismicity), uniform broad regional zones (regional zones), and local seismicity variations (special zones) used in California background seismicity model. Regions include: BSNRNG, Basin and Range; CASCAD, Cascadia; CSTCAL, Coastal California; SCARIZ, Southern California and Arizona; WGCEP, Working Group on California Earthquake Probabilities. Anisotropically smoothed seismicity sources: B, Brawley zone; C, creeping section of the San Andreas fault; M, Mendocino fracture zone. EC, Eastern California; N, Central Nevada seismic zone; SG, San Gorgonio; Z1–Z4 are zones of distributed shear discussed in text.

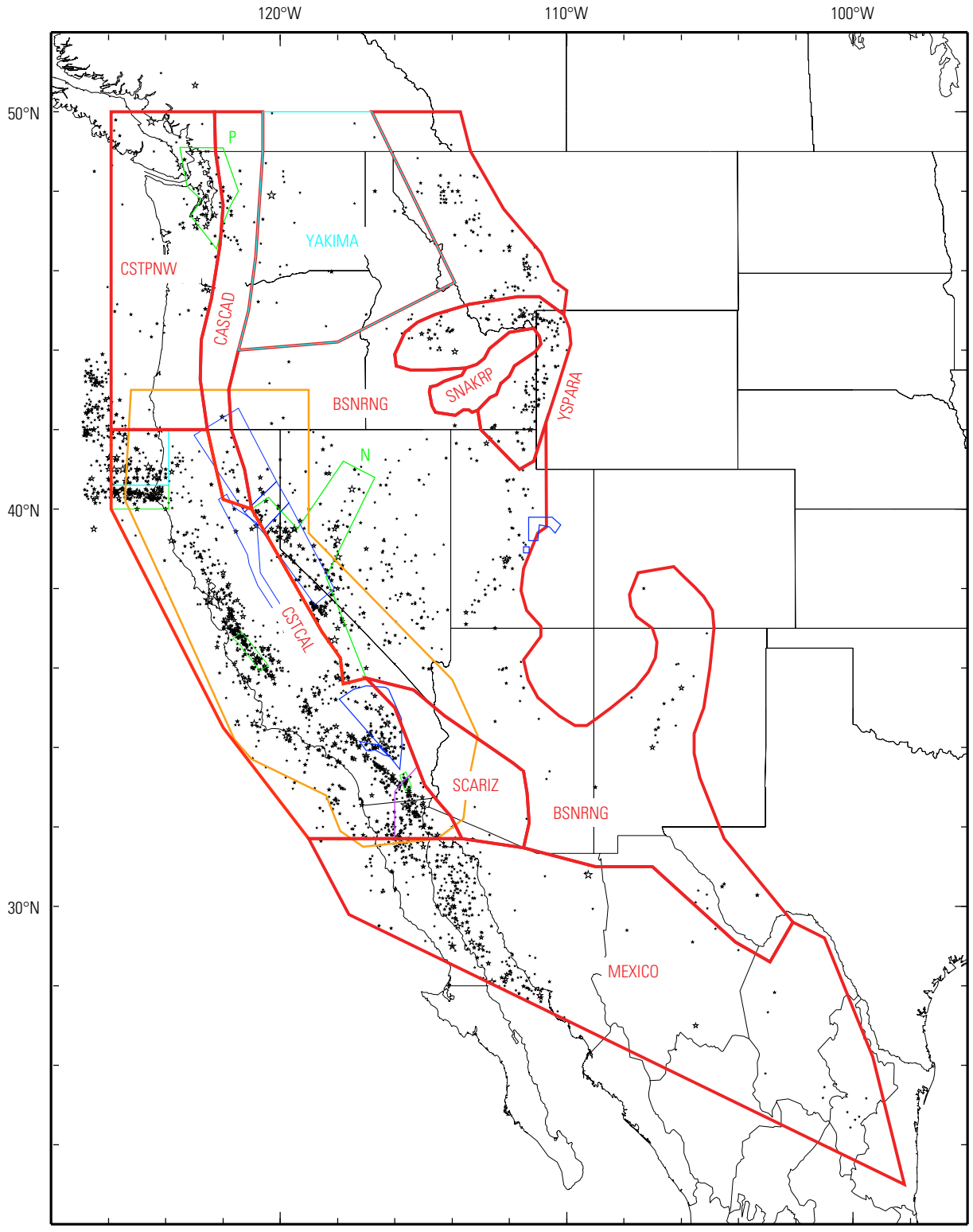

Figure 15. Historical seismicity patterns (gridded seismicity), uniform broad regional zones (regional zones), and local seismicity variations (special zones) used in Western United States background seismicity model. Regions include: BSNRNG, Basin and Range; CASCAD, Cascadia; CSTCAL, Coastal California; SCARIZ, Southern California and Arizona; SNAKRP, Snake River Plain; YSPARA, Yellowstone parabola; YAKIMA, Yakima; CSTPNW, coastal Pacific Northwest; MEXICO, Mexico; WGCEP, Working Group on California Earthquake Probabilities. Other regions: P, Puget Lowlands; see figure 14 for explanation.

We model a seismicity-based source zone for the Puget Lowland region to account for an observed deficit between geodetic and seismic deformation rates. An average seismicity rate is determined from the number of earthquakes in the zone with $M_w \geq 5.0$ since 1928, and M_{max} is increased from 7.0 to 7.3 as a proxy to account for 2.7 mm/yr of north-south contraction across the zone. We create two agrids for modeling the WUS gridded seismicity; one agrid is developed with the Puget zone earthquakes removed and the other a-grid includes those events. These two agrids are each weighted 50 percent. The Puget zone is a uniform zone that is added with 50 percent weight and fills in the hole remaining in the first agrid. This model allows for weight on the two models (1) earthquakes across the Puget region occur uniformly across the zone of high deformation and (2) future earthquakes occur close to past earthquakes.

Similar to the Puget Sound region, the M_{max} is increased from 7.0 to 7.5 in the background gridded-seismicity model in central Nevada as a proxy to account for part of the 2.0 mm/yr rate of geodetic extension observed in the region. Several large earthquakes occurred in this region during the early 20th century: 1915 Pleasant Valley, 1954 Dixie Valley, and 1954 Fairview Peak events. Treatment of these zones carries over from 2002, and further details can be found in the documentation (Frankel and others, 2002).

Gridded-seismicity models were included near the Cascadia subduction zone to account for potential deep earthquakes such as the 2001 Nisqually earthquake that caused damage near Seattle and Olympia, Wash. These zones are discussed in the gridded seismicity section since they are based on spatially smoothed earthquakes and include regions near the Puget Sound and in northern California. USGS/NEIC seismicity data indicate that since 1990 several deep, magnitude-2.5 earthquakes have occurred beneath Portland, Ore., at a rate of about 0.38/yr—about a factor of 10 less than the rate of magnitude-2.5 events beneath the Puget Lowland region. We included a new source zone for deep earthquakes near coastal Oregon. The new model is consistent with a Gutenberg-Richter distribution and a b-value of 0.8 that would predict a low rate of M6.5 events of about 0.003–0.005/yr.

Source Model—Geodetically Derived Areal Source Zones (C Zones)

Earthquake rates in zones of distributed shear are estimated from the geodetically determined rate of deformation across an area of high strain rate in areas where geologic strain rates are not well known. One outstanding issue in the Intermountain West region is that for several areas of the Basin and Range Province, the moment estimated from geology is about one-half the moment estimated from Global Positioning System (GPS) data (Pancha and others, 2006). Zones of distributed shear account for earthquakes in these areas where faults are poorly defined and geodetic or seismic data indicate a higher level of shear strain. These zones are implemented using geodetic data and Kostrov's formula (Kostrov, 1974) that converts strain rate to moment rate.

The 1996 and 2002 maps included four zones of distributed shear in northern California and Nevada. Similar zones were used in the 2008 maps but the geometries of the zones in northern California and Nevada were slightly modified to be consistent with recent geodetic strain-rate data. The shape of the updated C-zones was based on the shape of the maximum geodetic shear strain rate distribution in the area. We did not include the high shear strain rate in the central Nevada seismic belt because of significant post-seismic influences from the Pleasant Valley, Fairview Peak, and Dixie Valley earthquake sequences (Hammond and Thatcher, 2005). GPS velocities in and around those C-zones are modeled using a broadly distributed shear deformation belt (fig. 16, bottom panel) to obtain the shear rates in those zones. The shear rate of the eastern California Foothills fault system (zone 1) is based on fault slip-rate studies (for example, Clark and others, 1984). The rates of shear in zone 2 (northeastern California), zone 3 (Mohawk–Honey Lake), and zone 4 (western Nevada) are based on a composite of geodetic, geologic, and seismicity strain rates. We found average geodetic shear rates of 7, 7, and 10 mm/yr for zones 2, 3, and 4, respectively (fig. 16). The corresponding geologic shear rates in the same zones are 2.3, 2, and 0 mm/yr. The corresponding seismicity shear rates are 0.6, 1.0, and 1.5 mm/yr. We used 50 percent of the residual shear rate between the geodetic and the combined geologic and seismic shear rates as our final shear rates for those zones. Rates for each zone are shown in table 5.

Additionally, two new zones of distributed shear were added to the 2008 model in southern California based on research presented in the Working Group on California Earthquake Probabilities report (Field and others, 2008): the Mojave (eastern California) and San Gorgonio zones. Each of these zones was modeled using a shear strain rate of 2 mm/yr, which is about half of the geodetic strain rate leftover after considering known fault strain rates. Parameters used to define the zones are outlined in table 5.

These zones are characterized using a preferred strike and a Gutenberg-Richter magnitude-frequency distribution between M6.5 and 7.6. For the 2008 maps, we have selected M7.6 as the maximum magnitude for these zones based on the magnitude of the 1872 Owens Valley earthquake.

Source Model—Faults

Fault sources are based on published fault studies and recommendations from State geological surveys. We only include mapped structures for which we can estimate a mean slip rate or mean recurrence interval. Fault models applied to the WUS are described in Appendixes G (Intermountain West), H (Pacific Northwest), and I (California). Fault models depend on the fault geometry (segmentation) and slip rate or paleoseismic recurrence rates to establish the locations, sizes, and rates of future earthquakes. To model each rupture we

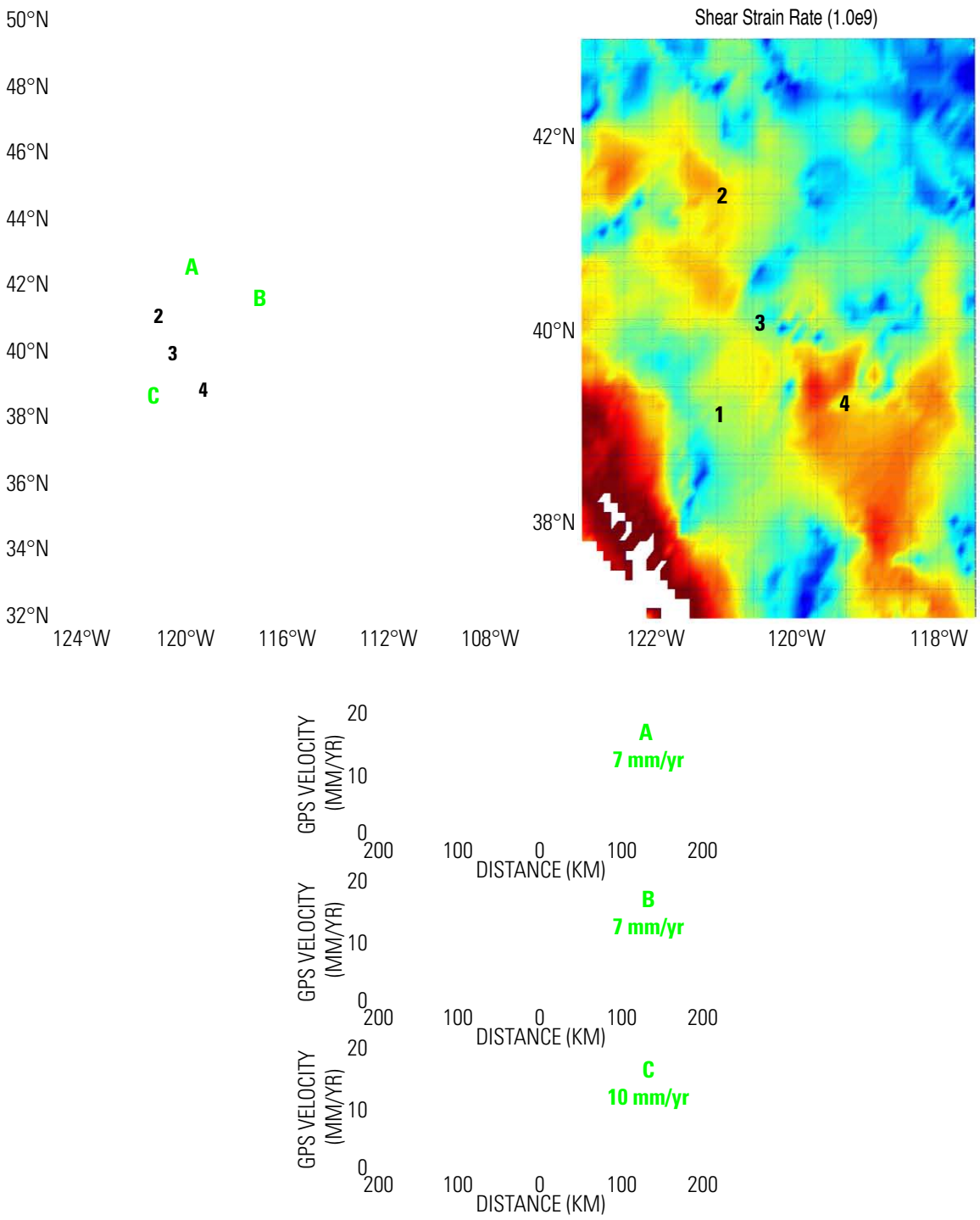

Figure 16. Moment estimated from Global Positioning System (GPS) data. mm/yr, millimeters per year; km, kilometers.

Table 5. Source parameters for geodetic zones of distributed shear.

[°, degree; mm/yr, millimeters per year; km, kilometers]

Zone	M_{min}	M_{max}	Virtual fault strike (°)	b-value	Ratio SS:Rev:Normal	Slip rate (mm/yr)	Length (km)	Width (km)
S. Calif.–Mojave	6.5	7.6	–47	0.8	1: 0: 0	2.0	219	15
S. Calif.–San Gorgonio	6.5	7.6	–67	0.8	1: 0: 0	2.0	102	18
Shear1–Calif. Foothills fault	6.5	7.6	–35	0.8	1: 0: 0	0.05	360	12
Shear2–NE Calif.	6.5	7.6	–25	0.8	1: 0: 0	2.0	230	15
Shear3–Mohawk-Honey Lake	6.5	7.6	–45	0.8	1: 0: 0	2.0	88	15
Shear4–W. Nev.	6.5	7.6	–45	0.8	1: 0: 0	4.0	245	15

estimate a fault rupture length and width. These parameters are obtained from geologic mapping (fault geometry and length) and seismicity characteristics (fault dip and rupture depth). To model the rate of each size of earthquake along crustal faults, we use weighted combinations of characteristic and Gutenberg-Richter magnitude-frequency distributions to characterize the sources.

Magnitudes

In the source model, we either use historical magnitudes or estimate magnitude based on fault area (California) or surface-rupture length (Intermountain West and Pacific Northwest regions). The equations of Ellsworth—type B equation (Ellsworth, 2003)—and Hanks and Bakun (2002) were applied for California; surface-rupture length relative to magnitude relations of Wells and Coppersmith—all fault types (Wells and Coppersmith, 1994) were applied to faults in the WUS outside of California.

A change in detail compared to 2002 fault-hazard modeling is that we now round derived magnitude estimates to two decimal places, compared to one decimal place in 2002 (see Appendix F4 for further discussion). One reason for this change is that epistemic uncertainty in the magnitude-area relation frequently is lost when we round to nearest tenth but is retained when rounding to nearest hundredth. This change alters earthquake recurrence rate estimates because larger events produce more slip per event. Changes in probabilistic ground motion that are associated with this change in rounding procedure change are apparent particularly in the new spectral acceleration (SA) ratio maps, even when the geology model for a given fault has not changed.

We include an epistemic uncertainty of ±0.2 magnitude units for the characteristic earthquake magnitude and the maximum magnitude of the Gutenberg-Richter distribution for most regions of the WUS. The uncertainty is applied with weights of 0.2 for the lower, 0.6 for the median, and 0.2 for the upper branches. However, no additional epistemic uncertainty in magnitude is applied within California; the two rupture area-magnitude relations that are used in that region account for some epistemic uncertainty.

In addition to the epistemic uncertainty, we also include aleatory uncertainty for characteristic earthquakes using a normal distribution with standard deviation of 0.12. For the 2008 maps we extend the value at which the distribution is truncated from ±0.15 magnitude units used in 2002 to a-value of 2 sigma or ±0.24 that was applied in the Working Group on California Earthquake Probabilities (2003) report. Most of the magnitude-frequency models are moment balanced using different characteristic magnitudes. Exceptions include the California Type-A fault a priori model and the Wasatch model. We do not apply any additional aleatory uncertainty for the models that use Gutenberg-Richter magnitude-frequency distributions (including the California Type-A fault unsegmented model) because these models are thought to already account for aleatory uncertainty in the size of earthquakes on a fault.

Earthquake Recurrence

The characteristic rate of earthquakes on a fault is determined by the ratio of the slip rate (vertical or horizontal) to the slip of the characteristic earthquake determined by the length or area of the fault. For Gutenberg-Richter relations, we use standard equations that relate slip rate and magnitude to the rate of earthquakes in each magnitude bin (Frankel and others, 2002; Petersen and others, 1996). In the 2002 source models, we applied a ratio of 67-percent characteristic and 33-percent Gutenberg-Richter magnitude-frequency distribution for faults in coastal California and have applied equal weighting for the rest of the WUS (including eastern California).

The Western State Seismic Policy Council (WSSPC) held a workshop to discuss issues for the Intermountain West region. One of their recommendations was to change the ratio of characteristic and Gutenberg-Richter magnitude-frequency distributions in the Intermountain West region to reflect similar event weighting to that used in coastal California, 67-percent characteristic and 33-percent Gutenberg-Richter (see Appendix J for discussion). Scientists in the Pacific

Northwest, however, did not accept this recommendation; they felt that uncertainties in recurrence are large in that region. Therefore, we have implemented the 2/3-characteristic 1/3-Gutenberg-Richter magnitude-frequency distribution for faults in the Intermountain West region but not in the Pacific Northwest region.

Intermountain West Fault Sources

Nearly 300 faults in the Intermountain West are included as sources in the 2008 model (fig. 17, Appendix G). We updated input parameters for more than 10 percent of those faults based on a literature review of parameters such as slip rate and recurrence. The majority of changes in our model resulted from the comprehensive reevaluation of all published paleoseismic studies by the Utah Quaternary Fault Working Group (Lund, 2005).

The WSSPC recommended that the USGS model allow for multisegment ruptures along the Wasatch fault (fig. 18). Therefore, in addition to a segmented model, similar to that applied in the 2002 maps, we include a floating M7.4 earthquake rupture model that assumes a 1.2 mm/yr mean slip rate for the Wasatch fault and that is weighted 0.1 in the model. This model allows for earthquakes that cross segment boundaries and was agreed on by the Utah Fault Working Group.

Another WSSPC recommendation was to change the default dip for normal faults from 60° to 50°. The WSSPC group and our own studies indicate that a default dip of 50° may be more consistent with global normal faulting seismic data (focal mechanisms). Therefore, we have modified the preferred dips of faults in the Basin and Range Province to adhere to their recommendation. The Lost River fault preferred dip was not modified; it was determined from the focal mechanism of the Borah Peak earthquake and the aftershock distribution. This change to the fault dips across the Intermountain West region generally increases the hazard by changing the distance from the source to the site and also increasing the fault-parallel slip rate (see Appendix J for further discussion).

Several WSSPC recommendations (Lund, 2006) were not adopted in this update of the maps, one of which was to promote all characteristic earthquakes on fault sources with M less than 6.5 to M6.5. This recommendation was based on the observation that earthquakes with M less than 6.5 often do not have well-defined surface ruptures. We applied this promotion in earlier versions of the map but reverted back to the calculated magnitudes in the final version because establishing a default minimum magnitude caused a higher rate of M6.5 events than have been observed in the historical earthquake catalog. Even though this recommendation was not implemented in this version of the maps, we agree that the suggestion needs further review. Another recommendation was to incorporate slip rate uncertainties in the models. Slip-rate uncertainties are not available for all the faults in the model, so it is premature to implement this recommendation (see Appendix J for the consensus uncertainty data). We plan to work with other State geological surveys to produce this information for the next version of the maps.

Pacific Northwest—Cascadia Fault Sources

The Pacific Northwest fault sources (fig. 19) are described in Appendix H, and the Cascadia subduction zone is described in Appendix K. The primary changes to the Pacific Northwest model are to the Cascadia subduction zone, which includes a broader magnitude-frequency distribution. In addition, one fault was modified (the South Whidbey Island fault) and three new faults have been added for 2008 maps (the Lake Creek–Boundary Creek fault, Stonewall anticline, and Boundary Creek fault—see Appendix H for further details).

The Cascadia subduction zone extends about 1,200 kilometers from Vancouver Island in British Columbia to Cape Mendocino in California. Adjacent to northern California the Gorda plate is consumed eastward beneath North America at a rate of about 40 mm/yr (Nishimura and others, 1984). The last great Cascadia rupture is thought to have occurred in January 1700, based on analysis of tsunami records in Japan, trees along the Pacific coast, study of onshore tsunami deposits, and other geophysical data (Satake and others, 2003).

We include the same Cascadia subduction-zone geometry and weighting scheme (fig. 20) as used in the 2002 model. Thermal models of Flück and others (1997) and global analogs of shallow-dipping subduction zones were used to develop alternative rupture models. These models include ruptures that extend (1) through various depth ranges thought to be related to the elastic and transitional properties of the crust and (2) down to a depth of about 30 kilometers similar to other large subduction earthquakes (fig. 21).

The primary constraint on the recurrence of Cascadia earthquakes is that great earthquakes occur on average every 500 years beneath all sites on the coast of the Cascadia subduction zone, based on paleoseismic studies of coastal subsidence and tsunami deposits (for example, Atwater and Hemphill-Haley, 1997). We considered two sets of rupture scenarios for these events: (1) M9.0±0.2 events that rupture the entire Cascadia subduction zone every 500 years on average and (2) M8.0–8.7 events with rupture zones that fill the entire zone over a period of about 500 years. Each of these large to great earthquakes is expected to rupture the entire seismogenic area. Ruptures in the latter set of scenarios float along the Cascadia subduction zone.

For these maps, we assign a probability of 0.67 to the M8.8–9.2 scenario and a probability of 0.33 for the set of M8.0–8.7 scenarios with floating ruptures (fig. 20). In the 2002 maps, M9.0 and M8.3 scenarios were given equal probabilities. The higher probability of the M8.8–9.2 rupture scenario in this update reflects consensus of scientists and others at the March 28–29, 2006, Pacific Northwest NSHMP workshop. In that meeting it was concluded that the M9.0± 0.2 scenario was more likely than more frequent, floating smaller earthquakes. Figure 22 shows the magnitude-frequency distribution of the Cascadia subduction zone and a map showing

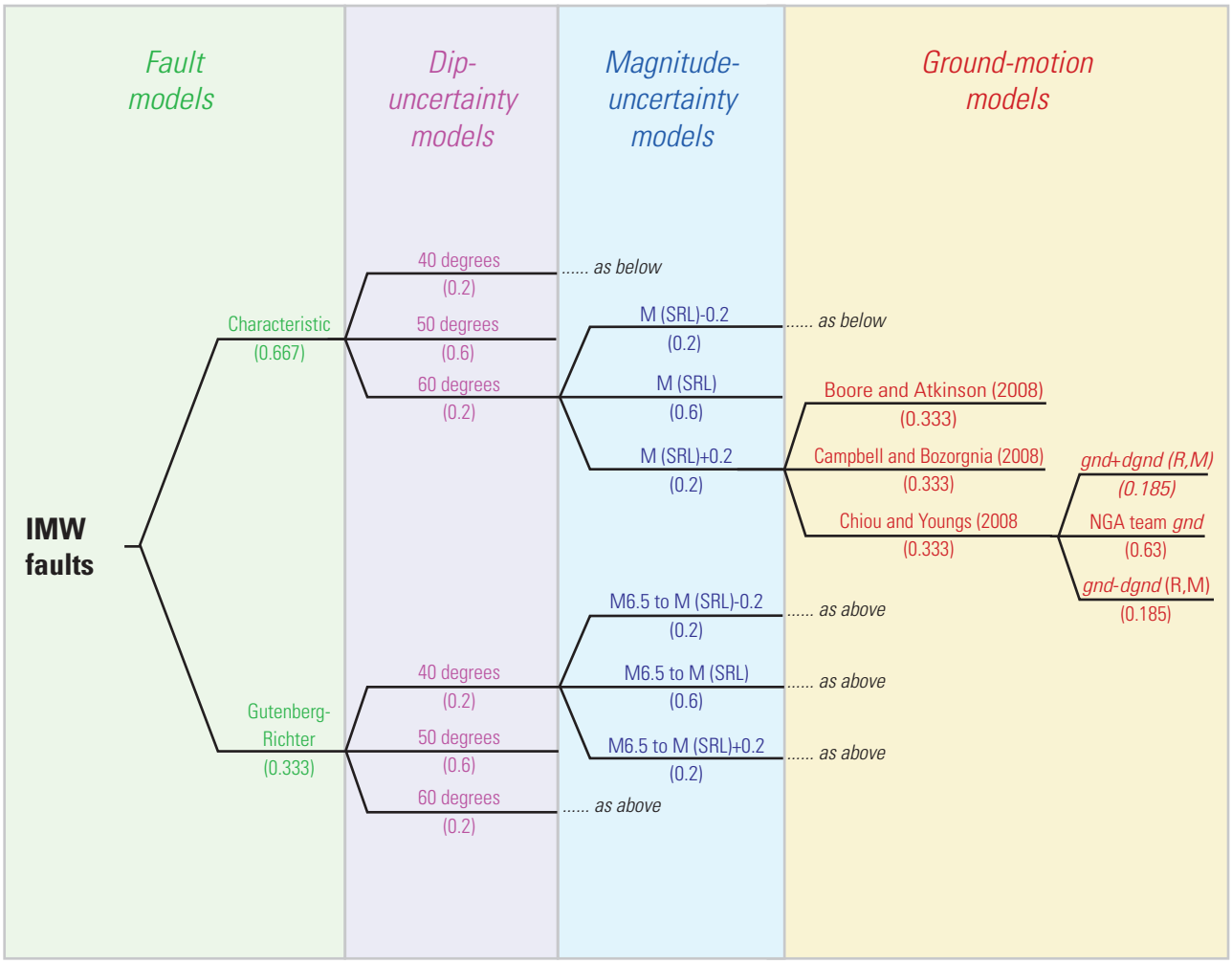

Figure 17. Logic tree for fault sources in the Intermountain West (IMW). Parameters in this table include some aleatory variability as well as depicted epistemic uncertainty. Additional aleatory variability may be associated with all models depicted. We treat aleatory variability in ground motion in the hazard code. Most faults in the Intermountain West have assigned characteristic magnitudes (see first panel) based on surface-rupture length except where historical earthquakes serve as analogs and where the characteristic magnitude is constrained to M7.5 (shown in table G-3 in Appendix G). Short faults (less than 17 kilometers) in the region with characteristic magnitude less than 6.5 are treated like the upper branch but with full weight. NGA, Next Generation Attenuation; *gnd* is the logarithm of median spectral acceleration or peak ground acceleration; *dgnd* is uncertainty in median spectral acceleration or peak ground acceleration at a given distance (R) and magnitude (M). See table 6.

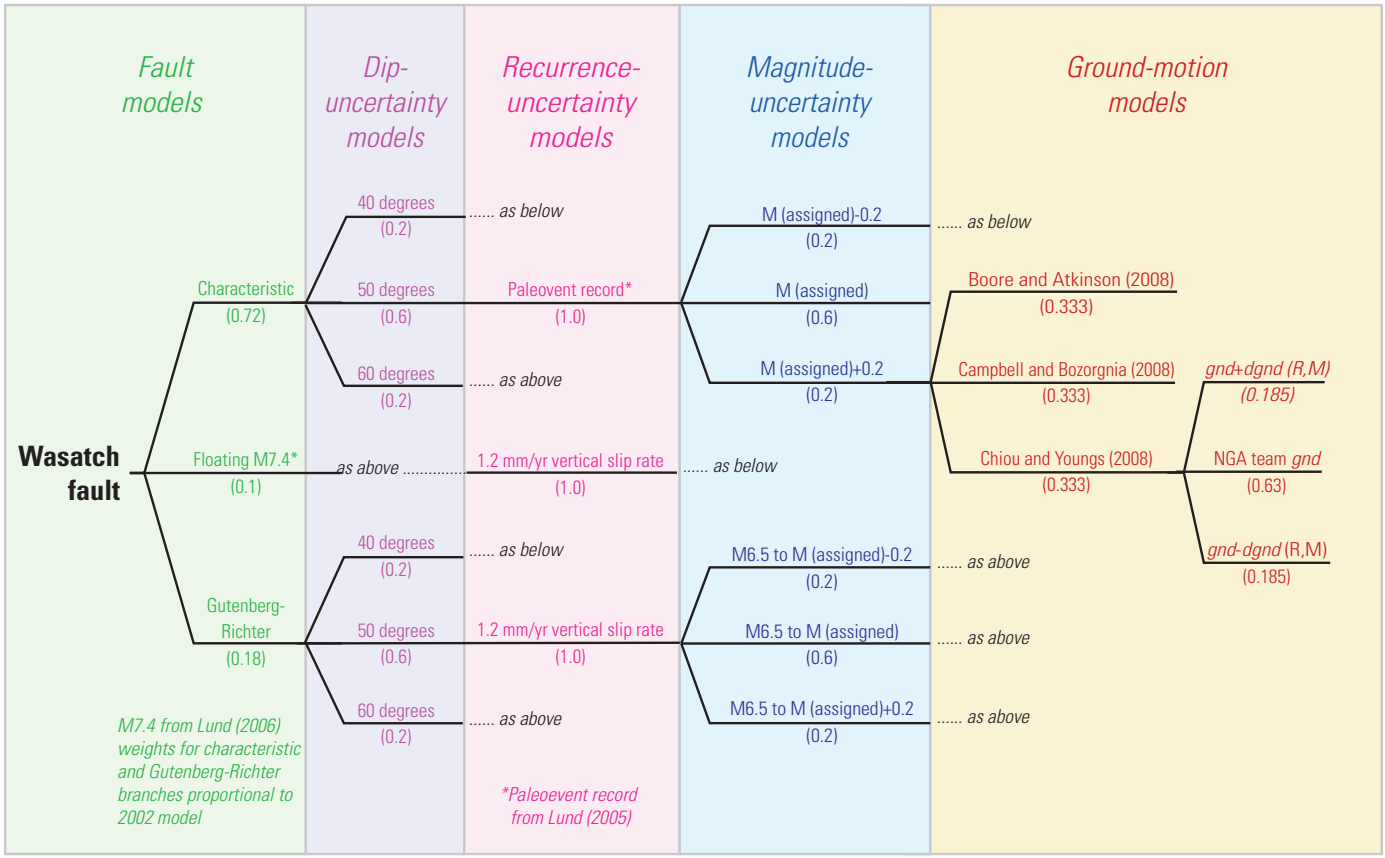

Figure 18. Logic tree for the Wasatch fault in Utah. Parameters in this figure include some aleatory variability as well as depicted epistemic uncertainty. Additional aleatory variability may be associated with all models depicted. We treat aleatory variability in ground motion in the hazard code. Assigned characteristic magnitudes for segments of the Wasatch fault retained from 2002 model. NGA, Next Generation Attenuation; *gnd* is the logarithm of median spectral acceleration or peak ground acceleration; *dgnd* is uncertainty in median spectral acceleration or peak ground acceleration at a given distance (R) and magnitude (M). See table 6.

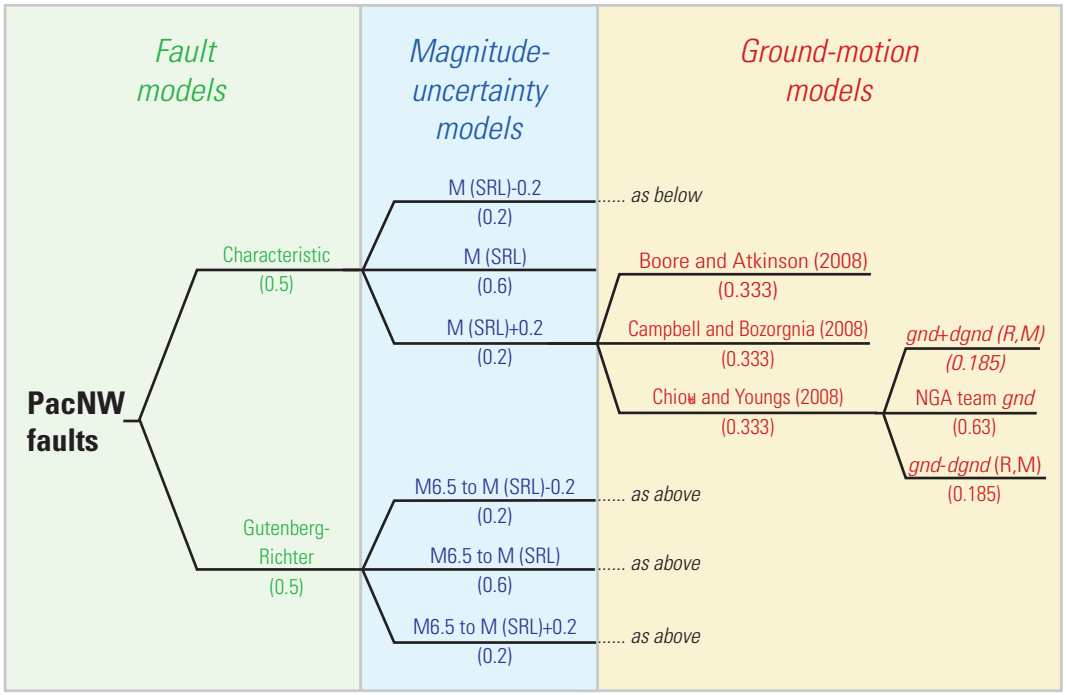

Figure 19. Logic tree for fault sources in the compressional region of the Pacific Northwest (PacNW). Parameters in this figure include some aleatory variability as well as depicted epistemic uncertainty. Additional aleatory variability may be associated with all models depicted. We treat aleatory variability in ground motion in the hazard code. Short faults (less than 17 kilometers) in the region with characteristic magnitude less than 6.5 are treated like the upper branch but with full weight. NGA, Next Generation Attenuation; *gnd* is the logarithm of median spectral acceleration or peak ground acceleration; *dgnd* is uncertainty in median spectral acceleration or peak ground acceleration at a given distance (R) and magnitude (M). See table 6.

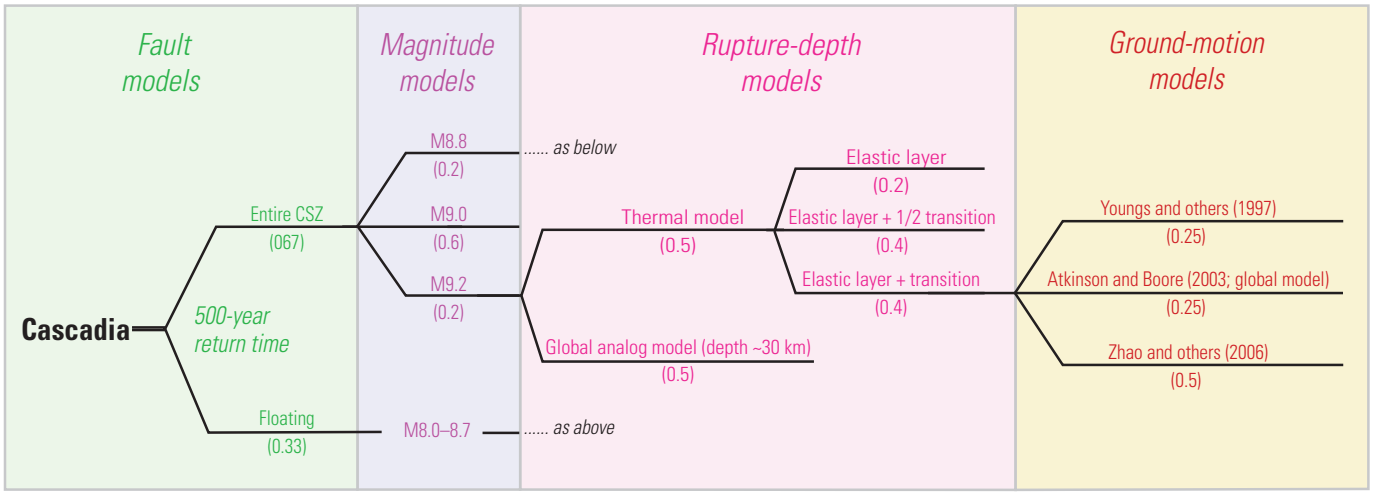

Figure 20. Logic tree for Cascadia subduction zone (CSZ). Parameters in this figure include some aleatory variability as well as depicted epistemic uncertainty. Additional aleatory variability shown in table K-1 in Appendix K.

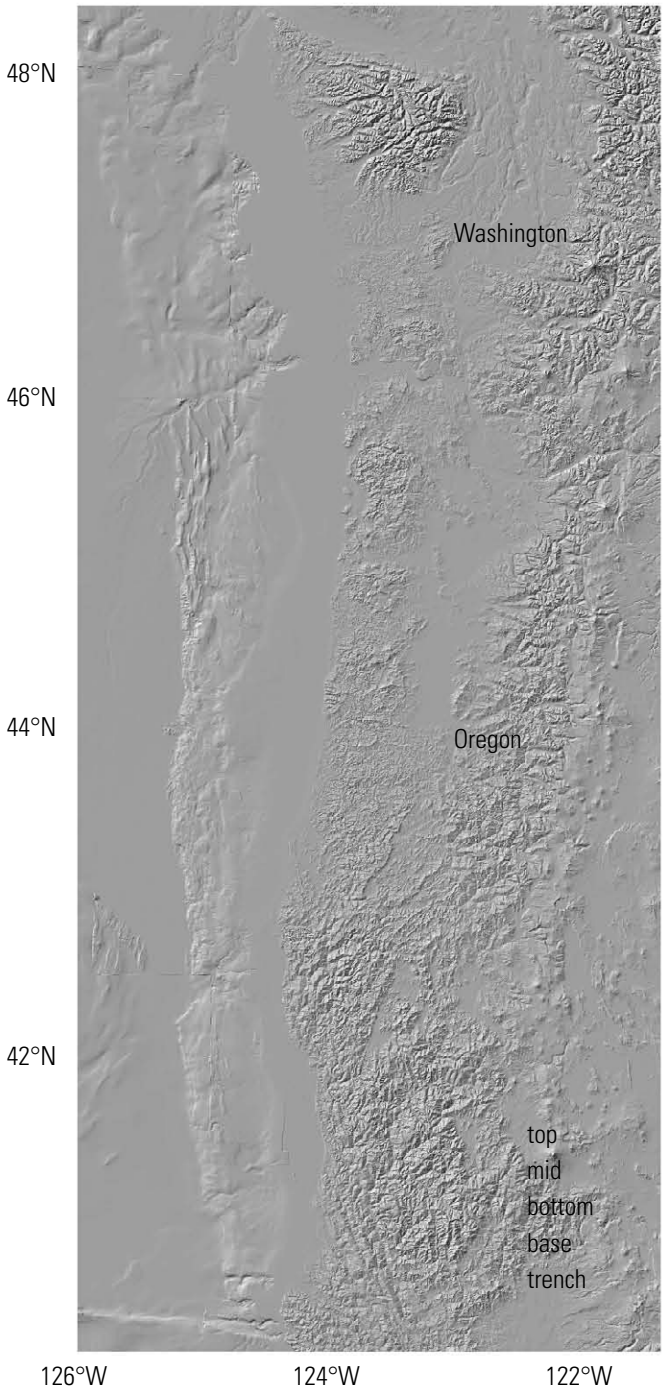

Figure 21. Location of the eastern edge of earthquake-rupture zones on the Cascadia subduction zone for the various models used in this study relative to the surficial expression of the trench: top, base of the elastic zone; mid, midpoint of the transition zone; bottom, base of the transition zones; base, base of the model that assumes ruptures extend to about 30-kilometers depth. Figure provided by Ray Weldon.

the geographic variation of frequency of floating earthquakes. The annual rates are calculated using the scenario probabilities previously listed. Recurrence rates and weights are shown in table K-1.

California Fault Sources

The 1996 and 2002 California seismic hazard models are described in Petersen and others (1996), Frankel and others (1996, 2002), and Cao and others (2003). For the 2008 seismic hazard maps we have updated the fault parameters by adopting new information from the Working Group on California Earthquake Probabilities (WGCEP). Changes to the fault source models are described in detail in Appendix A of the WGCEP report (Wills and others, 2008). The WGCEP modified fault locations, fault rupture parameters, and zones of distributed shear in California. The major changes to the fault parameters described in detail in the WGCEP report and appendixes (Field and others, 2008) and outlined below.

We incorporate two types of fault sources (Type A and B) into the seismic hazard maps for the WUS. Type-A faults are well-known faults that are defined using published information on fault geometry, earthquake sequences, slip rates, and dates of previous earthquakes. In California, major strands of the San Andreas fault system including the Calaveras, Hayward–Rodgers Creek, San Jacinto, and Elsinore fault zones, the Garlock fault zone, and the Cascadia subduction zone are modeled as Type-A faults. Detailed, fault-specific models are developed for each Type-A fault. The models include characteristic earthquakes on single segments, multisegment ruptures, and earthquakes that are shifted uniformly along the fault (the "floating earthquake" or "unsegmented" model). Type-B faults are characterized by published information on slip rates and fault geometry. Coastal California Type-B fault sources are modeled assuming 2/3 of the moment is released as characteristic earthquakes and 1/3 in earthquakes (fig. 23) that follow a truncated Gutenberg-Richter model from 6.5 to the maximum magnitude.

Among the most significant changes in the 2008 model was the revision of previously described "segments" of the southern San Andreas fault into 10 sections: the Parkfield, Cholame, Carrizo, Big Bend, Mojave north, Mojave south, San Bernardino north, San Bernardino south, San Gorgonio–Garnet Hill, and Coachella. These sections are defined by changes in trend, slip rate, style of faulting, or amount of displacement in past earthquakes. Sections were also revised on the San Jacinto and Elsinore faults in southern California. Slip rates were changed on sections of the San Andreas and San Jacinto faults based on recent geologic and geodetic studies suggesting that a larger part of the total slip may follow the San Jacinto rather than the southern San Andreas fault. Because there is significant uncertainty in how much of the total slip is on the San Andreas as opposed to the San Jacinto, alternative "deformation models" were developed to span the range of potential slip rates on the San Andreas and San Jacinto faults. The revised slip rates (in particular the

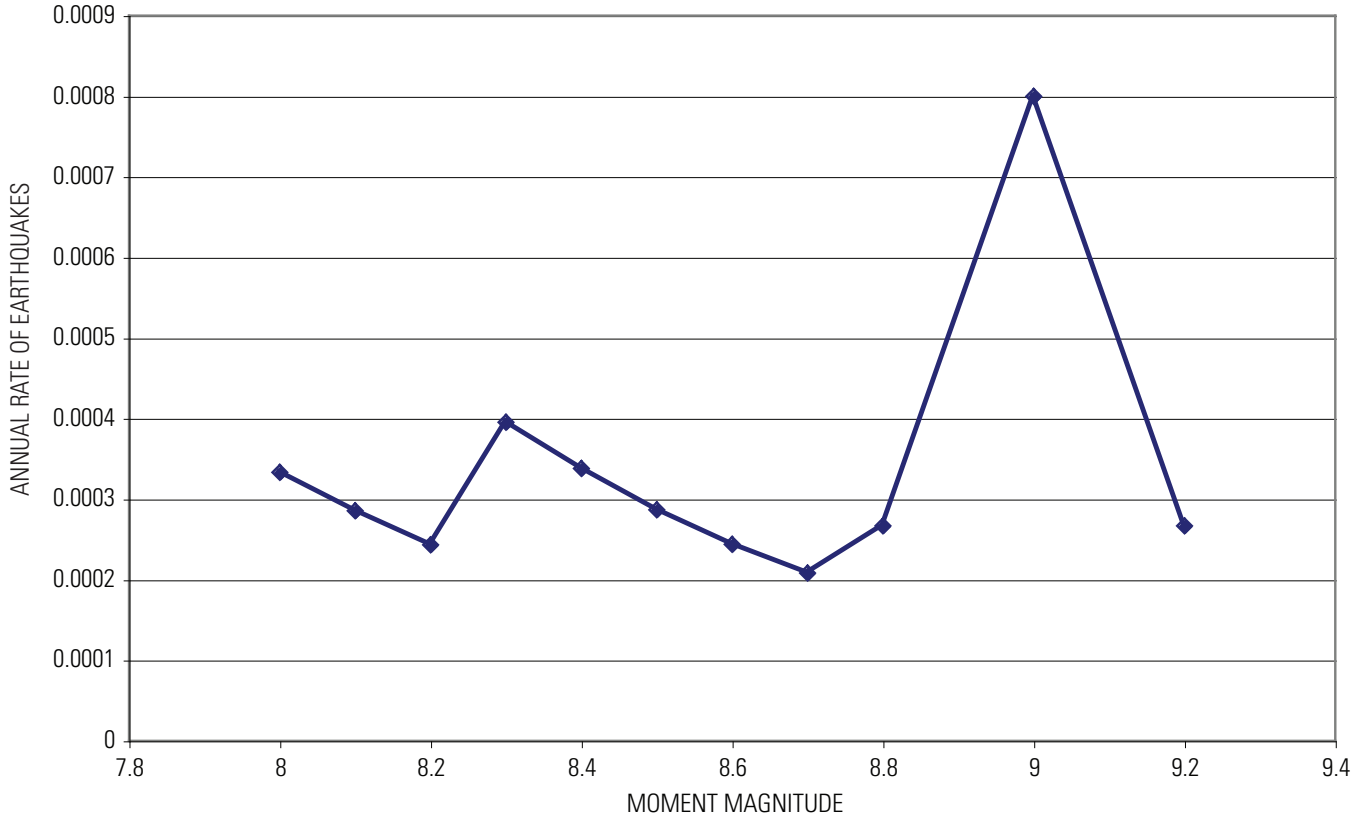

Figure 22. Magnitude-frequency distribution of the Cascadia subduction zone.

decreased slip rate on the section of the San Andreas fault through the San Gorgonio Pass) have major effects on the potential for large earthquakes to rupture multiple sections of the San Andreas fault. In addition to revised slip rates, all of the Type-A faults in southern California now have modified earthquake recurrence models based on paleoseismic data. Two different types of models were developed for California: (1) an event-rate model that honors the paleoseismic data precisely and (2) a moment-balanced model that is as consistent as possible with the event rates, while honoring the slip rates precisely. For each of these models, the magnitudes were calculated using the Ellsworth type B (Ellsworth, 2003) and Hanks and Bakun (2002) magnitude-area equations. The four resulting models are weighted equally (25 percent).

The slip rate on the San Andreas fault in San Gorgonio Pass is lower than other sections of the fault partly because some of the right-lateral shear related to the Pacific-North America plate boundary leaves the San Andreas fault near the north end of the Coachella Valley and follows right-lateral faults in a broad region across the Mojave Desert and along the east side of the Sierra Nevada. In the western Basin and Range, right-lateral faults including the Death Valley fault system accommodate approximately 8 mm/yr of right-lateral shear. South of the Garlock fault, slip rates on the faults within the eastern California shear zone were revised on the basis of recent work of Oskin and others (2007). Revision of fault slip rates and the zones of distributed shear, as previously discussed, result in a total right-lateral shear of about 8–10 mm/yr that continues from the San Andreas fault in the Coachella Valley northward across the Mojave Desert and through the western Basin and Range, which is consistent with geodetic deformation rates in the area.

For many faults in southern California, the fault traces, dips, and depth were revised using the new SCEC Community Fault Model (CFM) (Plesch and Shaw, 2003, 2007). The lower seismogenic depths in CFM are from the maximum depth of relocated background seismicity, following Nazareth and Hauksson (2004). In addition to providing more detailed information on the traces and depths of faults, the CFM provided alternative models for several areas where it is not clear how faults may interact at depth or which of two possible models of faults at depth is correct. The most complex of these models covers the Santa Barbara Channel, where one of the alternatives includes a low-angle fault that dips toward the shoreline. In this case, and possibly others, one of the alternatives may result in significantly higher ground motion than the other.

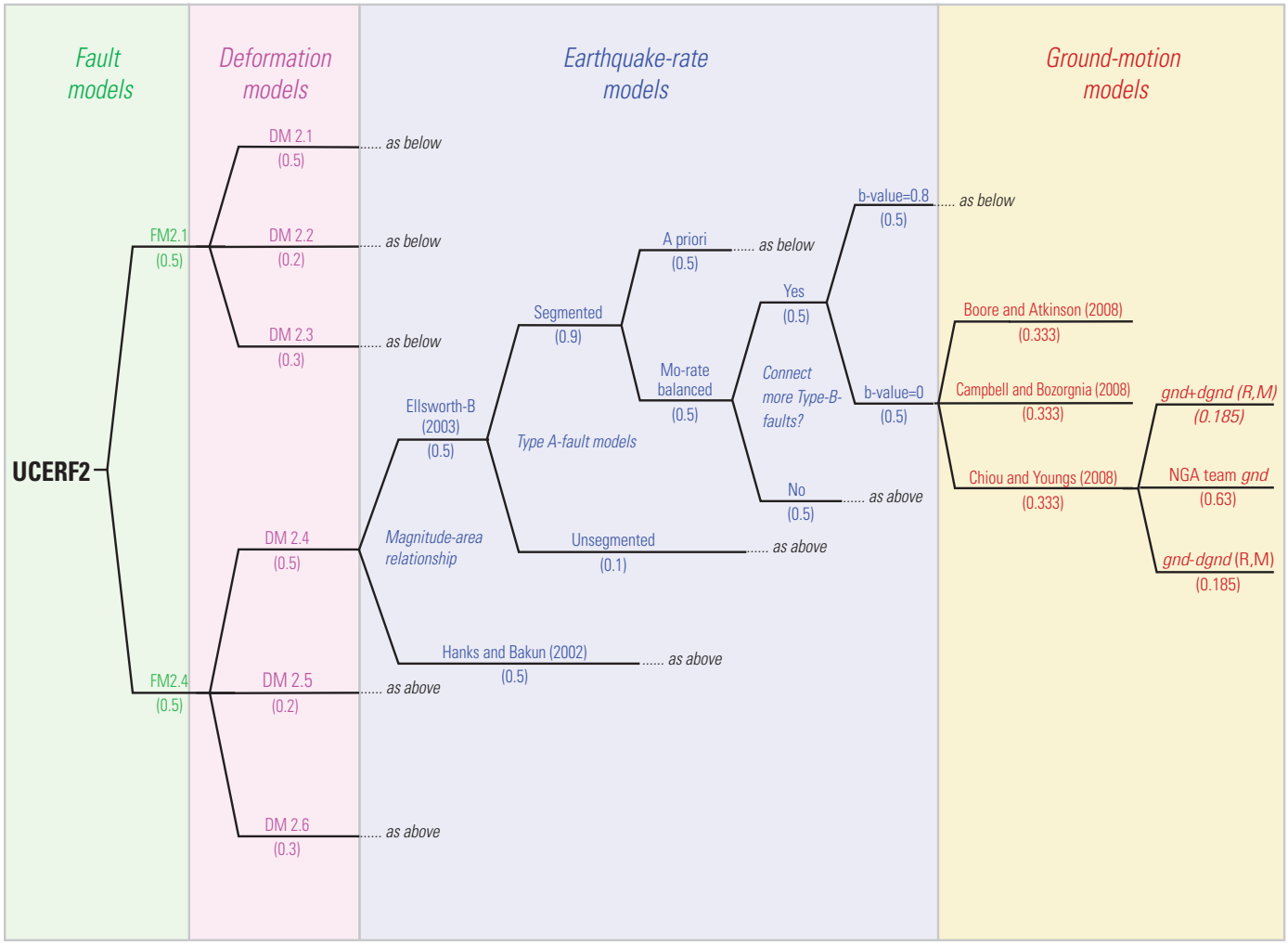

Figure 23. Logic tree for fault sources in California (UCERF2). Parameters in this table include some aleatory variability as well as depicted epistemic uncertainty. Additional aleatory variability may be associated with all models depicted. We treat aleatory variability in ground motion in the hazard code. Illustration modified from Working Group on California Earthquake Probabilities (Field and others, 2008). NGA, Next Generation Attenuation; *gnd* is the logarithm of median spectral acceleration or peak ground acceleration; *dgnd* is uncertainty in median spectral acceleration or peak ground acceleration at a given distance (R) and magnitude (M). See table 6.

In northern California, revisions since the 2002 NSHMP model are much less extensive. The location, dip, and slip rates of several faults along the west side of the southern Sacramento Valley have been updated on the basis of the work of O'Connell and Unruh (2000), and the West Tahoe fault has been added on the basis of the work of Kent and others (2005).

One of the major changes to the source model for California is that the moment rate on Type-A and B faults have been reduced by 10 percent to account for aseismic slip or aftershock slip that does not rupture in independent large earthquakes. This change reduces the rate of earthquakes in California and, with other modifications in the background seismicity and fault models, brings the California model rate of earthquakes within the estimated 95-percent confidence limits of the historical rate of earthquakes (Petersen and others, 2000; Frankel and others, 2002).

Ground-Motion Relations

We apply published ground-motion prediction equations (attenuation relations) to compute the ground motions resulting from each seismic source. The equations relate ground shaking to earthquake magnitude, distance from source, style of faulting, rupture characteristics (depth to top of rupture, hanging-wall and foot-wall shaking differences, and so forth), and ground-motion modifications along the path between the source and the site. These ground motions are typically quantified in terms of a median value and a probability distribution (aleatory variability). The ground motions are calculated for each attenuation relation separately then combined using a weighted logic tree analysis. We apply different attenuation relations for crustal, subduction-zone interface, and deep in-slab earthquakes.

Crustal Faults

The 2002 hazard maps applied up to five ground-motion prediction equations for crustal faults (Abrahamson and Silva, 1997; Boore and others, 1997; Campbell and Bozorgnia, 2003; Sadigh and others, 1997; and Spudich and others, 1999); all of these relations have been replaced by newly updated attenuation relations that are the result of Pacific Earthquake Engineering Research Center (PEER)—Next Generation Attenuation Relation Project (NGA). Results will be published in Earthquake Spectra (Power and others, 2008). The project developed a global strong-motion database containing strong-motion records from 173 earthquakes (fig. 24). Many new ground motion records were available for this effort that were not used in constructing previous equations, especially for large crustal fault ruptures. NGA modelers applied their own selection criteria for using earthquake ground motion records, but they had to justify why data was discarded and document reasons different choices were made in developing the models. Additional 1-d simulations of rock ground motions, 1-d simulations of shallow site response, and 3-d simulations of basin response were also developed to constrain the new models. NGA modelers interacted extensively with the each other and with the broader community in developing the models.

The new NGA equations differ significantly (especially at 1-s period) from previous equations. The USGS convened a workshop on NGA equations and a user workshop that gave the external community opportunities to comment on the equations and their effects on the maps. In addition to these workshops, we also convened an expert panel on strong ground motion to provide advice on implementing the NGA equations in the National Seismic Hazard Maps (September 2006). This panel felt strongly that the new hazard maps should be constructed using the new NGA equations exclusively and that additional epistemic uncertainty should be added to account for lack of data. The following is a summary of the consensus recommendations for the National Seismic Hazard Maps: (1) New NGA equations represent significant advances in fitting a larger standard dataset of ground motions and source and path parameters, and these equations should replace the older equations for crustal earthquakes in the WUS. (2) Three NGA attenuation models should be used for calculating ground motions from crustal WUS earthquake sources weighted equally: Boore and Atkinson (2008), Campbell and Bozorgnia (2008), and Chiou and Youngs (2008). (3) Additional epistemic uncertainty should be added to the equations to account for sparse data. (4) New hazard maps should not consider directivity because it is difficult to separate this effect in the current equations.

Figures 25 and 26 show plots comparing the new NGA equations and the older equations used in the 2002 maps for M6.5 and 7.5 earthquakes at 0.2-s and 1-s spectral acceleration (SA). Ground motions at 0.2-s period are similar for the new NGA and older equations for the M6.5 event. However, for earthquakes with M7.5, the new equations yield lower ground motions for three of the four relations out to distances of 100 kilometers. NGA equations for an M6.5 earthquake at 1-s period are generally lower for three of the four relations out to distances of about 20 kilometers and then are similar to the older equations at farther distances. NGA ground-shaking estimates are generally 50 percent lower for the M7.5 events out to distances of 100 kilometers. On the basis of recommendations from the expert panel on ground motions, we assign equal weights to each of the three NGA equations.

As in the previous maps, we use a reference site condition that is specified to be the boundary between NEHRP site classes B and C, with an average shear-wave velocity in the upper 30 meters of the crust of 760 m/s (as recommended by participants of the ATC/USGS workshop). The new NGA equations allow for direct calculations of ground motions for the 760 m/s shear wave velocity. In previous versions of most of the attenuation equations, it was impossible to identify the underlying shear-wave velocity that corresponded to "rock" relations. During the NGA project, the NGA modelers determined that the rock Vs30 measurements used in two of the attenuation relations averaged about 560 m/s rather than

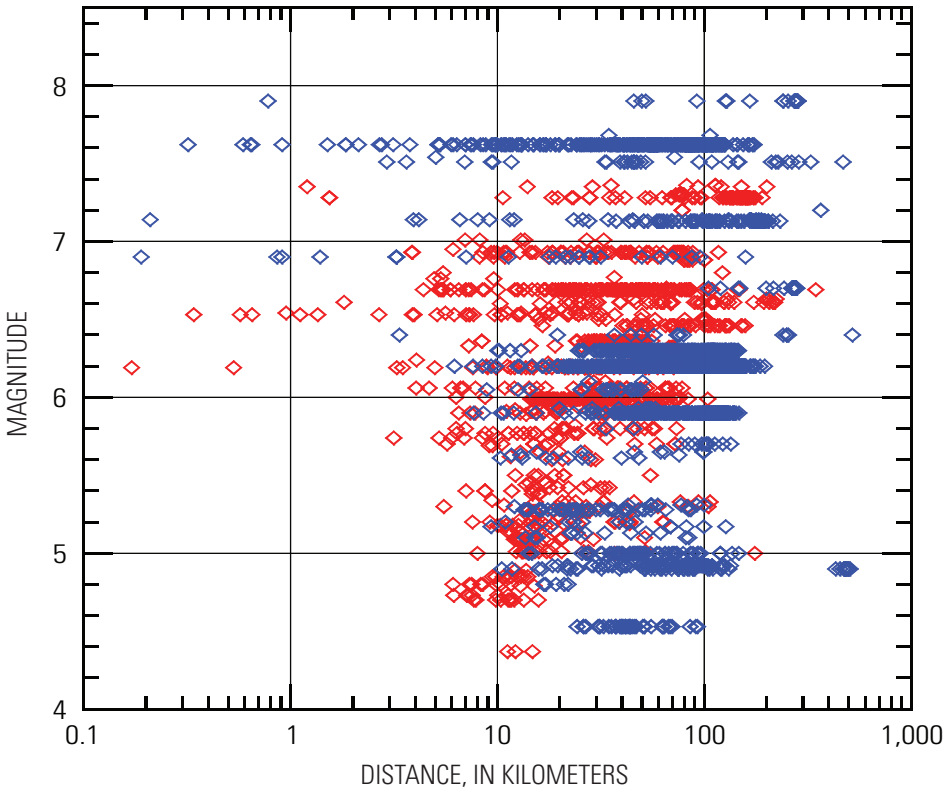

Figure 24. Pacific Earthquake Engineering Research Center (PEER) earthquake database. Red diamonds represent the previous data set and the blue diamonds represent the new data set. Illustration provided by Yousef Bozorgnia and Ken Campbell.

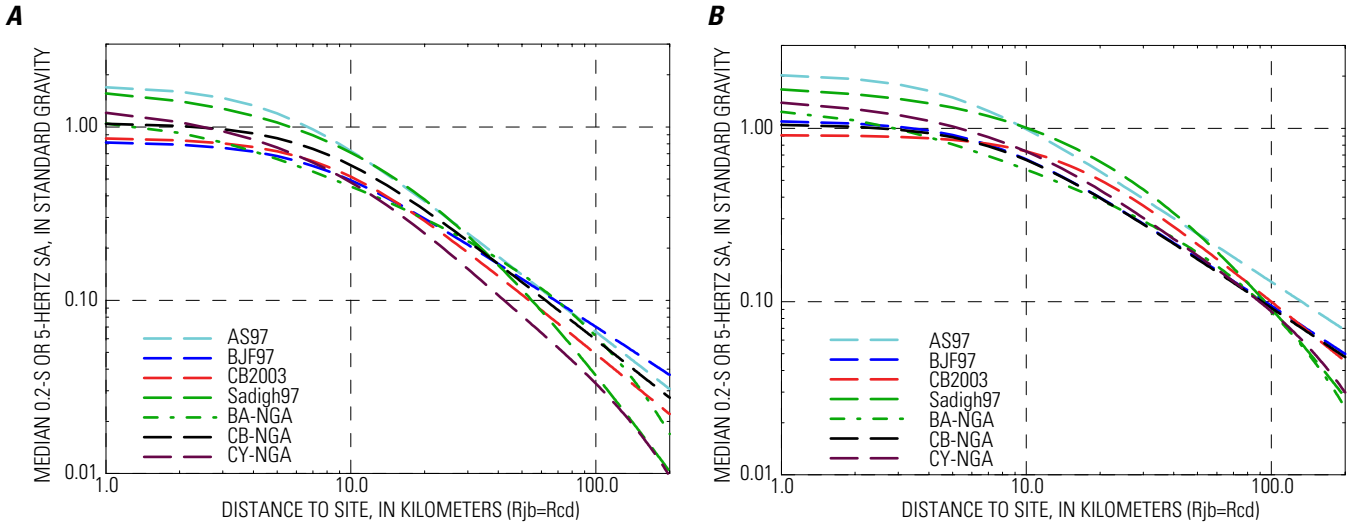

Figure 25. Western United States ground motion (0.2-s spectral acceleration) for (***A***) M6.5 earthquakes and (***B***) M7.5 earthquakes from strike-slip source at firm-rock site based on AS97 (Abrahamson and Silva, 1997), BJF97 (Boore and others, 1997), CB2003 (Campbell and Bozorgnia, 2003), Sadigh97 (Sadigh and others, 1997) BA-NGA (Boore and Atkinson, 2008), CB-NGA (Campbell and Bozorgnia, 2008), and CY-NGA (Chiou and Youngs, 2008).

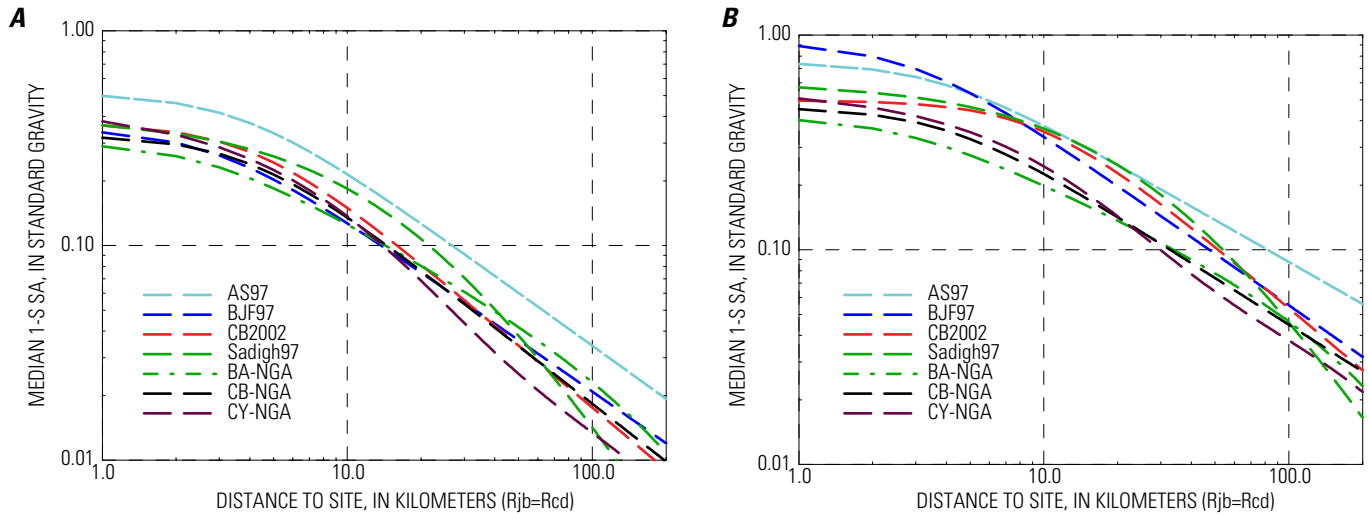

Figure 26. Western United States 1-s spectral acceleration (SA) for (***A***) M6.5 earthquakes and (***B***) M7.5 earthquakes from strike-slip source at firm-rock site based on AS97 (Abrahamson and Silva, 1997), BJF97 (Boore and others, 1997), CB2003 (Campbell and Bozorgnia, 2003), Sadigh97 (Sadigh and others, 1997) BA-NGA (Boore and Atkinson, 2008), CB-NGA (Campbell and Bozorgnia, 2008), and CY-NGA (Chiou and Youngs, 2008).

760 m/s. Therefore, the 2002 maps incorporated rock attenuation relations that were not 760 m/s, and some of the reduction in the new maps for 1-s period is due to this difference.

The NGA review panel also suggested that the national maps should incorporate additional epistemic uncertainty in the attenuation relations because of data limitations (especially for large earthquakes) and the considerable interaction between modelers. This was also discussed at the Applied Technology Council user workshop and the California regional workshop. We developed ground-motion epistemic uncertainty based on number of earthquakes in magnitude-distance bins in the NGA database. The ground-motion uncertainty is assumed to be 50 percent for M>7 and R<10 kilometers. This is an additive factor of 0.4 in log-space (90 percent confidence limits). The factors for other bins are $0.4*\sqrt{(n/N)}$ where N is the number of earthquakes recorded in another bin, and n is the number in the M≥7, R<10-kilometer bin. The other bins had uncertainties ranging from 10 percent to 50 percent. Following NGA modelers, we partitioned the source space into nine bins, three in distance and three in magnitude. Table 6 shows the number of earthquakes in each bin that two NGA modeling groups used for their ground-prediction estimation effort, and the resulting uncertainty using the square-root rule. Boore and Atkinson (2008) did not report this information in their paper. Finally, we averaged the two estimates (final column of table 6) and used this average value for the additional epistemic ground-motion uncertainty part of the hazard model. This uncertainty was applied symmetrically (that is, *gnd* + *dgnd* models were weighed equally with *gnd* – *dgnd* models, where *gnd* stands for the logarithm of median spectral acceleration or peak ground acceleration for a given ground-motion prediction model). The unmodified *gnd* model is weighted 0.63 and the *gnd* ±*dgnd* models are weighted 0.185 when the hazard curves from these three branches are added. The same *dgnd* terms are applied to all three NGA relations (Boore and Atkinson, 2008; Campbell and Bozorgnia, 2008; Chiou and Youngs, 2008) that are used with all WUS crustal sources in the hazard model.

Subduction Zone/Plate Interface

Ground motions for great Cascadia earthquakes were determined from: Youngs and others (1997), Atkinson and Boore (2003; global model), and a new equation published by Zhao and others (2006). In the 1996 and 2002 maps, we essentially followed the approach of Geomatrix Consultants, Inc. (1995) and included the Sadigh and others (1997) relations. The attenuation relations are compared in figure 27. The Sadigh and others (1997) relations were included for distances less than about 70 kilometers, to address the concern that the subduction-zone data may underestimate ground motions at close-in distances, since the data from close-in distances used in the Youngs and others (1997) relations were dominated by records from the Mexican subduction zone. At our workshops, concern was expressed about using crustal-attenuation relations for subduction-zone earthquakes (for example, Sadigh and others, 1997). In the 2008 update, we use the Zhao and others (2006) relation to essentially take the place of Sadigh and others (1997; although we apply the Zhao and others, 2006, relations at all distances). The Zhao and others (2006) relations are derived from strong-motion recordings from interface earthquakes in Japan. For distances less than about 100 kilometers, the Zhao and others (2006) relations predict

Table 6. Number of earthquakes (N) in each bin for the C&Y (Chiou and Youngs, 2008) and C&B (Cambell and Bozorgnia, 2008) attenuation relations.

M and Rrup range	N_{eq} (C&Y)	C&Y *dgnd* term	N_{eq} (C&B)	C&B *dgnd* term	Average *dgnd* term
5≤M<6,Rrup<10	24	0.22	4	0.53	±0.375
5≤M<6,10≤Rrup<30	50	0.15	15	0.27	0.21
5≤M<6, Rrup≥30	26	0.21	14	0.28	0.245
6≤M<7,Rrup<10	24	0.22	19	0.24	0.23
6≤M<7,10≤Rrup<30	26	0.21	20	0.25	0.225
6≤M<7, Rrup≥30	23	0.21	18	0.25	0.23
M≥7, Rrup<10	7	0.40	7	0.40	0.40
M≥7,10≤Rrup<30	8	0.37	9	0.35	0.36
M≥7, Rrup≥30	10	0.33	13	0.29	0.31

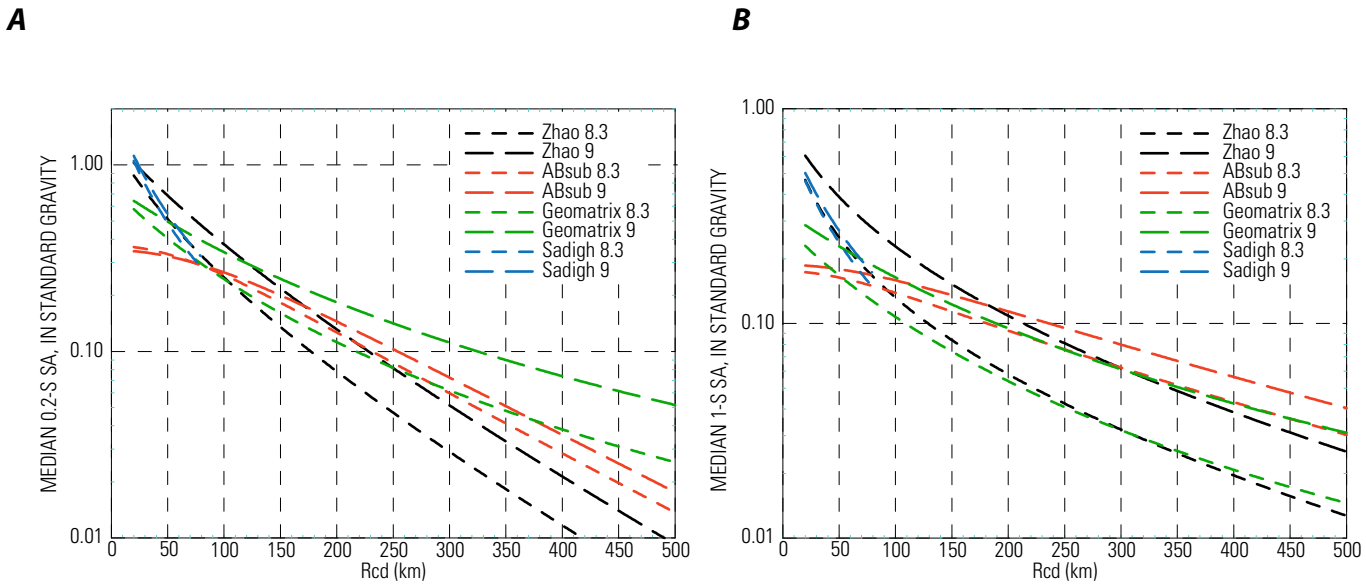

Figure 27. Plots comparing the ground-motion attenuation relations for the subduction zone interface at (***A***) 0.2-s and (***B***) 1-s spectral acceleration (SA) at firm-rock site based on Zhao 8.3 and Zhao 9, Zhao and others (2006); ABsub 8.3 and ABsub 9, Atkinson and Boore (); Geomatrix 8.3 and Geomatrix 9, Geomatrix Consultants, Inc. (1995); Sadigh 8.3 and Sadigh 9, Sadigh and others (1997).

higher ground motions than the Youngs and others (1997) and Atkinson and Boore (2003) relations.

Figure 27B shows the attenuation relations for Zhao and others (2006) along with recent data from the M8.3 Tokachi-Oki earthquake in Japan. The Zhao and others (2006) relation fits the recent data out to 250 kilometers but overpredicts the ground motions at larger distances. The overprediction at large distances may be caused by strong attenuation along the Japanese Island Arc, which may not be applicable to the case of the Cascadia subduction zone. We applied new weights to these relations giving the newest relation of Zhao and others (2006) half weight and equally distributing the remaining half weight to Youngs and others (1997) and Atkinson and Boore (2003).

Subduction Zone—In-Slab

To calculate ground motions for intermediate-depth earthquakes (depth greater than 35 kilometers), we incorporated two attenuation relations. We used the attenuation relation

by Geomatrix Consultants, Inc. (1993) with modification for depth dependence that was incorporated in the 1996 and 2002 maps. In addition, we included the Boore and Atkinson (2000) equations for intraslab earthquakes. Deep events were assumed to occur at 50-kilometer depth for the ground-motion calculations.

Results of the Seismic Hazard Calculations

To produce the National Seismic Hazard Maps, we calculated the hazard at several spectral accelerations (SA, periods 0.2, 0.3, 0.5, 0.75, 1.0, and 2.0 s) and peak horizontal ground acceleration (PGA). The hazard curves are then interpolated at 0.00211, 0.00103, and 0.00040 annual rate of exceedance to obtain the 10-percent, 5-percent, and 2-percent probability of exceedance in 50 years, respectively. The hazard model assumes Poisson (time-independent) event occurrence. Other levels can be interpolated from the hazard curves, but we caution use of these curves at low probability levels because inclusion of some very low activity faults that are omitted from the USGS source model may cause significant differences. These maps are based on uniform firm-rock site conditions defined as a site with average shear wave velocity of 760 m/s in the upper 30 meters of the crust (Vs30).

Central and Eastern United States Maps

The hazard at 2-percent probability of exceedance in 50 years in the CEUS is dominated by the New Madrid and Charleston seismic zones, but seismicity zones in eastern Tennessee and the northeast, as well as the two faults also contribute significantly. The hazard at the 2-percent probability of exceedance in a 50-year level is typically a factor of two to four higher than the 10 percent in 50-year values in the CEUS. Figures 28 to 30 show hazard maps for the CEUS at 2-percent probability of exceedance in 50 years for the 0.2- and 1-s SA and PGA, hazard values used in building codes. Figures 31 to 33 show hazard maps for the CEUS at 10-percent probability of exceedance in 50 years for the 0.2- and 1-s SA and PGA.

We made many comparisons of the 2008 and the 2002 hazard maps. Ratio maps can be found on the Web site: *http://earthquake.usgs.gov/research/hazmaps/*. The PGA and 0.2-s SA hazard at 2 percent in 50 years is lower by about 15–25 percent across much of the Northeastern United States. Near New Madrid the high-frequency ground motions are significantly lower within several kilometers of the fault and are typically lower by 2–15 percent at distances up to 1,000 kilometers from the fault. For the 1-s SA, the ground motions are decreased about 10–15 percent across much of the CEUS. Ground-motion hazards near the New Madrid Seismic Zone are lower than in 2002. In addition, the motions are also lower by 2–10 percent at distances up to 1,000 kilometers from sources. The cluster model causes the ground motions to be slightly elevated at sites to the northwest and southeast of the three modeled sources. Most of the decrease in ground motion in the hazard maps is caused by the new attenuation relations, changes to the New Madrid fault zone, and addition of magnitude uncertainties in the earthquake catalog.

Western United States Maps

The hazard at 2-percent probability of exceedance in 50 years in the WUS is controlled by the major faults described earlier in the faulting sections. The hazard at the 2-percent probability of exceedance in 50-year level is typically a factor of 1.5–2 higher than the 10 percent in 50-year values in coastal California and from 2–3.5 across the rest of the WUS. Figures 34 to 36 show hazard maps for the WUS at 2-percent probability of exceedance in 50 years for the 0.2- and 1-s SA and PGA, hazard values used in building codes. Figures 37 to 39 show hazard maps for the WUS at 10-percent probability of exceedance in 50 years for the 0.2- and 1-s SA and PGA.

Comparisons of the 2008 and the 2002 hazard maps for the WUS can also be found at the USGS National Seismic Hazard Map Web site. For high-frequency ground motions (PGA and 0.2-s SA), the ground motions are mostly within about 10 percent of the 2002 maps. The ground motions in the Pacific Northwest, coastal California (figs. 40 and 41), and the Wasatch fault regions are typically 5–10 percent higher whereas the ground motions are about 10 percent lower in areas of low seismicity. However, the changes are more substantial at longer periods (1-s SA) where ground motions have decreased by 5–30 percent in many areas of the Western United States (with the exception of rates in an area adjacent to the subduction zone, which rose by 10–20 percent). These large decreases are due primarily to changes in the attenuation relations for crustal and subduction earthquakes (including better specification of the Vs30 of 760 m/s in the attenuation equations for crustal faults), reductions in the rate of earthquakes due to magnitude-uncertainty introduced in the earthquake catalog, and source model changes.

Conclusions and Proposed Future Improvements to Maps

The 2008 National Seismic Hazard Maps represent the "best available science" based on input from scientists and engineers that participated in the update process. This does not mean that significant changes will not be made in future maps. Future earthquakes and science on earthquake recurrence and ground shaking continually improve our understanding of the seismic hazard. We plan on holding several workshops over the next several years to define uncertainties in the input parameters and to refine the methodologies used to produce

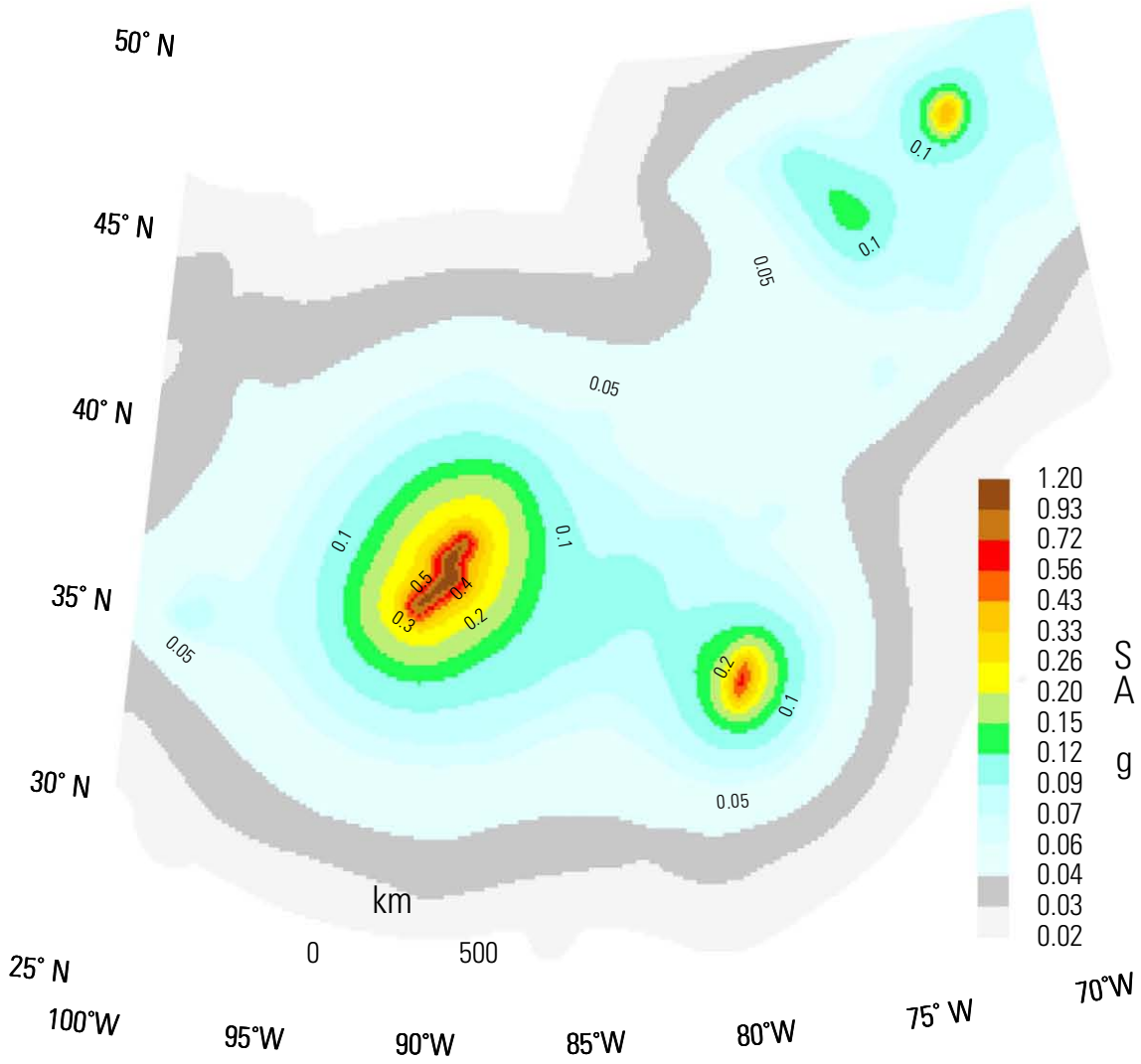

Figure 28. Map of 1-hertz spectral acceleration (SA) for 2-percent probability of exceedance in 50 years in the Central and Eastern United States in standard gravity (g).

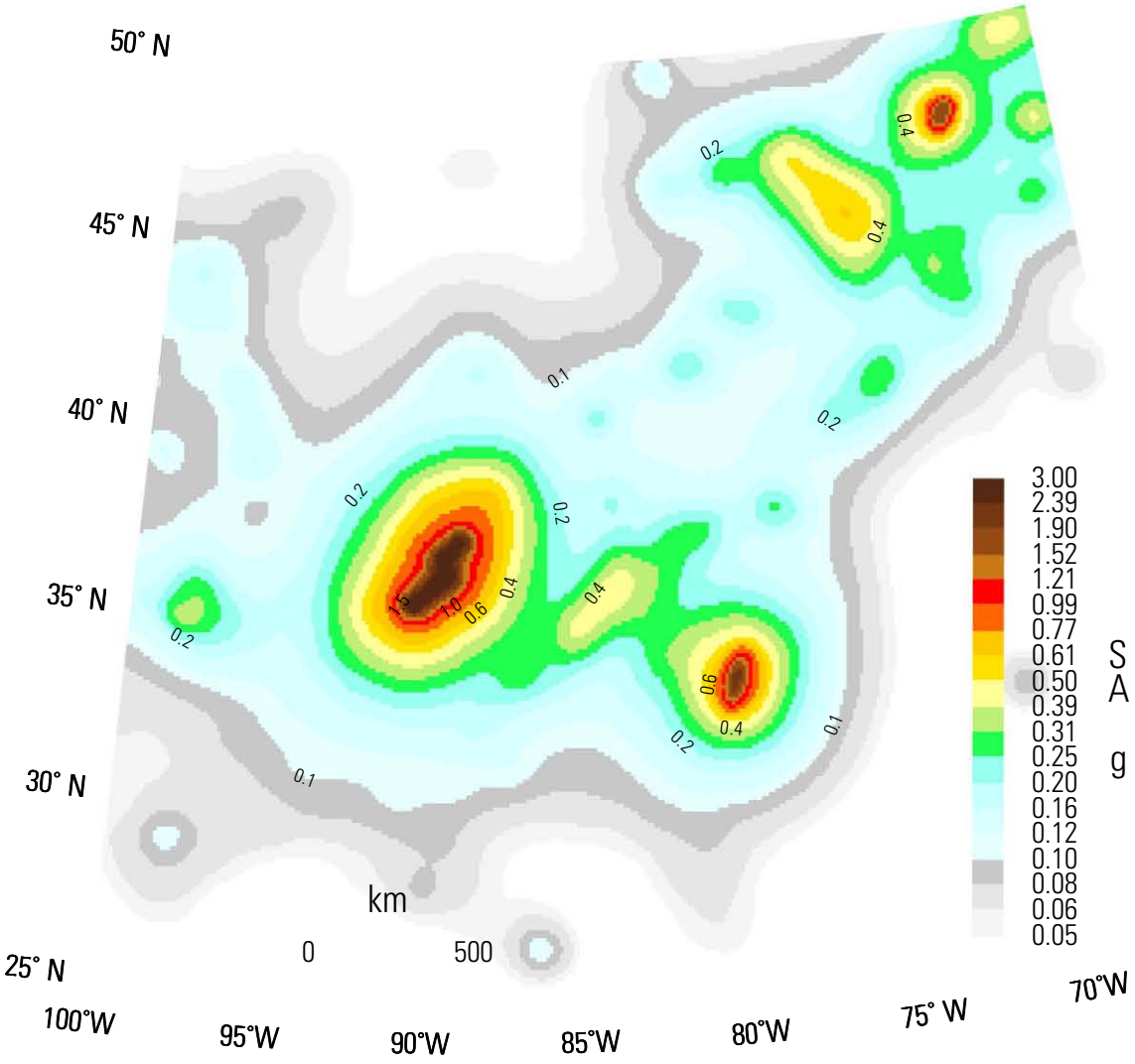

Figure 29. Map of 5-hertz spectral acceleration (SA) for 2-percent probability of exceedance in 50 years in the Central and Eastern United States in standard gravity (g).

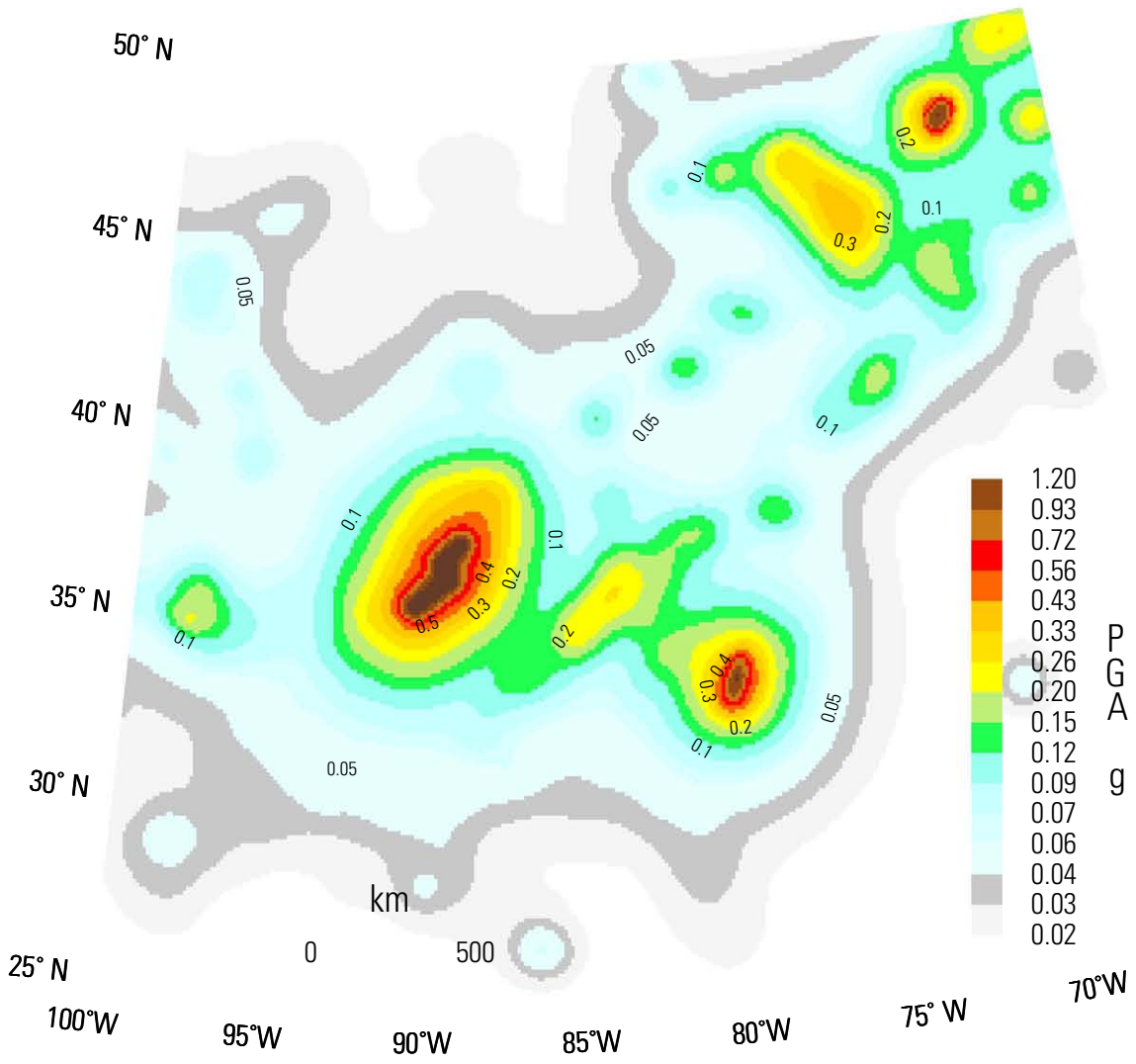

Figure 30. Map of peak ground acceleration (PGA) for 2-percent probability of exceedance in 50 years in the Central and Eastern United States in standard gravity (g).

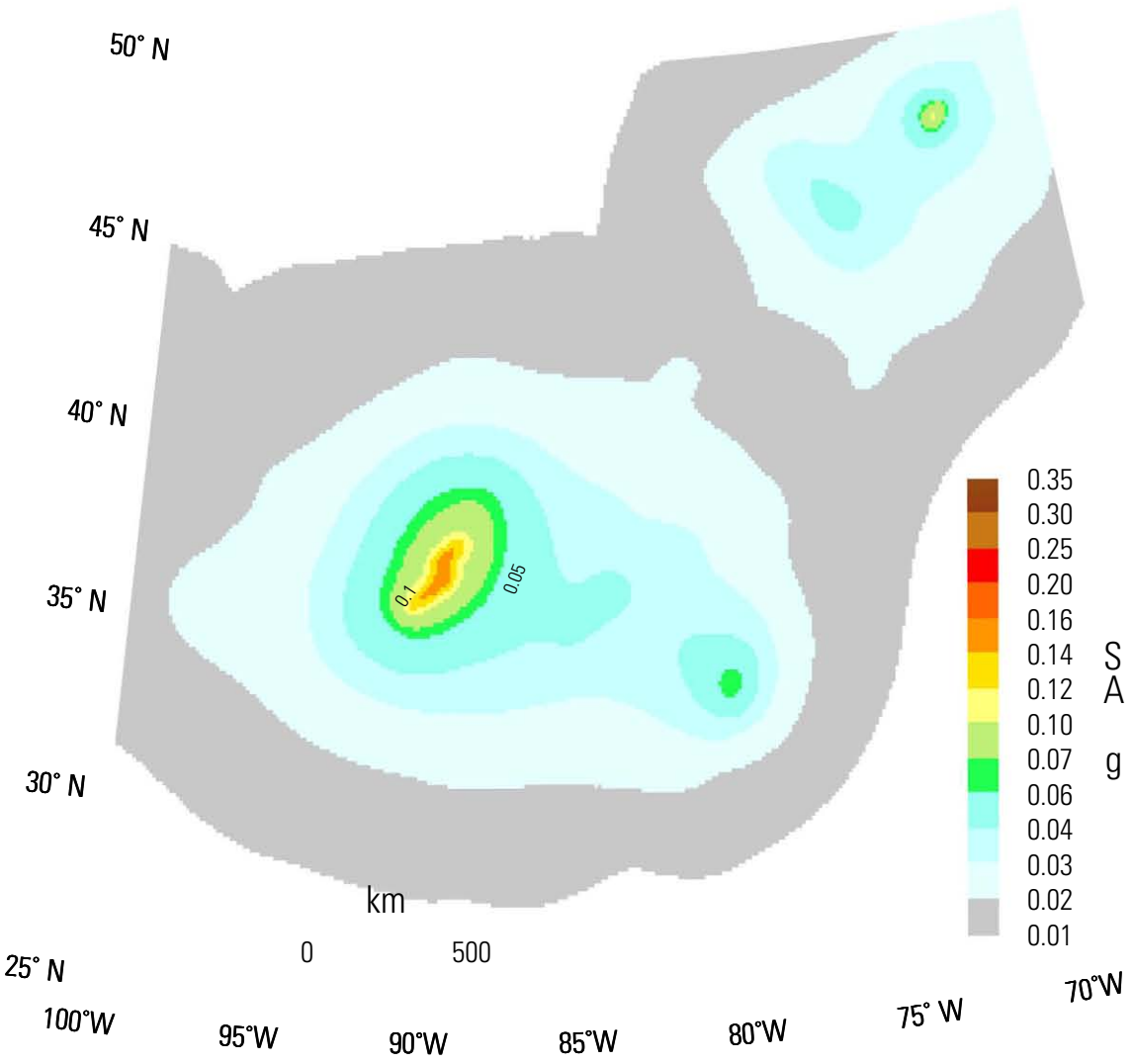

Figure 31. Map of 1-hertz spectral acceleration (SA) for 10-percent probability of exceedance in 50 years in the Central and Eastern United States in standard gravity (g).

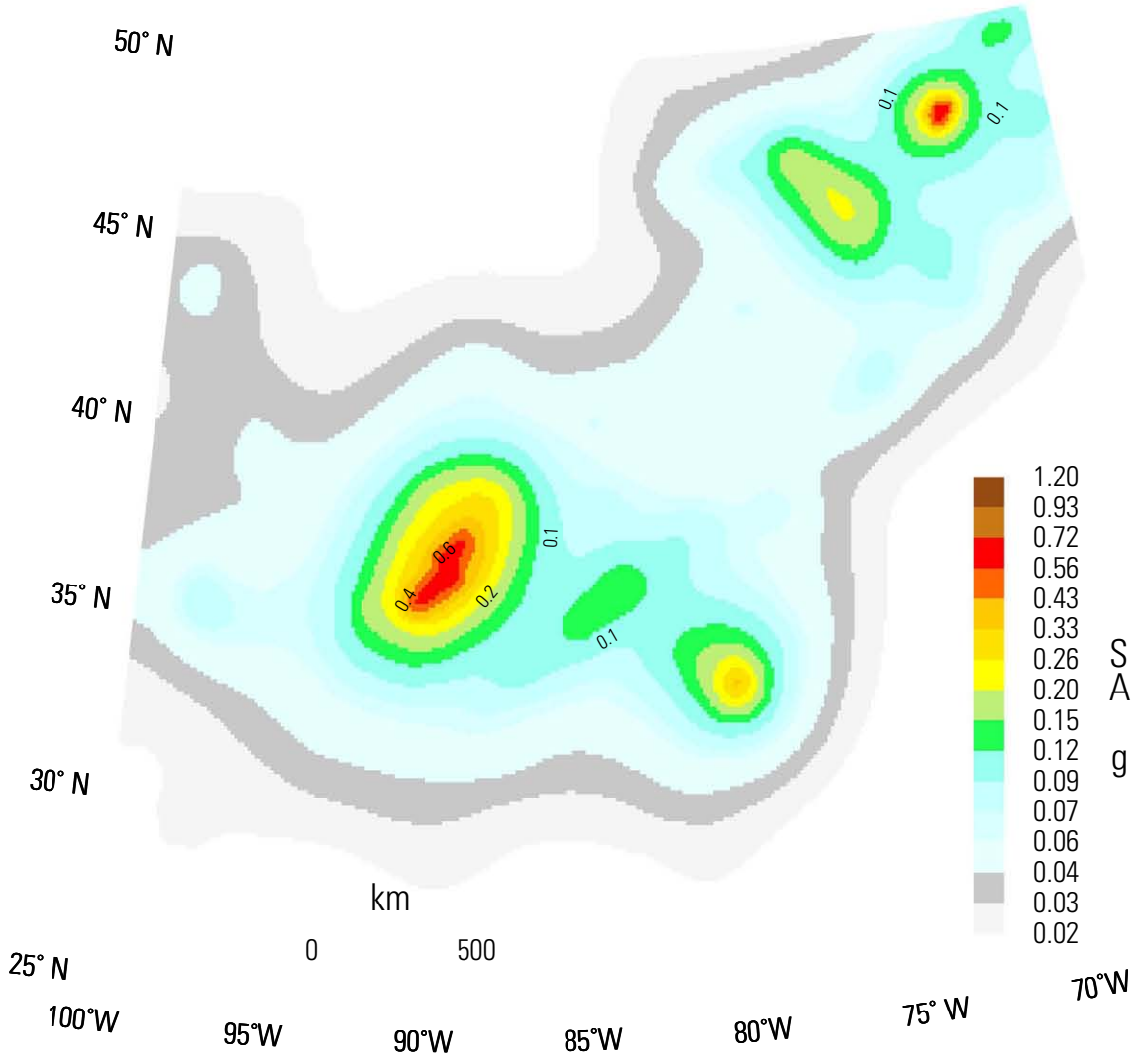

Figure 32. Map of 5-hertz spectral acceleration (SA) for 10-percent probability of exceedance in 50 years in the Central and Eastern United States in standard gravity (g).

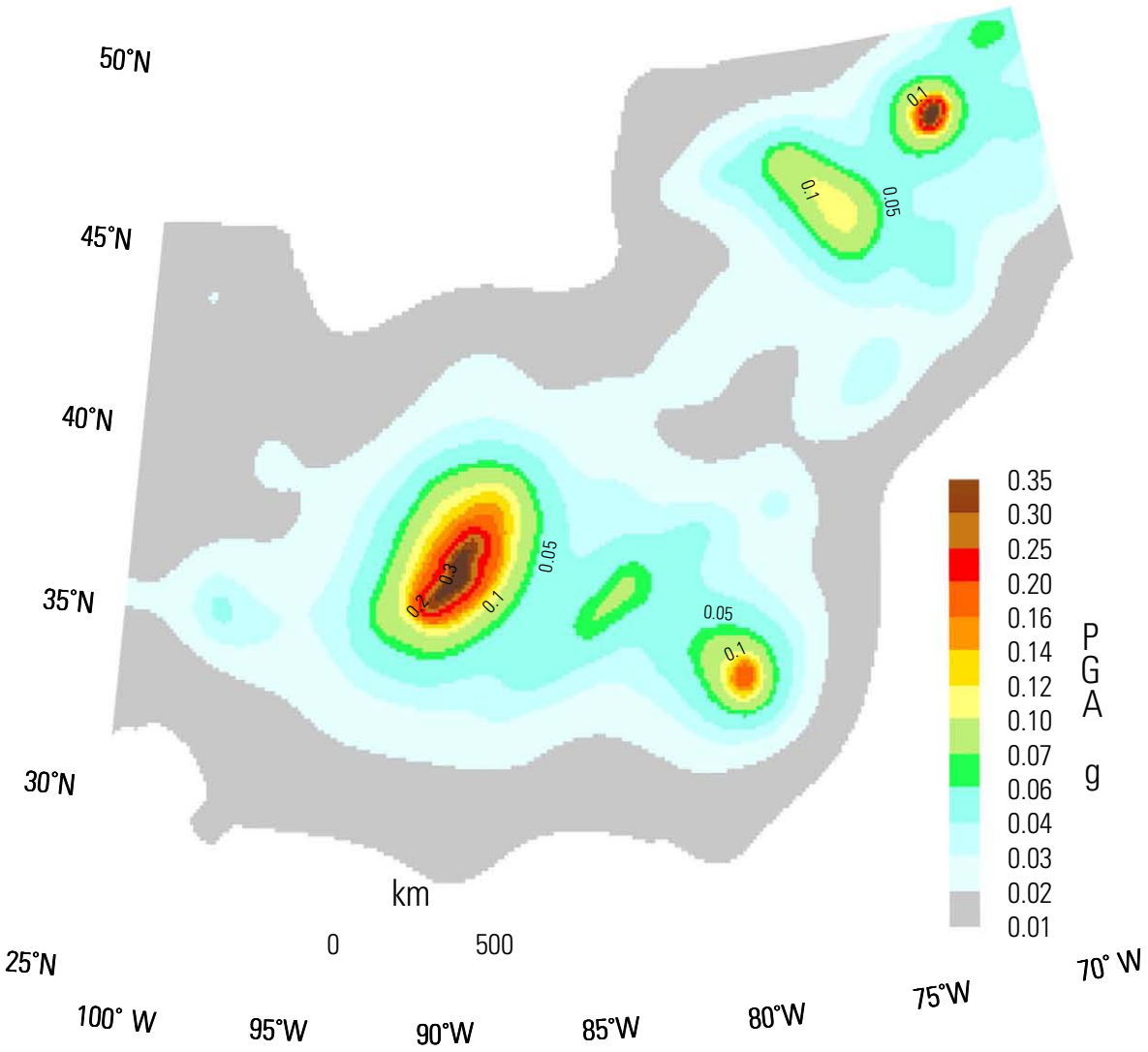

Figure 33. Map of peak ground acceleration (PGA) for 10 percent probability of exceedance in 50 years in the Central and Eastern United States in standard gravity (g).

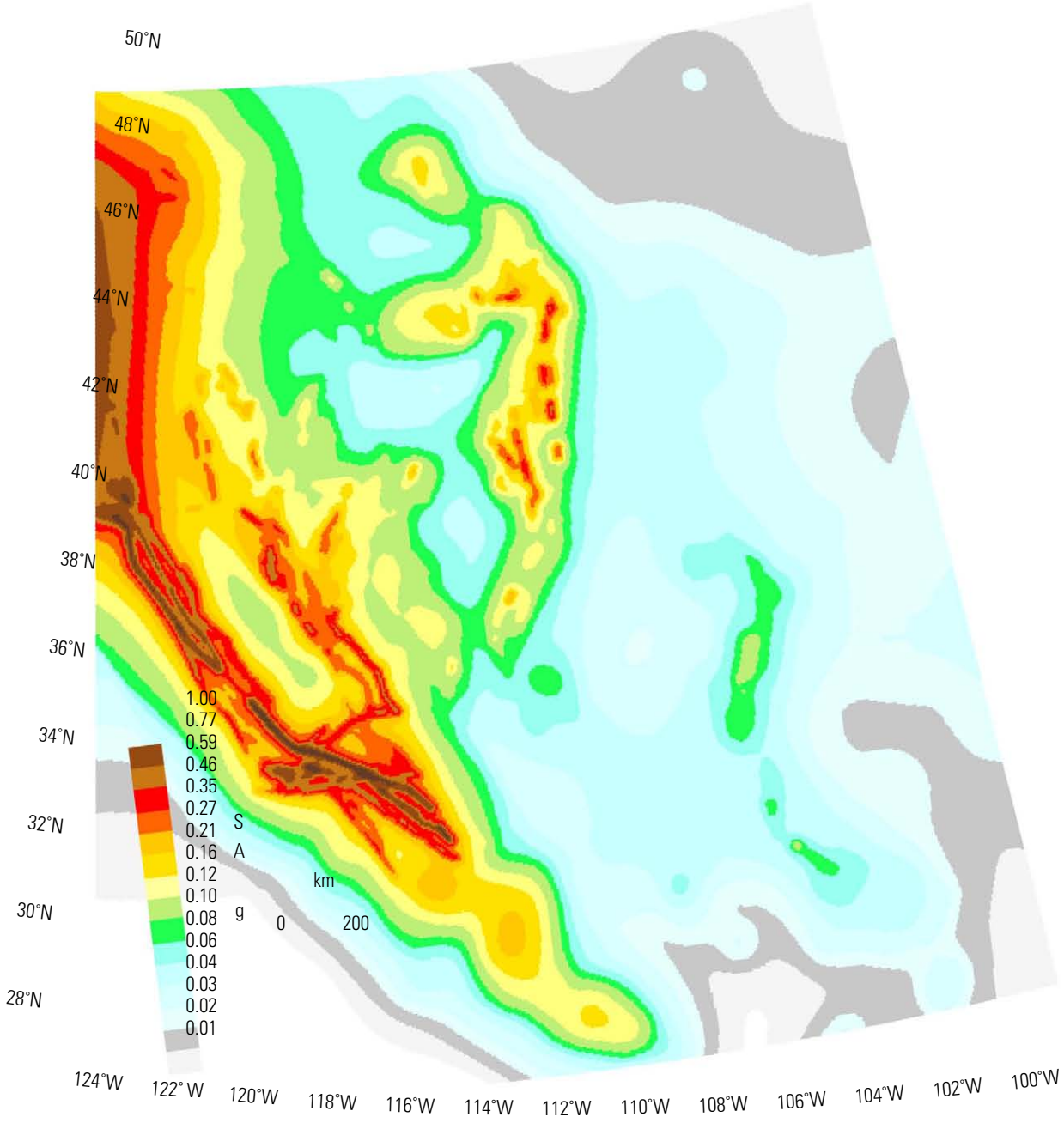

Figure 34. Map of 1-hertz spectral acceleration (SA) for 2-percent probability of exceedance in 50 years in the Western United States in standard gravity (g).

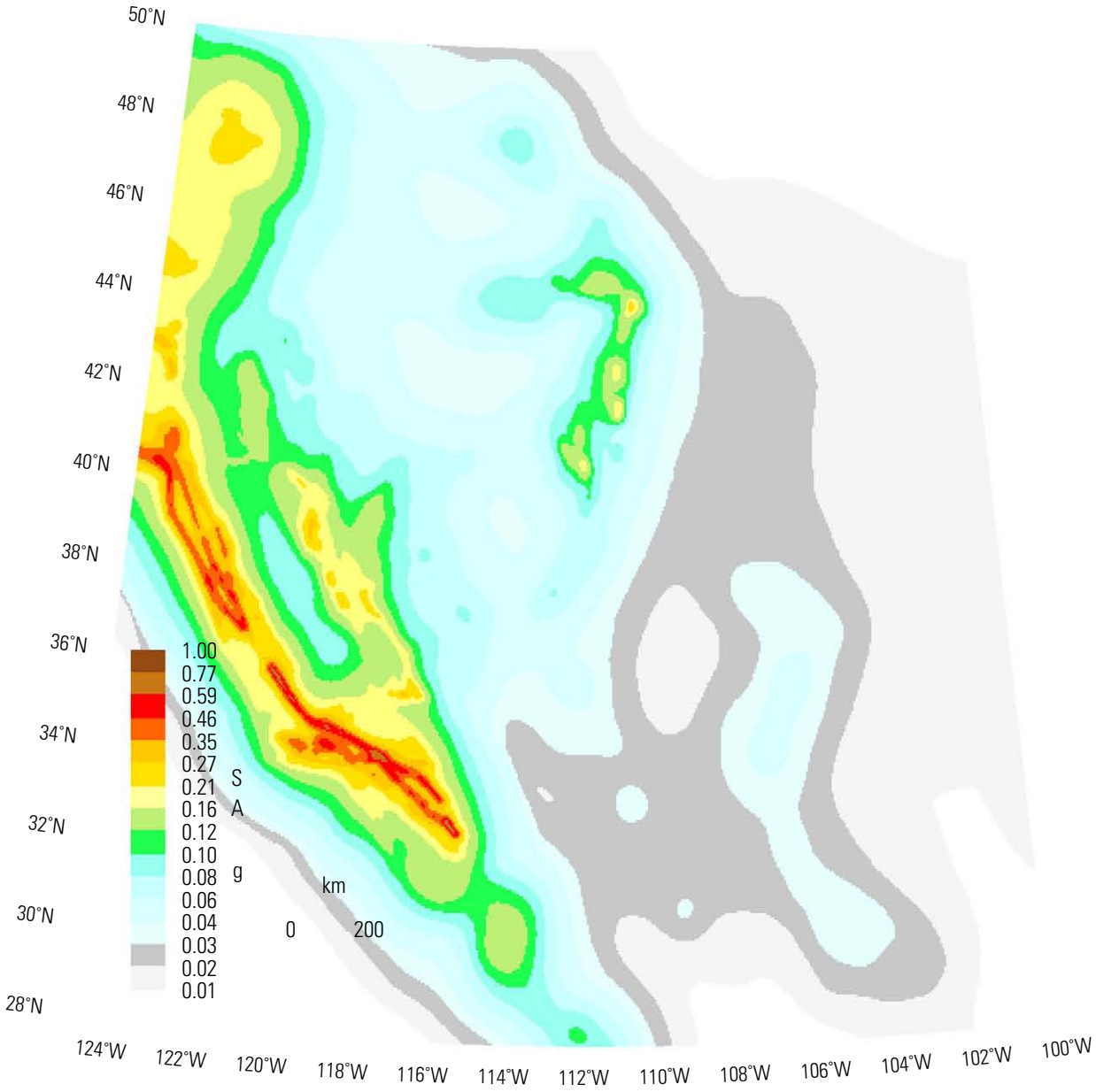

Figure 35. Map of 1-hertz spectral acceleration (SA) for 10-percent probability of exceedance in 50 years in the Western United States in standard gravity (g).

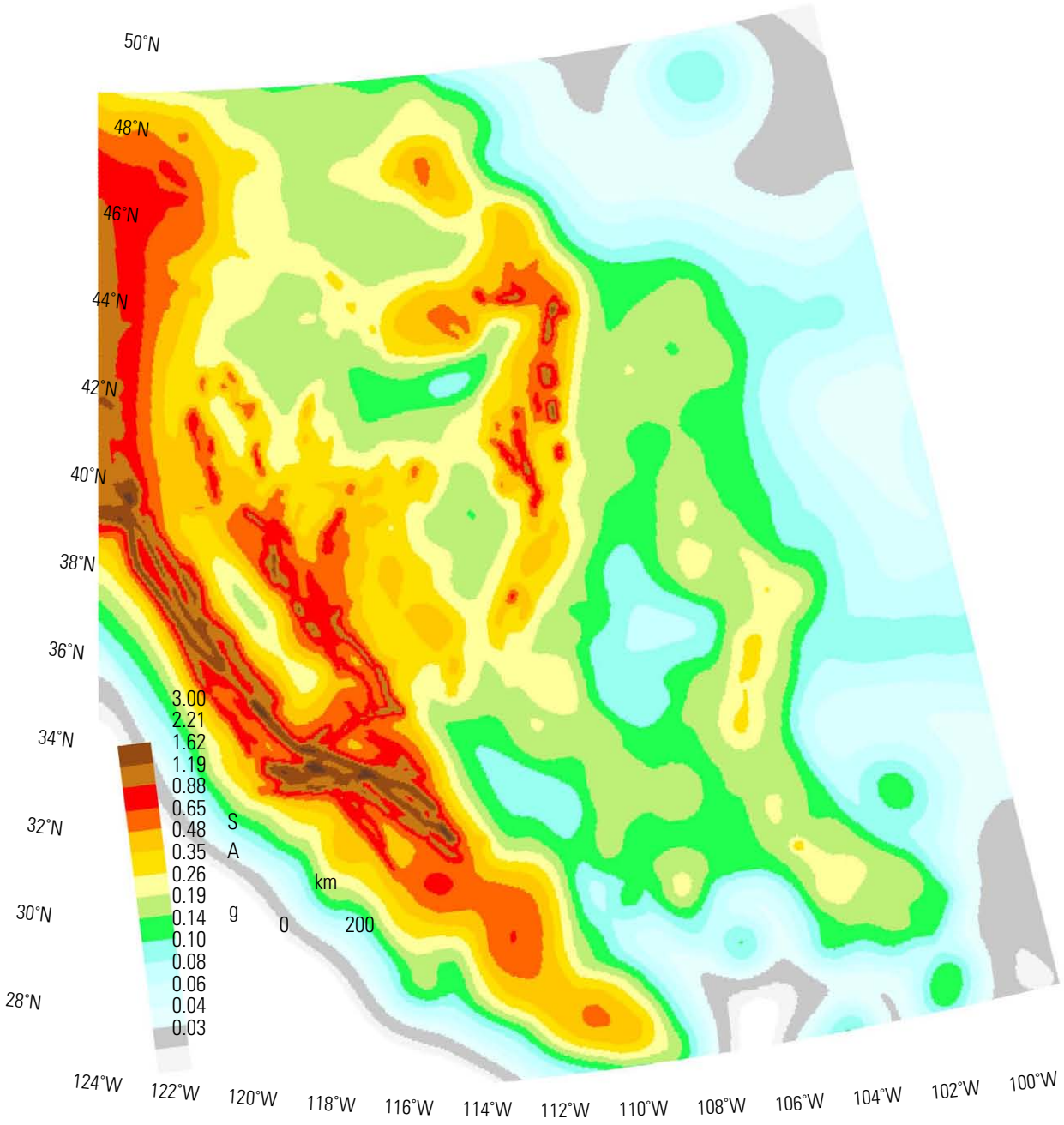

Figure 36. Map of 5-hertz spectral acceleration (SA) for 2-percent probability of exceedance in 50 years in the Western United States in standard gravity (g).

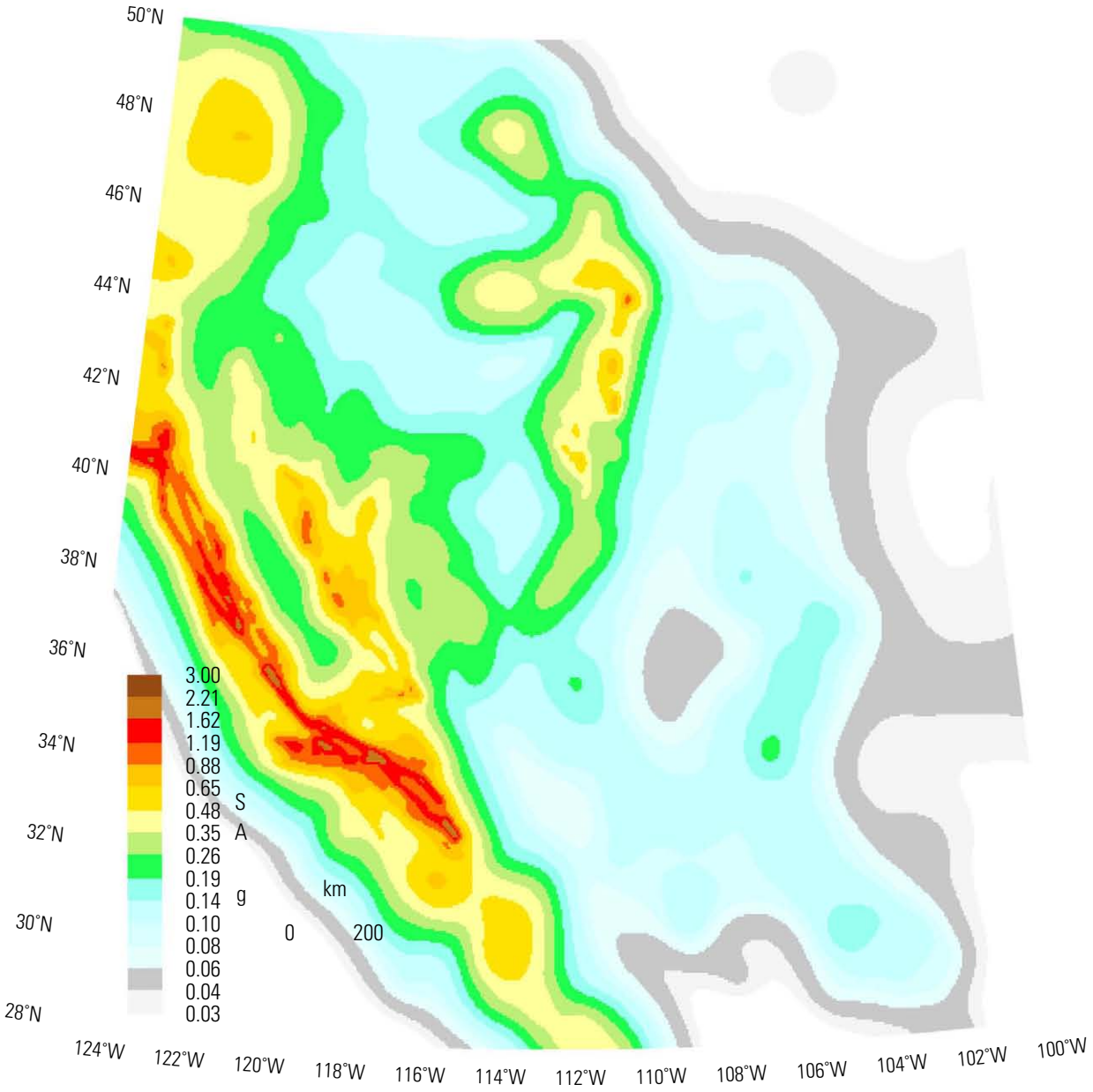

Figure 37. Map of 5-hertz spectral acceleration (SA) for 10-percent probability of exceedance in 50 years in the Western United States in standard gravity (g).

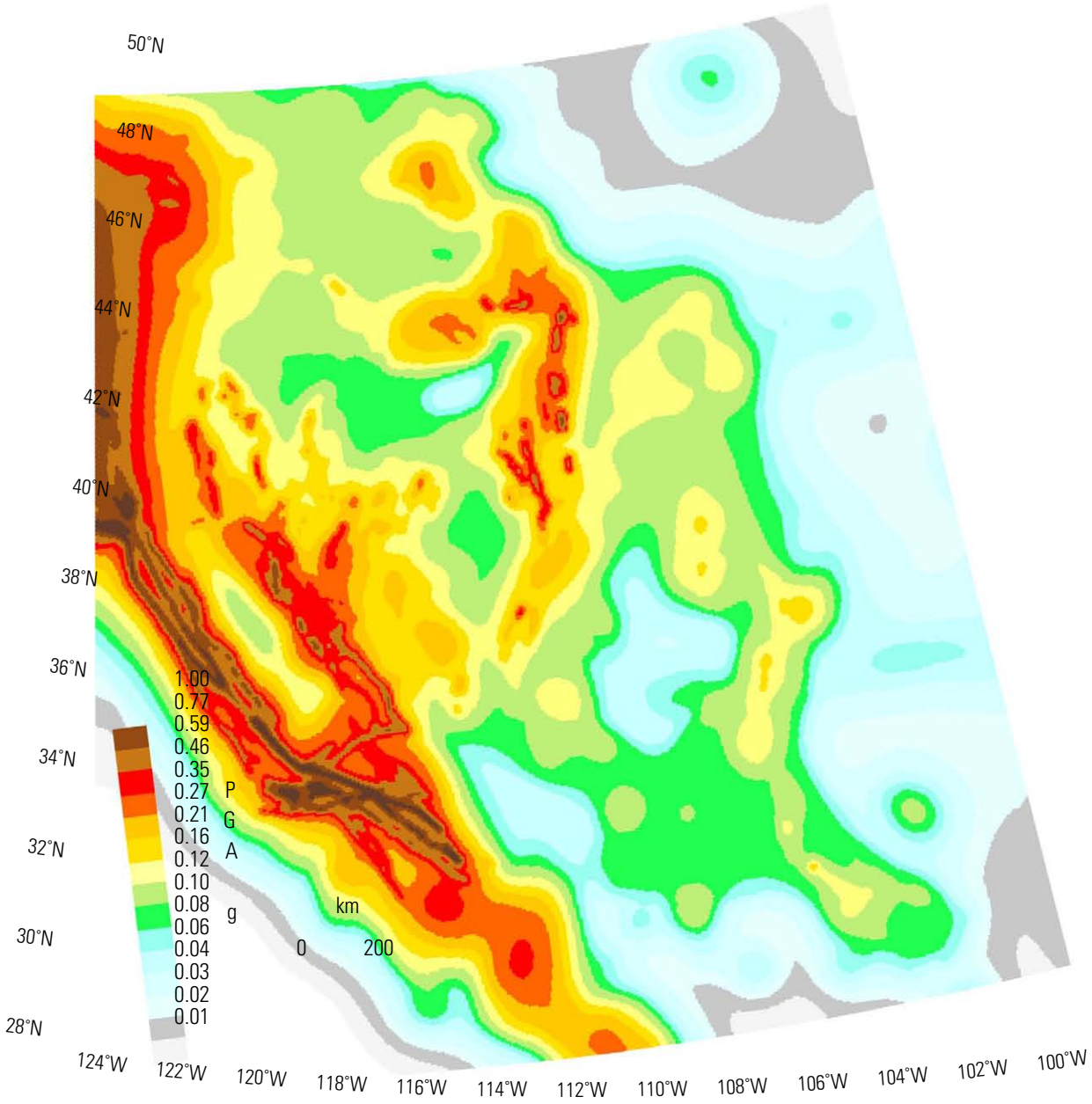

Figure 38. Map of peak ground acceleration (PGA) for 2-percent probability of exceedance in 50 years in the Western United States in standard gravity (g).

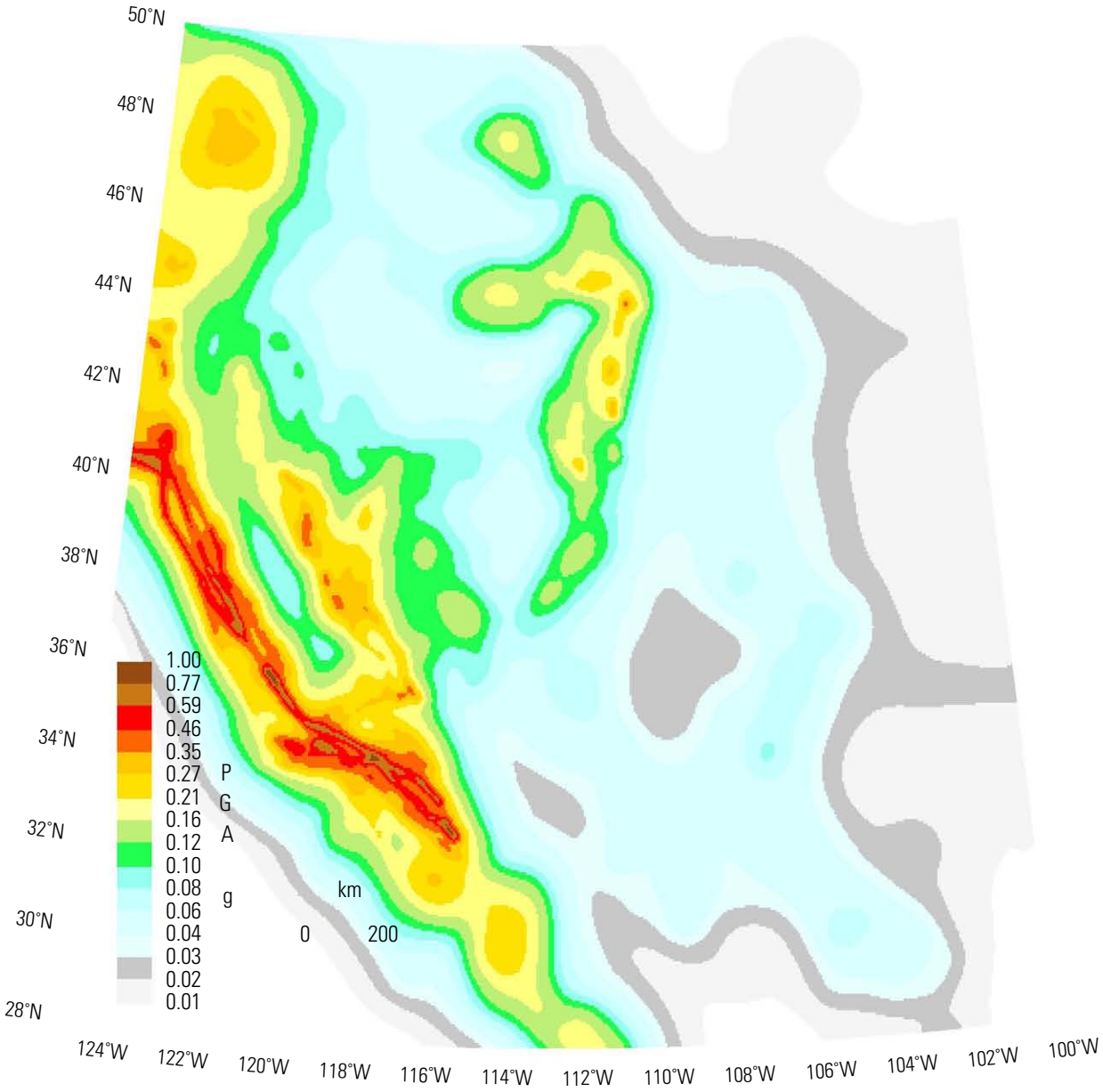

Figure 39. Map of peak ground acceleration (PGA) for 10-percent probability of exceedance in 50 years in the Western United States in standard gravity (g).

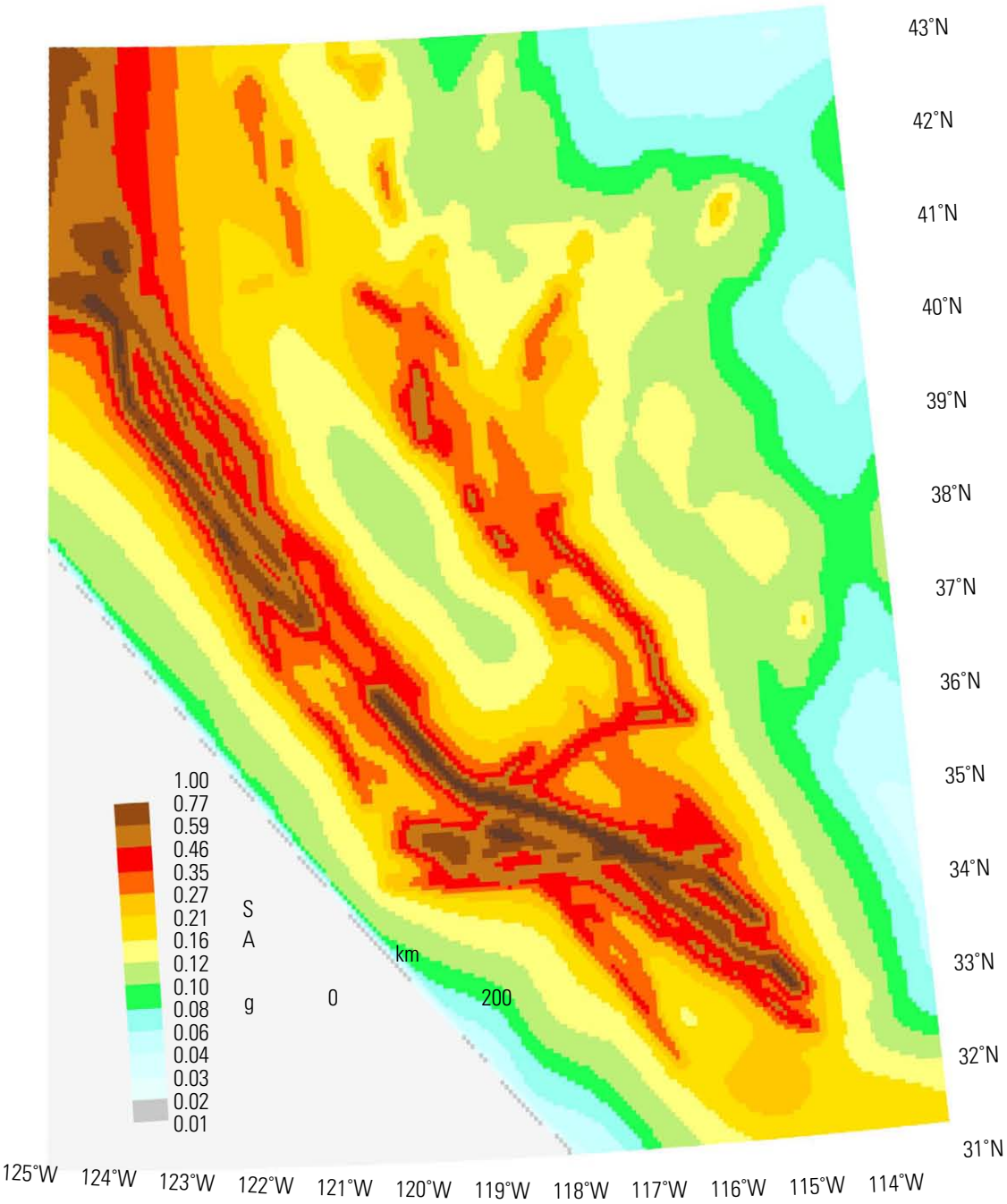

Figure 40. Map of 1-hertz spectral acceleration (SA) for 2-percent probability of exceedance in 50 years in California in standard gravity (g). Red lines are fault sources used in the model.

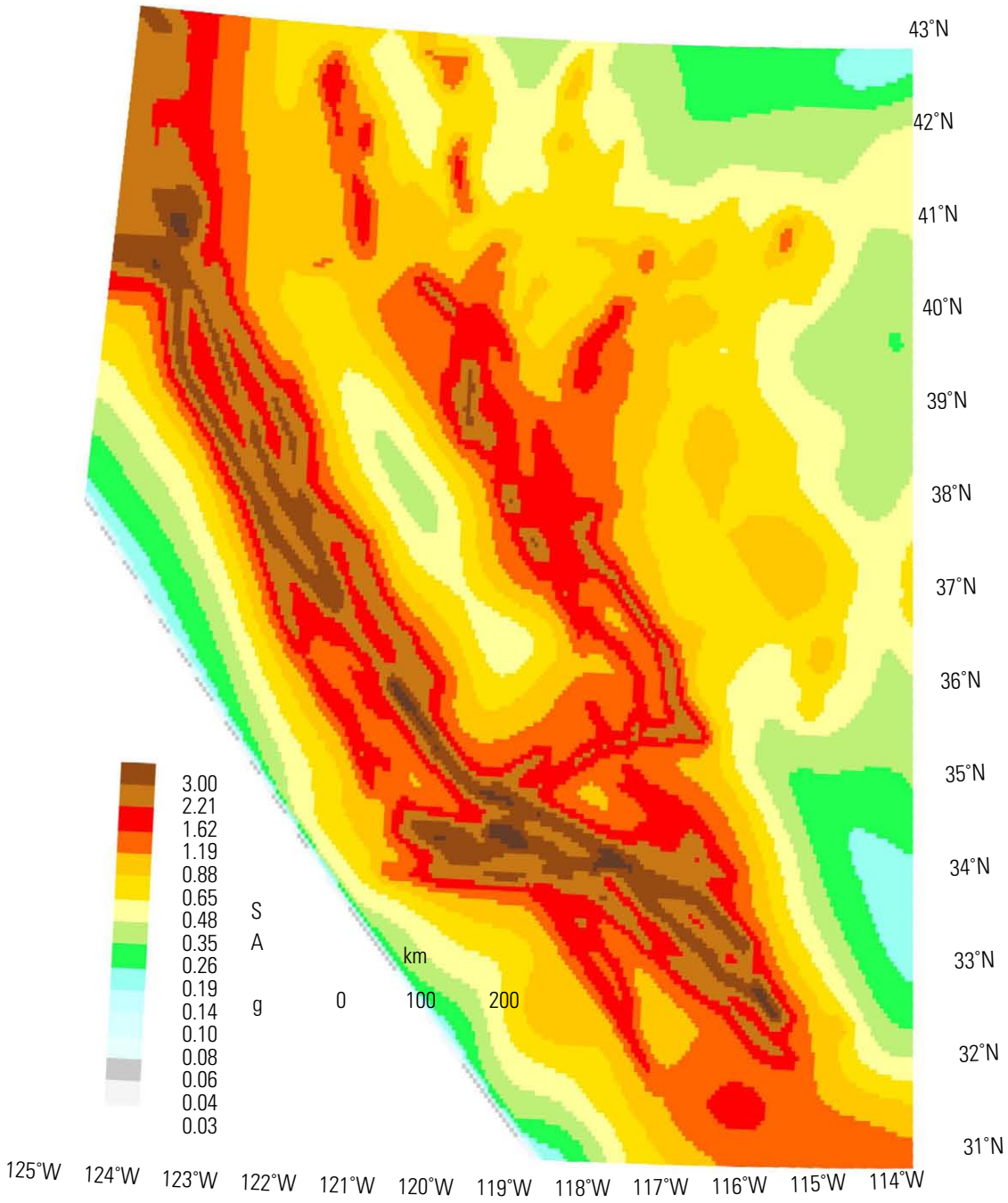

Figure 41. Map of 5-hertz spectral acceleration (SA) for 2-percent probability of exceedance in 50 years in California in standard gravity (g). Red lines are fault sources used in the model.

and distribute the hazard information. Specific recommendations for future research include:

CEUS:

1. Improve source magnitude-frequency distributions at sites across the CEUS (including M_{max}, b-values, a-values)
2. Estimate magnitude uncertainties and round-off errors, and uncertainties in rates implied in the earthquake catalog
3. Study the mechanism for earthquake generation along the New Madrid Fault Zone (understand relation of surface strain rate and paleoseismic earthquake rate)
4. Constrain the location of the Charleston, South Carolina, earthquake sources
5. Assess the range of ground shaking from earthquakes in the CEUS (consider regional tectonics and variability in stress drops, Kappa, and Q)
6. Convene workshops on CEUS issues: NGA-East ground motions, M_{max}, Charleston sources, New Madrid sources, urban hazard maps
7. Develop attenuation models for the Rocky Mountain and other transition regions.

WUS:

1. Reduce discrepancy between model and historical earthquake rates or explain differences
2. Assess fault seismic slip rates, geodetic strain rates, and paleoearthquake rates and associated uncertainties and resolve discrepancies between datasets
3. Constrain ratio of seismic and aseismic slip on faults and develop approach to routinely apply geodetic results to seismic hazard analysis
4. Continue to improve estimates of fault geometry, magnitude, and recurrence parameters (especially for urban areas)
5. Estimate the various source ruptures along faults including multisegment or multifault ruptures
6. Continue to improve models for depth of rupture
7. Assess the range of ground shaking from subduction-zone earthquakes (interface and in-slab)
8. Continue to improve crustal fault attenuation relations that include range of source parameters (for example, directivity) and path parameters (propagation effects and site amplification)
9. Incorporate sedimentary basin models and soil models into hazard studies
10. Develop time-dependent models of earthquake ruptures and determine how these should be included in future maps
11. Convene workshops and perform research on WUS issues: NGA-subduction zone, discrepancy between model and historical earthquake rates, slip rates and uncertainties, urban hazard maps

Acknowledgments

We wish to thank the hundreds of workshop participants and reviewers who made valuable suggestions that were incorporated in the maps that significantly improved the quality of this product. We give special thanks to the National Seismic Hazard Mapping Project Advisory Panel and the NGA expert panel (listed in the Introduction). We thank the National Earthquake Hazard Reduction Program (NEHRP) for funding the development of these maps. We thank Garry C. Rogers (Geological Survey of Canada) who provided a catalog of deep earthquakes beneath the Georgia Strait–Puget Sound region and Gail M. Atkinson for providing CEUS attenuation elations with different stress drops. The mapping tool GMT (Wessel and Smith, 1991) was used to create the maps.

References

Abrahamson, N.A., and Silva, W.J., 1997, Empirical response spectral attenuation relations for shallow crustal earthquakes: Seismological Research Letters, v. 68, p. 94–127.

Algermissen, S.T., and Perkins D.M., 1976, A probabilistic estimate of the maximum acceleration in rock in the contiguous United States: U.S. Geological Survey Open-File Report 76–416, 45 p., 2 pls., scale 1:7,500,000.

Algermissen, S.T., Perkins, D.M., Thenhaus, P.C., Hanson, S.L., and Bender, B.L. 1990, Probabilistic earthquake acceleration and velocity maps for the United States and Puerto Rico: U.S. Geological Survey Miscellaneous Field Studies Map MF-2120, 2 sheets, scale 1:7,500,000.

Atkinson, G.M., and Boore, D.M., 1995, Ground motion relations for eastern North America: Bulletin of the Seismological Society of America, v. 85, p. 17–30.

Atkinson, G.M., and Boore, D.M., 2003, Empirical ground-motion relations for subduction-zone earthquakes and their application to Cascadia and other regions: Bulletin of the Seismological Society of America, v. 93, p. 1703–1729.

Atkinson, G.M., and Boore, D.M., 2006, Earthquake ground-motion prediction equations for eastern North America: Bulletin of the Seismological Society of America, v. 96, p. 2181–2205.

Atwater, B.F., and Hemphill-Haley, E., 1997, Recurrence intervals for great earthquakes of the past 3,500 years at northeastern Willapa Bay, Washington: U.S. Geological Survey Professional Paper 1576, 108 p.

Bakun, W.H., and Hopper, M.G., 2004, Magnitudes and locations of the 1811–1812 New Madrid, Missouri, and the 1886 Charleston, South Carolina, earthquakes: Bulletin of the Seismological Society of America, v. 94, p. 64–75.

Behrendt, J.C., Hamilton, R.M., Ackermann, H.D., and Henry, V.J., 1981, Cenozoic faulting in the vicinity of the Charleston, South Carolina, 1886 earthquake: Geology, v. 9, p. 117–122.

Behrendt, J.C., and Yuan, A., 1987, The Helena Banks strike-slip(?) fault zone in the Charleston, South Carolina, earthquake area—Results from a marine, high-resolution, multichannel, seismic-reflection survey: Geological Society of America Bulletin, v. 98, p. 591–601.

Boore, D.M., and Atkinson, G.M., 2008, Ground-motion prediction equations for the average horizontal component of PGA, PGV, and 5%-damped PSA at spectral periods between 0.01 s and 10.0 s: Earthquake Spectra, v. 24, no. 1.

Boore, D.M., Joyner, W.B., and Fumal, T.E., 1997, Equations for estimating horizontal response spectra and peak acceleration from western North American earthquakes—A summary of recent work: Seismological Research Letters, v. 68, p. 128–153.

Campbell, K.W., 2003, Prediction of strong ground motion using the hybrid empirical method and its use in the development of ground-motion (attenuation) relations in eastern North America: Bulletin of the Seismological Society of America, v. 93, p. 1012–1033.

Campbell, K.W. and Bozorgnia, Y., 2003, Updated near-source ground-motion (attenuation) relations for the horizontal and vertical components of peak ground acceleration and acceleration response spectra: Bulletin of the Seismological Society of America, v. 93, p. 314–331.

Campbell, K.W., and Bozorgnia, Y., 2008, Ground motion model for the geometric mean horizontal component of PGA, PGV, PGD and 5% damped linear elastic response spectra for periods ranging from 0.01 to 10.0 s: Earthquake Spectra, v. 24, no. 1.

Cao, T., Bryant, W.A., Rowshandel, B., Branum, D., and Wills, C.J., 2003, The revised 2002 California probabilistic seismic hazard maps June 2003: California Geological Survey Web page *http://www.consrv.ca.gov/cgs/rghm/psha/fault_parameters/pdf/2002_CA_Hazard_Maps.pdf*.

Chiou, B., and Youngs, R., 2008, A NGA model for the average horizontal component of peak ground motion and response spectra: Earthquake Spectra, v. 24, no. 1.

Clark, M.M., 1984, Preliminary slip-rate table and map of late-Quaternary faults of California: U.S. Geological Survey Open-File Report 84–106, 12 p. pamphlet, 1 sheet, scale 1:100,000.

Cramer, C.H., 2001, A seismic hazard uncertainty analysis for the New Madrid seismic zone: Engineering Geology, v. 62, p. 251–266.

Crone, A.J., Machette, M.N., Bradley, L-A., and Mahan, S.A., 1997, Late Quaternary surface faulting on the Cheraw fault, southeastern Colorado: U.S. Geological Survey Miscellaneous Geologic Investigations I-2591, 7 p. pamphlet, 1 pl.

Ellsworth, W., 2003, Appendix D—Magnitude and area data for strike slip earthquakes, *in* Working Group on California Earthquake Probabilities, Earthquake probabilities in the San Francisco Bay region—2002–2031: U.S. Geological Survey Open-File Report 03–214, 6 p.

Engdahl, E.R., and Villaseñor, A., 2002, Global seismicity—1900–1999, *in* Lee, W.H.K., Kanamori, H., Jennings, P.C., and Kisslinger, C., eds., International handbook of earthquake and engineering seismology: International Association of Seismology and Physics of the Earth's Interior (IASPEI), p. 665–690.

Engdahl, E.R., and Rinehart, W.A., 1991, Seismicity map of North America project, *in* Slemmons, D.B., Engdahl, E.R., Zoback, M.D., and Blackwell, D.B., eds., Neotectonics of North America—Decade Map Volume 1, *in* the Decade of North American Geology: Geological Society of America, Boulder, p. 21-27.

Felzer, K., 2007, Appendix I—Calculating California seismicity rates, *in* Earthquake Rate Model 2.2 of the Working Group on California Earthquake Probabilities, *http://www.wgcep.org*.

Felzer, K., and Cao, T., 2007, Appendix H—WGCEP historical California earthquake catalog, *in* Earthquake Rate Model 2.2 of the Working Group on California Earthquake Probabilities, *http://www.wgcep.org*.

Field, E., Dawson, T., Ellsworth, W., Felzer, V., Frankel, A., Gupta, V., Jordan, T., Parsons, T., Petersen, M., Stein, R., Weldon, R., and Wills, C., 2008, The Uniform California Earthquake Rupture Forecast, Version 2 (UCERF 2): U.S. Geological Survey Open-File Report and California Geological Survey Special Report 203, 97 p.

Flück, P., Hyndman, R.D., and Wang, K., 1997, Three-dimensional dislocation model for great earthquakes of the Cascadia subduction zone: Journal of Geophysical Research, v. 102, p. 20539–20550.

Frankel, A., 1995, Mapping seismic hazard in the Central and Eastern United States: Seismological Research Letters, v. 66, p. 8–21.

Frankel, A., and Mueller, C., 2008, Calculation of the rate of M≥6.5 earthquakes for California and adjacent portions of Nevada and Mexico: U.S. Geological Survey Open-File Report 2008–1112.

Frankel, A.D., Petersen, M.D., Mueller, C.S., Haller, K.M., Wheeler, R.L., Leyendecker, E.V., Wesson, R.L., Harmsen, S.C., Cramer, C.H., Perkins, D.M., Rukstales, K.S., 2002, Documentation for the 2002 update of the National Seismic Hazard Maps: U.S. Geological Survey Open-File Report 2002–420, 39 p.

Frankel, A., Mueller, C., Barnhard, T., Perkins, D., Leyendecker, E., Dickman, N., Hanson, S., and Hopper, M., 1996, National Seismic Hazard Maps—Documentation June 1996: U.S. Geological Survey Open-File Report 96–532, 110 p.

Gardner, J.K., and Knopoff, L., 1974, Is the sequence of earthquakes in southern California, with aftershocks removed, Poissonian?: Bulletin of the Seismological Society of America, v. 64, p. 1363–1367.

Gardner, J.N., Lewis, C.J., Lavine, A., Reneau, S.L., and Schultz, E., 2005, Evaluating seismic hazards at Los Alamos National Laboratory—Geology and paleoseismology of the Pajarito fault system, Rio Grande Rift, New Mexico: Los Alamos National Laboratory Report LA-UR-05-4662, 42 p. (36 MB Microsoft Powerpoint file).

Geomatrix Consultants, Inc., 1993, Seismic margin earthquake for the Trojan site: Final unpublished report prepared for Portland General Electric Trojan Nuclear Plant, Ranier, Oregon. (Note: tables of these attenuation relationships are included in Geomatrix Consultants, 1995.)

Geomatrix Consultants, Inc., 1995, Seismic design mapping state of Oregon: Final report prepared for the Oregon Department of Transportation, Salem, Oregon.

Gregor, N.J., Silva, W.J., Wong, I.G., and Youngs, R.R., 2002, Ground-motion attenuation relationships for Cascadia subduction zone megathrust earthquakes based on a stochastic finite-fault model: Bulletin of the Seismological Society of America, v. 92, p. 1923–1932.

Gutenberg, B., and Richter, C.F., 1944, Frequency of earthquakes in California: Bulletin of the Seismological Society of America, v. 34, p. 185–188.

Hammond, W.C., and Thatcher, W., 2005, Northwest Basin and Range tectonic deformation observed with the Global Positioning System, 1999–2003: Journal of Geophysical Research, v. 110, no. B10, 12 p.

Hanks, T.C., and Bakun, W.H., 2002, A bilinear source-scaling model for M–log A observations of continental earthquakes: Bulletin of the Seismological Society of America, v. 92, p. 1841–1846.

Holbrook, J., Autin, W.J., Rittenour, T.M., Marshak, S., and Goble, R.J., 2006, Stratigraphic evidence for millennial-scale temporal clustering of earthquakes on a continental-interior fault—Holocene Mississippi River floodplain deposits, New Madrid seismic zone, USA: Tectonophysics, v. 420, p. 431–454.

Hough, S.E., Armbruster, J.G., Seeber, L., and Hough, J.F., 2000, On the Modified Mercalli intensities and magnitudes of the 1811–1812 New Madrid earthquakes: Journal of Geophysical Research, v. 105, no. B10, p. 23839–23864.

Hough, S.E., and Martin, S., 2002, Magnitude estimates of two large aftershocks of the 16 December 1811 New Madrid earthquake: Bulletin of the Seismological Society of America, v. 92, no. 8, p. 3259–3268.

Johnston, A.C., Coppersmith, K.J., Kanter, L.R., and Cornell, C.A., 1994, The earthquakes of stable continental regions: Palo Alto, California, Electric Power Research Institute, 5 v., 2,519 p., 16 folded plates, 1 diskette.

Johnston, A.C., 1996a, Seismic moment assessment of earthquakes in stable continental regions—I. Instrumental seismicity: Geophysical Journal International, v. 126, p. 381–414.

Johnston, A.C., 1996b, Seismic moment assessment of earthquakes in stable continental regions—III. New Madrid 1811–1812, Charleston 1886 and Lisbon 1755: Geophysical Journal International, v. 126, p. 314–344.

Johnston, A.C., and Schweig, E.S., 1996, The enigma of the New Madrid earthquakes of 1811–1812: Annual Review of Earth and Planetary Sciences, v. 24, p. 339–384.

Kafka, A.L., 2002, Statistical analysis of the hypothesis that seismicity delineates areas where future large earthquakes are likely to occur in the Central and Eastern United States: Seismological Research Letters, v. 73, no. 6, p. 992–1003.

Kafka, A.L., and Levin, S.Z., 2000, Does the spatial distribution of smaller earthquakes delineate areas where larger earthquakes are likely to occur?: Bulletin of the Seismological Society of America, v. 90, no. 3, p. 724–738.

Kanno, T., Narita, A., Morikawa, N., Fujiwara, H., and Fukushima, Y., 2006, A new attenuation relation for strong ground motion in Japan based on recorded data: Bulletin of the Seismological Society of America, v. 96, p. 879–897.

Kelson, K.I., and Swan, F.H., 1990, Paleoseismic history of the Meers fault, southwestern Oklahoma, and implications for evaluations of earthquake hazards in the Central and Eastern United States, *in* Weiss, A.J., ed., Seventeenth water reactor safety information meeting: Proceedings of the U.S. Nuclear Regulatory Commission NUREG/CP-0105, v. 2, p. 341–365.

Kent, G.M., Babcock, J.M., Driscoll, N.W., Harding, A.J., Dingler, J.A., Seitz , G.G., Gardner, J.V., Mayer, L.A., Goldman, C.R., Heyvaert, A.C., Richards, R.C., Karlin, R., Morgan, C.W., Gayes, P.T., and Owen, L.A., 2005, 60 k.y. record of extension across the western boundary of the Basin and Range province—Estimate of slip rates from offset shoreline terraces and a catastrophic slide beneath Lake Tahoe: Geology, v. 33, p. 365–368.

Kostrov, V.V., 1974, Seismic moment and energy of earthquakes: Izvestiya, Russian Academy of Sciences, Physics of the Solid Earth, v. 1, p. 23–44.

Lund, W.R., 2005, Consensus preferred recurrence-intervals and vertical slip-rate estimates—Review of Utah paleoseismic-trenching data by the Utah Quaternary Fault Parameters Working Group: Utah Geological Survey Bulletin 134, 114 p., *http://ugspub.nr.utah.gov/publications/bulletins/B-134.pdf*.

Lund, W.R., ed., 2006, Basin and Range Province Earthquake Working Group seismic-hazard recommendations to the U.S. Geological Survey National Seismic Hazard Mapping Program: Utah Geological Survey Open-File Report 477, 23 p., *http://geology.utah.gov/online/ofr/ofr-477.pdf*

McGuire, R.K., 2004, Seismic hazard and risk analysis: Earthquake Engineering Research Institute MNO-10, 221 p.

Mueller, C., Hopper, M., and Frankel, A., 1997, Preparation of earthquake catalogs for the National Seismic Hazard Maps—Contiguous 48 States: U.S. Geological Survey Open-File Report 97–464, 36 p.

Mueller, K., and Pujol, J., 2001, Three-dimensional geometry of the Reelfoot blind thrust—Implications for moment release and earthquake magnitude in the New Madrid seismic zone: Bulletin of the Seismological Society of America, v. 91, p. 1563–1573.

Nazareth, J.J., and Hauksson, E., 2004, The seismogenic thickness of the southern California crust: Bulletin of the Seismological Society of America, v. 94, p. 940–960.

Nishimura, C.E., Wilson, D.S., and Hey, R.N., 1984, Pole of rotation analysis of present-day Juan de Fuca plate motion: Journal of Geophysical Research, v. 89, p. 10283–10290.

O'Connell, D.R.H., and Unruh, J.R., 2000, Updated seismotectonic evaluation of faults within 10 km of Monitcello Dam, Solano Project, California: Bureau of Reclamation, Geophysics, Paleohydrology and Seismotectonics Group, Geotechnical Services, Denver, Colo., 101 p.

Oskin, M., Perg, L., Blumentritt, D., Mukhopadhyay, S., and Iriondo, A., 2007, Slip rate of the Calico fault—Implications for geologic versus geodetic rate discrepancy in the Eastern California shear zone: Journal of Geophysical Research—Solid Earth, v. 112, doi:10.1029/2006JB004451.

Pancha, A., Anderson, J.G., and Kreemer, C., 2006, Comparison of seismic and geodetic scalar moment rates across the Basin and Range Province: Bulletin of the Seismological Society of America, v. 96, p. 11–32.

Petersen, M.D., Cramer, C.H., Reichle, M.S., Frankel, A.D., and Hanks, T.C., 2000, Discrepancy between earthquake rates implied by historic earthquakes and a consensus geologic source model for California: Bulletin of the Seismological Society of America, v. 90, p. 1117–1132.

Petersen, M.D., Bryant, W.A., Cramer, C.H., Cao, T., Reichle, M.S., Frankel, A.D., Lienkaemper, J.J., McCrory, P.A., and Schwartz, D.P., 1996, Probabilistic seismic hazard assessment for the State of California: California Division of Mines and Geology Open-File Report 96–08, U.S. Geological Survey Open-File Report 96–706.

Plesch, A., and Shaw, J.H., 2003, SCEC CFM—A WWW accessible community fault model for Southern California: American Geophysical Union Fall Meeting Proceedings and Abstracts, v. 84, abstract number S12B-0395.

Plesch, A., and Shaw, J.H., 2007, Community Fault Model (CFM) for Southern California: Bulletin of the Seismological Society of America, v. 97, p. 1793–1802.

Sadigh, K., Chang, C.Y., Egan, J., Makdisi, F., and Youngs, R., 1997, Attenuation relationships for shallow crustal earthquakes based on California strong motion data: Seismological Research Letters, v. 68, p. 180–189.

Sanford, A.R., Lin, K., Tsai, I., and Jaksha, L., 1995, Preliminary listing and discussion of New Mexico earthquakes 1962–1994 with duration magnitudes of 3.0 and greater: Socorro, New Mexico Institute of Mining and Technology Geophysics Open-File Report 79.

Sanford, A.R., Mayeau, T., Schlue, J., Aster, R., and Jaksha, L., 2004, Earthquake catalogs for New Mexico and bordering areas II—1999–2004: New Mexico Tech on-line report *http://geoinfo.nmt.edu/publications/periodicals/nmg/28/n4/eqcat2004.pdf*.

Satake, K., Wang, K., and Atwater, B., 2003, Fault slip and seismic moment of the 1700 Cascadia earthquake inferred from Japanese tsunami descriptions: Journal of Geophysical Research, v. 108, 2535, doi:10.1029/2003JB002521.

Seeber, L., and Armbruster, J.G., 1991, NCEER-91 earthquake catalog: National Center for Earthquake Engineering Research Technical Report NCEER-91-0021, 110 p.

Shaw, J., Plesch, A., Planansky, G., 2004, Community Fault Model updated 1/4/04: Harvard College Geology Department, *http://structure.harvard.edu/cfm*, site accessed 5/06.

Silva, W., Gregor, N., and Darragh, R., 2002, Development of hard rock attenuation relations for central and eastern North America, internal report from Pacific Engineering, November 1, 2002, *http://www.pacificengineering.org/CEUS/Development%20of%20Regional%20Hard_ABC.pdf*

Sipkin, S.A., 2003, A correction to body-wave magnitude m_b based on moment magnitude M_w: Seismological Research Letters, v. 74, p. 739–742.

Somerville, P., Collins, N., Abrahamson, N., Graves, R., and Saikia, C., 2001, Ground motion attenuation relations for the Central and Eastern United States—Final report, June 30, 2001: Report to U.S. Geological Survey for award 99HQGR0098, 38 p.

Spudich, P., Joyner, W.B., Lindh, A.G., Boore, D.M., Margaris, B.M., and Fletcher, J.B., 1999, SEA99—A revised ground motion prediction relation for use in extensional tectonic regimes: Bulletin of the Seismological Society of America, v. 89, p. 1156–1170.

Stover, C.W., and Coffman, J.L., 1993, Seismicity of the United States, 1568–1989 (revised): U.S. Geological Survey Professional Paper 1527, 418 p.

Stover, C.W., Reagor, G., and Algermissen, S.T., 1984, United States earthquake data file: U.S. Geological Survey Open-File Report 84–225, 123 p.

Tavakoli, B**.,** and Pezeshk, S., 2005, Empirical-stochastic ground-motion prediction for eastern North America: Bulletin of the Seismological Society of America, v. 95, p. 2283–2296.

Tinti, S., and Mulargia, F., 1985, Effects of magnitude uncertainties on estimating the parameters in the Gutenberg-Richter frequency-magnitude law: Bulletin of the Seismological Society of America, v. 75, p. 1681–1697.

Toro, G.R., 2002, Modification of the Toro et al. (1997) attenuation relations for large magnitudes and short distances: Risk Engineering, Inc. report, *http://www.riskeng.com/PDF/atten_toro_extended.pdf*

Toro, G.R., Abrahamson, N.A., and Schneider, J.F., 1997, A model of strong ground motions from earthquakes in central and eastern North America—Best estimates and uncertainties: Seismological Research Letters, v. 68, p. 41–57.

Toro, G.R., and Silva, W.J., 2001, Scenario earthquakes for Saint Louis, MO, and Memphis, TN, and seismic hazard maps for the central United States region including the effect of site condition: Technical report to U.S. Geological Survey, Reston, Virginia, under Contract 1434-HQ-97-GR-02981, *http://www.riskeng.com/PDF/Scen_CEUS_Rept.pdf*.

Tuttle, M.P., Schweig, E.S., Sims, J.D., Lafferty, R.H., Wolf, L.W., and Hayes, M.L., 2002, The earthquake potential of the New Madrid seismic zone: Bulletin of the Seismological Society of America, v. 92, p. 2080–2089.

Tuttle, M.P., Schweig, E.S., III, Campbell, J., Thomas, P.M., Sims, J.D., Lafferty, R.H., III, 2005, Evidence for New Madrid earthquakes in A.D. 300 and 2350 B.C.: Seismological research leters, v. 76, p. 489–501.

Utsu, T., 2002, Relationships between magnitude scales, *in* Lee, W.H.K., Kanamori, H., Jennings, P.C., and Kisslinger, C., eds., International handbook of earthquake and engineering seismology: International Association of Seismology and Physics of the Earth's Interior (IASPEI), p. 733–746.

Weichert, D.H., 1980, Estimation of the earthquake recurrence parameters for unequal observation periods for different magnitudes: Bulletin of the Seismological Society of America, v. 70, p. 1337–1356.

Wells, D.L., and Coppersmith, K.J., 1993, Likelihood of surface rupture as a function of magnitude [abs.]: Seismological Research Letters, v. 64, p. 54.

Wells, D.L., and Coppersmith, K.J., 1994, New empirical relationships among magnitude, rupture length, rupture width, and surface displacements: Bulletin of the Seismological Society of America, v. 84, p. 974–1002.

Wessel, P., and Smith, W.H.F., 1991, Free software helps map and display data: EOS Transactions, American Geophysical Union, v. 72, no. 441, p. 445–446.

Wheeler, R.L., 1995, Earthquakes and the cratonward limit of Iapetan faulting in eastern North America: Geology, v. 23, p. 105–108.

Wheeler, R.L., and Cramer, C.H., 2002, Updated seismic hazard in the southern Illinois Basin—Geological and geophysical foundations for use in the 2002 USGS National Seismic-Hazard Maps: Seismological Research Letters, v. 73, p. 776–791.

Wheeler, R.L., and Frankel, A., 2000, Geology in the 1996 USGS seismic-hazard maps, Central and Eastern United States: Seismological Research Letters, v. 71, p. 273–282.

Wheeler, R.L., and Perkins, D.M., 2000, Research, methodology, and applications of probabilistic seismic-hazards mapping of the Central and Eastern United States—Minutes of a workshop on June 13–14, 2000, at Saint Louis University: U.S. Geological Survey Open-File Report 2000-0390, 18 p.

Wills, C.J., Weldon, R.J., II, and Bryant, W. A., 2008, California fault parameters for the National Seismic Hazard Maps and Working Group on California Earthquake Probabilities, Appendix A, in Field, E., Dawson, T., Ellsworth, W., Felzer, K., Frankel, A., Gupta, V., Jordan, T., Parsons, T., Petersen, M., Stein, R., Weldon, R., and Wills, C., 2008, The Uniform California Earthquake Rupture Forecast, Version 2 (UCERF 2): U.S. Geological Survey Open-File Report and California Geological Survey Special Report 203, 51 p.

Working Group on California Earthquake Probabilities, 2003, Earthquake probabilities in the San Francisco Bay region—2002–2031: U.S. Geological Survey Open-File Report 03-214.

Youngs, R.R., Chiou, S.J., Silva, W.J., and Humphrey, J.R., 1997, Strong ground motion attenuation relationships for subduction zone earthquakes: Seismological Research Letters, v. 68, p. 58–73.

Zhao J.X., Zhang, J., Asano, A., Ohno, Y., Oouchi, T., Takahashi, T., Ogawa, H., Irikura, K., Thio, H., Somerville, P., Fukushima, Y., and Fukushima, Y., 2006 Attenuation relations of strong ground motion in Japan using site classification based on predominant period: Bulletin of the Seismological Society of America, v. 96, p. 898–913.

Zoback, M.L., 1992, First- and second-order patterns of stress in the lithosphere—The World Stress Map Project: Journal of Geophysical Research, v. 97, no. B8, p. 11703–11728.

Appendixes A-K

Appendix A. Depth To The Top Of Rupture (*Ztor*) For Western United States Faults

By Stephen C. Harmsen and Yuehua Zeng

Several attenuation relations include terms as a function of depth to top of rupture (*Ztor*) in addition to the effect of geometric spreading. We discuss *Ztor* for two source specifications: (1) mapped Quaternary faults and (2) background seismicity.

(1) All Quaternary faults in the hazard model have specified depth to top of fault. Most of these have tops at the Earth's surface, and this (large) subset is the one we discuss now. In the 1996 and 2002 probabalistic seismic hazard analysis for the National Seismic Hazard Maps, all fault ruptures were modeled to fill the rupture width. Now, however, we attempt to produce a reasonable distribution of depths to top of rupture in our hazard model. The *Ztor* distribution is as follows. All characteristic-source scenarios continue to rupture over the entire fault width. Gutenberg-Richter scenarios, however, have a down-dip distribution of *Ztor* as shown in table A-1.

Currently, the Gutenberg-Richter distribution has a lower magnitude limit of 6.5. All fault sources with M≤6.5, because they are characteristic, rupture the entire fault width, as do all sources, characteristic or Gutenberg-Richter, with M>7.0. Thus, our implementation of down-dip rupture tops on Quaternary faults is confined to the Gutenberg-Richter part of the model, with magnitude range 6.5 to 7.0. For the special case of the creeping section of San Andreas fault, having a Gutenberg-Richter distribution of magnitude with magnitude from 6.0 to 6.7, the model excludes the possibility of non-zero *Ztor*.

(2) For background (gridded) hazard, that is, for sources for which no faults are identified, *Ztor* is currently fixed at 5.0 kilometers for M<6.5 sources, and *Ztor* is 1.0 kilometer for M>6.5 sources. Hazard from all such sources is, therefore, affected by nonsurface-rupture terms in several of the Next Generation Attenuation (NGA) ground-motion prediction models. For the dip-slip portion of background seismicity, an additional hanging-wall term (which is a function of *Ztor* and other parameters) is included for two of the Next Generation Attenuation (NGA) models. Figure A-1 shows the depth to top of rupture for all available earthquakes in the NGA database. The average *Ztor* is 1.0 kilometer for M<6.5 and 5.0 for 6.5<M<7.0, respectively. This is consistent with our current assumption on *Ztor* for M<6.5 and M>6.5 sources, respectively. The average *Ztor* for earthquakes with M>7.0 is about 0.0 kilometers in the NGA database. Since the background hazard is not related to any surface rupture, we decided to fix those M>7.0 events to *Ztor*=1.0.

Campbell and Bozorgnia (2006) suggested using surface rupture relative to magnitude probabilities proposed by Wells and Coppersmith (1993). Figure A-2 shows this distribution and shows an approximate graph of the expected distribution of

Table A-1. Depth to top of rupture.

Magnitude range	Pr [*ztor*=0]	Pr [*ztor*=2 km]	Pr [*ztor*=4 km]
6.5≤M≤6.75	0.333	0.333	0.333
6.75<M≤7.0	0.5	0.5	0
7.0 < M	1.0	0	0

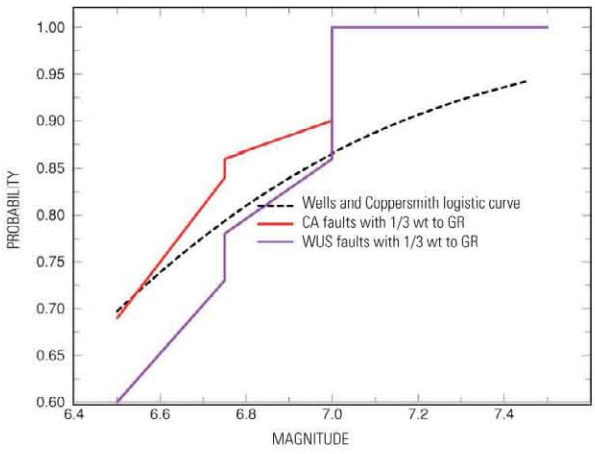

Figure A-1. Plot of probability of surface rupture relative to magnitude.

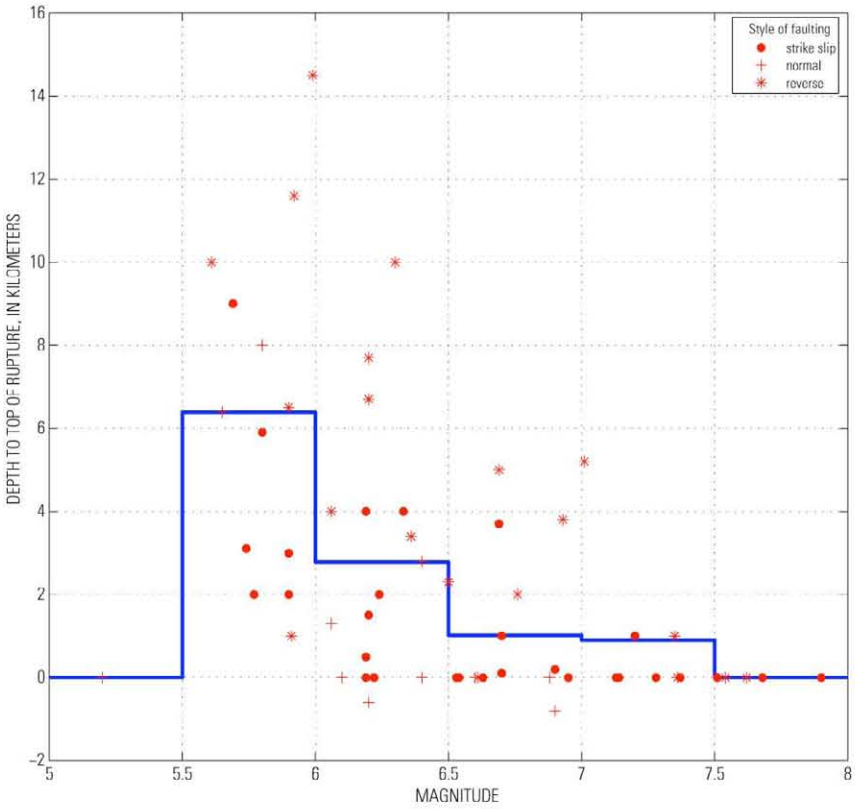

Figure A-2. Plot of depth to top of rupture relative to magnitude for all available earthquakes in the Next Generation Attenuation database.

Ztor for fault sources with M_{char} in the 6.5 to 7.0 range in our current implementation. This graph is approximate because there are complications associated with the epistemic and aleatory range of magnitudes associated with any given M_{char}. However, figure A-2 illustrates several features of the current model.

(1) For lower magnitudes, the probability of nonsurface rupturing is greater than for higher magnitudes.

(2) The probability of surface rupture increases as the weight applied to Gutenberg-Richter distribution decreases.

(3) There are two magnitudes, at M6.75 and M7.0, where the probability of surface rupture increases substantially.

The relative positions of the colored curves compared to the Wells and Coppersmith (1993) distribution will vary depending on the value of M_{char} and other details.

The above discussion pertained to faults that crop out on the Earth's surface. The growing inventory of blind thrusts (for example, those of the Great Valley, San Fernando Valley, and elsewhere in California) in the Quaternary fault database may need to be included when comparing our model with the Wells and Coppersmith (1993) distribution or other proposed distributions of depth of surface rupture.

One feature of the Wells and Coppersmith (1993) distribution that is not in our current Western United States fault model is the significant probability (greater than 10 percent) of nonsurface rupturing M>7 earthquakes on faults that crop out at the Earth's surface. Whether such events should be included in the seismic hazard model is a topic of current debate.

References

Campbell, K.W. and Bozorgnia, Y., 2006, Campbell-Bozorgnia NGA empirical ground motion model for the average horizontal component of PGA, PGV, PGD, and SA at selected periods ranging from 0.01–10.0 seconds, Pacific Earthquake Engineering Research Center report, ver. 1.0, October 2006.

Wells, D.L. and Coppersmith, K.J., 1993, Likelihood of surface rupture as a function of magnitude [abs.]: Seismological Research Letters, v. 64, p. 54.

Appendix B. Fault Distances to Nonplanar Fault

By Yuehua Zeng

In the 2008 update of the National Seismic Hazard Maps, the Joyner-Boore (JB) distance and closest fault distance to a nonplanar fault were developed. We defined the nonplanar fault based on the approach of Zeng and Chen (2001). The fault model is constructed by extending the surface trace of a multisegment rupture fault down a dipping direction based on the average strike for the fault. The average strike of the fault is obtained by taking the strike of the line connecting the first point with the last point of the surface trace. Mathematically, it is implemented by assuming x_0 and y_0 as the location of a given point on the fault-surface trace. By defining the origin of the coordinate at the first point of the fault trace, the direction of the x-axis is given by the vector connecting the first point with the last point of the fault trace. The y-axis is perpendicular to the x-axis along the surface projection of the average dip direction. For any point on the fault plane, its coordinate is given by

$$\begin{aligned} x &= x_0, \\ y &= y_0 + d * \cos(\delta), \\ z &= d * \sin(\delta) \end{aligned} \qquad (1B)$$

where d is the distance along the dip direction, and δ is the dip angle. Equation (1B) extends a multisegment fault trace along the free surface to a nonplanar fault plane at depth. Although the real fault structure at depth could differ, we assume that the fault model given in (1B) is sufficient to represent the earthquake rupture plane unless further evidence or data become available.

For a buried fault, we can revise equation (1B) to

$$\begin{aligned} x &= x_0, \\ y &= y_0 + d * \cos(\delta), \\ z &= d_0 + d * \sin(\delta) \end{aligned} \qquad (2B)$$

where d_0 is the depth to the top of the fault, and x_0 and y_0 are the location of a given point on the fault top.

In the previous multisegment fault model used in 1996 and 2002 National Seismic Hazard Maps, each segment bases the dip direction along the strike perpendicular to the segment. Such defined fault segments will fan out or pinch inward at the connecting point of those segments (fig. B-1). The current fault overcomes this problem and provides a continuous extending fault plane (fig. B-2). Each fault

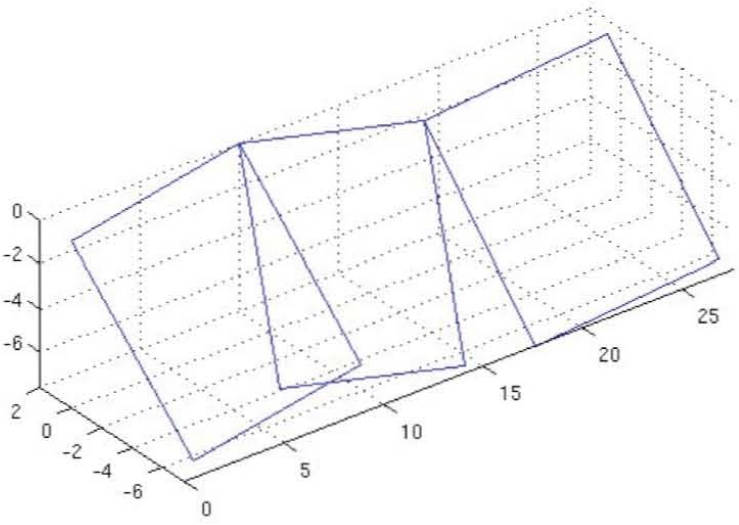

Figure B-1. Schematic plot of multisegment fault defined in previous National Seismic Hazard Maps. Dip direction is normal to the strike of each segment.

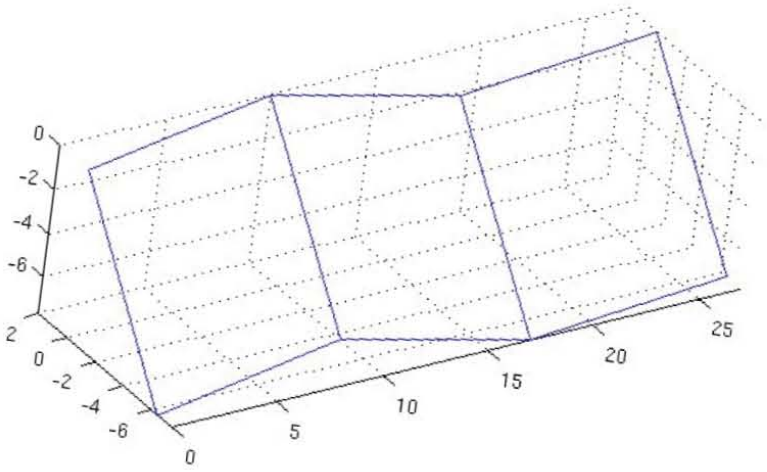

Figure B-2. Schematic plot of multisegment fault defined in the 2008 update of the National Seismic Hazard Maps. The fault plane is constrained to the down-dip direction based on the average strike of the fault. The average strike of the fault is the strike of the line connecting the first point with the last point of the surface trace of the fault.

segment is a parallelogram defined by equation (1B) or (2B). We calculate the fault distances to those parallelograms analytically. The calculation provides tenfold increase in computing time compared to the numerical solution for the previous fault distance calculation for the characteristic-fault hazard example.

Reference

Zeng, Y., and Chen, C.H., 2001, A combined GPS measurements and strong motion waveform inversion of the source rupture process during the 1999 Chi Chi, Taiwan earthquake: Bulletin of the Seismological Society of America, v. 91, p. 1088–1098.

Appendix C. Distance to a Fault with Random Strike

By Stephen C. Harmsen

In the 2008 update of the maps, background sources with random strike are assigned a mean distance when computing the ground-motion integral. The fault is assumed to have vertical dip. The Wells and Coppersmith (1994) formula of rupture length (L) as a function of moment magnitude is used to obtain L whenever M>6. Consider a line source with center at *P* and length L. Let L_0=L/2. Let the epicentral distance from *P* to site S to be *r*. There are two cases, $L_0 \geq r$ and $L_0 < r$.
The first case, $L_0 \geq r$:

The distance is found by elementary trigonometry to be $r \sin\theta$.

The mean distance is

$$<r_{jb}> = \int_0^{\pi/2} r \sin\theta U(\theta) d\theta = \frac{2r}{\pi}.$$

Here $U(\theta)$ is the uniform distribution,

$$U(\theta) = \frac{2}{\pi} \text{ for } 0 \leq \theta \leq \frac{\pi}{2}.$$

We assume that all source strikes are equally likely, and by symmetry, the domain of integration may be reduced to one mathematical quadrant.

The second case $L_0 < r$:

In this case, the distance to the fault either projects onto the nearest fault endpoint or onto an interior point. The angle where the changeover occurs is

$$\theta_0 = \arccos\left(\frac{L_0}{r}\right).$$

If $\theta \leq \theta_0$, the law of cosines is used to obtain the distance, $r_{jb}^2 = r^2 + l_0^2 - 2rl_0\cos(\theta) = a - b\cos\theta$ with $a = r^2 + l_0^2$ and $b = 2rl_0$ or $r_{jb} = \sqrt{a - b\cos\theta}$ and if $\theta > \theta_0$, then $r_{jb} = r\sin\theta$ as above. The mean distance is

$$<r_{jb}> = \frac{2}{\pi}\left[\int_0^{\theta_0} \sqrt{a - b\cos\theta}\, d\theta + \int_{\theta_0}^{\pi/2} r\sin\theta d\theta.\right]$$

The first term is found to have an analytic solution involving the elliptic integral of the second kind. See Gradshteyn and Ryzhik (1980), chapter 2, Indefinite integrals of elementary functions, eqn. 2 at bottom of p. 156, and then p. 905. The second term above integrates to $r\cos(\theta_0)$. The solution of the elliptic integral is available in many Fortran libraries, such as "Numerical Recipes in Fortran", by Press and others (1986). Some transformations are required to use the Press and others' *el2* function. While these are of limited interest to the general reader, they are included here for completeness and will be found in the Fortran code hazgridXnga2.f for example.

$$\delta_0 = \sqrt{\frac{(a+b)(1-\cos\theta_0)}{2(a-b\cos\theta_0)}},$$

$$\delta = a\sin\delta_0,$$

$$x = \tan\delta,$$

$$s^2 = 1 - \frac{2b}{a+b},$$

$$s = \sqrt{s^2},$$

$$e_2 = el2(x, s, 1., s^2),$$

$$f = 2\sqrt{a+b}$$

Here, *el2* is the output of the Numerical Recipes function call with four arguments. When calling *el2*, we need to ensure that s^2 is positive, which it is mathematically, but may fail to be in applications due to numerical precision. Finally, we define another term and get the solution,

$$t = \frac{2b\sin\theta_0}{\sqrt{a - b\cos\theta_0}},$$

$$I = e_2 f - t,$$

$$<r_{jb}> = \frac{2}{\pi}\left[I + r\cos\theta_0\right]$$

The grids of stations and sources are used to define a matrix of average distances, $<r_{jb}>$, as a

function of source magnitude from M6 to M7.5. These average distances are used, along with the companion distance, which we currently write as

$$r_{cd}=\sqrt{< r_{jb} >^2 + h^2}\ ,$$

in the attenuation models, which predict ground otion from M and r. In this formula, h is the depth to top of fault, which is assumed to have vertical dip. R_{jb} is the Joyner-Boore distance, and r_{cd} is the closest distance to any point on the fault or rupture surface. A more accurate determination of $<r_{cd}>$, which also involves the elliptic integral of the second kind, is possible. Because of limited sensitivity of the ground-motion prediction equations to small changes in r_{cd} we believe our estimate is adequate.

References

Gradshteyn, I.S., and Ryzhik, I.M., 1980, Table of integrals, series, and products, corrected and enlarged edition, *in* Jeffrey, A., ed.: New York, Academic Press.

Press, W.H., Flannery, B.P., Teukolsky, S.A., and Vettering, W.T., 1986, Numerical recipes—The art of scientific computing: New York, Cambridge University Press, 818 p.

Wells, D.L. and Coppersmith, K.J., 1994, New empirical relationships among magnitude, rupture length, rupture width, and surface displacements: Bulletin of the Seismological Society of America, v. 84, p. 974–1002.

Appendix D. Modeling Dip-Slip Background Sources

By Stephen C. Harmsen

This appendix discusses how we implement a hanging-wall effect in the current NSHMP PSHA for background sources (that is, faults with no specific information except for rate estimates from historical seismicity). For many of these gridded sources in the WUS, half of them are strike slip and half are dip slip. Several of the NGA relations that the 2008 PSHA uses to estimate seismic hazard in the WUS have a complex response to dip-slip sources, much of which is contained in a hanging-wall (hw) term. Because this hw term is not negligible in many instances, we need to model its effect in a fair and reasonable way.

For the dip-slip part of background seismic hazard, the hazard software computes an average hanging-wall effect. A set of faults with a random but uniformly distributed strike and fixed 50° dip is defined. The centers of all dipping faults have depth of 7.5 kilometers (not randomized). Furthermore, the centers of dipping faults, like the vertical-dip counterparts, are co-located with the rate grid at 0.1-degree increments in latitude and longitude. Our implementation of virtual dip-slip faults uses the Wells and Coppersmith (1994) all-source A(M) formula to estimate fault area A (in square kilometers), log(A)=(M–4.07)/0.98. From A, fault width is determined assuming an aspect ratio of 1.5; a minimum depth of top of fault of 0.5 kilometer below Earth's surface further constrains fault width. The hanging-wall term of the relevant Next Generation Attenuation (NGA) model is computed for each such fault strike for a given distance and magnitude, and the samples are averaged. Because attenuation model response is defined in "logged" ground-motion space, the averages are geometric in "unlogged" space.

Figure D-1 is a schematic diagram of a virtual dipping fault with the relevant distances labeled.

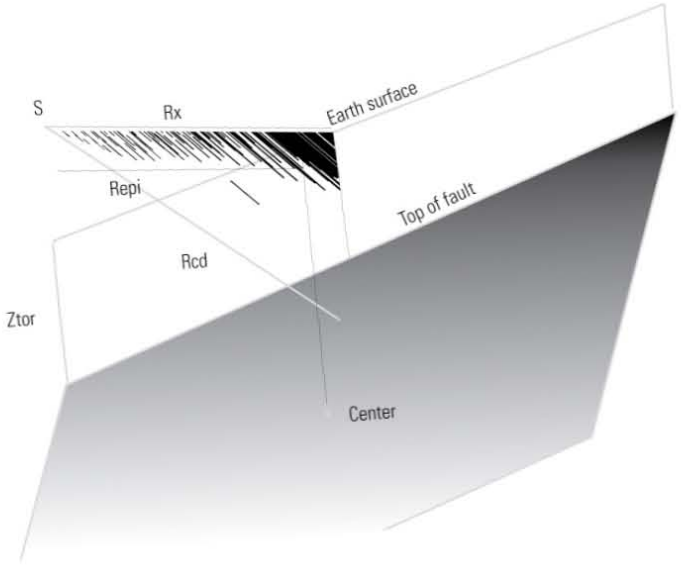

Figure D-1. Schematic diagram of virtual fault with associated distances to site S. Rcd, closest distance to fault; Rx, closest distance to top of fault projected indefinitely along strike; Rx<0 on footwall (Rx is used in the Chiou and Youngs relation); Repi, picentral distance to center projected to Earth surface; Ztor, depth of top of rupture, and θ is fault strike, a random variable.

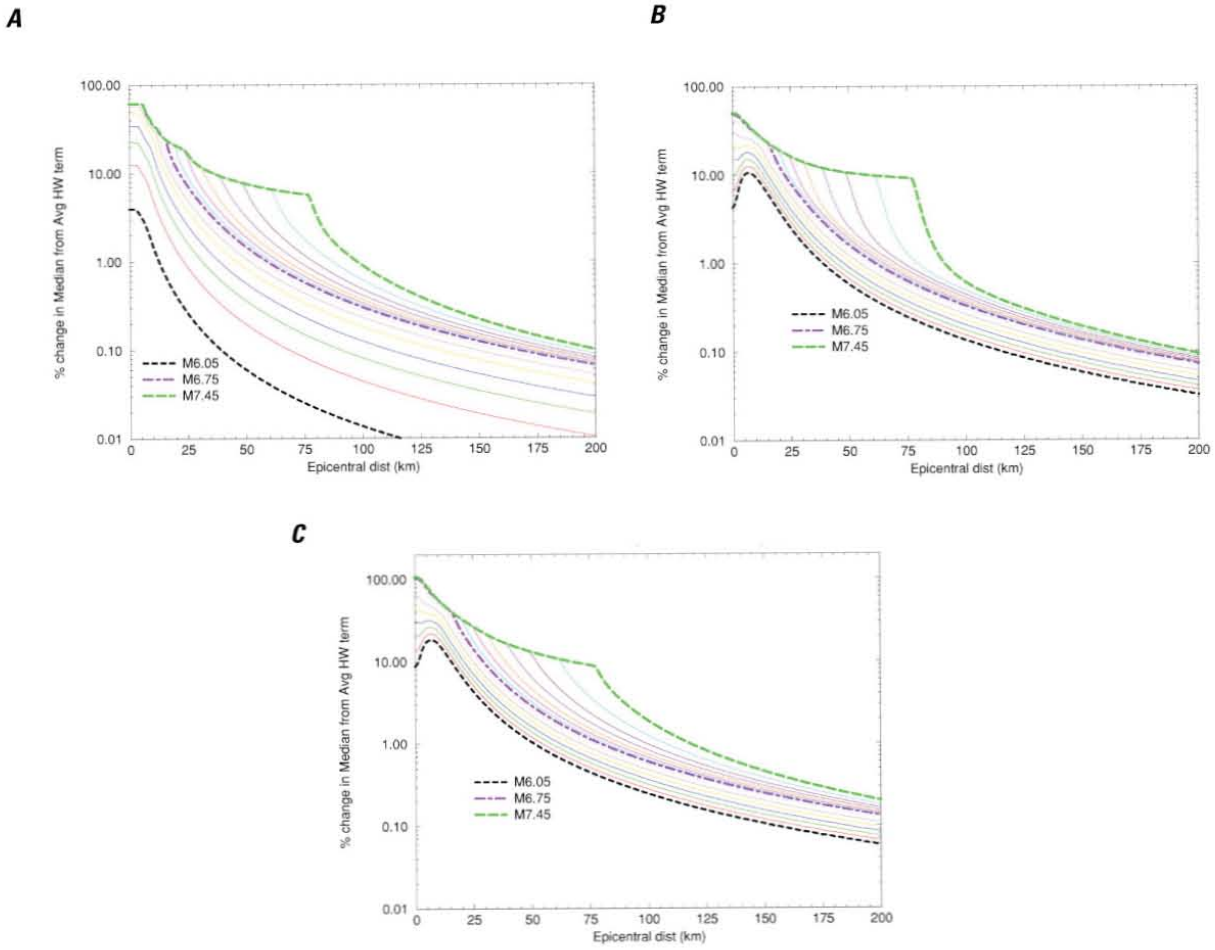

Figure D-2. Effect of including hanging-wall term on median ground motion considering (***A***) Campbell and Bozorgnia (2008), (***B***) Chiou and Youngs (2008) 1-hertz hanging-wall term, and (***C***) Chiou and Youngs (2008) 5-hertz hanging-wall term (M6.05–7.45 at 1-s period and 50° fault dip).

Each of the distances Rjb, Rcd, and Rx is computed for each virtual fault and is used to determine the hw term associated with that sample.

Figure D-2A shows the resulting average effect for the Campbell and Bozorgnia (2008) NGA model for M ranging from 6.05 to 7.45 and for 1-s SA (corresponding graphs for 0.2-s SA and PGA are identical). The x-axis labeled epicentral distance is site-to-source-center distance (projected to Earth's surface). The y-axis is the percent increase in the median ground motion associated with inclusion of this average hw term. For dip-slip background sources closest to any given site, this hw effect can be 40 percent.

Figures D-2B and D-2C show the corresponding results for the Chiou and Youngs (2008) NGA model for 1-s SA and 0.2-s SA, respectively. The Chiou and Youngs hanging-wall term has a stronger spectral frequency dependence than the Campbell and Bozorgnia model, rising with frequency in the 0.5-hertz to 5-hertz band. The maximum 1-hertz effect is similar to that of the Campbell and Bozorgnia model. For the 5-hertz SA, however, the median motion is increased by 100 percent at sites that are close to the dip-slip source. The Chiou and Youngs hw-effect on peak ground accleration is also relatively large at near-source sites.

When combined with strike-slip sources, this illustrated hw-effect is reduced. For the standard case in the 2008 update of the maps, 50 percent dip slip and 50 percent strike slip, the average hw term is multiplied by 0.5.

When the average hw term is applied to the median, it is applied at the average Joyner-Boore distance, or Rjb, associated with vertical strike-slip faulting, because this version of Rjb is the fundamental distance that the USGS gridded-hazard

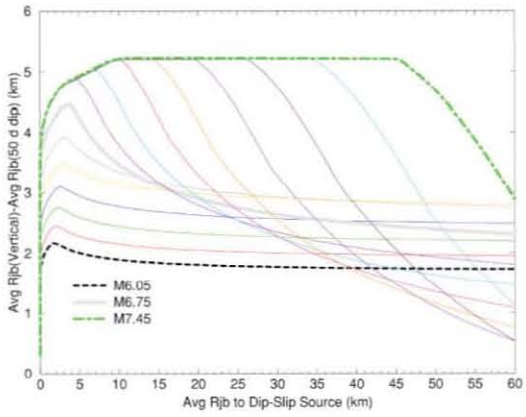

Figure D-3. Plot showing the increase in Rjb for vertical faults compared to 50°-dipping faults as a function of average Rjb for the random-strike

software uses to compute exceedance probability from random sourc or distances less than 60 kilometers. Figure D-3 shows the increase in Rjb for vertical faults compared to 50°-dipping faults as a function of average Rjb for the random-strike dipping fault. From figure D-3, the strike-slip source on average can be over 5 kilometers more distant than the dip-slip source for earthquakes of random orientation having M>7. The software uses an approximation to this fairly complicated functional relation to associate a given average hanging-wall effect with the fundamental distance measure, average Rjb for vertical faults.

References

Campbell, K.W. and Bozorgnia, Y., 2008, Ground motion model for the geometric mean horizontal component of PGA, PGV, PGD and 5% damped linear elastic response spectra for periods ranging from 0.01 to 10.0 s: Earthquake Spectra, v. 24, no. 1.

Chiou, B., and Youngs, R., 2008, A NGA model for the average horizontal component of peak ground motion and response spectra: Earthquake Spectra, v. 24, no. 1.

Wells, D.L. and Coppersmith, K.J., 1994, New empirical relationships among magnitude, rupture length, rupture width, and surface displacements: Bulletin of the Seismological Society of America, v. 84, p. 974–1002.

Appendix E. The Gutenberg-Richter Part of the Magnitude-Frequency Distribution for Western United States Faults

By Stephen C. Harmsen

The 2008 model for fault hazard, like earlier models, generally distributes hazard into characteristic-event and Gutenberg-Richter-event components. For events with M≤6.5, all hazard is assumed characteristic (noexception: San Andreas fault, creeping section). For events with M>6.5, the Gutenberg-Richter (GR) part of the hazard is developed by redistributing the seismic-moment rate that has been determined for that fault onto a set of events with M>6.5 and M<Mchar, where Mchar is the characteristic-event moment magnitude. The feature that is new in the 2008 model compared to earlier models is that Mchar is now computed to two decimal places rather than one (for example, 6.67 instead of 6.7) for non-California faults. We continue to sample events with a truncated GR-distribution with M from 6.5+dM/2 to Mchar–dM/2, and this requires us to redefine dM to be an interval-dependent quantity, rather than the fixed value of 0.1 that was used in earlier maps. The range Mchar–6.5 determines the number of samples, with more magnitudes sampled as the range increases. Table E-1 shows the number of samples, *k*, as a function of this range, which in turn determines dM. This information is contained in the Fortran program, *fltrate.v2.f*. The GR distribution is defined by its *a*- and *b*-values, where 10^a is the rate of M0 events and *b* is the slope in the equation log(N)=*a*–*b*M. In the past, we could say that 10^a is the rate of earthquakes in the interval M0±dM/2; now we say that 10^a is the rate of events in an (unspecified) interval of length dM containing 0 in its interior. The moment-rate-conserving calculation does not require further knowledge of this interval; it concentrates moment at each sampled M (as it always did) and does not use information about the distribution at nonsampled M values.

For California faults with a GR component of hazard (that is, the so-called Type-B faults) Mchar is still defined to one decimal-place accuracy, and dM remains 0.1 in the 2008 PSHA.

The main reason for defining Mchar with two-decimal-place accuracy in the 2008 PSHA was to assess the effects of additional epistemic uncertainty on approximated features such as fault dip and magnitude as a function of fault area. Sensitivity studies on *k* (for example, using *k*=10 instead of *k*=8) indicate that small changes in *k* in table E-1 yield a negligible effect on the seismic-hazard computation. Current upper limits of Mchar on non-California faults are 7.5 and 8.0 for dip-slip and strike-slip events, respectively. If these bounds were increased, it might be necessary to increase *k* for larger X.

Table E-1. Sampling interval details for non-California faults, truncated GR distribution.

X=Mchar – 6.5	*K*	dM
X≤0.1	1	X
0.1 <X≤0.3	2	X/2
0.3 <X≤0.5	4	X/4
0.5 <X≤0.7	6	X/6
0.7 < X	8	X/8

Appendix F. New Madrid Temporal Cluster Model

By Mark D. Petersen, Stephen C. Harmsen, and Oliver S. Boyd

In the 2008 hazard model, we have implemented a new cluster model that considers ground motions from three temporally clustered earthquakes on three separate segments of the New Madrid Seismic Zone, in contrast to the 2002 model that considers ground motions from one earthquake on the three segments (Toro and Silva, 2001). In this appendix we describe how the temporal cluster model affects the ground-motion hazard by showing two simple example calculations for the New Madrid seismic zone.

To calculate the probability of ground-motion exceedance from three temporally clustered earthquakes on three segments of the fault we apply the equation:

$$P = \alpha \times \{1-[(1-P1) \times (1-P2) \times (1-P3)]\}$$

where α is the time-independent cluster rate, P1 is the probability of exceeding a certain ground-motion level from a rupture of segment 1, P2 is the probability of exceeding the same ground-motion level from a rupture of segment 2, and P3 is the probability of exceeding the same ground-motion level from a rupture of segment 3. This formula is repeated for each ground-motion level included in the hazard curve. The New Madrid cluster model considers the ground motions from dependent earthquakes on the north, central, and south segments. The annual rate of the cluster for these is either 1/500, 1/750, 1/1,000, or 1/1500, as described in the logic tree (see fig. 6).

For this example, we calculate the probability for an M7.5 event with an annual occurrence rate of 1/500 on each of the three segments using the Toro and others (1997) attenuation relation with modifications by Toro (2002). Our example shows hazard calculations for two sites to emphasize the effect of the cluster model on the hazard. The first site is near the northern end of the northern segment in Paducah, Ky. (lat 37.072N., long 88.628°W.) and the second site is near the intersection of the southern and central segments in Tennessee (lat 36.0°N., long 89.0°W.). To calculate the hazard, we first need to calculate the conditional probability of exceeding each ground-motion level at a site, for an earthquake on each segment. The probabilities are shown in Figure F-1. At the Tennessee site, the probability of exceeding a ground motion of 0.4 g is 0.0527 for the northern rupture and 0.295 for the southern and central ruptures. The above formula yields a probability of 0.529 of exceeding 0.4 g PGA. This probability is then multiplied by the cluster rate 1/500 year. The

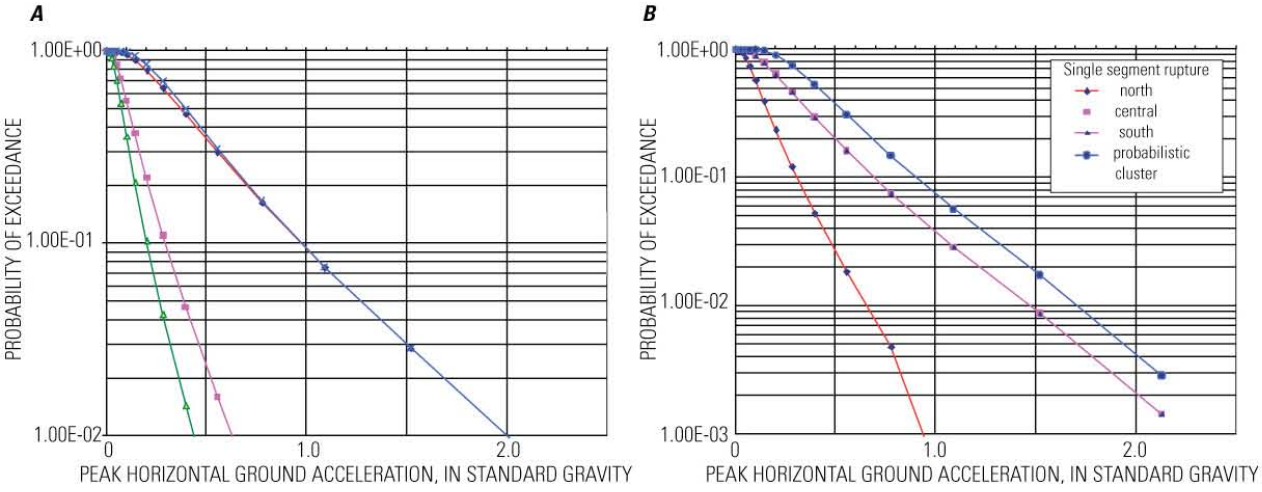

Figure F-1. Complementary cumulative plot for P=α×[1-(1-P1)*(1-P2)*(1-P3)] for a site in (A) Paducah, Kentucky, and (B) Tennessee. Curve for central and south segments are the same.

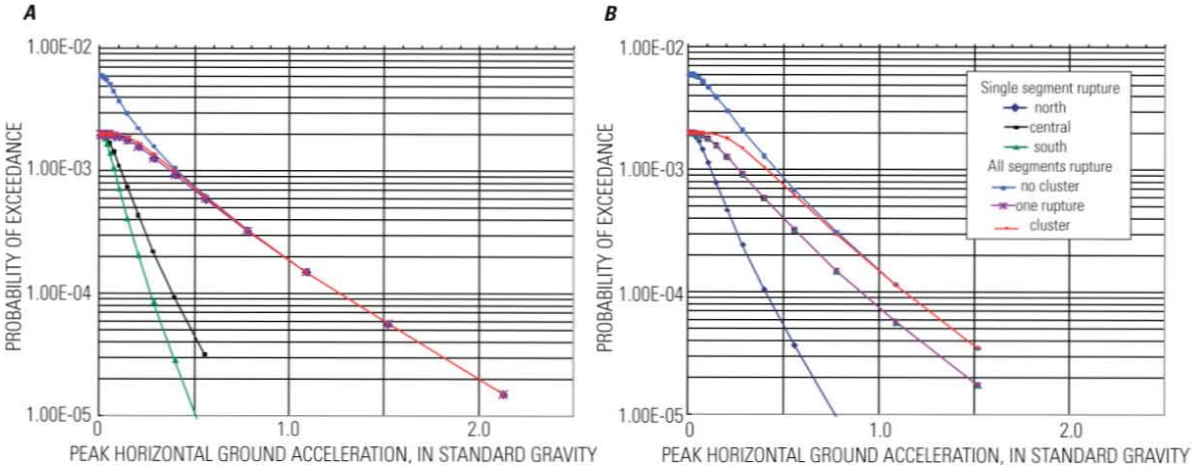

Figure F-2. Hazard curves for a site in (A) Paducah, Kentucky, and (B) Tennessee. Curves for central, south, and single rupture on three segments are the same. Curves for three independent segment ruptures and the three-segment cluster model are similar beyond ground motions of 0.5 g.

calculation using the above formula yields a 0.00106 annual rate of exceeding 0.4 g. This calculation is repeated for all the points on the hazard curve.

Figure F-2 shows the hazard curves for the same two sites for ruptures on each of the segments separately, three independent ruptures, one rupture of the three segments, and the temporal cluster of ruptures as described previously. For the site in Paducah, Ky., located north of the New Madrid sources, earthquakes on the northern segment contribute most to the hazard while earthquakes on the central and southern segments contribute little to the total hazard at the selected site. The curves for the three independent-rupture models, the single-rupture model on each of the three segments, the single northern-segment rupture, and the cluster model are all similar to each other. For the site in Tennessee, earthquakes on the more distant northern segment contribute less than earthquakes on the closer central and southern segments. The three independent ruptures and the cluster models are higher than the single rupture of the three segments by about a factor of 2. Thus, the result of incorporating this cluster model on the hazard maps is that the hazard near the central part of the New Madrid Seismic Zone is increased compared to the 2002 model, which only considered a single rupture of three New Madrid segments.

For the 2008 maps, we included several models that are depicted in the logic tree (see fig. 6). Half weight is given to the cluster model and half to the model with one independent rupture of all three segments (the 2002 model). The cluster models consider three different weighted scenarios: (1) each of the segments rupture on average in 500 years as three temporally clustered earthquakes, (2) each of the segments rupture on average in 1,000 years as three temporally clustered earthquakes, and (3) the northern segment ruptures every 750 years and the southern and central segments rupture every 500 years as temporally clustered earthquakes. To account for the latter alternative, we include a cluster every 750 years and a second cluster that ruptures only the southern two segments every 1,500 years. The sum of these two models results in rates of approximately 750 years for the north and 500 years $(=1/750+1/1500)^{-1}$ for the southern two segments.

References

Toro, G.R. and Silva, W.J., 2001, Scenario earthquakes for Saint Louis, MO, and Memphis, TN, and seismic hazard maps for the central United States region including the effect of site condition: Technical report to U.S. Geological Survey, Reston, Virginia, under Contract 1434-HQ-97-GR-02981, *http://www.riskeng.com/PDF/Scen_CEUS_Rept.pdf.*

Toro, G.R., 2002, Modification of the Toro et al. (1997) attenuation relations for large magnitudes and short distances: Risk Engineering, Inc. report, *http://www.riskeng.com/PDF/atten_toro_extended.pdf*

Toro, G.R., Abrahamson, N.A., and Schneider, J.F., 1997, A model of strong ground motions from earthquakes in central and eastern North America—Best estimates and uncertainties: Seismological Research Letters, v. 68, p. 41–57.

Appendix G. Parameters for Faults in the Intermountain West

By Kathleen M. Haller and Russell L. Wheeler

Fault sources in the Intermountain West, as defined in this appendix, are those that are located in the Western United States but not in the Pacific Coast States of Washington, Oregon, and California. Faults in those three states are discussed elsewhere in the documentation. The Intermountain West faults modeled in the National Seismic Hazard Maps include all Quaternary faults that have published geologic or paleoseismic investigations that, at a minimum, document slip rate, or sufficient data to calculate slip rate, and (or) rates of large-magnitude earthquakes resulting in permanent, geologically recognized surface deformation. In the Intermountain West, all faults with known Holocene (younger than 10 ka) surface faulting are included in this model, and many late Quaternary (younger than about 125–150 ka) faults are represented as well. Thousands of older faults exist in this broad region, which has a long history of tectonic deformation. The nearly 250 faults that we modeled as sources in this region are shown in figure G-1.

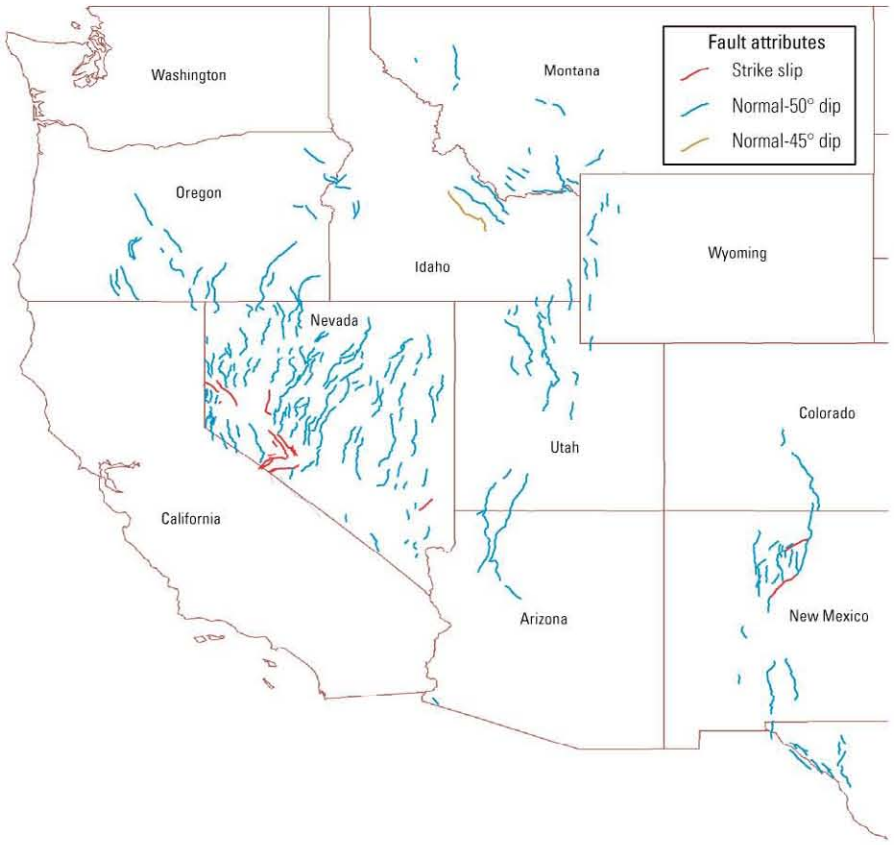

Figure G-1. Map of fault sources in the Intermountain West showing sense of slip by color.

We updated input parameters for more than 10 percent of the fault sources in the Intermountain West (table G-1) based on a literature review that focused on critical data such as slip rate and recurrence intervals. Most of the changes in our model resulted from the comprehensive reevaluation of all published paleoseismic studies by the Utah Quaternary Fault Working Group (Lund, 2005). Figure G-2 graphically shows changes that improve characterization of mean vertical slip rate, which is documented in table G-1. Additional modifications (shown in tables G-1 and G-2) were made to maintain internal consistency in the input parameters.

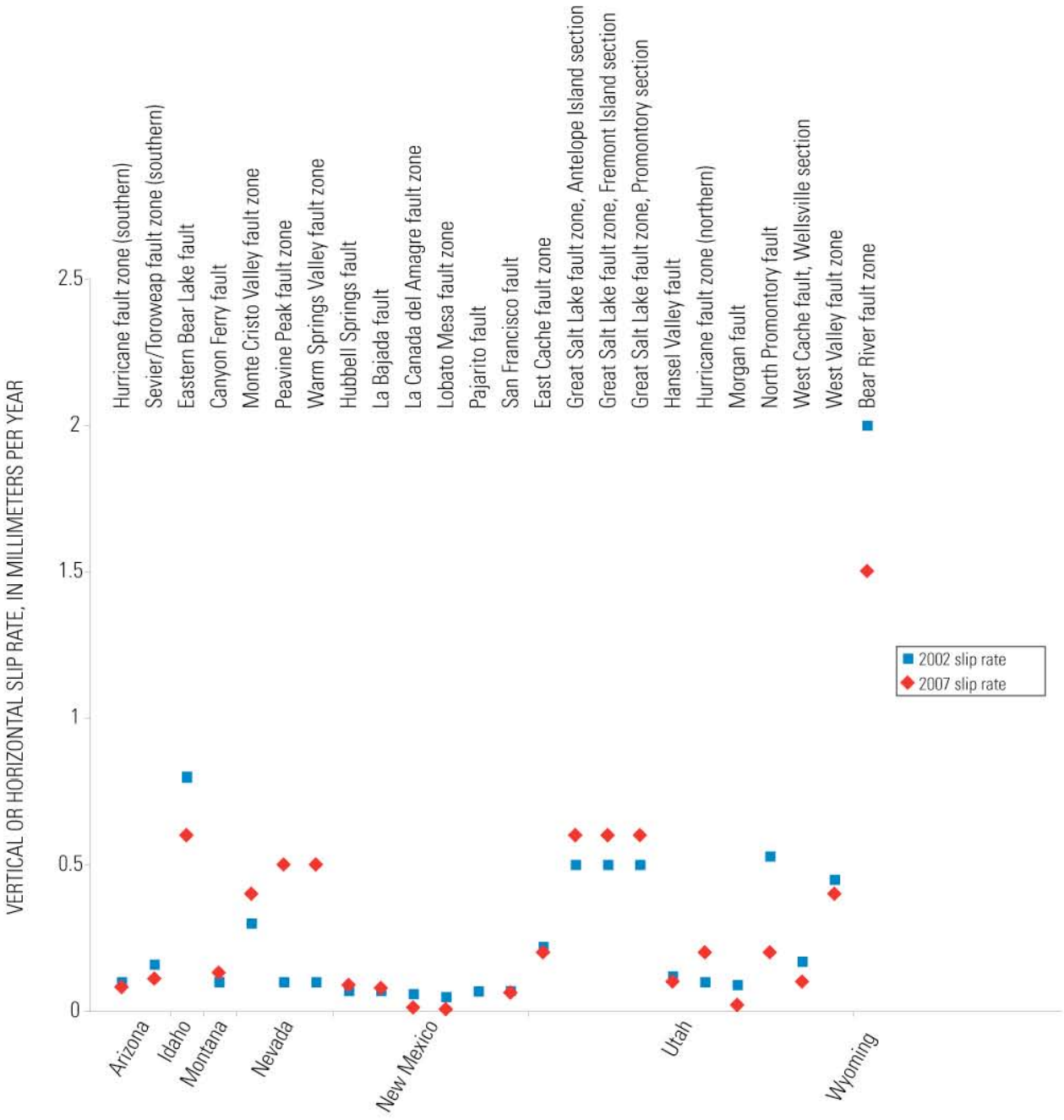

Figure G-2. Plot of comparison of assigned slip rates for Intermountain West faults grouped by State.

Table G-1. Updated Intermountain West fault parameters.
[See *http://gldims.cr.usgs.gov/webapps/cfusion/Sites/hazfaults_search/hf_search_main.cfm?hazmap=2008* for further documentation of source material.

Fault name	State	Updated parameter	2008 value	2002 value	References or comment
Hurricane fault zone (southern)	Arizona	vertical slip rate	0.081	0.1	Fenton and others (2001)
Sevier/Toroweap fault zone (southern)	Arizona	vertical slip rate	0.11	0.16	Fenton and others (2001)
Cuddy Mountain-Lick Creek fault	Idaho	length	30	52	Fault location updated based on improved mapping source
Eastern Bear Lake fault	Idaho	slip rate	0.6	0.8	Lund (2005) based on McCalpin (2003)
Lost River fault	Idaho	length (km)	141	159	Fault location updated based on improved mapping source
Squaw Creek fault	Idaho	length (km)	48	59	Fault location updated based on improved mapping source
Rush Peak fault	Idaho	length (km)	29	26	Fault location updated based on improved mapping source
Canyon Ferry fault	Montana	vertical slip rate	0.13	0.1	Anderson and LaForge (2003)
Hebgen Lake/Red Canyon fault	Montana	sources combined			Lund (2006)
Monte Cristo Valley fault zone	Nevada	horizontal slip rate	0.4	0.3	Bell and others (1999)
Peavine Peak fault	Nevada	vertical slip rate to recurrence rate	8.333E-4	0.1	Ramelli and others (2002)
Warm Springs Valley fault zone	Nevada	horizontal slip rate	0.5	0.1	dePolo (2006)
Calabacillas fault	New Mexico	source added	0.0069	NA[1]	McCalpin and Harrison (2000)
East Paradise fault	New Mexico	source added	0.0096	NA[1]	Personius and Mahan (2000)
Embudo fault	New Mexico	dip	60	90	
Hubbell Springs fault	New Mexico	vertical slip rate	0.089	0.07	Personius and Mahan (2003)
La Bajada fault	New Mexico	vertical slip rate	0.078	0.07	Wong and others (1995)
La Canada del Amagre fault zone	New Mexico	vertical slip rate	0.012	0.06	Wong and others (1995)
Lobato Mesa fault zone	New Mexico	vertical slip rate	0.0054	0.05	Wong and others (1995)
Pajarito fault	New Mexico	vertical slip rate to recurrence rate	5.74E-05*	0.068	Gardner and others (2005)
San Francisco fault	New Mexico	vertical slip rate	0.063	0.07	Wong and others (1995)
Socorro Canyon fault	New Mexico	source added	0.027	NA[1]	Phillips and others (2003)
East Cache fault zone	Utah	vertical slip rate	0.2	0.22	Lund (2005) based on McCalpin (1994)
Great Salt Lake fault zone (Antelope segment)	Utah	vertical slip rate	0.6	0.5	Lund (2005) based on Dinter and Pechmann (2000)

Table G-1. Updated Intermountain West fault parameters.—Continued

Fault name	State	Updated parameter	2008 value	2002 value	References or comment
Great Salt Lake fault zone (Fremont Island segment)	Utah	vertical slip rate	0.6	0.5	Lund (2005) based on Dinter and Pechmann (2000)
Great Salt Lake fault zone (Promontory segment)	Utah	vertical slip rate	0.6	0.5	Updated to be consistent with other two segments of the fault
Hansel Valley fault	Utah	vertical slip rate	0.1	0.12	Lund (2005) based on McCalpin (1985)
Hurricane fault zone (northern)	Utah	vertical slip rate	0.2	0.1	Lund (2005) based on Stenner and others (1999)
Joes Valley fault zone	Utah	vertical slip rate to recurrence rate	1.00 E-04	0.2	Lund (2005) based on Foley and others (1986)
Joes Valley fault zone west fault/ Joes Valley fault zone east fault	Utah	sources combined			Lund (2005)
Morgan fault	Utah	vertical slip rate	0.02	0.09	Lund (2005) based on Sullivan and others (1988) and Sullivan and Nelson (1992)
Oquirrh-Southern Oquirrh Mountain fault	Utah	fault extended to included Southern Oquirrh Mountain fault	63 km M7.17	27 km M6.7	Olig and others (2001)
North Promontory fault	Utah	vertical slip rate	0.2	0.53	Lund (2005) based on McCalpin and others (1992)
Wasatch fault (Brigham City segment)	Utah	recurrence rate	7.69 E-04	8.03 E-04	Lund (2005)
Wasatch fault (Weber segment)	Utah	recurrence rate	7.14 E-04	5.60 E-04	Lund (2005)
Wasatch fault (Salt Lake City segment)	Utah	recurrence rate	7.69 E-04	7.41 E-04	Lund (2005)
Wasatch fault (Provo segment)	Utah	recurrence rate	4.17 E-04	4.37 E-04	Lund (2005)
West Cache fault (Clarkston segment)	Utah	source added	0.4	NA[1]	Lund (2005) based on Black and others (2000)
West Cache fault (Wellsville segment)	Utah	vertical slip rate	0.1	0.17	Lund (2005)
West Valley fault zone	Utah	vertical slip rate	0.4	0.45	Lund (2005) based on Keaton and others (1987) and Keaton and Currey (1989)
Bear River fault zone	Wyoming	vertical slip rate	1.5	2	Lund (2005) based on West (1994)

[1] Fault source added in 2008 maps, value not applicable.

Table G-2. Updated fault names for Intermountain West faults.

2008 Name	2002 Name	State
Peavine Peak fault	North Peavine Mountain fault zone	Nevada
East Great Salt Lake fault zone, Antelope segment	Great Salt Lake fault zone, Antelope section	Utah
East Great Salt Lake fault zone, Fremont Island segment	Great Salt Lake fault zone, Fremont Island section	Utah
East Great Salt Lake fault zone, Promontory segment	Great Salt Lake fault zone, Promontory section	Utah

Four new sources were added to the model including the Calabacillas, East Paradise, and Socorro Canyon faults in New Mexico and the Clarkston segment of the West Cache fault in Utah. All were the targets of paleoseismologic investigations not considered in the 2002 maps. The Calabacillas fault was added based on two trenches that exposed evidence of four surface ruptures at approximately 14 ka, 32 ka, 77 ka, and 151 ka resulting in about 1 meter of offset (McCalpin and Harrison, 2000). The East Paradise fault was added based on evidence for three surface ruptures resulting in a total surface offset of 2.75±1 meters of an eolian sand deposit 286±26 ka (Personius and Mahan, 2000). Similarily, trenching and geologic mapping of the Socorro Canyon fault indicates three earthquakes have occurred in the past 122±18 ka (Phillips and others, 2003). We added the Clarkston segment of the West Cache fault in Utah based on Lund (2005).

Although assigned slip rate is commonly used to characterize fault activity and hence its contribution to seismic hazard, the parameter that is actually used is annualized rate of earthquakes of a predefined magnitude. In the Intermountain West, few faults have been trenched in more than one location; furthermore, far fewer trenching studies constrain the timing of more than a couple of events. Therefore, it is rare that we can use recurrence-interval data based on dated events in a trench to improve characterization of faults in our model. However, we were able to update the Peavine Peak fault in Nevada, Pajarito fault in New Mexico, and Joes Valley fault in Utah to better reflect their rates of activity. Using rate to characterize the Peavine Peak fault is a particularly good choice because the fault, as expressed at the surface, is very short. Its short length suggests a magnitude of M6.36. The large amount of reported Holocene displacement (Ramelli and others, 2002) results in exceptionally frequent events, a frequency that is not supported by the paleoseismic record. Additionally, the Utah Quaternary Fault Working Group (Lund, 2005) also updated mean recurrence intervals for the Wasatch fault (fig. G-3) based on consensus reevaluation of the tens of trenching studies that have been conducted since the 1980s and recommended that we implement multisegment rupture scenerio for the Wasatch fault (further discussed in Appendix J).

Finally, we have changed the default dip of normal fault in the Intermountain West to 50±10° (F1-3) as recommended by the Western States Seismic Policy Council (Lund, 2006). See Appendix J for further discussion of this decision.

Table G-3. Intermountain West fault parameters by State.
[Refer to *http://gldims.cr.usgs.gov/webapps/cfusion/Sites/hazfaults_search/hf_search_main.cfm?hazmap=2008* for further documentation of source material—M, characteristic magnitude; mm/yr, millimeters per year; °, degree; km, kilometers]

Fault name	Vertical or horizontal slip rate (mm/yr)	Dip (°)		Sense of slip	Width (km)	Length (km)	M	Characteristic rate	Gutenberg-Richter a-value	Gutenberg-Richter b-value
Arizona										
Algodones fault zone	0.15	50	NE	normal	20	19	6.57	2.74E-04	1.7188557	0.8
Aubrey fault zone	0.018	50	W	normal	20	65	7.18	1.35E-05	0.31276687	0.8
Big Chino fault	0.083	50	SW	normal	20	49	7.04	7.59E-05	0.9097004	0.8
Dutchman Draw fault	0.075	50	NW	normal	20	16	6.49	1.55E-04	NA	NA
Hurricane fault zone (central)	0.2	50	NW	normal	20	108	7.44	1.02E-04	1.3467844	0.8
Hurricane fault zone (southern)	0.081	50	NW	normal	20	100	7.4	4.39E-05	0.9379256	0.8
Sevier/Toroweap fault zone (southern)	0.11	50	W	normal	20	171	7.5*		1.2597	0.8
Colorado										
Cheraw fault	0.15	50	NW	normal	17	45	7	1.15E-04	2.14217	0.95
Northern Sangre de Cristo fault	0.18	50	W	normal	20	185	7.5*		1.5098404	0.8
Southern Sawatch fault	0.062	50	E	normal	20	45	6.99	6.19E-05	0.94294106	0.8
Idaho										
Beaverhead fault	0.12	50	SW	normal	20	134	7*		1.7037585	0.8
Big Flat-Jakes Creek fault	0.04	50	E	normal	20	31	6.81	5.13E-05	0.66017526	0.8
Cuddy Mountain-Lick Creek fault	0.05	50	NW	normal	20	30	6.79	6.67E-05	1.0533264	0.8
Eastern Bear Lake fault	0.6	50	W	normal	20	81	7.29	3.85E-04	1.7621624	0.8
Lemhi fault	0.22	50	SW	normal	20	147	7*		2.0074117	0.8
Lost River fault	0.15	45	SW	normal	21	141	7*		1.890967	0.8
Rush Peak fault	0.05	50	S	normal	20	29	6.78	6.69E-05	1.0435416	0.8
Squaw Creek fault	0.1	50	E	normal	20	48	7.03	9.43E-05	0.99330914	0.8
Montana										
Blacktail fault	0.03	50	NE	normal	20	40	6.94	3.17E-05	0.5970158	0.8
Canyon Ferry fault	0.13	50	SW	normal	20	39	6.92	1.43E-04	1.2292868	0.8
Centennial fault	0.9	50	N	normal	20	64	7.17	6.90E-04	2.0111513	0.8
Emigrant fault	0.25	50	NW	normal	20	57	7.12	2.03E-04	1.4244301	0.8

Table G-3. Intermountain West fault parameters by State.—Continued

Fault name	Vertical or horizontal slip rate (mm/yr)	Dip (°)		Sense of slip	Width (km)	Length (km)	M	Characteristic rate	Gutenberg-Richter a-value	Gutenberg-Richter b-value
Georgia Gulch fault	0.031	50	W	normal	20	14	6.42	7.14E-05	NA	NA
Hebgen-Red Canyon fault	0.5	50	SW	normal	20	25	7.3*	4.99E-05	1.1747674	0.8
Helena Valley fault	0.01	50	S	normal	20	20	6.6	1.75E-05	0.5579098	0.8
Jocko fault	0.08	50	NW	normal	20	16	6.47	1.71E-04	NA	NA
Madison fault	0.4	50	W	normal	20	111	7.45	2.02E-04	1.6542257	0.8
Mission fault	0.32	50	W	normal	20	92	7.36	1.84E-04	1.5176541	0.8
Red Canyon fault	0.5	60	SW	normal	17	22	6.6	7.44E-04	2.18657	0.8
Red Rock Hills fault	0.17	50	W	normal	20	11	6.27	4.89E-04	NA	NA
Red Rock fault	0.5	50	E	normal	20	27	6.73	7.29E-04	2.0244016	0.8
Sweetwater fault	0.04	50	NE	normal	20	13	6.38	9.64E-05	NA	NA
Thompson Valley fault	0.08	50	W	normal	20	10	6.22	2.45E-05	NA	NA
Nevada										
Antelope Range-Kingsley Mountains fault zone	0.01	50	E	normal	20	71	7.23	6.90E-06	-0.04907726	0.8
Antelope Valley	0.8	50	E	normal	20	41	6.95	8.46E-04	0.11249995	0.8
Bare Mountain fault	0.008	50	E	normal	20	19	6.57	1.47E-05	0.44757023	0.8
Battle Mountain fault	0.1	50	W	normal	20	26	6.72	1.47E-04	1.3179169	0.8
Benton Spring fault, southern section	0.26	90		strike slip	15	85	7.32	9.33E-05	1.1789495	0.8
Beowawe fault	0.1	50	W	normal	20	48	7.03	9.37E-05	0.99032956	0.8
Bettles Well-Petrified Springs fault	0.1	90		strike slip	15	71	7.23	4.07E-05	0.72174894	0.8
Black Hills fault	0.1	50	SE	normal	20	9	6.18	3.23E-04	NA1	NA
Black Rock fault zone	0.19	50	W	normal	20	80	7.29	1.20E-04	1.2578105	0.8
Bloody Run Hills fault	0.01	50	W	normal	20	27	6.74	1.44E-05	0.3311862	0.8
Bonham Ranch fault zone	0.2	50	E	normal	20	56	7.11	1.66E-04	1.3262955	0.8
Buena Vista Valley fault zone	0.1	50	W	normal	20	92	7.36	5.71E-05	1.0087095	0.8
Buffalo Creek fault zone	0.1	50	W	normal	20	28	6.77	1.36E-04	1.340194	0.8
Buffalo Mountain fault	0.1	50	SE	normal	20	18	6.54	1.91E-04	1.5277609	0.8

Table G-3. Intermountain West fault parameters by State.—Continued

Fault name	Vertical or horizontal slip rate (mm/yr)	Dip (°)		Sense of slip	Width (km)	Length (km)	M	Characteristic rate	Gutenberg-Richter a-value	Gutenberg-Richter b-value
Buffalo Valley fault zone	0.1	50	E	normal	20	41	6.95	1.05E-04	1.1279789	0.8
Butte Mountains fault zone	0.01	50	W	normal	20	61	7.15	7.90E-06	0.04790682	0.8
California Wash fault	0.28	50	W	normal	20	35	6.87	3.32E-04	1.5380037	0.8
Carico Lake Valley fault zone	0.1	50	E	normal	20	42	6.96	1.04E-04	1.1336586	0.8
Carson City fault	0.1	50	E	normal	20	16	6.48	2.11E-04		
Carson Range fault	2	50	E	normal	20	53	7.08	1.75E-03	2.3154082	0.8
Carson Range-Kings Canyon faults	2	50	E	normal	20	71	7.23	1.38E-03	2.2523534	0.8
Clan Alpine fault zone	0.15	50	SE	normal	20	35	6.87	1.78E-04	1.2685935	0.8
Coaldale fault 1	0.1	90		strike slip	15	65	7.19	4.30E-05	0.8277135	0.8
Coaldale fault 2	0.1	90		strike slip	15	17	6.51	1.18E-04	1.2846416	0.8
Cortez Mountain fault zone	0.1	50	NW	normal	20	67	7.2	7.23E-05	1.0636964	0.8
Coyote Spring fault	0.01	50	W	normal	20	15	6.45	2.19E-05		
Crescent Dunes fault	0.01	50	W	normal	20	45	7	9.75E-06	0.15092339	0.8
Desatoya Mountains fault zone	0.1	50	SE	normal	20	47	7.02	9.57E-05	0.98844993	0.8
Diamond Mountains fault	0.1	50	E	normal	20	85	7.32	6.11E-05	0.99556833	0.8
Diamond Valley fault	0.1	50	E	normal	20	23	6.67	1.58E-04	1.2925441	0.8
Dixie Valley fault zone	0.3	50	E	normal	20	119	7*	7.73E-04	2.0502302	0.8
Dry Lake fault	0.008	50	W	normal	20	49	7.04	7.34E-06	-0.104764714	0.8
Dry Valley-Smoke Creek Ranch fault zone	0.1	50	E	normal	20	50	7.05	9.12E-05	1.0006925	0.8
Duck Flat fault	0.1	50	SW	normal	20	16	6.49	2.05E-04	NA	NA
Dunn Glenn fault	0.1	50	W	normal	20	16	6.48	2.10E-04	NA	NA
East Tahoe fault	0.3	50	W	normal	20	26	6.7	3.79E-04	1.70588	0.8
Eastern Bilk Creek Mountains fault zone	0.01	50	E	normal	20	30	6.8	1.31E-05	0.055391836	0.8
Eastern Edwards Creek Valley fault zone	0.1	50	NW	normal	20	39	6.92	1.10E-04	1.1135823	0.8
Eastern Granite Range fault	0.1	50	E	normal	20	34	6.85	1.22E-04	1.0813034	0.8

Table G-3. Intermountain West fault parameters by State.—Continued

Fault name	Vertical or horizontal slip rate (mm/yr)	Dip (°)		Sense of slip	Width (km)	Length (km)	M	Characteristic rate	Gutenberg-Richter a-value	Gutenberg-Richter b-value
Eastern Independence Valley fault zone	0.1	50	W	normal	20	46	7.01	9.57E-05	0.97741973	0.8
Eastern Monitor Range fault zone	0.1	50	E	normal	20	105	7.43	5.16E-05	1.039428	0.8
Eastern Osgood Mountains fault zone	0.01	50	SE	normal	20	33	6.84	1.24E-05	0.07651044	0.8
Eastern Osgood Mountains piedmont fault	0.01	50	SE	normal	20	30	6.79	1.33E-05	0.35366117	0.8
Eastern Pine Forest Range fault zone	0.1	50	E	normal	20	10	6.25	2.94E-04	NA	NA
Eastern Pyramid Lake fault	0.1	50	W	normal	20	44	6.99	9.85E-05	1.1444507	0.8
Eastern Tuscarora Mountains fault zone	0.01	50	E	normal	20	52	7.07	8.81E-06	0.007714621	0.8
Edna Mountain fault	0.1	50	SE	normal	20	35	6.88	1.15E-04	1.0907553	0.8
Eglington fault	0.1	50	SE	normal	20	11	6.5	7.1E-05*	NA	NA
Emigrant Peak fault zone	0.76	50	W	normal	20	29	6.78	1.03E-03	2.2327015	0.8
Eugene Mountains fault	0.1	50	W	normal	20	10	6.24	3.00E-04	NA	NA
Fairview fault zone	0.1	50	E	normal	20	34	7.2	3.70E-05	0.7732189	0.8
Fox Range fault zone	0.1	50	W	normal	20	35	6.86	1.21E-04	1.0893043	0.8
Freds Mountain fault	0.1	50	E	normal	20	29	6.78	1.36E-04	1.351704	0.8
Frenchman Mountain fault	0.015	50	W	normal	20	20	6.59	2.66E-05	0.727833	0.8
Golden Gate fault	0.01	50	E	normal	20	36	6.89	1.14E-05	0.09563966	0.8
Granite Springs Valley fault zone	0.2	50	E	normal	20	49	7.05	1.80E-04	1.2957662	0.8
Grass Valley fault zone	0.1	50	W	normal	20	54	7.09	8.56E-05	1.0170091	0.8
Hiko fault zone	0.01	50	W	normal	20	15	6.46	2.15E-05	NA	NA
Hoppin Peaks fault zone	0.1	50	E	normal	20	103	7.41	5.40E-05	1.0377592	0.8
Hot Springs fault zone	0.1	50	W	normal	20	24	6.68	1.58E-04	1.3026237	0.8
Huntoon Valley fault system	0.1	90		strike slip	15	38	6.92	6.40E-05	0.8796344	0.8
Independence Valley fault zone	0.1	50	W	normal	20	66	7.19	7.40E-05	1.0632656	0.8

Table G-3. Intermountain West fault parameters by State.—Continued

Fault name	Vertical or horizontal slip rate (mm/yr)	Dip (°)		Sense of slip	Width (km)	Length (km)	M	Characteristic rate	Gutenberg-Richter a-value	Gutenberg-Richter b-value
Indian Head fault	0.1	90		strike slip	15	15	6.45	1.29E-04	NA	NA
Indian Hill fault	0.1	50	E	normal	20	8	6.13	3.53E-04	NA	NA
Ione Valley fault	0.1	50	W	normal	20	79	7.28	6.50E-05	0.97885894	0.8
Jackson Mountains fault zone	0.1	50	E	normal	20	75	7.25	6.80E-05	0.96608203	0.8
Jakes Valley fault zone	0.01	50	E	normal	20	35	6.88	1.16E-05	0.092969574	0.8
Jersey Valley fault zone	0.1	50	W	normal	20	34	6.86	1.20E-04	1.0840122	0.8
Kane Spring Wash fault	0.01	90		strike slip	15	43	6.97	6.00E-06	-0.09340974	0.8
Kawich-Hot Creek Ranges fault zone	0.2	50	SE	normal	20	121	7.49	9.61E-05	1.373548	0.8
Kings Canyon fault zone	0.2	50	SE	strike slip	20	18	6.52	3.97E-04	1.8220319	0.8
Little Fish Lake Valley fault	0.1	50	W	normal	20	43	6.98	1.00E-04	1.1416051	0.8
Little Valley fault	0.2	50	E	normal	20	18	6.54	3.84E-04	1.8298311	0.8
Lone Mountain fault zone	0.13	50	W	normal	20	41	6.95	1.37E-04	1.2428901	0.8
Marys Mountain fault	0.001	50	E	normal	20	20	6.58	1.81E-06	-0.4508271	0.8
McGee Mountain fault zone	0.01	50	E	normal	20	42	6.96	1.03E-05	0.13084666	0.8
Middlegate fault zone	0.1	50	W	normal	20	38	6.92	1.10E-04	1.1128118	0.8
Montana Mountains/Desert Valley fault zone	0.1	50	W	normal	20	102	7.41	5.37E-05	1.0355022	0.8
Monte Cristo Valley fault zone	0.4	90		strike slip	15	29	6.78	3.17E-04	1.7190449	0.8
Mount Irish Range fault	0.01	50	W	normal	20	12	6.32	2.67E-05	NA	NA
Mount Rose fault zone	1.5	50	E	normal	20	36	6.89	1.71E-03	2.2719285	0.8
Nightingale Mountains fault	0.1	50	W	normal	20	36	6.88	1.18E-04	1.0987121	0.8
Northern Butte Valley fault	0.1	50	W	normal	20	17	6.49	2.08E-04	NA	NA
Northern Huntington Valley fault zone	0.1	50	W	normal	20	39	6.93	1.08E-04	1.1160657	0.8
Northern Roberts Mountains fault	0.1	50	NW	normal	20	23	6.65	1.63E-04	1.2830935	0.8
Northern Simpson Park Mountains fault zone	0.1	50	N	normal	20	13	6.37	2.46E-04	NA	NA
Paradise Range fault zone	0.1	50	W	normal	20	43	6.97	1.02E-04	1.1375	0.8

Table G-3. Intermountain West fault parameters by State.—Continued

Fault name	Vertical or horizontal slip rate (mm/yr)	Dip (°)		Sense of slip	Width (km)	Length (km)	M	Characteristic rate	Gutenberg-Richter a-value	Gutenberg-Richter b-value
Peavine Peak fault zone	0.5	50	NE	normal	20	13	6.36	8.33E-04	NA	NA
Penoyer fault	0.016	50	W	normal	20	56	7.11	1.34E-05	0.23221329	0.8
Petersen Mountain fault	0.1	50	E	normal	20	26	6.72	1.47E-04	1.3177838	0.8
Petersen Mountain fault 2	0.05	50	E	normal	20	16	6.49	1.03E-05	NA	NA
Pleasant Valley fault zone	0.1	50	W	normal	20	68	7.6*	1.85E-05	0.77481645	0.8
Pyramid Lake fault zone	2	90		strike slip	15	77	7.27	7.71E-04	2.0423502	0.8
Railroad Valley fault zone	0.07	50	W	normal	20	159	7.5*		1.031487	0.8
Rainbow Mountain fault zone	0.15	90		strike slip	15	72	7.23	6.18E-05	0.9029679	0.8
Rattlesnake Flat fault	0.1	90		strike slip	15	15	6.46	1.27E-04	NA	NA
Ruby Mountains fault zone	0.28	50	W	normal	20	53	7.08	2.45E-04	1.4626777	0.8
Ruby Mountains fault zone	0.28	50	W	normal	20	37	6.9	3.18E-04	1.553986	0.8
Ruby Valley fault zone	0.1	50	E	normal	20	81	7.3	6.23E-05	0.9819613	0.8
San Emidio fault zone	0.2	50	W	normal	20	34	6.86	2.38E-04	1.3822703	0.8
Sand Springs Range fault	0.1	50	E	normal	20	42	6.96	1.03E-04	1.1316223	0.8
Schell Creek Range fault system	0.01	50	E	normal	20	105	7.43	5.14E-06	0.038450907	0.8
Selenite Range fault zone	0.1	50	W	normal	20	18	6.53	1.96E-04	1.5275263	0.8
Seven Troughs Range fault zone	0.1	50	E	normal	20	39	6.93	1.08E-04	1.1189233	0.8
Sheep Basin fault	0.044	50	W	normal	20	22	6.65	7.14E-05	0.92446565	0.8
Sheep Creek Range southeastern fault	0.1	50	SE	normal	20	38	6.92	1.10E-04	1.1131995	0.8
Shoshone Range fault zone	0.1	50	W	normal	20	121	7.5*	4.67E-05	1.0706302	0.8
Simpson Park Mountains fault zone	0.22	50	W	normal	20	73	7.24	1.51E-04	1.3009341	0.8
Singatse Range fault zone	0.1	50	E	normal	20	34	6.85	1.22E-04	1.0814091	0.8
Smith Valley fault	0.38	50	E	normal	20	94	7.37	2.16E-04	1.5970038	0.8
Southwest Reese River Valley fault	0.1	50	NE	normal	20	80	7.29	6.35E-05	0.97973024	0.8
Spanish Springs Peak fault	0.1	90		strike slip	15	5	6.0	1.97E-04	NA	NA

Table G-3. Intermountain West fault parameters by State.—Continued

Fault name	Vertical or horizontal slip rate (mm/yr)	Dip (°)		Sense of slip	Width (km)	Length (km)	M	Characteristic rate	Gutenberg-Richter a-value	Gutenberg-Richter b-value
Spanish Springs Valley fault	0.1	50	E	normal	20	21	6.62	1.72E-04	1.2713587	0.8
Spruce Mountain Ridge fault zone	0.1	50	W	normal	20	33	6.83	1.27E-04	1.0750724	0.8
The Lava Beds fault	0.1	50	E	normal	20	26	6.73	1.44E-04	1.3206738	0.8
Toiyabe Range fault zone	0.22	50	E	normal	20	127	7.5*		1.4322273	0.8
Unnamed faults	0.1	90		strike slip	15	40	6.93	6.38E-05	0.88942795	0.8
Warm Springs Valley fault zone	0.5	90		strike slip	15	38	6.92	3.20E-04	1.5781618	0.8
Wassuk Range fault zone	0.55	50	E	normal	20	119	7.49	2.61E-04	1.8082168	0.8
West Gate fault	0.1	50	W	normal	20	25	6.69	1.55E-04	1.3073386	0.8
West Spring Mountains fault	0.045	50	W	normal	20	53	7.08	3.90E-05	0.6648692	0.8
Western Diamond Mountains fault zone	0.1	50	W	normal	20	65	7.18	7.49E-05	1.0574684	0.8
Western Granite Range fault	0.2	50	SW	normal	20	28	6.76	2.77E-04	1.637748	0.8
Western Humboldt Range fault zone	0.1	50	W	normal	20	78	7.28	6.44E-05	0.97469764	0.8
Western Smoke Creek Desert fault 2	0.1	50	E	normal	20	19	6.57	1.85E-04	1.548334	0.8
Western Toiyabe Range fault zone	0.2	50	NW	normal	20	139	7.5*		1.4317641	0.8
White River Valley fault zone	0.045	50	W	normal	20	105	7.42	2.39E-05	0.6941244	0.8
Faults in Excelsior Mountains	0.1	90		strike slip	15	27	6.74	8.33E-05	1.0934577	0.8
New Mexico										
Alamogordo fault	0.11	50	W	normal	20	121	7.5	5.11E-05	1.1098998	0.8
Black Mesa fault zone	0.02	50	NW	normal	20	18	6.54	3.81E-05	0.82740765	0.8
Caballo fault	0.025	50	W	normal	20	22	6.64	4.17E-05	0.67914515	0.8
Calabacillas fault	0.0069	50	E	normal	20	33	6.83	8.73E-06	-0.086238175	0.8
Cañones fault	0.02	50	W	normal	20	31	6.81	2.56E-05	0.3580615	0.8
County Dump fault	0.038	50	E	normal	20	37	6.89	4.40E-05	0.68327254	0.8
East Paradise fault zone	0.0096	50	W	normal	20	13	6.38	2.33E-05	NA	NA

Table G-3. Intermountain West fault parameters by State.—Continued

Fault name	Vertical or horizontal slip rate (mm/yr)	Dip (°)		Sense of slip	Width (km)	Length (km)	M	Characteristic rate	Gutenberg-Richter a-value	Gutenberg-Richter b-value
Embudo fault	0.09	90		strike slip	15	66	7.19	3.90E-05	0.7851453	0.8
Gallina fault	0.02	50	E	normal	20	39	6.93	2.17E-05	0.41997	0.8
Hubbell Springs fault	0.089	50	W	normal	20	45	7	8.72E-05	1.1024992	0.8
Jemez-San Ysidro fault	0.02	50	E	normal	20	54	7.09	1.70E-05	0.31491816	0.8
La Bajada fault	0.078	50	W	normal	20	42	6.96	8.10E-05	1.0260626	0.8
La Canada del Amagre fault zone	0.012	50	E	normal	20	17	6.5	2.44E-05	NA	NA
La Jencia fault	0.021	50	E	normal	20	33	6.84	2.57E-05	0.3945969	0.8
Lobato Mesa fault zone	0.0054	50	W	normal	20	19	6.56	1.00E-05	0.27112764	0.8
Nacimiento fault	0.02	50	E	normal	20	83	7.3	1.27E-05	0.2915034	0.8
Nambe fault	0.02	50	W	normal	20	50	7.05	1.81E-05	0.29710352	0.8
Organ Mountains fault	0.15	50	E	normal	20	30	6.79	1.98E-04	1.5264946	0.8
Pajarito fault	NA	50	E	normal	20	50	7.05	9.90E-05	1.0362936	0.8
Picuris-Pecos fault	0.05	50	W	normal	20	99	7.39	2.78E-05	0.7286884	0.8
Pojoaque fault	0.02	50	W	normal	20	48	7.03	1.87E-05	0.29133075	0.8
Puye fault	0.03	50	E	normal	20	20	6.59	5.31E-05	1.028595	0.8
San Andres Mountains fault	0.1	50	E	normal	20	130	7.5*		1.100531	0.8
San Felipe fault zone	0.043	50	E	normal	20	43	6.97	4.42E-05	0.7741354	0.8
San Francisco fault	0.063	50	W	normal	20	28	6.76	8.77E-05	1.1385194	0.8
Sawyer Canyon fault	0.024	50	E	normal	20	8	6.15	8.24E-05	NA	NA
Socorro Canyon fault zone	0.027	50	E	normal	20	49	7.04	2.50E-05	0.42780202	0.8
Southern Sangre de Cristo fault	0.13	50	W	normal	20	104	7.42	6.83E-05	1.1506004	0.8
Tijeras-Canoncito fault	0.09	90		strike slip	15	81	7.29	3.40E-05	0.708118	0.8
Zia fault	0.038	50	E	normal	20	33	6.84	4.68E-05	0.65372443	0.8
Texas										
Acala fault	0.088	50	SW	normal	20	7	6.09	3.27E-04	NA	NA
Amargosa fault	0.11	50	NE	normal	20	70	7.22	7.77E-05	0.9918686	0.8
Arroyo Diablo fault	0.013	50	SW	normal	20	14	6.41	3.03E-05	NA	NA

Table G-3. Intermountain West fault parameters by State.—Continued

Fault name	Vertical or horizontal slip rate (mm/yr)	Dip (°)		Sense of slip	Width (km)	Length (km)	M	Characteristic rate	Gutenberg-Richter a-value	Gutenberg-Richter b-value
Caballo fault	0.11	50	SW	normal	20	42	6.97	1.12E-04	1.1767493	0.8
Campo Grande fault	0.048	50	SW	normal	20	45	7	4.67E-05	0.8312168	0.8
East Baylor Mountain - Carizzo Mountain fault	0.008	50	SE	normal	20	41	6.96	8.22E-06	0.03237028	0.8
East Franklin Mountains fault	0.1	50	E	normal	20	48	7.03	9.40E-05	0.99157643	0.8
East Sierra Diablo fault	0.02	50	E	normal	20	35	6.86	2.42E-05	0.3905596	0.8
West Delaware Mountains fault zone	0.024	50	SW	normal	20	25	6.7	3.65E-05	0.6902017	0.8
West Eagle Mountains-Red Hills fault	0.013	50	SW	normal	20	24	6.69	2.00E-05	0.4178935	0.8
West Indio Mountains fault	0.044	50	SW	normal	20	23	6.66	7.13E-05	0.9353471	0.8
West Lobo Valley fault zone	0.034	50	E	normal	20	61	7.15	2.69E-05	0.5796732	0.8
Utah										
East Cache fault zone	0.2	50	W	normal	20	83	7.31	1.23E-04	1.2883028	0.8
Great Salt Lake fault zone, Antelope Island segment	0.6	50	W	normal	20	39	6.93	6.52E-04	1.8982953	0.8
Great Salt Lake fault zone, Fremont Island segment	0.6	50	W	normal	20	32	6.83	7.46E-04	1.8456042	0.8
Great Salt Lake fault zone, Promontory segment	0.6	50	W	normal	20	54	7.09	5.11E-04	1.793224	0.8
Hansel Valley fault	0.1	50	E	normal	20	13	6.6	1.13E-04	1.3680598	0.8
Hurricane fault zone (northern)	0.2	50	NW	normal	20	47	7.02	1.89E-04	1.2834035	0.8
Joes Valley fault zone	NA	50	W	normal	20	47	7	1.02E-04	1.4678782	0.8
Morgan fault	0.02	50	W	normal	20	17	6.52	3.93E-05	0.81770503	0.8
North Promontory fault	0.2	50	W	normal	20	27	6.73	2.92E-04	1.6267301	0.8
Oquirrh fault zone	0.2	50	W	normal	20	27	6.7	2.59E-04	1.54073	0.8
Oquirrh-Southern Oquirrh Mountains fault zone	0.2	50	W	normal	20	63	7.17	1.53E-04	1.3553717	0.8
Paragonah fault	0.46	50	NW	normal	20	27	6.75	6.47E-04	1.995324	0.8
Sevier/Toroweap fault zone (northern)	0.36	50	W	normal	20	87	7.33	2.18E-04	1.5575325	0.8

Table G-3. Intermountain West fault parameters by State.—Continued

Fault name	Vertical or horizontal slip rate (mm/yr)	Dip (°)		Sense of slip	Width (km)	Length (km)	M	Characteristic rate	Gutenberg-Richter a-value	Gutenberg-Richter b-value
Stansbury fault zone	0.4	50	W	normal	20	54	7.09	3.43E-04	1.6193315	0.8
Strawberry fault	0.1	50	W	normal	20	39	6.92	1.11E-04	1.1174334	0.8
Utah Lake faults	0.4	50	W	normal	20	31	6.81	5.17E-04	1.6635933	0.8
Wasatch fault *(floating M7.4)*	1.2	50	W	normal	20	327	7.4		3.21964	0.8
Wasatch fault, Brigham City segment		50	W	normal	20	41	6.9 6.7 7.1	7.7E-4 0.6 7.7E-4 0.2 7.7E-4 0.2	2.29257	0.8
Wasatch fault, Levan segment		50	W	normal	20	32	6.8 6.6 7.0.	2.37E-4 0.6 2.37E-4 0.2 2.37E-4 0.2	1.56260	0.8
Wasatch fault, Nephi segment		50	W	normal	20	44	7.0 6.8 7.2.	4E-4 0.6 4E-4 0.2 4E-4 0.2	2.20522	0.8
Wasatch fault, Provo segment		50	W	normal	20	77	7.4 7.2 7.6	4.2E-4 0.6 4.2E-4 0.2 4.2E-4 0.2	2.03881	0.8
Wasatch fault, Salt Lake City segment		50	W	normal	20	48	7.0 7.2 6.8	7.7E-4 0.6 7.7E-4 0.2 7.7E-4 0.2	2.26023	0.8
Wasatch fault, Weber segment		50	W	normal	20	63	7.2 7.0 7.4.	7.1E-4 0.6 7.1E-4 0.2 7.1E-4 0.2	2.11524	0.8
West Cache fault, Clarkston segment	0.4	50	E	normal	20	23	6.66	6.48E-04	1.8939321	0.8
West Cache fault, Wellsville segment	0.1	50	NE	normal	20	20	6.6	1.76E-04	1.559867	0.8
West Valley fault zone	0.4	50	E	normal	20	16	6.48	8.45E-04		

Table G-3. Intermountain West fault parameters by State.—Continued

Fault name	Vertical or horizontal slip rate (mm/yr)	Dip (°)		Sense of slip	Width (km)	Length (km)	M	Characteristic rate	Gutenberg-Richter a-value	Gutenberg-Richter b-value
Wyoming										
Bear River fault zone	1.5	50	W	normal	20	37	6.9	4.35E-04	1.6894047	0.8
Eagle Bay fault	0.48	50	E	normal	20	32	6.82	6.13E-04	1.748995	0.8
East Mount Sheridan faults	1.4	50	E	normal	20	22	6.64	2.32E-03	2.4247884	0.8
Grand Valley fault	1.1	50	W	normal	20	55	7.1	9.31E-04	2.0645933	0.8
Greys River fault	0.62	50	W	normal	20	50	7.05	5.64E-04	1.7916788	0.8
Hoback fault	0.071	50	SW	normal	20	19	6.56	1.33E-04	1.39176	0.8
Rock Creek fault	1.7	50	W	normal	20	41	6.95	1.79E-03	2.3599827	0.8
Teton fault	1.3	50	E	normal	20	62	7.16	9.96E-04	2.1593647	0.8
Upper Yellowstone Valley faults	0.37	50	E	normal	20	18	6.54	7.06E-04	2.0950741	0.8

References

Anderson, L.W., and LaForge, R., 2003, Seismotectonic study for Canyon Ferry Dam, Missouri River Basin Project, Montana: Bureau of Reclamation Seismotectonic Report 2003-1, 70 p.

Bell, J.W., dePolo, C.M., Ramelli, A.R., Sarna-Wojcicki, A.M., Meyer, C.E., 1999, Surface faulting and paleoseismic history of the 1932 Cedar Mountain earthquake area, west-central Nevada, and implications for modern tectonics of the Walker Lane: Geological Society of America Bulletin, v. 111, p. 791–807.

Black, B.D., Giraud, R.E., and Mayes, B.H. , 2000, Paleoseismic investigation of the Clarkston, Junction Hills, and Wellsville faults, West Cache fault zone, Cache County, Utah: Utah Geological Survey Special Study 98, 23 p.

dePolo, C.M., 2006, Determination of fault slip rates, paleoearthquake history, and segmentation of the Warm Springs Valley fault system: Technical report to U.S. Geological Survey, Reston, Virginia, under Contract 04HQGR0082, 35 p.

Dinter, D.A., and Pechmann, J.C., 2000, Paleoseismology of the East Great Salt Lake fault: U.S. Geological Survey National Earthquake Hazards Reduction Program, Annual Summary, v. 42, USGS External Grant award no. 98HQGR1013, 6 p. Available at *http://erp-web.er.usgs.gov/reports/annsum/vol42/ni/ni_vol42.htm*.

Fenton, C.R., Webb, R.H., Pearthree, P.A., Cerling, T.E., and Poreda, R.J., 2001, Displacement rates on the Toroweap and Hurricane faults—Implications for Quaternary downcutting in the Grand Canyon, Arizona: Geology, v. 29, p. 1035–1038.

Foley, L.L., Martin, R.A., Jr., and Sullivan, J.T., 1986, Seismotectonic study for Joes Valley, Scofield and Huntington North Dams, Emery County and Scofield Projects, Utah: Bureau of Reclamation Seismotectonic Report 86-7, 132 p., 3 pls.

Gardner, J.N., Lewis, C.J., Lavine, A., Reneau, S.L., and Schultz, E., 2005, Evaluating seismic hazards at Los Alamos National Laboratory—Geology and paleoseismology of the Pajarito fault system, Rio Grande Rift, New Mexico: Los Alamos National Laboratory Report LA-UR-05-4662, 42 p. (36 MB Microsoft Powerpoint file).

Keaton, J.R., and Currey, D.R., 1989, Earthquake hazard evaluation of the West Valley fault zone in the Salt Lake City urban area, Utah: Technical report to U.S. Geological Survey, Salt Lake City, under Contract 14-08-001-G1397, 69 p.

Keaton, J.R., Currey, D.R., and Olig, S.J., 1987, Paleoseismicity and earthquake hazards evaluation of the West Valley fault zone, Salt Lake urban area: Technical report to U.S. Geological Survey, under Contract 14-08-0001-22048, April 1986 (Draft), 18 p.

Lund, W.R., 2005, Consensus preferred recurrence-intervals and vertical slip-rate estimates—Review of Utah paleoseismic-trenching data by the Utah Quaternary Fault Parameters Working Group: Utah Geological Survey Bulletin 134, 114 p., http://ugspub.nr.utah.gov/publications/bulletins/B-134.pdf.

Lund, W.R., ed., 2006, Basin and Range Province Earthquake Working Group seismic-hazard recommendations to the U.S. Geological Survey National Seismic Hazard Mapping Program: Utah Geological Survey Open-File Report 477, 23 p.

McCalpin, J.P., 1985, Quaternary fault history and earthquake potential of the Hansel Valley area, north-central Utah: U.S. Geological Survey Final Technical Report, 37 p.

McCalpin, J.P., 1994, Neotectonic deformation along the East Cache fault zone, Cache County, Utah: Utah Geological Survey Special Study 83, 37 p.

McCalpin, J.P., 2003, Neotectonics of the Bear Lake Valley, Utah and Idaho; A preliminary assessment: Utah Geological Survey Miscellaneous Publication 03-4, 43 p.

McCalpin, J.P., and Harrison, J.B.J., 2000, Paleoseismicity of Quaternary faults near Albuquerque, New Mexico: Final Technical Report to U.S. Geological Survey for contract 99HQGR0056, 46 p.

McCalpin, J., Robison, R.M., and Garr, J.D., 1992, Neotectonics of the Hansel Valley-Pocatello Valley corridor, northern Utah and southern Idaho, *in* Gori, P.L., and Hays, W.W., eds., Assessment of regional earthquake hazards and risk along the Wasatch front, Utah: U.S. Geological Survey Professional Paper 1500, p. G1–G18.

Olig, S.S., Gorton, A.E., Black, B.D., and Forman, S.L., 2001, Paleoseismology of the Mercur fault and segmentation of the Oquirrh-East Great Salt Lake fault zone, Utah: Technical report to U.S. Geological Survey, Reston, Virginia, under Contract 98HQGR1036, January 25, 2001, variously paginated.

Personius, S.F., and Mahan, S.A., 2003, Paleoearthquakes and eolian-dominated fault sedimentation along the Hubbell Spring fault zone near Albuquerque, New Mexico: Bulletin of the Seismological Society of America, v. 93, no. 3, p. 1355–1369.

Personius, S.F., and Mahan, S.A., 2000, Paleoearthquake recurrence on the East Paradise fault zone, metropolitan Albuquerque, New Mexico: Bulletin of the Seismological Society of America, v. 90, no. 2, p. 357–369.

Phillips, F.M., Ayarbe, J.P., Harrison, J.B.J., and Elmore, D., 2003, Dating rupture events on alluvial fault scarps using cosmogenic nuclides and scarp morphology: Earth and Planetary Science Letters, v. 215, p. 203–218.

Ramelli, A.R., Bell, J.W., dePolo, C.M., and Yount, J.C., 1999, Large-magnitude, late Holocene earthquakes on the Genoa fault, west-central Nevada and eastern California: Bulletin of the Seismological Society of America, v. 89, p. 1458–1472.

Ramelli, A.R., dePolo, C.M., and Bell, J.W., 2002, Paleoseismic studies of the Peavine Peak fault: Technical report to U.S. Geological Survey, Reston, Virginia, under Contract 01HQGR0167, 14 p.

Stenner, H.D., Lund, W.R., Pearthree, P.A., and Everitt, B.L., 1999, Paleoseismic investigation of the Hurricane fault in northwestern Arizona and southwestern Utah: Arizona Geological Survey Open-File Report 99-8, 137 p.

Sullivan, J.T., and Nelson, A.R., 1992, Late Quaternary displacement on the Morgan fault, a back valley fault in the Wasatch Range of northeastern Utah, *in* Gori, P.L., and Hays, W.W., eds., Assessment of regional earthquake hazards and risk along the Wasatch front, Utah: U.S. Geological Survey Professional Paper 1500, p. I1–I19.

Sullivan, J.T., Nelson, A.R., LaForge, R.C., Wood, C.K., and Hansen, R.A., 1988, Central Utah regional seismotectonic study for USBR dams in the Wasatch Mountains: Bureau of Reclamation Seismotectonic Report 88-5, 269 p.

West, M.W., 1994, Paleoseismology of Utah, Volume 4—Seismotectonics of north-central Utah and southwestern Wyoming: Utah Geological Survey Special Study 82, 93 p., 5 pls.

Wong, I., Kelson, K., Olig, S., Kolbe, T., Hemphill-Haley, M., Bott, J., Green, R., Kanakari, H., Sawyer, J., Silva, W., Stark, C., Haraden, C., Fenton, C., Unruh, J., Gardner, J., Reneau, S., and House, L., 1995, Seismic hazards evaluation of the Los Alamos National Laboratory: Technical report to Los Alamos National Laboratory, Las Alamos, New Mexico, February 24, 1995, 3 volumes, 12 pls., 16 appendixes

Appendix H. Parameters for Faults in the Pacific Northwest

By Kathleen M. Haller and Russell L. Wheeler

In the 2008 model, we made several subtle changes in the treatment of crustal faults in the Pacific Coast States of Oregon and Washington to integrate feedback from the Working Group on Pacific Northwest faults, Western Seismic Safety Policy Council (WSSPC), and the regional Pacific Northwest workshop. First, we included region of predominately normal faults in southeastern Oregon into a set of files, orwa_n.* to reduce the default dip to 50° (fig. H-1) as applied in adjacent regions to the east and southeast. We also allow for variable dip as discussed in Appendix J. These faults are modeled following the logic tree in figure 17. The other crustal faults in Oregon and Washington are modeled following the logic tree in figure 19, which does not carry dip uncertainty, and truncated Gutenberg-Richter and characteristic magnitude distributions are given equal weight, as in the 2002 model. This compressional-zone weight scheme has roughly the same effect on probabilistic ground motion as including dip uncertainty and a 2/3 char, 1/3 GR weight scheme that is used for the faults in the extensional region.

Three new sources were added to the model including the Lake Creek–Boundary Creek and Boulder Creek faults and the Stonewall anticline feature. The Lake Creek–Boundary Creek fault is located near Port Angeles, Wash. Recent paleoseismic investigations of this fault suggest that two closely spaced late Holocene events were preceded by a period of quiescence up to 10 k.y. (Nelson and others, 2007), which complicates assigning mean slip rate. However, we assigned a mean slip rate of 0.43 mm/yr to this fault. The Boulder Creek fault is near the Canadian border near Bellingham, Wash.

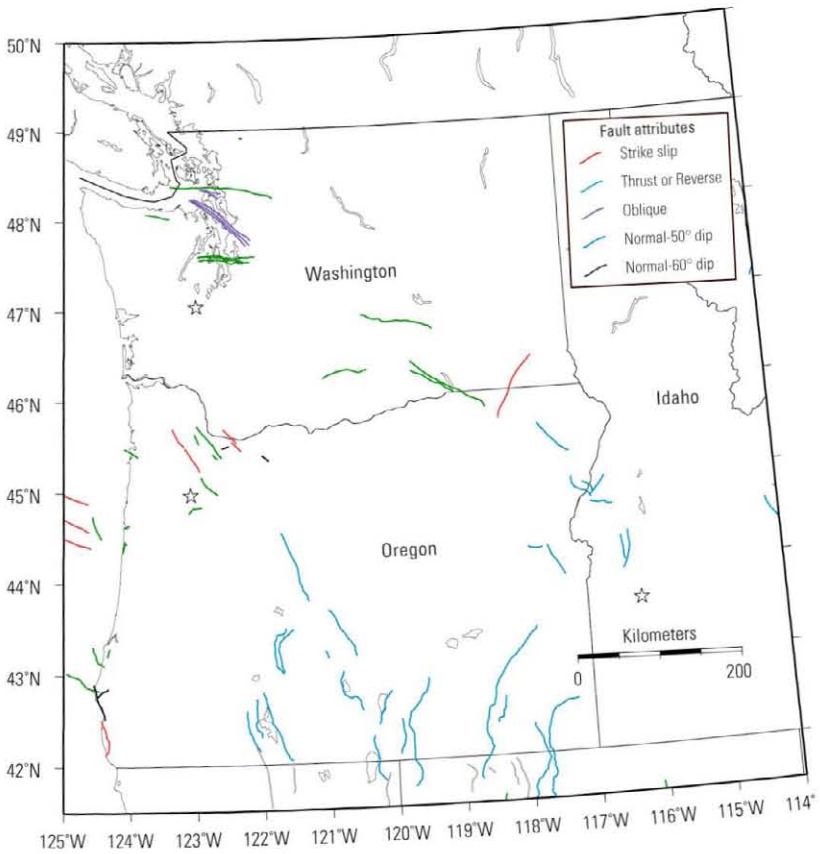

Figure H-1. Map of fault sources in the Pacific Northwest showing sense of slip by color.

Paleoseismic investigations (Haugerud and others, 2005; Barnett and others, 2006, 2007; Siedlecki and Schermer, 2007) indicate 2.5 meters of slip has occurred over 7,600 years, which suggests slip rate of 0.33 mm/yr. The fault is expressed as two short scarps. We assigned a fixed characteristic magnitude of M6.8 based on reported average slip per event of 70 cm. Because of the short length of the fault and the initial work on this fault is ongoing, we do not currently carry the truncated Gutenburg-Richter branch for this source. The Stonewall anticline had not been considered in previous versions of the maps; we add it to this version based on Yeats and others (1998).

Based on input from the Pacific Northwest workshop, we changed the single fault location for the South Whidbey Island fault to three subparallel faults that share the total 0.6 mm/yr slip rate used in prior models. The faults in the new fault representation are longer; thus, the characteristic magnitudes have increased approximately 0.2 magnitude units.

Table H-1. Pacific Northwest fault parameters by State.
[Refer to *http://gldims.cr.usgs.gov/webapps/cfusion/Sites/hazfaults_search/hf_search_main.cfm?hazmap=2008* for further documentation of source material—mm/yr, millimeters per year; °, degree; km, kilometers]

Fault name	Vertical or horizontal slip rate (mm/yr)	Dip (°)		Sense of slip	Width (km)	Length (km)	Magnitude	Characteristic rate	Gutenberg-Richter a-value	Gutenberg-Richter b-value
Oregon										
Abert Rim fault	0.5	50	W	normal	20	45	7	4.92E-04	1.8536639	0.8
Alvin Canyon fault	6.4	90		strike slip	15	71	7.23	2.61E-03	2.529093	0.8
Battle Rock fault zone	0.1	50	NE	normal	20	45	7	9.73E-05	1.1503175	0.8
Beaver Creek fault zone	0.2	50	SE	normal	20	17	6.52	3.96E-04	1.8206571	0.8
Bolton fault	0.013	60	SW	reverse	17	9	6.19	3.28E-05	NA	NA
Cape Blanco anticline	1.4	45	S	thrust	21	47	7.02	1.56E-03	2.20199	0.8
Chemult graben fault system (east)	0.052	50	W	normal	20	62	7.16	3.98E-05	0.76154273	0.8
Chemult graben fault system (west)	0.44	50	E	normal	20	68	7.21	3.13E-04	1.5856717	0.8
Coquille anticline	0.24	60	SW	reverse	17	29	6.78	2.54E-04	1.6225786	0.8
Cottonwood Mountain fault	0.09	50	NE	normal	20	42	6.97	9.16E-05	1.09056	0.8
Daisy Bank fault	5.7	90		strike slip	15	81	7.3	2.08E-03	2.5063807	0.8
Gales Creek fault zone	0.016	90		strike slip	15	27	6.75	1.31E-05	0.3024114	0.8
Goose Lake	0.1	50	W	normal	20	60	7.14	7.99E-05	1.0417969	0.8
Grant Butte fault	0.11	50	NW	normal	20	9	6.21	3.41E-04	NA	NA
Happy Camp fault	0.025	60	N	reverse	17	20	6.58	3.55E-05	0.8424882	0.8
Helvetia fault	0.014	60	NE	reverse	17	14	6.4	2.56E-05	NA	NA
Juniper Mountain fault	0.01	50	N	normal	20	18	6.53	1.94E-05	0.52264785	0.8
Klamath graben fault system (east)	0.2	50	W	normal	20	92	7.36	1.15E-04	1.3133024	0.8
Klamath graben fault system (west)	0.16	50	E	normal	20	51	7.06	1.42E-04	1.2051246	0.8
Lacamas Lake fault	0.026	90		strike slip	15	24	6.67	2.44E-05	0.48052972	0.8
Metolius fault zone	0.038	50	SW	normal	20	92	7.36	2.18E-05	0.5904285	0.8

Table H-1. Pacific Northwest fault parameters by State.—Continued

Fault name	Vertical or horizontal slip rate (mm/yr)	Dip (°)		Sense of slip	Width (km)	Length (km)	Magnitude	Characteristic rate	Gutenberg-Richter a-value	Gutenberg-Richter b-value
Mount Angel fault	0.067	60	NE	reverse	17	30	6.8	6.85E-05	0.77476245	0.8
Mount Hood fault	0.16	50	NE	normal	20	11	6.29	4.45E-04	NA	NA
Newberg fault	0.016	90		strike slip	15	34	6.85	1.14E-05	0.053293127	0.8
Paulina Marsh fault	0.29	50	SW	normal	20	10	6.26	8.41E-04	NA	NA
Pine Valley graben fault system, Brownlee section	0.008	50	SW	normal	20	19	6.56	1.50E-05	0.445314	0.8
Pine Valley graben fault system, Halfway-Posey Valley section	0.008	50	NE	normal	20	38	6.91	8.96E-06	0.014196634	0.8
Portland Hills fault	0.1	60	SW	reverse	17	50	7.05	7.07E-05	0.8903394	0.8
Sandy River fault zone	0.016	90		strike slip	15	17	6.5	1.89E-05	NA	NA
Santa Rosa fault system	0.13	50	W	normal	20	171	7.5*	5.39E-05	1.3327227	0.8
Sky Lakes fault zone	0.28	50	E	normal	20	53	7.08	2.45E-04	1.4632595	0.8
South Slough thrust and reverse faults	0.62	60	W	reverse	17	11	6.29	1.33E-03	NA	NA
Southeast Newberry fault zone	0.51	50	SW	normal	20	68	7.2	3.74E-04	1.7777597	0.8
Steens fault zone	0.3	50	E	normal	20	214	7.5*	1.24E-04	1.7935853	0.8
Tule Springs Rim fault	0.1	50	W	normal	20	37	6.9	1.12E-04	1.1019461	0.8
Turner and Mill Creek faults	0.007	60	SE	reverse	17	20	6.59	9.79E-06	0.29409804	0.8
Waldport fault	0.14	60	E	reverse	17	15	6.43	2.47E-04	NA	NA
Wallowa fault	0.14	50	NE	normal	20	53	7.08	1.21E-04	1.1553462	0.8
Warner Valley faults (east)	0.11	50	W	normal	20	147	7.5		1.1963375	0.8
Warner Valley faults (west)	0.11	50	E	normal	20	44	6.99	1.08E-04	1.1843001	0.8
Wecoma fault	8.5	90		strike slip	15	88	7.34	2.95E-03	2.7000494	0.8
Whaleshead fault zone	2.55	90		strike slip	15	46	7.01	1.45E-03	2.1573264	0.8
Winter Rim fault system	0.43	50	E	normal	20	66	7.19	3.18E-04	1.6960521	0.8
Yaquina faults	0.6	60	N	reverse	17	8	6.14	1.62E-03	NA	NA

Table H-1. Pacific Northwest fault parameters by State.—Continued

Fault name	Vertical or horizontal slip rate (mm/yr)	Dip (°)		Sense of slip	Width (km)	Length (km)	Magnitude	Characteristic rate	Gutenberg-Richter a-value	Gutenberg-Richter b-value
Washington										
Boulder Creek fault	0.33	60		reverse	17	11	6.8*	3.24E-04*		
Devils Mountain fault	0.15	60	N	reverse	17	125			1.1531128	0.8
Hite fault system	0.02	90		strike slip	15	88	7.34	6.92E-06	0.0706793	0.8
Horse Haven Hills structure (NW trend)	0.031	60	W	reverse	17	59	7.14	1.92E-05	0.4226207	0.8
Lake Creek-Boundary Creek fault	0.43	60	N	reverse	17	30	6.79	6.64E-04	1.8786485	0.8
Mill Creek Thrust fault	0.038	60	S	reverse	17	56	7.11	2.48E-05	0.5012743	0.8
Rattlesnake-Wallula fault system	0.043	60	SW	reverse	17	109	7.44	1.73E-05	0.5754388	0.8
Saddle Mountain fault	0.052	60	S	reverse	17	91	7.35	2.39E-05	0.6193971	0.8
Seattle fault zone-middle		45	S	thrust	21	64	7.2		1.11	0.8
Seattle fault zone-northern		45	S	thrust	21	71	7.2	2.00E-04	1.15	0.8
Seattle fault zone-southern		45	S	thrust	21	56	7.1		1.16	0.8
Southern Whidbey Island fault-middle	0.2	60	N	oblique	17	109	7.44	1.34E-04	1.24270	0.8
Southern Whidbey Island fault northern	0.2	60	N	oblique	17	105	7.42	1.40E-04	1.23295	0.8
Southern Whidbey Island fault-southern	0.2	60	N	oblique	17	105	7.42	1.40E-04	1.23519	0.8
Strawberry Point fault	0.25	90		oblique	15	26	6.73	2.11E-04	1.4862921	0.8
Stonewall anticline		60		reverse	17	30	6.8		1.6484004	0.8
Utsalady Point fault	0.15	90		oblique	15	25	6.69	1.36E-04	1.2508161	0.8

References

Barnett, E.A., Kelsey, H.M., Sherrod, B.L., Blakely, R.J., Hughes, J.F., Schermer, E.R., Haugerud, R.A., Weaver, C.S., and Siedlecki, E., 2006, Active faulting at the northeast margin of the greater Puget Lowland—A paleoseismic and magnetic-anomaly study of the Kendall Scarp, Whatcom County, northwest Washington: Eos, Transactions, American Geophysical Union, v. 87, Abstract S31A-0183.

Barnett, E.A., Kelsey, H.M., Sherrod, B., Blakely, R.J., Hughes, J., Schermer, E.R., Haugerud, R.A., Weaver, C., Siedlecki, E.M., and Blakely, R.J., 2007, Active faulting at the northeast margin of the greater Puget Lowland; a trenching and wetland coring study of the Kendall Fault scarp, Whatcom County, northwest Washington: Geological Society of America Abstracts with Programs, v. 39, p. 61.

Haugerud, R.A., Sherrod, B.L., Wells, R.E., Hyatt, T., 2005, Holocene displacement on the Boulder Creek Fault near Bellingham, WA and implications for kinematics of deformation of the Cascadia Forearc: Geological Society of America Abstracts with Programs, v. 37, p. 476.

Nelson, A.R., Personius, S.F., Buck, J., Bradley, L-A., Wells, R.E., and Schermer, E.R., 2007, Field and laboratory data from an earthquake history study of scarps of the Lake Creek-Boundary Creek fault between the Elwha River and Siebert Creek, Clallam County, Washington: U.S. Geological Survey Scientific Investigations Map SIM-2961, 2 sheets.

Siedlecki, E.M., and Schermer, E.R., 2007, Paleoseismology of the Boulder Creek fault, Kendall, WA: Geological Society of America Abstracts with Programs, v. 39, p. 26.

Yeats, R.S., Kulm, L.D., Goldfinger, C., and McNeill, L.C., 1998, Stonewall anticline—an active fold on the Oregon continental shelf: Geological Society of America Bulletin, v. 110, p. 527–587.

Appendix I. Parameters for Faults in California

From Working Group on California Earthquake Probabilities report (Field and others, 2008; Wills and others, 2008)

Table I-1. Rupture-model data for Type-A faults. Rupture names include the segments involved; see table 2 of Field and others (2008) for segment name definitions. "Ellsworth" and "Hanks and Bakun" represent Ellsworth (2003) B magnitude-area relationship and Hanks and Bakun (2002) magnitude-area relationships, respectively. The values under "Ellsworth-B Rate" and "Hanks and Bakun Rate" are for the moment-balanced models (using Deformation Model D2.1).

Rupture name (segments involved)	Area (km2)	Ellsworth mag	Hanks and Bakun mag	A-priori rate	Ellsworth-B rate	Hanks and Bakun rate
Elsinore fault						
W	674.8	7.03	6.84	7.14E–04	9.27E–04	1.37E–03
GI	488.6	6.89	6.67	2.55E–03	1.19E–03	2.19E–03
T	734.9	7.07	6.89	6.10E–04	1.24E–04	3.46E–04
J	1426.1	7.35	7.28	Unlikely	3.85E–05	2.48E–05
CM	517.3	6.91	6.69	5.71E–04	1.04E–03	2.11E–03
W+GI	1163.4	7.27	7.16	Unlikely	2.48E–05	1.42E–04
GI+T	1223.5	7.29	7.19	8.90E–04	1.25E–04	1.25E–04
T+J	2161	7.53	7.52	Unknown	1.27E–04	1.26E–04
J+CM	1943.3	7.49	7.45	Unknown	1.74E–04	2.92E–04
W+GI+T	1898.3	7.48	7.44	Unlikely	2.48E–05	9.07E–05
GI+T+J	2649.6	7.62	7.63	Unknown	1.26E–04	1.27E–04
T+J+CM	2678.2	7.63	7.64	2.50E–04	2.83E–04	2.54E–04
W+GI+T+J	3324.4	7.72	7.77	Unlikely	2.52E–05	2.48E–05
GI+T+J+CM	3166.9	7.7	7.74	2.50E–04	1.83E–04	1.27E–04
W+GI+T+J+CM	3841.7	7.78	7.85	Unlikely	2.49E–05	2.52E–05
Total				*5.84E–03*	*4.43E–03*	*7.37E–03*
Garlock fault						
GE	519.3	6.92	6.7	6.80E–04	3.61E–04	6.21E–04
GC	1276.1	7.31	7.21	7.84E–05	9.26E–05	8.32E–05
GW	1290.9	7.31	7.22	2.36E–04	2.19E–04	2.61E–04
GE+GC	1795.4	7.45	7.41	7.84E–05	9.05E–05	8.32E–05
GC+GW	2567.1	7.61	7.62	3.13E–04	5.99E–04	5.50E–04
GE+GC+GW	3086.3	7.69	7.72	3.13E–04	5.83E–04	5.78E–04
Total				*1.70E–03*	*1.95E–03*	*2.18E–03*
San Jacinto fault						
SBV	725.7	7.06	6.88	2.31E–03	4.39E–04	4.42E–04
SJV	686.7	7.04	6.85	2.43E–03	4.50E–04	4.49E–04
A	1193.9	7.28	7.17	Unlikely	8.83E–05	8.82E–05
C	786.1	7.1	6.93	Unlikely	8.87E–05	8.98E–05
CC	681.5	7.03	6.85	8.89E–04	4.50E–04	4.48E–04
B	403.6	6.81	6.59	4.82E–03	4.45E–04	4.43E–04
SM	325.8	6.71	6.49	1.09E–03	1.50E–03	4.01E–03

Table I-1. Rupture-model data for Type-A faults.—Continued

Rupture name (segments involved)	Area (km2)	Ellsworth mag	Hanks and Bakun mag	A-priori rate	Ellsworth-B rate	Hanks and Bakun rate
SBV+SJV	1412.4	7.35	7.27	1.32E–03	4.49E–04	4.41E–04
SJV+A	1880.6	7.47	7.44	Unknown	4.41E–04	4.50E–04
A+C	1980.1	7.5	7.47	3.15E–03	1.21E–03	1.16E–03
A+CC	1875.4	7.47	7.43	Unlikely	8.82E–05	9.00E–05
CC+B	1085.1	7.24	7.12	8.89E–04	4.50E–04	4.47E–04
B+SM	729.4	7.06	6.89	1.09E–03	4.40E–04	4.43E–04
SBV+SJV+A	2606.4	7.62	7.62	Unknown	4.47E–04	4.48E–04
SJV+A+C	2666.8	7.63	7.64	Unknown	4.48E–04	4.51E–04
SJV+A+CC	2562.2	7.61	7.61	Unlikely	8.91E–05	8.93E–05
A+CC+B	2279.1	7.56	7.55	Unlikely	9.02E–05	8.95E–05
CC+B+SM	1411	7.35	7.27	8.89E–04	4.48E–04	4.40E–04
SBV+SJV+A+C	3392.5	7.73	7.78	1.05E–03	4.49E–04	4.41E–04
SBV+SJV+A+CC	3287.9	7.72	7.76	Unlikely	8.94E–05	9.03E–05
SJV+A+CC+B	2965.8	7.67	7.7	Unlikely	8.82E–05	8.89E–05
A+CC+B+SM	2604.9	7.62	7.62	Unlikely	8.93E–05	8.96E–05
SBV+SJV+A+CC+B	3691.5	7.77	7.83	Unlikely	8.80E–05	8.97E–05
SJV+A+CC+B+SM	3291.6	7.72	7.76	Unlikely	8.94E–05	9.03E–05
SBV+SJV+A+CC+B+SM	4017.3	7.8	7.88	Unlikely	8.90E–05	8.82E–05
Total				*1.99E–02*	*9.05E–03*	*1.15E–02*
Northern San Andreas fault						
SAO	1469.9	7.37	7.29	4.93E–04	1.16E–03	1.01E–03
SAN	2044.4	7.51	7.48	2.09E–05	2.00E–05	1.99E–05
SAP	1078.4	7.23	7.11	5.31E–04	1.22E–04	1.05E–05
SAS	838.5	7.12	6.97	7.64E–04	2.09E–03	2.40E–03
SAO+SAN	3514.3	7.75	7.8	1.07E–03	2.77E–03	2.99E–03
SAN+SAP	3122.8	7.69	7.73	Unlikely	2.08E–06	2.11E–06
SAP+SAS	1916.9	7.48	7.45	1.03E–03	2.19E–03	3.63E–03
SAO+SAN+SAP	4592.7	7.86	7.95	8.21E–05	7.10E–05	4.91E–05
SAN+SAP+SAS	3961.3	7.8	7.87	2.52E–05	2.32E–05	2.27E–05
SAO+SAN+SAP+SAS	5431.1	7.93	8.05	2.84E–03	9.97E–04	3.09E–04
Total				*6.85E–03*	*9.45E–03*	*1.05E–02*
Southern San Andreas fault						
PK	78	6.09	5.87	3.46E–02	2.49E–02	5.26E–02
CH	750.2	7.08	6.9	5.00E–05	5.21E–05	5.46E–05
CC	891.2	7.15	7	3.00E–04	1.60E–04	5.74E–05
BB	751	7.08	6.9	3.00E–04	5.68E–04	5.26E–04
NM	556.5	6.95	6.73	2.00E–04	1.05E–04	1.44E–04
SM	1279	7.31	7.21	5.00E–04	6.45E–04	6.78E–04
NSB	451.9	6.86	6.64	7.00E–04	7.12E–04	6.64E–04
SSB	555.5	6.94	6.73	5.00E–05	5.10E–05	5.17E–05
BG	843	7.13	6.97	5.00E–04	1.88E–04	1.35E–05
CO	693.4	7.04	6.86	2.50E–03	6.70E–03	1.21E–02

Table I-1. Rupture-model data for Type-A faults.—Continued

Rupture name (segments involved)	Area (km2)	Ellsworth mag	Hanks and Bakun mag	A-priori rate	Ellsworth-B rate	Hanks and Bakun rate
PK+CH	828.2	7.12	6.96	1.60E–03	4.36E–03	7.01E–03
CH+CC	1641.4	7.42	7.36	3.00E–04	2.39E–04	2.15E–04
CC+BB	1642.2	7.42	7.36	Unknown	5.02E–06	5.07E–06
BB+NM	1307.5	7.32	7.23	Unlikely	1.01E–06	1.01E–06
NM+SM	1835.4	7.46	7.42	7.00E–04	4.95E–06	5.04E–06
SM+NSB	1730.9	7.44	7.39	6.00E–04	8.79E–04	8.90E–04
NSB+SSB	1007.4	7.2	7.07	8.00E–04	1.05E–03	1.22E–03
SSB+BG	1398.5	7.35	7.26	9.00E–04	5.03E–06	4.95E–06
BG+CO	1536.4	7.39	7.32	7.00E–04	2.83E–04	4.10E–04
PK+CH+CC	1719.4	7.44	7.38	7.00E–04	4.26E–04	4.19E–04
CH+CC+BB	2392.4	7.58	7.58	Unlikely	9.94E–07	9.93E–07
CC+BB+NM	2198.7	7.54	7.53	Unlikely	1.00E–06	1.01E–06
BB+NM+SM	2586.4	7.61	7.62	2.50E–04	1.88E–04	2.67E–04
NM+SM+NSB	2287.4	7.56	7.55	1.00E–04	7.24E–05	6.69E–05
SM+NSB+SSB	2286.4	7.56	7.55	4.00E–04	6.05E–04	7.55E–04
NSB+SSB+BG	1850.4	7.47	7.43	4.00E–04	2.22E–04	3.05E–05
SSB+BG+CO	2091.9	7.52	7.5	4.00E–04	2.23E–04	2.48E–04
PK+CH+CC+BB	2470.4	7.59	7.59	4.00E–04	8.20E–04	8.34E–04
CH+CC+BB+NM	2948.8	7.67	7.7	Unlikely	9.91E–07	9.99E–07
CC+BB+NM+SM	3477.7	7.74	7.79	4.00E–04	1.95E–04	4.99E–06
BB+NM+SM+NSB	3038.4	7.68	7.71	Unlikely	9.95E–07	1.00E–06
NM+SM+NSB+SSB	2842.9	7.65	7.68	2.00E–04	1.04E–04	1.02E–04
SM+NSB+SSB+BG	3129.4	7.7	7.73	3.00E–04	2.92E–04	1.97E–04
NSB+SSB+BG+CO	2543.8	7.61	7.61	4.00E–04	2.23E–04	2.17E–04
PK+CH+CC+BB+NM	3026.9	7.68	7.71	7.00E–04	1.54E–03	1.66E–03
CH+CC+BB+NM+SM	4227.8	7.83	7.9	5.00E–04	4.16E–04	2.67E–04
CC+BB+NM+SM+NSB	3929.6	7.79	7.86	1.00E–04	8.64E–05	5.55E–05
BB+NM+SM+NSB+SSB	3593.9	7.76	7.81	5.00E–05	4.92E–05	5.42E–05
NM+SM+NSB+SSB+BG	3685.9	7.77	7.83	1.00E–04	6.19E–05	3.29E–05
SM+NSB+SSB+BG+CO	3822.8	7.78	7.85	4.00E–04	3.58E–04	4.16E–04
PK+CH+CC+BB+NM+SM	4305.9	7.83	7.92	2.00E–03	1.04E–03	6.43E–04
CH+CC+BB+NM+SM+NSB	4679.8	7.87	7.96	Unlikely	9.91E–07	9.89E–07
CC+BB+NM+SM+NSB+SSB	4485.1	7.85	7.94	1.00E–04	9.04E–05	6.76E–05
BB+NM+SM+NSB+SSB+BG	4436.9	7.85	7.93	Unlikely	1.01E–06	1.01E–06
NM+SM+NSB+SSB+BG+CO	4379.2	7.84	7.93	1.00E–04	6.01E–05	3.90E–05
PK+CH+CC+BB+NM+SM+NSB	4757.8	7.88	7.97	5.00E–04	4.21E–04	3.49E–04
CH+CC+BB+NM+SM+NSB+SSB	5235.3	7.92	8.03	5.00E–05	5.00E–05	5.09E–05
CC+BB+NM+SM+NSB+SSB+BG	5328.1	7.93	8.04	5.00E–05	4.44E–05	3.00E–05
BB+NM+SM+NSB+SSB+BG+CO	5130.2	7.91	8.02	5.00E–05	4.50E–05	4.70E–05
PK+CH+CC+BB+NM+SM+NSB+SSB	5313.3	7.93	8.04	1.00E–04	1.00E–04	1.09E–04
CH+CC+BB+NM+SM+NSB+SSB+BG	6078.2	7.98	8.12	Unlikely	9.95E–07	1.01E–06

Table I-1. Rupture-model data for Type-A faults.—Continued

Rupture name (segments involved)	Area (km2)	Ellsworth mag	Hanks and Bakun mag	A-priori rate	Ellsworth-B rate	Hanks and Bakun rate
CC+BB+NM+SM+NSB+SSB+BG+CO	6021.5	7.98	8.11	1.00E–05	9.66E–06	9.24E–06
PK+CH+CC+BB+NM+SM+NSB+SSB+BG	6156.3	7.99	8.12	5.00E–05	4.65E–05	4.09E–05
CH+CC+BB+NM+SM+NSB+SSB+BG+CO	6771.6	8.03	8.18	Unlikely	1.01E–06	9.93E–07
PK+CH+CC+BB+NM+SM+NSB+SSB+BG+CO	6849.7	8.04	8.18	1.00E–04	8.29E–05	6.59E–05
Total				*5.42E–02*	*4.88E–02*	*8.37E–02*
Hayward–Rogers Creek fault						
RC	734.5	7.07	6.89	4.36E–03	2.69E–03	5.21E–03
HN	250.7	6.6	6.38	3.48E–03	2.73E–03	4.27E–03
HS	377.7	6.78	6.56	3.72E–03	2.86E–03	4.59E–03
RC+HN	985.2	7.19	7.06	5.22E–04	4.67E–04	5.68E–04
HN+HS	628.3	7	6.8	2.64E–03	1.43E–03	3.97E–03
RC+HN+HS	1362.8	7.33	7.25	3.09E–04	2.75E–04	3.62E–04
Total				*1.50E–02*	*1.05E–02*	*1.90E–02*
Calaveras fault						
CN	470.2	6.87	6.65	1.03E–03	1.29E–03	2.31E–03
CC	155.5	6.39	6.17	7.66E–03	6.82E–03	1.45E–02
CS	42.5	5.83	5.61	1.05E–02	1.98E–02	4.25E–02
CN+CC	625.7	7	6.8	1.29E–04	1.34E–04	1.58E–04
CC+CS	198	6.5	6.28	2.60E–03	3.28E–03	6.32E–03
CN+CC+CS	668.2	7.02	6.84	9.07E–04	1.25E–03	2.85E–03
Total				*2.28E–02*	*3.26E–02*	*6.86E–02*

Table I-2. Significant changes to California Type-B fault models. Following changes represent all updated slip rates and changes in length, width, and dip of the fault of more than 10 percent.

[mm/yr, millimeters per year; km^2, square kilometers]

Fault name	Updated parameter	2008 value	2002 value
Anacapa-Dume	length	51	75
	width	21.9	28
Blackwater	slip rate	0.5	0.6
Burnt Mtn	dip	-67	90
	width	17.3	13
Calico-Hidalgo	length	117	95
	slip rate	1.8	0.6
Casmalia (Orcutt Frontal fault)	slip rate	0.2	0.25
Channel Island Thrust	dip	20	17
	width	21.3	34
Chino-Central Ave	length	24	28
	width	14.8	17

Table I-2. Significant changes to California Type-B fault models.—Continued

Fault name	Updated parameter	2008 value	2002 value
Clamshell-Sawpit	dip	50	45
Cleghorn	width	15.5	13
Coronado Bank	width	8.6	13
Cucamonga	dip	-45	45
	width	11	18
Death Valley-graben	dip	-60	60
	length	76	54
Death Valley-south	length	42	62
Deep Springs	dip	-60	60
Earthquake Valley	width	18.8	15
Eureka Peak	width	15	13
Fish Slough	dip	-60	60
Gravel Hills-Harper Lake	width	11.4	13
Great Valley 13	dip	-15	15
	top of rupture	9.1	7
	width	23.6	10
Great Valley 14	dip	-22	15
	top of rupture	8.1	7
	width	38.4	10
Great Valley 3	dip	20	15
	slip rate	1.2	1.5
	top of rupture	9	7
	width	14.6	10
Great Valley 5	dip	90	15
	Length	32	28
	slip rate	1	1.5
	top of rupture	10	7
Hat Creek-McArthur-Mayfield	dip	-60	60
Helendale-S. Lockhart	length	114	97
Hollywood	width	18.4	14
Holser	dip	58	65
	width	21.9	14
Hosgri	dip	-80	90
	width	6.9	12
Independence	dip	64	60
	length	54	49
Johnson Valley N	width	15.9	13
Landers	length	95	83
	width	15.1	13
Lenwood-Lockhart-Old Woman Springs	slip rate	0.9	0.6
Malibu Coast	dip	74	75
	width	17.3	13
Mission Ridge-Arroyo Parida-Santa Ana	dip	70	60
	width	8.1	15
Newport-Inglewood	width	15.1	13
Newport-Inglewood offshore	width	10.2	13

Table I-2. Significant changes to California Type-B fault models.—Continued

Fault name	Updated parameter	2008 value	2002 value
North Channel Slope	dip	-26	26
	length	51	68
	slip rate	1	2
	top of rupture	1.1	10
	width	7.8	23
North Frontal fault zone-eastern	dip	41	45
	width	25.3	18
North Frontal fault zone-western	dip	49	45
	width	20.8	18
Northridge	dip	35	42
	top of rupture	7.4	5
	width	16.4	22
Oakridge Mid Channel Montalvo-Oak	dip	16	28
	length	30.2551	36.5286
	slip rate	3	1
	top of rupture	0.4	5
	width	44.6	11
Owens Valley	length	86	121
Pinto Mtn	width	15.5	13
Pisgah-Bullion Mtn-Mesqite Lk	slip rate	0.8	0.6
Pleito Thrust	dip	-46	45
	width	18.9	16
Raymond	dip	-79	75
	width	15.9	13
Red Mountain	dip	56	60
	length	101	39
	width	17	15
Rose Canyon	width	7.7	13
S. Sierra Nevada	length	113	76
San Cayetano	dip	-42	60
	width	23.9	15
San Gabriel	dip	-61	90
	width	16.8	13
San Joaquin Hills Thrust	dip	-23	23
	width	26.6	15
San Jose	dip	74	75
	width	16.4	13
Santa Cruz Island	length	69	50
Santa Monica	dip	-50	75
	width	15.1	13
Santa Rosa Island	width	8.7	13
Santa Susana	dip	-53	55
	length	43	27
	width	13.3	16
Santa Ynez-east segment	dip	-70	80
Santa Ynez-west segment	dip	-70	80
	width	9.8	13
Sierra Madre	dip	53	45

Table I-2. Significant changes to California Type-B fault models.—Continued

Fault name	Updated parameter	2008 value	2002 value
Simi-Santa Rosa	dip	-60	60
	width	12.8	15
Tank Canyon	dip	-53	60
	width	10.4	15
Upper Elysian Park	width	15.7	13
Ventura-Pitas Point	dip	64	75
	width	15.6	13
Verdugo	dip	55	45
White Wolf	dip	75	60
	width	15.1	21

Table I-3. Type-B Faults and Connected-B Faults. "Ellsworth-B" and "Hanks and Bakun" represent Ellsworth (2003) B magnitude-area relationship and Hanks and Bakun (2002) magnitude-area relationships, respectively.

Name	Ellsworth-B mag	Hanks and Bakun mag	Slip rate (mm/yr)	Area (km^2)	Length (km)	Moment rate (Newton-meters/yr)	Fault model
Anacapa-Dume, alt 1	7.2	7.1	3	1115.8	50.9	9.038E+16	F2.1
Anacapa-Dume, alt 2	7.2	7.1	3	1006.2	64.7	8.15E+16	F2.2
Bartlett Springs	7.3	7.2	6	1305.2	174	2.114E+17	F2.1, F2.2
Battle Creek	6.7	6.5	0.5	330.6	29	4.463E+15	F2.1, F2.2
Big Lagoon-Bald Mtn	7.5	7.5	0.5	2041.9	90.1	2.757E+16	F2.1, F2.2
Birch Creek	6.6	6.4	0.7	262.8	15.5	4.967E+15	F2.1, F2.2
Blackwater	7.1	6.9	0.5	720	59.5	9.72E+15	F2.1, F2.2
Burnt Mtn	6.8	6.5	0.6	364.7	21.1	5.908E+15	F2.1, F2.2
Calico-Hidalgo	7.4	7.4	1.8	1624.3	116.9	7.894E+16	F2.1, F2.2
Casmalia (Orcutt Frontal)	6.7	6.5	0.25	300.7	29	2.03E+15	F2.1, F2.2
Cedar Mtn-Mahogany Mtn	7.1	7	1	852.9	77.8	2.303E+16	F2.1, F2.2
Channel Islands Thrust	7.3	7.2	1.5	1263	59.2	5.115E+16	F2.1, F2.2
Chino, alt 1	6.7	6.4	1	285.9	24.3	7.719E+15	F2.1
Chino, alt 2	6.8	6.6	1	424	28.7	1.145E+16	F2.2
Clamshell-Sawpit	6.7	6.4	0.5	293.3	16	3.959E+15	F2.1, F2.2
Cleghorn	6.8	6.6	3	391.9	25.3	3.174E+16	F2.1, F2.2
Collayomi	6.7	6.4	0.6	284.9	28.5	4.615E+15	F2.1, F2.2
Coronado Bank	7.4	7.3	3	1602.2	186.3	1.298E+17	F2.1, F2.2
Cucamonga	6.7	6.5	5	308.8	28	4.169E+16	F2.1, F2.2
Death Valley (Black Mtns Frontal)	7.3	7.1	4	1141.5	76	1.233E+17	F2.1, F2.2
Death Valley (No of Cucamongo)	7.2	7.1	5	998.3	76.8	1.348E+17	F2.1, F2.2
Death Valley (No)	7.3	7.3	5	1385	106.5	1.87E+17	F2.1, F2.2
Death Valley (So)	6.9	6.7	4	544.6	41.9	5.881E+16	F2.1, F2.2
Deep Springs	6.8	6.6	0.8	429.9	25.3	9.285E+15	F2.1, F2.2
Earthquake Valley	6.8	6.6	2	382.8	20.4	2.067E+16	F2.1, F2.2
Elmore Ranch	6.7	6.5	1	330.5	29	8.924E+15	F2.1, F2.2
Elysian Park (Upper)	6.7	6.5	1.3	315.7	20.2	1.108E+16	F2.1, F2.2

Table I-3. Type-B Faults and Connected-B Faults.—Continued

Name	Ellsworth-B mag	Hanks and Bakun mag	Slip rate (mm/yr)	Area (km^2)	Length (km)	Moment rate (Newton-meters/yr)	Fault model
Eureka Peak	6.7	6.4	0.6	282.7	18.8	4.58E+15	F2.1, F2.2
Fickle Hill	7.1	6.9	0.6	728	32.1	1.179E+16	F2.1, F2.2
Fish Slough	6.8	6.6	0.2	440.7	26	2.38E+15	F2.1, F2.2
Gillem-Big Crack	6.8	6.6	1	412.8	32.5	1.115E+16	F2.1, F2.2
Gravel Hills-Harper Lk	7.1	6.9	0.7	742	65.1	1.402E+16	F2.1, F2.2
Great Valley 1	6.8	6.6	0.1	438.8	43.7	1.185E+15	F2.1, F2.2
Great Valley 10	6.5	6.3	1.5	216.6	21.6	8.773E+15	F2.1, F2.2
Great Valley 11	6.6	6.4	1.5	245.8	24.5	9.954E+15	F2.1, F2.2
Great Valley 12	6.4	6.2	1.5	175.2	17.4	7.096E+15	F2.1, F2.2
Great Valley 13 (Coalinga)	7.1	6.9	1.5	743.7	31.6	3.012E+16	F2.1, F2.2
Great Valley 14 (Kettleman Hills)	7.2	7	1.5	922.3	24	3.735E+16	F2.1, F2.2
Great Valley 2	6.5	6.3	0.1	219.8	21.9	5.935E+14	F2.1, F2.2
Great Valley 3, Mysterious Ridge	7.1	6.9	1.25	751.5	51.4	2.536E+16	F2.1, F2.2
Great Valley 4a, Trout Creek	6.6	6.4	1.25	280.3	19.2	9.459E+15	F2.1, F2.2
Great Valley 4b, Gordon Valley	6.8	6.6	1.25	416.1	28.5	1.404E+16	F2.1, F2.2
Great Valley 5, Pittsburg Kirby Hills	6.7	6.5	1	319	31.9	8.613E+15	F2.1, F2.2
Great Valley 7	6.9	6.6	1.5	447.8	44.6	1.814E+16	F2.1, F2.2
Great Valley 8	6.8	6.6	1.5	409.7	40.8	1.659E+16	F2.1, F2.2
Great Valley 9	6.8	6.6	1.5	391.5	39	1.586E+16	F2.1, F2.2
Hartley Springs	6.8	6.6	0.5	418.6	24.7	5.65E+15	F2.1, F2.2
Hat Creek-McArthur-Mayfield	7.2	7.1	1.5	1071.5	96.7	4.34E+16	F2.1, F2.2
Helendale-So Lockhart	7.4	7.3	0.6	1459.2	114	2.364E+16	F2.1, F2.2
Hilton Creek	6.9	6.7	2.5	497.4	29.3	3.357E+16	F2.1, F2.2
Hollywood	6.7	6.5	1	309.9	16.8	8.366E+15	F2.1, F2.2
Holser, alt 1	6.8	6.6	0.4	430.1	19.6	4.645E+15	F2.1
Honey Lake	7	6.8	2.5	631.8	57.4	4.264E+16	F2.1, F2.2
Hosgri	7.3	7.2	2.5	1182.2	171.2	7.98E+16	F2.1, F2.2

Table I-3. Type-B Faults and Connected-B Faults.—Continued

Name	Ellsworth-B mag	Hanks and Bakun mag	Slip rate (mm/yr)	Area (km^2)	Length (km)	Moment rate (Newton-meters/yr)	Fault model
Hunter Mountain-Saline Valley	7.2	7	2.5	897.2	72.4	6.056E+16	F2.1, F2.2
Hunting Creek-Berryessa	7.1	6.9	6	715.8	59.6	1.16E+17	F2.1, F2.2
Imperial	7	6.8	20	607.2	45.8	3.279E+17	F2.1, F2.2
Independence	7.2	7.1	0.2	1028.8	54	5.556E+15	F2.1, F2.2
Johnson Valley (No)	6.9	6.7	0.6	559.8	35.2	9.068E+15	F2.1, F2.2
Laguna Salada	7.3	7.2	3.5	1322.9	99.5	1.25E+17	F2.1, F2.2
Landers	7.4	7.3	0.6	1427.2	94.5	2.312E+16	F2.1, F2.2
Lenwood-Lockhart-Old Woman Springs	7.5	7.4	0.9	1915.8	145.1	4.655E+16	F2.1, F2.2
Likely	7	6.9	0.3	703.7	64	5.7E+15	F2.1, F2.2
Lions Head	6.8	6.6	0.02	428.2	41.4	2.312E+14	F2.1, F2.2
Little Lake	6.9	6.7	0.7	516.1	39.7	9.755E+15	F2.1, F2.2
Little Salmon (Offshore)	7.3	7.2	1	1183.3	45.5	3.195E+16	F2.1, F2.2
Little Salmon (Onshore)	7.1	7	5	890.7	34.3	1.202E+17	F2.1, F2.2
Los Alamos-West Baseline	6.9	6.7	0.7	555.4	27.8	1.05E+16	F2.1, F2.2
Los Osos	7	6.8	0.5	627.9	44.4	8.477E+15	F2.1, F2.2
Maacama-Garberville	7.4	7.3	9	1590.6	220.9	3.865E+17	F2.1, F2.2
Mad River	7.2	7	0.7	943.2	41.6	1.783E+16	F2.1, F2.2
Malibu Coast, alt 1	6.7	6.5	0.3	305.1	37.8	2.471E+15	F2.1
Malibu Coast, alt 2	7	6.8	0.3	652.4	37.8	5.285E+15	F2.2
McKinleyville	7.2	7.1	0.6	1073	47.3	1.738E+16	F2.1, F2.2
Mission Ridge-Arroyo Parida-Santa Ana	6.9	6.7	0.4	556.7	68.8	6.013E+15	F2.1, F2.2
Mono Lake	6.8	6.6	2.5	436.1	25.7	2.944E+16	F2.1, F2.2
Monte Vista-Shannon	6.5	6.3	0.4	223.2	45.1	2.411E+15	F2.1, F2.2
Monterey Bay-Tularcitos	7.3	7.2	0.5	1168.2	83.4	1.577E+16	F2.1, F2.2
Mount Diablo Thrust	6.7	6.5	2	325.1	25	1.756E+16	F2.1, F2.2
Newport-Inglewood (Offshore)	7	6.8	1.5	677.5	66.4	2.744E+16	F2.1, F2.2

Table I-3. Type-B Faults and Connected-B Faults.—Continued

Name	Ellsworth-B mag	Hanks and Bakun mag	Slip rate (mm/yr)	Area (km^2)	Length (km)	Moment rate (Newton-meters/yr)	Fault model
Newport-Inglewood, alt 1	7.2	7.1	1	980.5	65.3	2.647E+16	F2.1
Newport-Inglewood, alt 2	7.2	7.1	1	991.9	65.7	2.678E+16	F2.2
North Channel	6.8	6.6	1	392.8	50.6	1.061E+16	F2.2
North Frontal (East)	7	6.8	0.5	678	26.8	9.153E+15	F2.1, F2.2
North Frontal (West)	7.2	7.1	1	1043	50.1	2.816E+16	F2.1, F2.2
North Tahoe	6.7	6.5	0.43	332.1	19.6	3.856E+15	F2.1, F2.2
Northridge	6.9	6.7	1.5	546.4	33.3	2.213E+16	F2.1, F2.2
Oak Ridge (Offshore)	7	6.7	3	565.4	37.9	4.58E+16	F2.2
Oak Ridge (Onshore)	7.2	7.1	4	1001.4	49.3	1.082E+17	F2.1, F2.2
Ortigalita	7.1	6.9	1	771.5	70.1	2.083E+16	F2.1, F2.2
Owens Valley	7.3	7.2	1.5	1156.9	85.7	4.686E+16	F2.1, F2.2
Owl Lake	6.7	6.5	2	302.4	25.2	1.633E+16	F2.1, F2.2
Palos Verdes	7.3	7.2	3	1347.9	99.1	1.092E+17	F2.1, F2.2
Panamint Valley	7.4	7.3	2.5	1424.5	109.6	9.615E+16	F2.1, F2.2
Pinto Mtn	7.3	7.1	2.5	1147.8	74.1	7.748E+16	F2.1, F2.2
Pisgah-Bullion Mtn-Mesquite Lk	7.3	7.2	0.8	1158.8	88.5	2.503E+16	F2.1, F2.2
Pitas Point (Lower)-Montalvo	7.3	7.2	2.5	1349.1	30.2	9.107E+16	F2.1
Pitas Point (Lower, West)	7.3	7.1	2.5	1127.2	34.7	7.608E+16	F2.1
Pitas Point (Upper)	6.9	6.6	1	449	34.9	1.212E+16	F2.2
Pleito	7.1	7	2	823.8	43.6	4.449E+16	F2.1, F2.2
Point Reyes	6.9	6.7	0.3	557.2	47.4	4.513E+15	F2.1, F2.2
Puente Hills	7.1	7	0.7	835.7	44.1	1.579E+16	F2.1
Puente Hills (Coyote Hills)	6.9	6.6	0.7	467.4	17.4	8.834E+15	F2.2
Puente Hills (LA)	7	6.8	0.7	622	21.9	1.176E+16	F2.2
Puente Hills (Santa Fe Springs)	6.7	6.4	0.7	288	11.4	5.443E+15	F2.2
Quien Sabe	6.6	6.3	1	228.5	22.8	6.168E+15	F2.1, F2.2
Raymond	6.8	6.5	1.5	357.2	22.5	1.447E+16	F2.1, F2.2

Table I-3. Type-B Faults and Connected-B Faults.—Continued

Name	Ellsworth-B mag	Hanks and Bakun mag	Slip rate (mm/yr)	Area (km^2)	Length (km)	Moment rate (Newton-meters/yr)	Fault model
Red Mountain	7.4	7.4	2	1709.6	100.5	9.232E+16	F2.1, F2.2
Rinconada	7.5	7.4	1	1907.7	190.8	5.151E+16	F2.1, F2.2
Robinson Creek	6.7	6.4	0.5	283	16.7	3.821E+15	F2.1, F2.2
Rose Canyon	6.9	6.7	1.5	538.1	69.9	2.179E+16	F2.1, F2.2
Round Valley	7.1	6.9	1	734.7	43.3	1.984E+16	F2.1, F2.2
San Andreas (Creeping Segment)	6.7	6.7	34	131.6	121.8	3.859E+16	F2.1, F2.2
San Cayetano	7.2	7.1	6	1005	42	1.628E+17	F2.1, F2.2
San Gabriel	7.3	7.2	1	1198.7	71.3	3.236E+16	F2.1, F2.2
San Joaquin Hills	7.1	6.9	0.5	730.1	27.4	9.856E+15	F2.1, F2.2
San Jose	6.7	6.5	0.5	322.8	19.6	4.357E+15	F2.1, F2.2
San Juan	7.1	7	1	880.3	67.7	2.377E+16	F2.1, F2.2
San Luis Range (So Margin)	7.2	7	0.2	901.6	63.8	4.869E+15	F2.1, F2.2
Santa Cruz Island	7.2	7	1	919	69.1	2.481E+16	F2.1, F2.2
Santa Monica, alt 1	6.6	6.4	1	267.4	14.4	7.22E+15	F2.1
Santa Monica, alt 2	6.8	6.6	1	423.6	28	1.144E+16	F2.2
Santa Rosa Island	6.9	6.7	1	500.5	57.5	1.351E+16	F2.1, F2.2
Santa Susana, alt 1	6.9	6.7	5	540.7	27.2	7.299E+16	F2.1
Santa Ynez (East)	7.2	7.1	2	967.5	68.4	5.224E+16	F2.1, F2.2
Santa Ynez (West)	7	6.8	2	660.5	67.5	3.567E+16	F2.1, F2.2
Sierra Madre	7.2	7.1	2	1012	56.9	5.465E+16	F2.1, F2.2
Sierra Madre (San Fernando)	6.7	6.5	2	332.6	18.1	1.796E+16	F2.1, F2.2
Simi-Santa Rosa	6.9	6.7	1	501.8	39.1	1.355E+16	F2.1, F2.2
So Emerson-Copper Mtn	7.1	6.9	0.6	761.8	54	1.234E+16	F2.1, F2.2
So Sierra Nevada	7.5	7.5	0.1	1996.2	112.4	5.39E+15	F2.1, F2.2
Superstition Hills	6.8	6.6	4	410.3	36.2	4.431E+16	F2.1, F2.2
Surprise Valley	7.2	7.1	1.3	1094	87.3	3.84E+16	F2.1, F2.2
Bluff	7.2	7	0.6	897.9	48.8	1.455E+16	F2.1, F2.2

Table I-3. Type-B Faults and Connected-B Faults.—Continued

Name	Ellsworth-B mag	Hanks and Bakun mag	Slip rate (mm/yr)	Area (km^2)	Length (km)	Moment rate (Newton-meters/yr)	Fault model
Tank Canyon	6.4	6.2	1	173	16	4.672E+15	F2.1, F2.2
Trinidad	7.5	7.5	0.7	2003.3	88.4	3.786E+16	F2.1, F2.2
Ventura-Pitas Point	7	6.8	1	681.8	43.8	1.841E+16	F2.1, F2.2
Verdugo	6.9	6.7	0.5	513.5	29	6.932E+15	F2.1, F2.2
West Napa	6.7	6.5	1	295.7	29.6	7.983E+15	F2.1, F2.2
West Tahoe	7.1	7	0.6	870.3	51.3	1.41E+16	F2.1, F2.2
San Cayetano	7.2	7.1	6	1005	42	1.628E+17	F2.1, F2.2
White Mountains	7.4	7.3	1	1438.3	110.6	3.883E+16	F2.1, F2.2
White Wolf	7.2	7	2	957.6	63.4	5.171E+16	F2.1, F2.2
Zayante-Vergeles	7	6.9	0.1	694.4	57.9	1.875E+15	F2.1, F2.2

Table I-4. Connected-B Faults. Ellsworth (2003) and Hanks and Bakun (2002). "Ellsworth-B" and "Hanks and Bakun" represent Ellsworth (2003) B magnitude-area relationship and Hanks and Bakun (2002) magnitude-area relationships, respectively.

[mm/yr, millimeters per year; km^2, square kilometers]

Name	Ellsworth -B mag	Hanks and Bakun mag	Slip rate (mm/yr)	Area (km^2)	Length (km)	Moment rate (Newton-meters/yr)	Fault model	Connected B-Fault Names
Death Valley Connected	7.8	7.9	4.58568	4069.4	301.3	5.038E+17	F2.1, F2.2	Death Valley (No of Cucamongo); Death Valley (No); Death Valley (Black Mtns Frontal); Death Valley (So)
Green Valley Connected	6.8	6.6	4.66633	412	56.4	5.19E+16	F2.1, F2.2	Concord; Green Valley (So); Green Valley (No)
Greenville Connected	7	6.8	2	676.4	50.1	3.652E+16	F2.1, F2.2	Greenville (So); Greenville (No)
Hunter Mountain Connected	7.6	7.6	2.5	2321.6	181.9	1.567E+17	F2.1, F2.2	Hunter Mountain-Saline Valley; Panamint Valley
Little Salmon Connected	7.5	7.5	2.71787	2074	79.8	1.522E+17	F2.1, F2.2	Little Salmon (Onshore); Little Salmon (Offshore)

Table I-4. Connected-B Faults.—Continued

Name	Ellsworth -B mag	Hanks and Bakun mag	Slip rate (mm/yr)	Area (km^2)	Length (km)	Moment rate (Newton-meters/yr)	Fault model	Connected B-Fault Names
Newport Inglewood Connected alt 1	7.5	7.5	1.27675	2196.1	201.6	7.571E+16	F2.1	Rose Canyon; Newport-Inglewood (Offshore); Newport-Inglewood, alt 1
Newport Inglewood Connected alt 2	7.5	7.5	1.27533	2207.5	202	7.601E+16	F2.2	Rose Canyon; Newport-Inglewood (Offshore); Newport-Inglewood, alt 2
Oak Ridge Connected	7.4	7.3	3.63915	1566.8	87.3	1.539E+17	F2.2	Oak Ridge (Offshore), west extension; Oak Ridge (Offshore); Oak Ridge (Onshore)
Palos Verdes Connected	7.7	7.7	3	2950.2	285.4	2.39E+17	F2.1, F2.2	Palos Verdes; Coronado Bank
Pitas Point Connected	7.3	7.1	1	1130.8	78.7	3.053E+16	F2.2	Pitas Point (Upper); Ventura-Pitas Point
San Gregorio Connected	7.5	7.4	5.49298	1899.5	175.9	2.817E+17	F2.1, F2.2	San Gregorio (South); San Gregorio (North)
Santa Monica Connected alt 1	7.3	7.3	2.61336	1383.2	65.3	9.76E+16	F2.1	Anacapa-Dume, alt 1; Santa Monica, alt 1
Santa Monica Connected alt 2	7.4	7.3	2.40751	1429.8	92.7	9.294E+16	F2.2	Anacapa-Dume, alt 2; Santa Monica, alt 2
Santa Ynez Connected	7.4	7.4	2	1628	135.8	8.791E+16	F2.1, F2.2	Santa Ynez (West); Santa Ynez (East)
Sierra Madre Connected	7.3	7.2	2	1344.5	75	7.26E+16	F2.1, F2.2	Sierra Madre (San Fernando); Sierra Madre

References

Ellsworth, W., 2003, Appendix D—Magnitude and area data for strike slip earthquakes, *in* Working Group on California Earthquake Probabilities, Earthquake probabilities in the San Francisco Bay region—2002–2031: U.S. Geological Survey Open-File Report 03-214, 6 p.

Field, E., T. Dawson, W. Ellsworth, K. Felzer, A. Frankel, V. Gupta, T. Jordan, T. Parsons, M. Petersen, R. Stein, R. Weldon, C. Wills, 2008, The Uniform California Earthquake Rupture Forecast, Version 2 (UCERF 2): U.S. Geological Survey Open File Report and California Geological Survey Special Report 203, 97 p.

Hanks, T.C., and Bakun, W.H., 2002, A bilinear source-scaling model for M–log A observations of continental earthquakes: Bulletin of the Seismological Society of America, v. 92, pp. 1841–1846.

Kent, G.M., Babcock, J.M., Driscoll, N.W., Harding, A.J., Dingler, J.A., Seitz , G.G., Gardner, J.V., Mayer, L.A., Goldman, C.R., Heyvaert, A.C., Richards, R.C., Karlin, R., Morgan, C.W., Gayes, P.T., and Owen, L.A., 2005, 60 k.y. record of extension across the western boundary of the Basin and Range province: Estimate of slip rates from offset shoreline terraces and a catastrophic slide beneath Lake Tahoe: Geology, v. 33, no. 5, p. 365-368.

O'Connell, D.R.H., and Unruh, J.R., 2000, Updated Seismiotectonic Evaluation of faults within 10 km of Monitcello Dam, Solano Projedt, California: Bureau of Reclamation, Geophysics, Paleohydrology and Seismotectonics Group, Geotechnical Services, Denver Co. 101 p.

Oskin, M., Perg, L., Blumentritt, D., Mukhopadhyay, S., and Iriondo, A., 2007: Slip rate of the Calico fault: Implications for geologic versus geodetic rate discrepancy in the Eastern California shear zone, Journal of Geophysical Research - Solid Earth, v. 112, doi:10.1029/2006JB004451

Wills, C.J., Weldon, R.J., II, and Bryant, W.A., 2008, California Fault Parameters for the National Seismic Hazard Maps and Working Group on California Earthquake Probabilities, Appendix A, *in* Field, E., Dawson, T., Ellsworth, W., Felzer, K., Frankel, A., Gupta, V., Jordan, T., Parsons, T., Petersen, M., Stein, R., Weldon, R., and Wills, C., The Uniform California Earthquake Rupture Forecast, Version 2 (UCERF 2): U.S. Geological Survey Open File Report and California Geological Survey Special Report 203, 51 p.

Appendix J. Fault-Model Changes in the Western United States

By Kathleen M. Haller and Stephen C. Harmsen

We changed the 2002 fault source model for this update based on recommendations submitted by a number of different sources; these changes impact the maps in a variety of ways. We will address the most significant changes first followed by the less significant changes in this appendix.

Rounding M

In these maps, characteristic magnitude for faults outside of California, which is assigned based on fault length-magnitude relation of Wells and Coppersmith (1994), was rounded to two decimal places instead of one decimal place as in prior versions of the maps. Although originally considered to better capture epistemic uncertainty in the magnitude-area relations implemented in the California part of the maps (discussed elsewhere in the documentation), we retained rounding magnitude to nearest hundredth outside of California. This change in methodology affects earthquake recurrence-rate estimates and probabilistic ground motions through either increasing or decreasing the assigned characteristic magnitude for the source by up to 0.05-magnitude units. An overestimate by 0.05 magnitude units can mean a lowering of event rate by 16 percent. Similarly, an underestimate by 0.05-magnitude units can increase event rates by 20 percent as depicted by the blue diamonds in figure J-1. For sites near these faults, this has considerable impact.

Dip of Normal Faults

The Western States Seismic Policy Council (WSSPC) held a workshop to address issues of importance in the Intermountain West region. One of their recommendations was to reduce the average dip of normal faults from 60° to 50±10° (Lund, 2006). Although we cannot resolve the question of how steep Intermountain West normal faults dip or even if they are planar in nature; multiple lines of evidence exist that support implementing their recommendation. The basis for 60° dip is grounded in fault mechanics (Anderson, 1951), which later was supported by studies by Doser and Smith (1989) who determined that the dip of normal faults in the Western United States range from 40° to 90°, with an average dip of 60°. Seismic reflection studies and other subsurface information support this average dip (Walsh and Watterson, 2002; Smith and Bruhn, 1984; Zoback, 1983). Jackson (2002) compiled a worldwide data set of normal surface faulting earthquakes that shows that at the depth of the historical normal earthquakes fault planes dip between 30° and 70°. The mode of this dataset is 40–50°, and the mean somewhere between 40° and 60°. Although this particular data set is small, no nodal-plane solution suggests very gently dipping or very steeply dipping seismically active normal faults. Jackson (2002) does not include a list of earthquakes considered in his analysis, but historical earthquakes in the Intermountain West also were on planes dipping around 40°–60°. Therefore, we have changed the preferred dip of most normal faults to 50°. In addition, we give modest weight (20 percent each) to alternative models that characterize fault dip as 40° and 60° (see fig. 17). An exception is the Lost River fault, which is assigned 45±10° dip. As in past versions of the maps, all of our assigned slip rates are expressed as either vertical or horizontal rates; therefore, any change in dip will subsequently increase or decrease the fault parallel slip rate used in

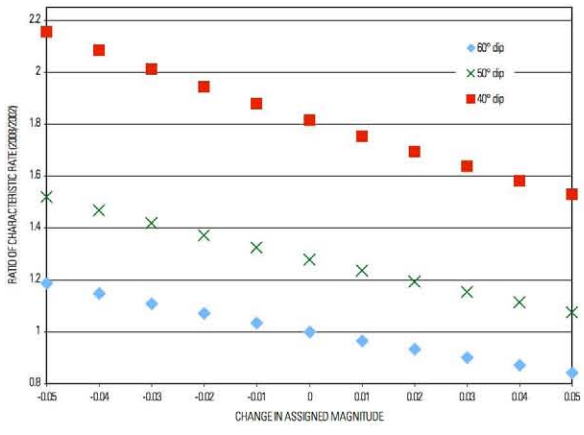

Figure J-1. Plot of the ratio (2008/2002 hazard maps) of rate of characteristic earthquakes resulting from rounding characteristic magnitude (M) to two decimal places and alternative fault-dip models.

our calculations. When one changes the dip of faults in the model from 60° to 50°, the rate of earthquakes increases by more than 20 percent in addition to the change in earthquake rate due to magnitude rounding. When the dip of the fault is changed from 60° to 40° the rate of earthquakes increases nearly 55 percent. Figure J-1 demonstrates the combined result when changes in default dip are combined with rounding the characteristic magnitude to two decimal places. For some faults that dip 50°, the rate of earthquakes is increased up to 66 percent. Similarly for some of our fault sources that dip 40°, the rate of earthquakes increases nearly 45 percent. Faults modeled with a dip of 60° show the same plus or minus 20 percent variation as other faults in the model that did not have a change in dip (fig. J-1). Therefore, assuming that the normal faults dip at a lower angle than our previous preferred dip of 60° can significantly affect probabilistic ground motions due to increases the rate of events.

Ratio of Magnitude-Frequency Distributions in the Intermountain West

Contribution by Robert L. Wesson

Another WSSPC recommendation was to change the ratio of characteristic and Gutenberg-Richter magnitude-frequency distributions in the Intermountain West region to reflect similar event weighting used in coastal California: 67 percent characteristic and 33 percent Gutenberg-Richter. This has generally lowered the hazard, but the specific amount depends on the assigned characteristic magnitude; the longer the fault, the larger the impact. Many faults in the Intermountain West, as they are depicted in these maps, are actually long fault zones that contain considerable complexity, and until this version of the map, the competing models were weighted the same, or equal likelihood of being the failure mode.

The problem of estimating the magnitude-frequency distribution of future earthquakes along a fault zone is not resolved but is hotly contested in the scientific community. In some instances, paleoseismic data may be available to provide some constraints on the interpretation of the behavior of the fault in the past. The estimation of the future magnitude-frequency behavior of the fault, even in the presence of these kinds of data, remains controversial. Owing to the relative youth of earthquake science, we have yet to have complete observations of repeated ruptures on the same fault. Thus the models used in hazard estimation are simplistic and uncertain.

In the preparation of the National Seismic Hazard Maps, two kinds of magnitude-frequency relationships are considered. These are termed the "characteristic" and the "truncated Gutenberg-Richter" models. Both of these terms may have different meanings in different contexts; the ways they are used in these maps are described here. The "characteristic" model means that all future ruptures along the fault will occur only as ruptures of individual, predefined segments; the magnitude for each segment is estimated from the length of the segment. The "characteristic" model enjoyed considerable popularity in the 1980s and 1990s, but historical earthquake ruptures show complex rupture patterns that include such phenomena as significant stopovers (for example, Landers) and branching on to other faults (for example, Denali). Therefore, the concept of segmentation (at least based on current knowledge) is increasingly questioned. In the application of this model, the magnitude (or moment) of the earthquakes is determined from the length of a segment, and the frequency of the characteristic earthquakes is determined by dividing the moment of an individual event by the long-term moment rate of the fault (that is, the slip rate multiplied by the area of the characteristic event).

The alternative model considered in the National Seismic Hazard Maps is the "truncated Gutenberg-Richter" model. The word "truncated" is used because in all cases a lower magnitude of 6.5 is considered. The general Gutenberg-Richter frequency-magnitude relation, found to be typical of any significant-sized region over a long period of time, says that the logarithm number of earthquakes in a specified magnitude interval is a linear function of the magnitude, that is

$$\log(n) = a - bM$$

(It can be shown that a similar relation with the same value of b, but a different value of a, holds for the logarithm of the number of earthquakes above a particular value of magnitude. Knowing the value of b and the magnitude interval, one type of a-value can be calculated from the other.) So the "truncated Gutenberg-Richter" magnitude-frequency distribution describes a model with a b-value typically determined from regional seismicity, a maximum magnitude determined from the length of the fault segment, and the a-value calculated such that the sum of the moments of all the earthquakes with this magnitude-frequency relationship between 6.5 and the maximum magnitude equals the moment rate determined for the fault from the slip rate. In essence, the "truncated Gutenberg-Richter" provides for the possibility that earthquakes less than the maximum will occur. In the calculations, all possible positions of the smaller earthquakes along the fault are considered. This is referred to as letting the earthquakes "float." The difficulty with the "truncated

Gutenberg-Richter" relation is that it suggests more earthquakes smaller than the maximum magnitude than are actually observed.

The fact that neither of these relations appears to be satisfactory led to the use of using a weighted sum from these two models. Originally, the two models were each weighted 50 percent, but subsequently in some regions (California in particular), where arguments were made that the earthquakes favored the characteristic model, the weights were two-thirds characteristic and one-third truncated Gutenberg-Richter.

As mentioned previously, the weight of opinion has been moving against a pure application of the "characteristic" model for the reasons described. For example, the Working Group for the San Francisco Bay Region (2003) considered such a wide variety of multisegment ruptures, uncertainties in magnitude-area relations, floating earthquakes and other issues, in a region where one would think that we know a good deal about the faults, as to represent a very significant backing away from the "characteristic" model. A similar approach was adopted in the current statewide review in California (Field and others, 2008).

In the Intermountain West we have only a few historical ruptures; furthermore, few faults have been the target of more than one or two paleoseismic investigations. Thus we have a rather limited basis of experience on which to define fault segments, notwithstanding the arguments above. Over 10 percent of the faults are more than 100 kilometers long and assigned characteristic M7.4 or greater; another 10 percent are between 66 and 100 kilometers long and are assigned characteristic M7.2 or M7.3. To overemphasize the likelihood that most of the seismic moment is released in only the largest earthquakes risks very significantly underestimating the frequency of small but still potentially damaging earthquakes.

Probabilities and Magnitudes of Multisegment Rupture

Issue 4 of the Western States Seismic Policy Council recommendations (Lund, 2006) addresses how fault segmentation is characterized in the National Seismic Hazard maps. We recognize that faults in the region are capable of producing M7.3 earthquakes (for example, Pleasant Valley, Nev., and Hebgen Lake, Mont., earthquakes) in which surface rupture jumped across gaps that some investigators assume to be the location of a fundamental boundary. Even though many faults in the Intermountain West have tentative segmentation models, most segments are short less than 20–25 kilometers) and, thus, would be modeled with frequent low-magnitude earthquakes. Therefore, most faults in the Intermountain West in our model are considered in the model to rupture from end to end in the "characteristic" part of the model. This practice permits many "multisegment" ruptures by constraining "characteristic" magnitude large enough to sustain rupture of the entire fault and floating earthquakes of magnitudes from M6.5 to the characteristic magnitude without explicitly defining segments boundaries. Explicit segmentation results in artificially high hazard at segment boundaries due to the influence of earthquakes on adjoining segments. If we consider the Lost River fault in Idaho as an example, using the existing segmentation model would overestimate the frequency of known Holocene surface-rupturing earthquakes by nearly a factor of five.

The longest faults in the region are divided into smaller parts of the fault, which are defined in the literature as multiple segments. The Hurricane fault that crosses the border between Utah and Arizona is divided into three parts, and the nearby Sevier-Toroweap fault is divided into two parts. Explicit segmentation models for the Wasatch fault in Utah and the Carson Range system in Nevada were modified in these maps to, in a sense, permit "multisegment" rupture that was not part of the 2002 maps.

Wasatch Fault

The Wasatch fault, bounding the eastern side of the Utah urban corridor, is one of the few faults in the model with explicit segmentation defined. Twenty years of trenching studies conducted on every segment but the northernmost makes this the second best studied fault in the Western United States. Over the years, studies have reviewed and analyzed the reasonably well dated event chronology to determine if individual surface ruptures crossed segment boundaries forming "multisegment" ruptures. In these maps, we have included a "floating" M7.4 (10 percent probability) to include that possibility (see fig. 18), with recurrence interval of 500 years somewhere along strike. Assigned maximum magnitude for each segment is retained from the 2002 models and therefore does not carry two-decimal-place rounding as other faults in the Intermountain West. However, we added aleatory uncertainty on the characteristic magnitudes. This was done using a similar a priori model as we now use in California for Type-A faults (that is, the recurrence model does not change, but some variation in the characteristic magnitude is permitted). The aleatory uncertainty is distributed

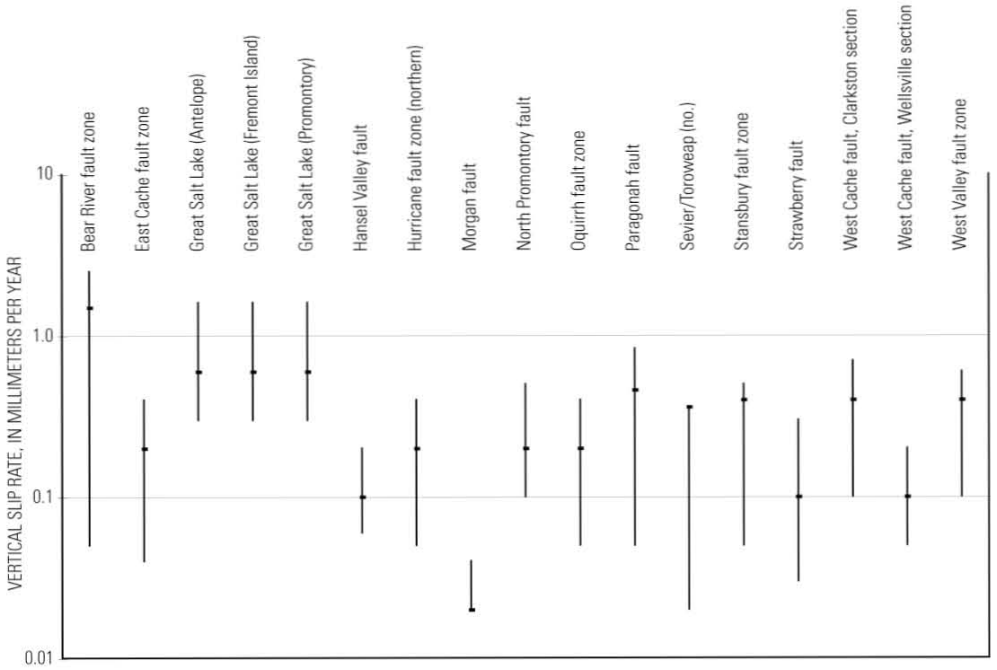

Figure J-2. Plot of results of Utah Quaternary Fault Parameter Working Group showing the preferred slip rate for 16 faults in Utah with associated uncertainties.

with dM of 0.2 on either side of the preferred M.

Carson Range System

We have included a new model for the Carson Range (Genoa) fault system near Carson City, Nev., based on recommendations from the Nevada Bureau of Mines and Geology and Ramelli and others (1999). The Carson Range fault (as named in our model) extends along the precipitous east front of the Sierra Nevada from south of Markleeville, Calif., northward to south of U.S. Highway 50, northwest of Carson City, Nev. Near the north end of the Carson Range fault, the Indian Hill, Carson City, and Kings Canyon faults splay off of the Carson Range fault and trend northeast, away from the range front. All three of these faults are short, less than 17 kilometers long, and are characterized in the 2002 model as having characteristic earthquakes of magnitudes 6.5 or less. Although historical surface faulting has occurred as the result of earthquakes of M6.5 and less, the size of the fault scarps near Carson City and their lateral continuity suggest they were formed in larger events that also ruptured the Carson Range fault (Ramelli and others, 1999). We assign 75-percent probability of synchronous rupture along these faults based on evidence that likely characterizes the fault behavior in the past two events; however, we cannot rule out the possibility that rupture occurred so closely spaced in time that they are geologically indistinguishable. In addition, the four faults may rupture independently; therefore, each are assigned a 25-percent probability that they are independent sources.

Similar treatment was given to the Mount Rose and Little Valley faults to the north, between Carson City and Reno. The Little Valley fault is parallel to and sympathetic to the Mount Rose fault; their proximity suggests that they probably merge at depth. Therefore, in this model the Little Valley fault is assigned a 25-percent probability that it ruptures independently from the nearby Mount Rose fault.

Western States Seismic Policy Council Recommendations

One of the short-term recommendations of WSSPC was to incorporate uncertainties in slip rates and recurrence intervals for the more significant faults in the Basin and Range Province. Specifically, they recommended incorporating the uncertainties determined by the Utah Quaternary Fault Parameters Working Group (Lund, 2005) The working group's effort is the first in the region to assemble uncertainty

in fault slip rate and recurrence intervals to augment preferred values; their results show the range in uncertainty generally is between one-half the preferred value and 2 times the preferred value (fig. J-2). Before we incorporate these types of uncertainties, we would like to expand the dataset to include faults in adjacent States.

Another recommendation focused on improving, or at least including, alternative models for determining characteristic magnitude. As has been stated many times in this documentation, we assign characteristic magnitude in the Intermountain West based on the regression relations of Wells and Coppersmith (1996). However, there is considerable uncertainty in surface-rupture length due to incomplete knowledge of the extent of individual ruptures on long faults and variable preservation of deformation features in the landscape. To compensate for possible longer or shorter ruptures, we use magnitude uncertainty (see fig. 17). For instance, for a fault having an assigned characteristic magnitude of M7.0 based on a surface-rupture length of 45 kilometers, we also allow epistemic uncertainty in the characteristic magnitude of 0.2 magnitude units larger or smaller than the characteristic event. Thus, the modeled surface-rupture length approximates 30–60 kilometers. Probably a more vexing problem is faults in our model that are so short they are assigned characteristic magnitudes less than M6.5.

There are nearly 30 faults in the Intermountain West that fall into this category (about 13 percent, fig. J-3). Fault scarps that are large enough to be preserved on the landscape for thousands of years identify the location and extent of these faults. Therefore, it is unlikely that they are the result of earthquakes that generally do not rupture the surface and when they do, have very small surface offsets. Wells and Coppersmith (1993) showed that only one-fourth of the historical M5±0.1 to 6±0.1 earthquakes rupture the surface, and fewer than one in three M6.0±0.1 to 6.4±0.1 earthquakes rupture the surface. In their data set all the earthquakes above M7.4±0.1 ruptured the surface. Youngs and others (2003) show, however, that the probability of surface rupture is higher in the Great Basin and northern Basin and Range above M5.6 and 6.25, respectively. Arbitrarily promoting the short faults in our model to M6.5 only exacerbates the excess of earthquakes at that magnitude. This step also requires creating hypothetical faults of the proper length or large stress-drop earthquakes. We did not implement this recommendation at this time.

References

Anderson, E.M., 1951, The dynamics of faulting: Edinburgh, Oliver & Boyd, 2d edition, 206 p.

Doser, D.I., and Smith, R.B., 1989, An assessment of source parameters of earthquakes in the cordillera of the western United States: Bulletin of the Seismological Society of America, v. 79, p. 1383–1409.

Field, E., T. Dawson, W. Ellsworth, K. Felzer, A. Frankel, V. Gupta, T. Jordan, T. Parsons, M. Petersen, R. Stein, R. Weldon, C. Wills, 2008, The Uniform California Earthquake Rupture Forecast, Version 2 (UCERF 2): U.S. Geological Survey Open File Report and California Geological Survey Special Report 203, 97 p.

Jackson, J.A., 2002, Active normal faulting and crustal extension, *in* Holdsworth, R.E., and Turner, J,P., compilers, Extensional tectonics—Faulting and related processes: The Geological Society, Key Issues in Earth Sciences, part 2, p. 135–149.

Lund, W.R., ed., 2006, Basin and Range Province Earthquake Working Group seismic-hazard recommendations to the U.S. Geological Survey National Seismic Hazard Mapping Program: Utah Geological Survey Open-File Report 477, 23 p.

Smith, R.B., and Bruhn, R.L., 1984, Intraplate extensional tectonics of the eastern Basin-Range; inferences on structural style from seismic reflection data, regional tectonics, and thermal-mechanical models of brittle-ductile deformation: Journal of Geophysical Research, v. 89, p. 5733–5762.

Walsh, J.J., and Watterson, J., 2002, Dips of normal faults in British Coal Measures and other sedimentary sequences, *in* Holdsworth, R.E., and Turner, J,P., compilers, Extensional tectonics—Faulting and related processes: The Geological Society, Key Issues in Earth Sciences, part 2, p. 25–39.

Wells, D.L. and Coppersmith, K.J., 1994, New empirical relationships among magnitude, rupture length, rupture width, and surface displacements: Bulletin of the Seismological Society of America, v. 84, p. 974–1002.

Working Group on California Earthquake Probabilities, 2003, Earthquake probabilities in the San Francisco Bay region—2002–2031: U.S. Geological Survey Open-File Report 03-214.

Youngs, R.R., Arabaz, W.J., Anderson, R.E., Ramelli, A.R., Ake, J.P., Slemmons, D.B., McCalpin, J.P., Doser, D.I., Fridrich, C.J., Swan, F.H., III, Rogers, A.M., Yount, J.C., Anderson, L.W., Smith, K.D., Bruhn, R.L., Knuepfer, P.L.K., Smith, R.B., dePolo, C.M., O'Leary, D.W., Coppersmith, K.J., Pezzopane, S.K., Schwartz, D.P., Whitney, J.W., Olig, S.S., Toro, G.R., 2003, A methodology for probabilistic fault displacement hazard analysis: Earthquake Spectra, v. 19, p. 191–217.

Zoback, M.L., 1983, Structure and Cenozoic tectonism along the Wasatch fault zone, Utah, *in* Miller, D.M., Todd, V.R., and Howard, K.A., eds., Tectonic and stratigraphic studies in the eastern Great Basin: Geological Society of America Memoir 157, p. 3–27.

Appendix K. Cascadia Subduction Zone

By Arthur D. Frankel and Mark D. Petersen

The geometry and recurrence times of large earthquakes associated with the Cascadia Subduction Zone (CSZ) were discussed and debated at a March 28–29, 2006, Pacific Northwest workshop for the USGS National Seismic Hazard Maps.

The CSZ is modeled from Cape Mendocino in California to Vancouver Island in British Columbia. We include the same geometry and weighting scheme as was used in the 2002 model (Frankel and others, 2002) based on thermal constraints (fig. 21) (Flück and others, 1997, and a reexamination by Wang and others, 2003, fig. 11, eastern edge of intermediate shading). This scheme includes four possibilities for the lower (eastern) limit of seismic rupture: the base of elastic zone (weight 0.1), the base of transition zone (weight 0.2), the midpoint of the transition zone (weight 0.2), and a model with a long north-south segment at long 123.8°W. in the southern and central portions of the CSZ, with a dogleg to the northwest in the northern portion of the zone (weight 0.5). The latter model was derived from the approximate average longitude of the contour of the 30-kilometer depth of the CSZ as modeled by Flück and others. (1997). A global study of the maximum depth of thrust earthquakes on subduction zones by Tichelaar and Ruff (1993) indicated maximum depths of about 40 kilometers for most of the subduction zones studied, although the Mexican subduction zone had a maximum depth of about 25 kilometers (Roland LaForge, oral commun., 2006). The recent inversion of GPS data by McCaffrey and others (2007) shows a significant amount of coupling (a coupling factor of 0.20.3) as far east as long 123.8°W. in some portions of the CSZ. Both of these lines of evidence lend support to the model with a north-south segment at long 123.8°W.

The primary constraint on our Cascadia earthquake model is that great earthquakes occur on average once every 500 years beneath sites on the coast over the CSZ, based on paleoseismic studies of coastal subsidence and tsunami deposits (for example, Atwater and Hemphill-Haley, 1997). We considered two sets of rupture scenarios for these events: (1) M9.0±0.2 events that rupture the entire CSZ every 500 years on average and (2) M8.0–8.7 events whose rupture zones fill up the entire zone over a period of about 500 years. The rupture zones in the latter set of scenarios are moved systematically or floated along the strike of the CSZ.

Various lines of evidence are used to assess the relative likelihood of these two sets of rupture scenarios. The A.D. 1700 earthquake that caused a tsunami in Japan is thought to have ruptured the entire zone in an earthquake about M9.0 (Satake and others 1996, 2003). Furthermore, recent sedimentation studies along the continental shelf also provide evidence that great earthquakes usually rupture most of the Cascadia subduction interface (Goldfinger and others, 2003). In contrast, Nelson and others (2006) and Kelsey and others (2002, 2005) reported tsunami deposits along northern California and southern Oregon that give evidence for additional M8.0–8.6 earthquakes that are not apparent in studies along the Washington coast. We have applied the M8.0–8.7 model for the entire CSZ lacking any evidence for different rupture behavior between the north and southern portions of the fault.

For the WGCEP and the NSHMP model we assign a probability of 0.67 to the M8.8–9.2 scenario and a probability of 0.33 for the set of M8.0–8.7 scenarios with floating rupture zones. In the 2002 maps, we used M9.0 and M8.3 scenarios with equal probabilities. To be clear, when we say “probability of a scenario” this indicates that the effective rate of the scenario in the hazard calculation is the probability of that scenario multiplied by the recurrence rate calculated for that scenario as if it were the only scenario. The higher probability of the M8.8–9.2 complete CSZ rupture scenario in the 2008 update compared to that in the 2002 maps reflects the consensus of attendees at the Pacific Northwest workshop that the former represents a more likely scenario for the great earthquakes than the set of floating M8 scenarios.

Here we describe the scenarios in more detail. In the first model, we consider rupture of the entire length of the CSZ with great earthquakes having a magnitude of M8.8 (weight 0.2), M9.0 (0.6), and M9.2 (0.2). The average recurrence time for such an event was taken to be 500 years based on the palesoeismic evidence. In the second model we consider a set of floating ruptures between M8.0 and M8.7. The key constraint of the second model is that the annual rate of having a rupture zone beneath any given site along

the coast is 1/500, to be consistent with the paleoseismic observations. This procedure is similar to the model applied in Geomatrix Consultants, Inc. (1995), where rupture zones for each magnitude were assumed to fill the CSZ every 500 years. We calculate the overall rate of earthquakes for the CSZ for a given magnitude so that the rate of having a rupture zone occurring beneath any given site is 1/500, on average. When rupture zones are floated along the CSZ using equal distance increments, sites near the middle of the CSZ will have a higher rate of ruptures beneath them compared to sites near the northern and southern ends of the CSZ. We used the magnitude-length relation for subduction-zone earthquakes determined by Geomatrix Consultants, Inc. (1995). The rupture zones were floated using 5-kilometer increments. The average rate of rupture zones under a site was calculated for a set of sites along the coast separated by 0.1 degree in latitude and extending the entire length of the CSZ. Probabilities were assigned to scenarios with magnitudes at one-tenth magnitude unit intervals from M8.0 to M8.7. The recurrence parameters for each magnitude interval are shown in table K-1; probabilities in the last column of table K-1 sum to 0.33, which is the weight of this model. The magnitude-frequency distribution of earthquakes along the Cascadia subduction zone can be observed in figure 22 of the main text. The implied recurrence intervals for M8.0 to M8.2 earthquakes are between 78 and 107 years, shorter than the observed seismic history that does not contain any of these events. To account for this lack of historical earthquakes between M8 and M8.2, we have weighted the probability of these rupture scenarios by one-half, compared to the intervals between M8.3 and M8.7, to make the rates more compatible with the earthquake record.

The effective recurrence rate of each scenario in the hazard calculation is the recurrence rate multiplied by the probability of that scenario. In the final model, considering all of the M9 and floating M8 rupture scenarios and their probabilities, the effective recurrence time (reciprocal of the mean rate) for earthquakes with M≥8.0 is 270 years. The reason for this relatively short recurrence time is that we are treating the M8 earthquakes as independent events, whereas they were likely clustered in time in order to explain the similar timing of coastal subsidence events found along the CSZ.

Table K-1. Recurrence parameters for M8.0–8.7 events.
[yr, years]

Magnitude	a-value	b-value	Recurrence (yr) under any site, on average	Recurrence (yr) along entire CSZ	Number of ruptures in 500 years	Probability of scenario
8.0	4.51	0.8	500	78	6	0.026
8.1	4.52	0.8	500	91	5	0.026
8.2	4.53	0.8	500	107	5	0.026
8.3	4.53	0.8	500	129	4	0.051
8.4	4.54	0.8	500	151	3	0.051
8.5	4.55	0.8	500	178	3	0.051
8.6	4.56	0.8	500	209	2	0.051
8.7	4.57	0.8	500	245	2	0.051

References

Atwater, B.F., and Hemphill-Haley, E., 1997, Recurrence intervals for great earthquakes of the past 3,500 years at northeastern Willapa Bay, Washington: U.S. Geological Survey Professional Paper 1576, 108 p.

Flück, P., Hyndman, R.D., and Wang, K., 1997, Three-dimensional dislocation model for great earthquakes of the Cascadia subduction zone: Journal of Geophysical Research, v. 102, p. 20539–20550.

Frankel, A.D., Petersen, M.D., Mueller, C.S., Haller, K.M., Wheeler, R.L., Leyendecker, E.V., Wesson, R.L., Harmsen, S.C., Cramer, C.H., Perkins, D.M., Rukstales, K.S., 2002, Documentation for the 2002 update of the National Seismic Hazard Maps: U.S. Geological Survey Open-File Report 02-420, 39 p.

Goldfinger, C., Nelson, C.H., Johnson, J.E., and the Shipboard Scientific Party, 2003, Deep-water turbidites as Holocene earthquake proxies—The

Cascadia subduction zone and northern San Andreas fault systems: Annuals of Geophysics, v. 46, p. 1169–1194.

Geomatrix Consultants, Inc., 1995, Seismic design mapping state of Oregon: Final report prepared for the Oregon Department of Transportation, Salem, Oregon.

Kelsey, H.M., Nelson, A.R., Hemphill-Haley, E., and Witter, R.C., 2005, Tsunami history of an Oregon coastal lake reveals a 4600 yr record of great earthquakes on the Cascadia subduction zone: Geological Society of America Bulletin, v. 117, p. 1009–1032.

Kelsey, H.M., Witter, R.C., and Hemphill-Haley, E., 2002, Plate-boundary earthquakes and tsunamis of the past 5500 yr, Sixes River estuary, southern Oregon: Geological Society of America Bulletin, v. 114, p. 298–314.

McCaffrey, R., Qamar, A.I., King, R.W., Wells, R., Khazaradze, G. , Williams, C.A., Stevens, C.W., Vollick, J.J., and Zwick, P.C., 2007, Fault locking, block rotation and crustal deformation in the Pacific Northwest: Geophysical Journal International, v. 169, p. 1315–1340.

Nelson, A.R., Kelsey, H.M., and Witter, R.C., 2006, Great earthquakes of variable magnitude at the Cascadia subduction zone: Quaternary Research, v. 65, p. 354–365.

Satake, K., Shimazaki, K., Tsuji, Y., and Ueda, K., 1996, Time and size of a giant earthquake in the Cascadia inferred from Japanese tsunami records of January 1700: Nature, v. 379, p. 246–249.

Satake, K., Wang, K., and Atwater, B., 2003, Fault slip and seismic moment of the 1700 Cascadia earthquake inferred from Japanese tsunami descriptions: Journal of Geophysical Research, v. 108, 2535, doi:10.1029/2003JB002521.

Tichelaar, B.W., and Ruff, L.J., 1993, Depth of seismic coupling along subduction zones: Journal of Geophysical Research, v. 98, 2017–2037.

Wang, K., Wells, R., Mazzotti, S., Hyndman, R.D., and Sagiya, T., 2003, A revised dislocation model of interseismic deformation of the Cascadia subduction zone: Journal of Geophysical Research, v. 108, no. B1, 2026, doi:10.1029/2001JB001227.